



University
of Glasgow

Du Beau, Amy (2013) *Neurotransmitter phenotypes of descending systems in the rat lumbar spinal cord*. PhD thesis.

<http://theses.gla.ac.uk/4721/>

Copyright and moral rights for this thesis are retained by the author

A copy can be downloaded for personal non-commercial research or study, without prior permission or charge

This thesis cannot be reproduced or quoted extensively from without first obtaining permission in writing from the Author

The content must not be changed in any way or sold commercially in any format or medium without the formal permission of the Author

When referring to this work, full bibliographic details including the author, title, awarding institution and date of the thesis must be given

Neurotransmitter phenotypes of descending systems in the rat lumbar spinal cord

Amy Du Beau (BS, MS)

Thesis submitted in fulfilment for the degree of Doctor of Philosophy
Institute of Neuroscience and Psychology
College of Medical, Veterinary and Life Sciences



November 2013

Summary

Descending systems from the brain exert a major influence over sensory and motor processes within the spinal cord. Although many descending systems are known to have an excitatory effect on spinal interneurons, there is a paucity of knowledge regarding their neurotransmitter phenotypes. Each descending pathway has distinctive anatomical, neurochemical and physical attributes which contribute to the selection and execution of appropriately adaptive motor patterns.

The overarching aims of this study were (1) to determine the neurotransmitter phenotypes of axons descending from the reticular formation, specifically the medial longitudinal fasciculus (MLF) and the caudal ventral lateral medulla (CVLM), and the corticospinal tract (CST) within lower lumbar segments of the rat spinal cord, (2) to investigate the neuronal targets of these systems, and (3) to classify these neurons according to their morphological and geometric properties within laminar boundaries.

Descending pathways of adult rats were anterogradely labelled using the b-subunit of cholera toxin (CTb) injected into the MLF and CVLM to label medullary axons and into the sensorimotor cortex to label CST axons. Spinal cord sections containing labelled axons were immunoreacted with various antibody combinations. Immunofluorescent tissues were examined with confocal microscopy in the transverse, parasagittal and horizontal planes. To investigate the targets of these descending systems, labelled sections were reacted with antibody against choline acetyltransferase (ChAT) and immunoreactive interneurons were reconstructed in three dimensions.

A series of complimentary immunoreactions revealed that the volumetric densities of descending medullary axons contained a heterogeneous combination of transmitters and that the phenotypes and proportions of transmitters used by the MLF and CVLM do not differ significantly. The majority of medullary axons were excitatory, expressing vesicular glutamate transporter 2 (VGLUT2), with fewer axons expressing glycine or γ -aminobutyric acid (GABA). A small population

expressed both of these inhibitory amino acids. A portion of these medullary axonal populations were not immunoreactive to the tested antibodies and were not serotonergic. CST axons were homogeneously glutamatergic, expressing vesicular glutamate transporter 1 (VGLUT1).

Contact densities of ChAT interneurons revealed that the dorsal horn received more input from the CST than partition cells populating the intermediate zone (laminae VI/VII) and central canal cells (lamina X), but all targeted cell populations were richly innervated by VGLUT1. Dendrites that were orientated dorsally relative to their soma were observed to have a greater density of combined inputs from the CST and VGLUT1. Findings suggest that ChAT interneurons in lamina III were activated by cutaneous primary afferents, which are known to be involved in presynaptic inhibition. The CST may act through these defined populations of ChAT interneurons to influence the processing of incoming sensory information.

Excitatory and inhibitory medullary axons descending from the CVLM were found to target ChAT interneurons and populations were classified according to their dendritic orientation in the transverse plane as either mediolateral or dorsoventral. In lamina X, cells orientated dorsoventrally received significantly greater excitatory CVLM input than those situated more dorsally whereas mediolaterally orientated cells received significantly greater inhibitory CVLM input than partition cells, located in the laminae VI/VII region. The CVLM pathway is likely to sculpt motor activity using both excitatory and inhibitory transmitters via morphologically and geometrically defined populations of ChAT interneurons.

Axons descending from the MLF were found to target ChAT interneurons. In the intermediate regions of laminae VI/VII and lamina X, the majority of ChAT interneurons were immunoreactive to neuronal nitric oxide synthase (nNOS), designated as ChAT::nNOS interneurons. Interneurons targeted by the MLF were contacted by serotonin (5-HT) containing terminals and these cells also received contacts from axons immunoreactive to dopamine β -hydroxylase (DBH), an enzyme that converts dopamine (DA) to noradrenalin (NA). The contact densities of partition cells were compared to central canal cells and inputs from 5-HT and MLF

axons were similar. However, the ChAT::nNOS population received comparably greater modulation from 5-HT not contained within descending MLF axons. ChAT partition cells that do not contain nNOS are considered to be the likely source of central boutons (C boutons) onto motoneurons in the ventral horn. Although some descending systems can directly affect motoneurons, most of their actions are mediated via interneurons and properties of these populations have been further elucidated by findings from this study.

Table of contents

Summary.....	ii
List of Figures.....	viii
List of tables.....	xi
Acknowledgement.....	xiii
Author's Declaration.....	xiv
Abbreviations.....	xv
Chapter 1. General introduction	18
1.1 Descending pathways of the mammalian spinal cord.....	19
1.2 Spinal cord organisation	19
1.3 Characterising descending pathways.....	20
1.3.1 Corticospinal tract.....	22
1.3.2 Reticulospinal tracts.....	23
1.3.3 Other descending systems	25
1.4 Axonal pathfinding.....	26
1.5 Neurotransmission at the synapse.....	27
1.6 Neuroreceptors and neurotransmitters of spinal neurons	32
1.6.1 Glutamate.....	32
1.6.2 Glycine and GABA.....	33
1.6.3 Monoamines.....	35
1.7 Neuronal specification in sensorimotor systems	37
1.7.1 Group Ia, Ib and II interneurons	38
1.7.2 Commissural interneurons	42
1.7.3 ChAT interneurons	42
1.8 Neural Networks	44
1.9 Physical properties of spinal neurons.....	45
1.10 Scope of this research and overarching aims.....	46
Chapter 2. General experimental methods.....	47
2.1 Surgical procedures and anaesthesia	48
2.2 Perfusion, dissection and tissue preparation for immunocytochemistry ..	53
2.3 Identification of injection sites	54
2.4 Orientation of immunofluorescent spinal cord tissue	55
2.5 Antibody characterisation	57
2.6 Image acquisition and confocal microscopy	58
2.7 Tissue allocation for experiments.....	60

2.8	Statistical analyses	65
Chapter 3. Neurotransmitter phenotypes of medullary axonal projections within lower lumbar spinal segments		
3.1	Introduction	68
3.2	Methods	70
3.2.1	Image acquisition	70
3.2.2	Derivation of laminar volume	70
3.2.3	Statistical Analysis	73
3.3	Results.....	75
3.3.1	Aim 1: To determine the distribution of medullary axons projecting to lower lumbar spinal cord segments.....	75
3.3.2	Aim 2: To determine the neurotransmitter phenotypes of axon terminals descending from the MLF and CVLM within lower lumbar spinal cord segments.....	81
3.3.3	Aim 3: To determine the neurotransmitter phenotypes of inhibitory axon terminals from the MLF and the CVLM within lower lumbar spinal cord segments.....	90
3.3.4	Aim 4: To determine if medullary axons projecting to lower lumbar spinal cord segments contain serotonin.....	98
3.4	Discussion	101
3.4.1	Qualitative summary	101
3.4.2	Labelling of descending systems.....	102
3.4.3	Identification of neurotransmitter phenotypes.....	102
Chapter 4. Axon terminals descending from the sensorimotor cortex and their neuronal targets in lower lumbar spinal cord segments		
4.1	Introduction	106
4.2	Methods	109
4.2.1	Image acquisition and analyses	109
4.2.2	Laminar boundaries in the parasagittal plane	112
4.2.3	Stereological techniques to examine neuronal targets.....	115
4.3	Results.....	119
4.3.1	Aim 1: To determine the distribution of axon terminals descending from the sensorimotor cortex within lower lumbar spinal cord segments....	119
4.3.2	Aim 2. To identify the neurotransmitter phenotype of CST axons in lower lumbar segments.....	123
4.3.3	Aim 3: To investigate immunoreactive contacts onto ChAT interneurons receiving input from the CST across laminar boundaries.....	125
4.3.4	Aim 4: Classification of ChAT dendritic orientations as related to their contact densities	132
4.4	Discussion	136

4.4.1	Distribution of excitatory descending sensorimotor axons	136
4.4.2	Neuronal targets of descending sensorimotor axon terminals	137
4.4.3	Stereologically classified interneuronal populations	139
	Chapter 5. Targets of the descending reticulospinal pathways	141
5.1	Introduction	142
5.2	Methods	145
5.2.1	Image acquisition and analyses	145
5.2.2	Laminar boundaries in the horizontal plane	146
5.3	Results.....	150
5.3.1	Aim 1: To identify the neurochemical content of contacts onto ChAT interneurons from descending CVLM axons across laminar boundaries in the transverse plane	150
5.3.2	Aim 2: To investigate neuromodulation of intermediate zone interneurons innervated by the MLF in the horizontal plane	157
5.3.3	Aim 3: To determine the relationship of ChAT::nNOS interneurons in laminae VI, VII and X.....	164
5.3.4	Aim 4: To qualitatively compare ChAT interneurons in naïve rat tissue receiving modulatory input from monoamines in the parasagittal plane	168
5.4	Discussion	173
5.4.1	Excitatory and inhibitory CVLM inputs onto ChAT interneurons across laminar boundaries.....	173
5.4.2	Serotonergic inputs onto interneurons in laminae VI, VII and X innervated by the MLF.....	175
5.4.3	The relationship of ChAT::nNOS interneurons in laminae VI, VII and X with 5-HT	176
5.4.4	Qualitative comparison of ChAT interneurons in naïve rat tissue receiving modulatory input from monoamines.....	177
	Concluding Remarks	179
	Appendices for Chapter 1.....	185
	Appendices for Chapter 2.....	188
	Appendices for Chapter 3.....	190
	Appendices for Chapter 4.....	194
	Appendices for Chapter 5.....	203
	List of references.....	213
	Publication	241

List of Figures

Figure 1.1 Neurotransmitter synthesis and release at the synapse.....	31
Figure 1.2 General schematic of recurrent inhibition	41
Figure 2.1 Injection sites for the descending systems in the sagittal plane	49
Figure 2.2 The stereotaxic frame.....	51
Figure 2.3 Bregma, lambda and the sagittal sutures of the rat skull	52
Figure 2.4 Anterograde transport of CTb labelling terminals in a lower lumbar segment	55
Figure 2.5 Three-dimensional spinal cord block in transverse, parasagittal and horizontal spatial planes.....	56
Figure 2.6 Confocal microscope instrument schematic	61
Figure 2.7 Sequential immunoreaction diagram.....	63
Figure 2.8 Diagram of general image acquisition and data collection methods ...	64
Figure 2.9 Normal probability plot	66
Figure 3.1 Conceptual model of bilateral laminar regions containing CTb terminals.....	72
Figure 3.2 Derivation of laminar volume using hexagons.....	73
Figure 3.3 Brain reconstructions for MLF and CVLM injection sites.....	77
Figure 3.4 Distributon of labelled terminals from the MLF.....	78
Figure 3.5 Distribution of labelled terminals from the CVLM.....	79
Figure 3.6 Immunochemistry of MLF terminals.....	84
Figure 3.7 Immunochemistry of CVLM terminals.....	85
Figure 3.8 Example of an <i>a priori</i> histogram plot.....	86
Figure 3.9 Volumetric density comparison of MLF and CVLM terminal transmitter content.....	87
Figure 3.10 Laminar densities of excitatory and inhibitory medullary axon terminals.....	89
Figure 3.11 Immunochemistry of inhibitory axons.....	92

Figure 3.12 Scatter plot comparison of glycine and GABA volumetric densities from MLF and CVLM axonal populations.....	93
Figure 3.13 Transverse medial and lateral regions.....	94
Figure 3.14 Volumetric densities of glycinergic axons from the MLF and CVLM across laminae.....	95
Figure 3.15 Volumetric densities of GABAergic axons from the MLF and CVLM across laminae.....	96
Figure 3.16 Volumetric densities of axons from the MLF and CVLM containing both inhibitory amino acids across laminae.....	97
Figure 3.17 Immunofluorescent axons from the MLF and serotonin.....	99
Figure 3.18 Immunofluorescent axons from the CVLM and serotonin.....	100
Figure 3.19 Qualitative summary of medullary axon neurochemicals.....	101
Figure 4.1 ChAT interneuron conceptually visualised in spinal cord grey matter	111
Figure 4.2 Laminal boundary maps in the parasagittal plane	114
Figure 4.3 Derivation of XY Ratios.....	116
Figure 4.4 Dendritic orientation in the parasagittal plane	117
Figure 4.5 Brain reconstruction for CST injection site	120
Figure 4.6 Distribution of labelled terminals from the CST.....	121
Figure 4.7 ChAT neurons revealed in an L4 transverse and parasagittal section .	122
Figure 4.8 Immunoreactive CST axon terminals.....	124
Figure 4.9 Descending CST inputs onto ChAT interneuron in the transverse plane	126
Figure 4.10 Neuronal densities of ChAT interneurons receiving CST input across transverse laminar boundaries.....	127
Figure 4.11 ChAT interneuron in laminae III / IV of an L4 spinal segment in the parasagittal plane	130
Figure 4.12 Neuronal densities of ChAT interneurons receiving CST input across parasagittal laminar boundaries.....	131
Figure 4.13 Dendritic orientations of reconstructed ChAT interneurons in the parasagittal plane, Part I (Dorsal).....	133
Figure 4.14 Dendritic orientations of reconstructed ChAT interneurons in the parasagittal plane, Part II (Ventral).....	134

Figure 4.15 Dendritic orientations relative to total contact density in the parasagittal plane	135
Figure 5.1 Laminar boundaries in the horizontal plane	148
Figure 5.2 ChAT interneuron in lamina VII receiving excitatory CVLM input	152
Figure 5.3 ChAT soma receiving inhibitory CVLM input	153
Figure 5.4 Neuronal densities of morphologically defined ChAT interneurons receiving CVLM boutons containing VGLUT2 across transverse laminar boundaries	154
Figure 5.5 Neuronal densities of morphologically defined ChAT interneurons receiving CVLM boutons containing VGAT across transverse laminar boundaries .	155
Figure 5.6 Dendritic densities of ChAT interneurons classified according to distance of immunoreactive CVLM boutons from soma	156
Figure 5.7 ChAT::nNOS interneuron receiving input from the MLF and 5-HT	159
Figure 5.8 Reconstructed ChAT interneuron receiving input from the MLF and 5-HT	160
Figure 5.9 Density comparison nNOS::ChAT interneurons receiving input from the MLF and 5-HT	161
Figure 5.10 Relationship of ChAT and ChAT::nNOS interneuronal populations receiving input from the MLF and 5-HT across intermediate laminar boundaries in the horizontal plane.....	162
Figure 5.11 Bilateral comparison of densities of interneurons targeted by 5-HT and descending MLF axons.....	163
Figure 5.12 Relationship of ChAT::nNOS immunoreactive interneurons in the intermediate zone with 5-HT	166
Figure 5.13 The relationship of ChAT, nNOS and ChAT::nNOS expressing interneurons in laminae VI - VII and X	167
Figure 5.14 Neuromodulation of ChAT interneurons.....	169
Figure 5.15 ChAT interneurons neuromodulated by 5-HT and NA near the central canal.....	171
Figure 5.16 Density comparison of ChAT interneurons in the parasagittal plane receiving modulatory input from monoamines	172

List of tables

Table 1.1 Characterisitcs of descending pathways.....	21
Table 2.1 Stereotaxic coordinates for the descending systems.....	49
Table 3.1 Summary of primary and secondary antibody combinations and concentrations.....	74
Table 3.2 Laminar volumes for L3, L4 and L5 lumbar spinal segments.....	80
Table 4.1 Summary of primary and secondary antibody combination and concentrations	118
Table 5.1 Summary of primary and secondary antibody combinations and concentration	149
Appendices 1	
Figure 1 Brain reconstructions for all MLF brain injection sites.....	185
Figure 2 Brain reconstructions for all CVLM brain injection sites.....	186
Figure 3 Brain reconstructions for all sensorimotor cortex brain injection sites.....	187
Appendices 2	
Table 1 Laboratory reagents.....	188
Table 2 Primary antibody characterisation.....	189
Table 3 Allocation of processed spinal cord tissue containing anterograde labelled axons (and naïve tissue) for all experiments.....	190
Appendices 3	
Table 1 Glutamatergic axon terminals from the MLF and CVLM.....	191
Table 2 Excitatory and inhibitory axon terminals from the MLF and CVLM.....	192
Table 3 Inhibitory axon terminals from the MLF and CVLM.....	193
Appendices 4	
Table 1 CST axon terminals immunoreacted with antibodies against VGLUT1 and VGLUT2.....	194
Table 2 CST axon terminals immunoreacted with antibodies against VGLUT1, VGLUT2 and VGAT.....	195
Table 3 Immunoreactive boutons onto laminae I-V ChAT interneurons targeted by the CST in the transverse plane.....	196

Table 4 Immunoreactive boutons onto laminae VI-VII ChAT interneurons targeted by the CST in the transverse plane.....	197
Table 5 Immunoreactive boutons onto laminae X ChAT interneurons targeted by the CST in the transverse plane.....	198
Table 6 Immunoreactive boutons onto laminae I-V ChAT interneurons targeted by the CST in the parasagittal plane.....	199
Table 7 Immunoreactive boutons onto laminae VI-VII ChAT interneurons targeted by the CST in the parasagittal plane.....	200
Table 8 Immunoreactive boutons onto laminae X ChAT interneurons targeted by the CST in the parasagittal plane.....	201
Table 9 Densities of ChAT dorsoventral and rostrocaudal interneurons related to dendritic orientations.....	202

Appendices 5

Table 1 Glutamatergic contacts onto laminae III-V ChAT interneurons targeted by the CVLM in the transverse plane.....	203
Table 2 Glutamatergic contacts onto laminae VI-VII ChAT interneurons targeted by the CVLM in the transverse plane.....	204
Table 3 Glutamatergic contacts onto laminae X ChAT interneurons targeted by the CVLM in the transverse plane.....	205
Table 4 Inhibitory contacts onto laminae III-V ChAT interneurons targeted by the CVLM in the transverse plane.....	206
Table 5 Inhibitory contacts onto laminae VI-VII ChAT interneurons targeted by the CVLM in the transverse plane.....	207
Table 6 Inhibitory contacts onto laminae X ChAT interneurons targeted by the CVLM in the transverse plane.....	208
Table 7 Laminae VI-VII ChAT interneurons targeted by the MLF and 5-HT in the horizontal plane.....	209
Table 8 Laminae X ChAT interneurons targeted by the MLF and 5-HT in the horizontal plane.....	210
Table 9 The relationship of ChAT, nNOS and ChAT::nNOS interneurons in laminae VI, VII and X in the transverse plane.....	211
Table 10 Monoaminergic contacts onto ChAT interneurons in laminae VI, VII and X in the parasagittal plane.....	212

Acknowledgement

Many thanks to those within the Spinal Cord Group for all your contributions. To Drs. Anne Bannatyne and Erika Polgár for being so kind and offering practical advice, delivered with understanding plus a sense of humour. Thanks to Robert Kerr and Christine Watt for all you do and much more. And to Professor Andrew Todd. Thanks to Andrew Toft for always listening to my zany ideas and sharing your own. Thanks to Leanne and Debbie for being extra helpful. Thanks to Professor David Maxwell for supervising this project.

Thanks to Dr. David Simmons and all those within the “psychology side” of our Institute of Neuroscience and Psychology for always including me. Amber, for mulling it over with coffee even on the rainiest days.

Thanks to my former professor, my friend and confidante, Dr. Rudy Candler for being the best “old timey” Alaskan chemist, for your encouragement and because you let me lead. Thanks to my Aunt Mozelle, Catherine and Pierre for your continual support. For Fran, for never forgetting. Thank you Birch, because you are my friend.

Author's declaration

I declare that this thesis has been written by me and that the work presented in this thesis is my own. Professor David Maxwell contributed to this work by performing surgical procedures in rats with my assistance. I confirm that this thesis has not been submitted in any previous application for a higher degree.

Amy Du Beau

Date

Abbreviations

Prefixes:

α	anti
Δ	<i>change in</i>
n	10 ⁻⁹ nano
μ	10 ⁻³ micro
m	10 ⁻² milli
12	cerebellar lobule 12
4V	4 th ventricle
5-HT	serotonin (5-hydroxytryptamine)
ACh	acetylcholine
Alexa 488	Alexa-fluor 488
Amb	ambiguus nucleus
AMPA	α-amino-3-hydroxy-5-methyl-4-isoxazolepropionic acid
ANOVA	analysis of variance
AP	anterior-posterior
ATP	adenosine triphosphate
Ave.	average
AvPB	avidin Pacific Blue
C	caudal
C	Celsius (degrees)
C boutons	central boutons
cc	central canal
Cg2	cingulate cortex 2
ChAT	choline acetyltransferase; cholinergic
CIN	commissural interneuron
CNS	central nervous system
contra	contralateral
CPu	caudate putamen, striatum
CPG	central pattern generator
CS	corticospinal
CST	corticospinal tract
CTb	b-subunit of cholera toxin
CVLM	caudal ventral lateral medulla
Cy5	Cyanine 5
D	dorsal
D ₁ , D ₂	dopaminergic receptors
DA	dopamine
DAB	3, 3'-diaminobenzidine

DBH	dopamine β -hydroxylase
DV	dorsoventral
Dyl 649	Dylight 649
e	Euler's number (≈ 2.72)
EtOH	ethanol
g	grams
g.pig	guinea pig
GABA	γ -aminobutyric acid
GAD65, 67	glutamic acid decarboxylase isoform 65, 67
Gi	granular insular cortex
GlyT2	glycine transporter 2
gt.	goat
H ⁺ -ATPase	H ⁺ -adenosine triphosphate
HRP	horseradish peroxidase
Ia I IN	Ia inhibitory interneuron
ICC	immunocytochemistry
IgG	immunoglobulin
IOBe	inferior olive beta subnucleus
<i>ip</i>	intraperitoneal
ipsi	ipsilateral
kDa	kilodalton
L	lateral
L	litre
L3, L4, L5	lumbar spinal segment(s) 3, 4, 5
log	logarithmic, base 10
LRtS5	lateral reticular nucleus, subtrigeminal part
LV	lateral ventricle
m	metre
M	molar = moles (or mol) per litre
M1	primary motor cortex
M2	secondary motor cortex
ML	mediolateral
MLF	medial longitudinal fasciculus
MN	motoneuron
mo.	mouse
mRNA	messenger ribonucleic acid
NA	noradrenaline
NADPH	nicotinamide adenine dinucleotide phosphate
NMDA	<i>N</i> -methyl-D-aspartate
nNOS	neuronal nitric oxide synthase
No.	number
NOS	nitric oxide synthase
PB	phosphate buffer

PBS	phosphate buffer saline
PBST	phosphate buffer saline plus Triton X-100 ©
PCRt	parvicellular reticular nucleus
PMn	paramedian reticular nucleus
PMT	photomultiplier
psi	pound-force per square inch absolute
py	pyramidal tract
r	radius or radii
R	rostral
rbt.	rabbit
RC	Renshaw cell
REM	rapid-eye movement
RetS	reticulospinal
RetST	reticulospinal tract
Rh Red	rhodamine red
Ro	raphé obscurus
ROb	raphé obscurus nucleus
rs	Spearman correlation test
SD	standard deviation
Sp5I	spinal trigeminal nucleus, interpolar part
UV vis	ultra-violet visible
V0,1,2,3	embryonic interneurons
V	ventral
V	volt
VGAT	vesicular GABA transporter
VGLUT	vesicular glutamate transporter (VGLUT1, 2 ,3)
vhc	ventral hippocampal commissure
VIAAT	vesicular inhibitory amino acid transporter
VST	vestibulospinal tract
wm	white matter
Δ pH	chemical gradient
$\Delta\Psi$	electrical gradient
Υ	gamma
λ	wavelength (nanometre)
π	pi (≈ 3.14)

Chapter 1. General introduction

1.1 Descending pathways of the mammalian spinal cord

Descending pathways are differentially involved in motor processes resulting from mechanisms involving the entire motor network rather than the brain commanding the spinal cord. Each descending pathway has distinctive neurochemical, anatomical and functional features. Since the advent of anterograde labelling techniques, these pathways can be traced. The aim of this chapter is to introduce a contextual common denominator by highlighting prominent literature reporting all aspects of the corticospinal and reticulospinal tracts terminating in the lower lumbar rat spinal cord. Because the spinal cord is highly conserved evolutionarily, the rat model may translate to phylogenetically higher vertebrates. Topics in this chapter include organisation of select descending systems, connectivity of neurons, neurotransmission at molecular and cellular levels, neuronal specification and geometry.

1.2 Spinal cord organisation

The spinal cord is a tubular bundle of tissue extending from the brain that acts as a conduit for electrochemical signals that drive motor circuits. Transverse sections are comprised of the peripheral white matter tracts and the central grey matter containing neurons. The posterior median sulcus is the groove located dorsally and the anterior median fissure is ventral groove such that the cord assumes an elliptical shape. Three meninges cover the spinal cord: the outer dura mater, the arachnoid mater, and the inner pia mater. The subarachnoid space between the arachnoid and delicate pia mater is filled with cerebrospinal fluid. Sixty years ago, Bror Rexed identified anatomically distinct areas corresponding to horizontally stacked layers to classify cat spinal laminae based upon cytoarchitectonic features and this scheme was later adapted to others species including the rat (Molander et al., 1984).

1.3 Characterising descending pathways

Mammalian motor pathways incorporate many different phylogenetically conserved descending systems and others which may have appeared later in evolution. In order to investigate descending pathways, their key characteristics must be defined. Signature features such as their origin in the brain, pattern of terminations, neurochemical properties and neuronal targets within the spinal cord are recognised (Table 1.1). As of yet, these key characteristics have not been fully elucidated for any major descending pathway. Adaptively appropriate motor movements are recruited and instantiated neurons must integrate information from descending pathways by tempering sensory and segmental inputs (Lemon, 2008). Mechanisms controlling features such as firing thresholds and synaptic gain may play major roles in integrating motor responses (Hultborn et al., 2004). An important consideration when investigating descending systems is that any single neuroanatomical pathway can mediate multiple functions (Lemon, 2008).

Characteristic	Specification
Origin	Location of neurons of origin in the brain of the given descending pathway
Synaptic input	Nature of the major inputs to these neurons of origin
Fibre number and size/length	Numbers and lengths of descending fibres and distribution of fibre diameters along the pathway
Course	Trajectory followed by fibres belonging to the pathway
Target/terminations	Location and type of interneurons or motoneurons receiving terminations from the pathway as defined by both level within the spinal cord and laminae within the grey matter
Collaterals	Other supraspinal targets innervated by axon collaterals from the same pathway
Molecular identity	Characteristic surface and other molecules important for axonal pathfinding
Transmitter(s) and neuromodulators	Transmitters employed at synaptic and presynaptic targets of the descending pathway
Transmission	Timing, patterns and type of activity exhibited by neurons contributing to pathway
Lesion/inactivation	Behavioural effects resulting from damaged descending pathway

Table 1.1 Characteristics of descending pathways

Key features of any given descending pathway are specified (adapted from Lemon, 2008).

1.3.1 Corticospinal tract

The only input to the spinal cord originating above the brainstem is from the cerebral cortex. The mammalian CST represents the longest and most direct pathway by which the cerebral cortex affects spinal activity (Armand, 1982, Miller, 1987). The CST makes a substantial contribution to volitional movements and precisely controlled coordinated actions, such as fractionated movements of the digits (Curfs et al., 1996, Lawrence and Hopkins, 1976, Lawrence and Kuypers, 1968, Liang et al., 1991). Goal-directed limb movements are controlled mostly by the CST and also rubrospinal pathways, with the latter originating from the magnocellular division of the red nucleus (Kuypers, 1981).

In rats, the neurons of origin of the CST are located principally in motor and somatosensory cortices (Donoghue and Wise, 1982, Hicks and D'Amato, 1977, Leong, 1983, Wise and Jones, 1977) and this organisation is highly conserved in vertebrates. Corticospinal (CS) fibres descend through the internal capsule and enter the midbrain to the cerebral peduncles. Descending cortical fibres disperse into smaller bundles in the pons. Cortical fibres descending to the medulla congregate into discreet triangular bundles known as the pyramidal tract. Most CS fibres decussate at the level of the spinomedullary junction, entering the lateral white matter of the spinal cord, which accounts for why one side of the body is controlled by the opposite side of the brain. CS axons were found to directly project contralaterally to laminae I and II (Casale et al., 1988, Liang et al., 1991) and ramify in laminae III - VII with few projections found in the ventral horn (Antal, 1984, Brown, 1971, Casale et al., 1988, Liang et al., 1991). The highest density of ipsilateral CS fibres is in the region of lamina VIII and medial lamina VII, both in cervical and lumbar segments (Jankowska and Edgley, 2006). Although these ipsilateral ramifications are rare, they do exist (Kuypers and Brinkman, 1970, Nyberg-Hansen, 1966) and these ipsilateral CS terminations are a viable source of axonal sprouting which are postulated to enhance recovery of contralaterally projecting neurons after injury (Dum and Strick, 1996).

Electrophysiological techniques have demonstrated that coordinated movements of forelimbs and digits in rats are directly attributed to strong cortico-

motoneuronal connections (Elger et al., 1977) and this connectivity may confer adaptive motor behaviours to distal extremities (Lemon, 2008). In many phylogenetically higher species such as primates (Curfs et al., 1996, Kuypers, 1960, Lawrence and Hopkins, 1976, Lawrence and Kuypers, 1968, Liang et al., 1991) and cats, CS axons descend in both the ipsilateral lateral funiculus and the ipsilateral ventral funiculus (Jankowska and Edgley, 2006). In more primitive forms such as edentates, marsupials and lagomorphs, CS fibres have been shown to overlap in areas of CS terminations with brainstem pathways (Kuypers, 1981). In mammals such as rodents, carnivores and primates, CS projections are more extensive, descending to all levels of the spinal cord (see Kuypers, 1981 and Lemon, 2008).

During development, axon terminations from the CST compete with each other for synaptic space on spinal neurons (Martin, 2005) and with specificity. Sensorimotor axons extend to spinal cord levels differentially. Axons from neurons originating in the forelimb area project to the cervical enlargement while axons from the hindlimb area descend further into lower lumbar spinal cord segments in rats (Brosamle and Schwab, 1997, Li et al., 1990). CST motor control functions are not expressed until development of connectional specificity to spinal cord neurons whereby the cortical “motor map” is formed (Martin, 2005).

The CS pathway is widely accepted to be glutamatergic. In rats specifically, experiments using combinations of retrograde tracers and immunostaining techniques have demonstrated that CS neurons contain excitatory amino acid (Giuffrida and Rustioni, 1989). Later studies of CS axons have confirmed immunoreactivity to excitatory amino acids, which suggests that CS pathways are glutamatergic (Valtschanoff et al., 1993).

1.3.2 Reticulospinal tracts

Descending axons coalesce in the brainstem and unlike other neurons within the central nervous system (CNS), neurons in the brainstem’s reticular formation are functionally and neurochemically indistinct. The descending reticulospinal tracts (RetST) play an important role in postural control and movement (Drew

and Rossignol, 1990a, Drew and Rossignol, 1990b, Grillner and Dubuc, 1988, Peterson et al., 1978). Neurons in the pontomedullary reticular formation are known to control posture and stability during reaching and walking in cats (Prentice and Drew, 2001, Schepens and Drew, 2004). Medullary axons projecting to lumbar segments were found to use a combination of excitatory and inhibitory transmitters and act directly on contralateral motoneurons, or indirectly via interneurons found outside motor nuclei (Bannatyne et al., 2003).

The RetST arises in the medial medulla and descends into the dorsolateral funiculus of the cord (Holmqvist and Lundberg, 1959, Holmqvist and Lundberg, 1961) with bilateral ramifications. This terminal distribution pattern may be similar at each spinal segmental level (Matsuyama et al., 1999) as demonstrated by anterograde tracing studies in cat. Retrograde tracer transport studies have shown that the medial pontomedullary reticular formation projects to the entire length of the spinal cord in the cat (Hayes and Rustioni, 1981, Tohyama et al., 1979), the opossum (Martin et al., 1979) and monkey (Coulter et al., 1979, Kneisley et al., 1978).

Neurons projecting from the reticular formation descend through or adjacent to the medial longitudinal fasciculus (MLF), further extending to the spinal ventromedial funiculus to ultimately ramify in laminae VI - IX at all segmental levels of the cord (Nyberg-Hansen, 1965, Petras, 1967a). Collateral fibres of these neurons are bilaterally distributed with ramifications in laminae VI-VIII and X at all levels of the cord (Holstege and Kuypers, 1982, Martin et al., 1979). The medial RetST arises from neurons in the pons and gigantocellular reticular nuclei (Ito et al., 1970, Peterson et al., 1975). Bilateral pathways in the ventral and ventrolateral funiculi arise from the nucleus reticularis gigantocellularis (Basbaum et al., 1978). Findings from retrograde tracing studies in rat suggest that neurons originating from gigantocellular reticular nuclei are commissural and project to cervical, thoracic and lumbar segments (Reed et al., 2008). However, most projections from the gigantocellular reticular nucleus are principally ipsilateral (Sakai et al., 2009, Tohyama et al., 1979). Stimulation of the gigantocellular nucleus activates axial musculature and this synaptic connectivity is proposed to be excitatory (Robbins et al., 1992) and a proportion

of fibres from the gigantocellular complex can be either serotonergic or peptidergic (Bowker et al., 1981a, Bowker et al., 1982).

The caudal ventral lateral medulla (CVLM) plays a major role in autonomic regulation. Some CVLM neurons make direct inhibitory connections with neurons in the reticular formation of the rostral ventrolateral medulla that project to the spinal cord and presumably affect the excitability of sympathetic preganglionic neurons (Agarwal et al., 1990, Aicher et al., 1995, Gieroba et al., 1992, Li et al., 1992). The RetST controls autonomic functions by influencing preganglionic cells and most of these influential fibres are derived from the lateral RetST with few components from the medial RetST. However, other descending tracts, e.g. CS, vestibulospinal, are assumed to exert regulatory effects of autonomic functions as well (Lemon, 2008). Glycinergic neurons in the ventromedial medulla may mediate motor atonia during rapid-eye movement (REM) sleep yet within this same anatomical region there is an embedded anatomical structure, the supraolivary medulla, purely containing glutamatergic neurons (Vetrivelan et al., 2009).

1.3.3 Other descending systems

The ventromedial brainstem pathway, which generally is inclusive of the RetST, includes the tectospinal tract and interstitiospinal tract arising from the midbrain, and lateral and medial vestibulospinal tracts (VST) (Sugiuchi et al., 2004). Propriospinal axons from these pathways project bilaterally into the cervical enlargements (tectospinal) and can reach lumbar segments. Kuypers considered this group of pathways as a bilateral postural control system for head, neck, trunk and proximal limb movements (Kuypers, 1981, Lawrence and Kuypers, 1968).

The dorsolateral brainstem pathways, including the rubrospinal tract arising from the magnocellular red nucleus (Kennedy, 1990, Kuchler et al., 2002, Muir and Whishaw, 2000) and the pontospinal tract descend contralaterally in the dorsolateral funiculus. These pathways provide additional capacity for flexion movements involving more distal limb segments (Kuypers, 1981).

“Emotional motor pathways” can influence motor functions at the spinal level as well (Holstege, 1998). The raphé spinal pathway includes a diffuse system arising from the lower brainstem and fibres terminate widely at all spinal levels. Transmitters and neuromodulators in these pathways include 5-HT and NA (Mason, 1997). This pathway is involved in various adaptive motor activities such as defensive postures, pupil dilation, cardiovascular changes, vocalisation and sexual behaviours, all of which are integral to an organism’s fitness and survival (Vanderhorst et al., 2000).

1.4 Axonal pathfinding

The connectivity of heterogeneous neurons within the spinal cord give insights into complex sensorimotor systems. The complexity of such connections has been referred to as “the wiring problem” whereby axons must selectively find pathways to reach their neuronal targets that enable formation of appropriate synaptic connections (see Spitzer, 2004). Axon terminals contacting cells can be either boutons terminals, which are terminations of axonal branches, or boutons *en passant*, which appear as swellings along non-myelinated axons and at nodes of Ranvier along myelinated axons (Hammond, 2001). Molecular cues, e.g. ambient thermal and/or pH fluctuations, can promote synapse formation by guiding axons and mediating their association with targets, but much less is known about physical cues, e.g. physical constraints, of axonal pathfinding (Nguyen et al., 2002). Axonal sprouting is not just an abortive attempt at regeneration, but part of a defined sequence of events that can enable transected axons to reconnect to their intended target. In contrast to peripheral nerves, central axons cannot regenerate (Bareyre et al., 2002). To further elucidate how axonal pathfinding may not only structure but actually predict properties of networks of neurons, an outstanding issue is to identify the common neurochemistry of axonal targets and then pair these populations with their morphology, geometry and functionality.

1.5 Neurotransmission at the synapse

From Hebb's rule (1949), if two neurons fire simultaneously, the synapses between them are strengthened and the activity of several neurons converging onto a single neuron further strengthens these synapses. Properties of individual neurons are adaptive and synaptic strength may vary in response to sensory input and central modulation (Buchanan and Grillner, 1991, Takahashi et al., 2001) as well as their inherent membrane properties (Dale and Kuenzi, 1997, Wallen et al., 1989).

Neurotransmission at chemical synapses is a sequence of temporal and spatial events initiated when a change in action potential (in units volt (V)) invades the presynaptic terminal (Figure 1.1). Synapses are specialised cell-to-cell contacts where electrical signals are converted to chemical signals that diffuse between cells. Although there are multitudes of kinds of synapses, they exist in two prevailing forms: electrical and chemical. Electrical coupling is achieved through extremely close apposition (≈ 3 nanometre (nm)) of the presynaptic to postsynaptic membrane (Wang, 2008). Electrical synapses are either rectifying where current flows in both directions or non-rectifying with unidirectional current flow. Because electrical transmission is independent of chemical signalling translation, it is advantageously fast.

In contrast, chemical synapses are, by nature, rectifying as the presynapse sends transmitter molecules across the cleft. For this reason, chemical synapses can be structurally asymmetrical as evidenced at the ultrastructural level. Postsynaptic density areas range from 0.01 to 0.5 micrometre² (μm^2) (Wang, 2008) and in three dimensions, the surfaces of pre- and postsynaptic membranes would have the shape of two plates facing each other. Chemical synapses are characterised as a cluster of small vesicles (30-50 nm in diameter) at the presynapse (Wang, 2008). Chemical transmission confers changing the sign of the signal. Electrical depolarisation of the cell membrane opens the Ca^{2+} permeable receptor channel. Presynaptic depolarisation elicited by an action potential can trigger the release of an inhibitory transmitter, which then causes hyperpolarisation at the postsynapse. This flux changes the threshold potential and propagates an electrochemical cascade along the length of the axon. Signal conversion occurs primarily at active zones, specialised electron-dense

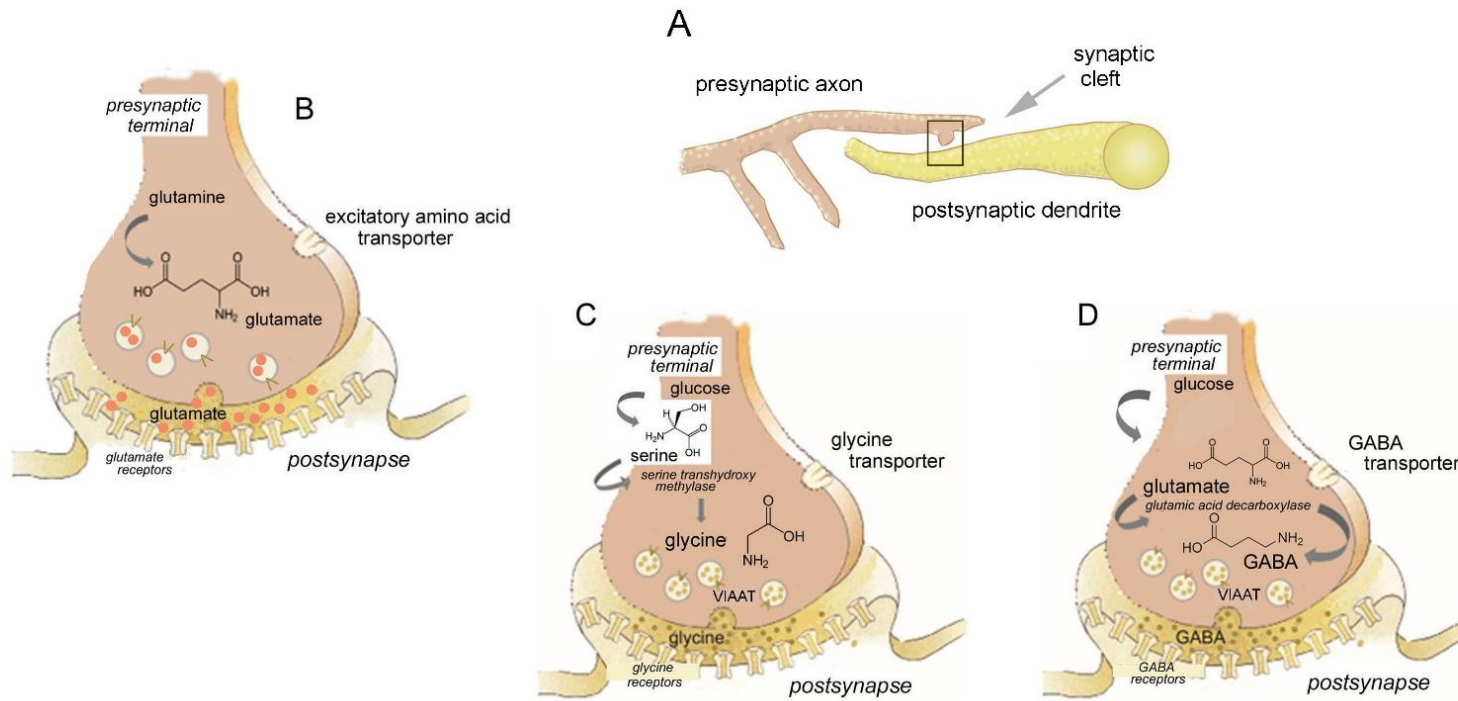
proteinaceous sites on the presynaptic nerve terminal (Couteaux and Pecot-Dechavassine, 1970). Excitation can thus become inhibition. Reducing tonic presynaptic inhibition in intraspinal terminals would effectively “open the gate” and allow signals to flow (Rudomin and Schmidt, 1999).

Inhibition of afferent activity can occur at any place in the synaptic pathway, but it is most strategic for inhibition to occur at the closest site, even before the unnecessary afferent activity has produced any appreciable disturbance in the CNS. There are three prime locations in the afferent pathway that can accomplish presynaptic inhibition: (1) the sensory receptor, (2) the primary afferent terminal, and (3) the second-order cell that is the postsynapse. While direct inhibition of peripheral receptors is common in invertebrates, presynaptic inhibition is preferentially employed in vertebrates. Presynaptic inhibition can be comparatively advantageous since it suppresses information flow in some intraspinal branches, but not in other branches of the same afferent and therefore may allow for selective excitation of neuronal target as needed for appropriately refined motor control and sensory discrimination (Rudomin and Schmidt, 1999).

Data suggest that each synaptic vesicle has a single H⁺-adenosine triphosphate (H⁺-ATPase) (Takamori et al., 2006). This H⁺-ATPase couples hydrolysis of one adenosine triphosphate (ATP) molecule to the inward transmembrane movement of two protons and generation of a chemical gradient (ΔpH) and an electrical gradient ($\Delta\Psi$). Under normal physiological conditions, there is an estimated 1-2 pH unit gradient and a 40-80 mV potential across the synaptic vesicle membrane. Anions such as Cl⁻ can permeate the synaptic vesicle membrane and reduce $\Delta\Psi$ which facilitates formation of a larger ΔpH (Johnson, 1988). Both forms of synaptic transmission, electrical and chemical, coexist on cells throughout the CNS. Synaptic transmission is not a static process as connectivity strength may be depressed or potentiated. Such potentiated changes in synaptic strength/weakness is plasticity. Depression is a complex phenomenon with both pre- and postsynaptic components entailing the depletion of readily releasable pools of vesicles, saturation, or desensitization of postsynaptic receptors (Neher, 1998). Control of temporal and spatial patterns of neurotransmitter signalling is optimally achieved by removing the transmitter from the synaptic cleft.

Although glial cells do not actively participate in synaptic transmission, they help define synaptic connectivity by maintaining signalling of neurons. Mechanisms of synaptic transmission and reuptake are shown in Figure 1.1.

Pre- & postsynapse



VIAAT = vesicular inhibitory amino acid transporter

Figure 1.1 Neurotransmitter synthesis and release at the synapse

Electrical current flows across the presynaptic membrane when depolarized and neurotransmitters are released into the synaptic cleft, targeting receptors at the postsynaptic site (A). The inset box (A) shows the synaptic site at the cleft. Excitatory glutamate from mitochondrial glutamine is synthesized and released into the synaptic cleft (B) with postsynaptic uptake. Glutamate is transported into neurons via excitatory amino acid transporters and then loaded into synaptic vesicles via vesicular glutamate transporters. Inhibitory transmitter glycine (C) is synthesized by various pathways (e.g. serine) and GABA (D) which is synthesized from glutamate by the enzyme glutamic acid decarboxylase and loaded into vesicles via vesicular inhibitory amino acid transporters (VIAAT). High affinity transporters terminate the activity of these transmitters, which are then recycled to the synaptic terminal for reuse.

1.6 Neuroreceptors and neurotransmitters of spinal neurons

Two broadly distinct types of neuroreceptors have evolved to bind neurotransmitter molecules and execute postsynaptic signalling: ionotropic and metabotropic receptors. Ligand-gated ionotropic receptors are further subdivided into three groups, kainite, α -amino-3-hydroxy-5-methyl-4-isoxazolepropionic acid (AMPA) and *N*-methyl-D-aspartate (NMDA), each of which are comprised of various subunits with unique stoichiometry. The overriding principle of neuroreception is that transmitter molecules in the cleft are received at complementary postsynaptic receptors that give measured and detectable synaptic responses.

1.6.1 Glutamate

In the spinal cord, glutamate is used by primary afferents, excitatory interneurons, projection neurons and some descending axons (Broman, 1993). Glutamate is expressed throughout the CNS and contributes to both normal and pathological neural activities. Synaptically released glutamate activates both AMPA and NMDA ionotropic receptors although not necessarily at the same synapse within the spinal cord (Dale, 1986, Dale and Roberts, 1985). Once glutamate is released from the presynaptic nerve terminal, AMPA receptors mediate rapid depolarisation whereas NMDA receptors mediate a much slower response that is permeable to Ca^{2+} and blocked by Mg^{2+} (Alford et al., 2003). In vertebrates, locomotor networks rely upon the co-activation of AMPA and NMDA receptors activated by glutamate released from descending fibres such as from the RetST (Brodin et al., 1988, Dale and Roberts, 1984, Jordan, 1998, Roberts et al., 1985). Glutamate can excite neurons by activating several different types of postsynaptic receptors. In particular, the NMDA activated receptor is of interest due to its putative role in synaptic plasticity (Houk et al., 1993). Glutamate uptake in vesicles depends primarily on $\Delta\Psi$ rather than ΔpH with affinities in the low millimolar (mM) range (Wang, 2008).

Three unique vesicular glutamate transporters have been identified. VGLUT1 messenger ribonucleic acid (mRNA) predominates within the neocortex and cerebellar cortex. Within the cord, VGLUT1 is associated specifically with large-diameter myelinated primary afferents (Varoqui et al., 2002). VGLUT2 mRNA is found within brainstem nuclei, thalamic nuclei and cerebellar deep nuclei (Wang, 2008). Within the cord, VGLUT2 is associated with populations of interneurons (Varoqui et al., 2002) and its expression in nociceptors is essential for normal perception of acute pain and heat hyperalgesia (Scherrer et al., 2010). Throughout the CNS, including the spinal cord, neurons containing VGLUT1 and VGLUT2 exist as independent populations (see Aihara et al., 2000, Bellocchio et al., 2000, Fremeau Jr et al., 2001, Kaneko et al., 2002, Ni et al., 1995, Sakata-Haga et al., 2001, Takamori et al., 2000). However, for unknown reasons, colocalisation of these transporters is commonly observed in the developing CNS (Nakamura et al., 2005), occurring infrequently in the adult (Hioki et al., 2003). In contrast, the transporter of glutamate's third isoform, VGLUT3, is expressed in neurons not classically considered glutamatergic (Fremeau Jr et al., 2001, Gras et al., 2002, Schafer et al., 2002) as it is not necessarily confined to glutamatergic neurons. VGLUT3's function remains enigmatic (Fremeau et al., 2004). In terms of the functional significance of VGLUT3, this excitatory transmitter may increase acetylcholine (ACh) vesicular filling, ultimately stimulating ChAT transmission. VGLUT3 accelerates 5-HT transmission at the level of specific 5-HT terminals and can exert inhibitory control at the raphé level. Findings indicate that loss of VGLUT3 expression leads to anxiety-associated behaviours (Amilhon et al., 2010).

1.6.2 Glycine and GABA

Inhibition of the vertebrate CNS is necessary to temper surplus afferent impulses (see Rudomin and Schmidt, 1999) and many spinal neurons are inhibited by glycine and GABA (Curtis et al., 1981). These amino acids act on ligand-gated chloride channels: glycine and GABA_A receptors, respectively. GABA transport relies on both ΔpH and $\Delta\Psi$ (Wang, 2008). Glycine is the smallest amino acid with a molecular mass \approx 50% less than glutamate (75 vs. 147 kilodalton (kDa)).

Comparatively low molecular mass leads to better permeability penetration in tissues.

For spinal interneurons, the balance between the activity of GABAergic and serotonergic fibres may set the level of excitability (Holstege, 1991). GABA may modify the time course of synaptic inputs with a much lower affinity than glycine (Lu et al., 2008), shortening the duration of glycinergic inhibition to control postsynaptic excitability with precision. GABAergic neurons throughout the CNS contain high levels of parvalbumin, a slow Ca²⁺ buffer associated with regulation of short-term plasticity (Caillard et al., 2000).

An important function of GABAergic inhibition is to suppress the response of dorsal horn neurons to low-threshold mechanical stimuli. GABAergic neurons and ionotropic GABA_A receptors are also found in the spinal dorsal horn where they control the propagation of pain signals from the periphery to higher CNS areas (Zeilhofer et al., 2009). In the ventral horn, GABA acts at both pre- and postsynaptic sites to regulate motoneuron activity and consequently is vital for normal motor function. Dysfunction of inhibitory systems leads to exaggerated reflexes associated with spasticity (see Baldissera et al., 1981). GABA may be especially important for regulating burst intensity, which affects the speed of motor responses (Houk et al., 1993). Inhibitory synaptic transmission is mediated by glycine and GABA is considered to be a prerequisite for coordinated action of muscles during locomotion (Nishimaru and Kakizaki, 2009). Abnormal synchronous gait may be due to a local defect in the mammalian lumbar spinal cord circuitry, and at the level of the synapse, sarcosine, an agent that blocks the reuptake of glycine, restores normal synchronous activation patterns (Kullander, 2005). Immunocytochemistry (ICC) studies on development changes of the distribution of inhibitory neurons demonstrate that GABAergic neurons are amongst the earliest to populate ventral regions of the rat lumbar spinal cord (Ma et al., 1992) and as synaptic inhibition begins to function, fetal motoneurons transition from being GABAergic to glycinergic (Nishimaru and Kakizaki, 2009).

Because many boutons in the spinal cord contain both glycine and GABA (Ornung et al., 1994, Taal and Holstege, 1994, Todd et al., 1995) the notion that they may act as cotransmitters is plausible. Neurons with axons ascending to the midbrain principally show GABAergic markers, or coincident GABAergic and

glutamatergic function (Martin et al., 2011). However, the coincident presence of glycine and GABA in axon terminals does not prove that they both transmit at synapses formed by these axons. For instance, glycine and GABA coexist in cerebellar Golgi cells (Ottersen et al., 1988) but there is reasonable doubt that glycine functions as a transmitter in this situation (Luque et al., 1995). Further, these amino acids coexist at axo-axonic synapses in the cord (Todd et al., 1995) although glycine is likely not involved in presynaptic inhibition (Todd et al., 1996).

1.6.3 Monoamines

Neuromodulators can change neural information processing by regulating synaptic transmitter release, altering baseline membrane potential and spiking activity, and modifying long-term synaptic plasticity (Jankowska et al., 2000). Axons containing 5-HT are especially abundant in the grey matter of the cord and corroborative evidence indicates that while some classes of spinal neurons are heavily innervated by 5-HT, others receive few inputs (Alvarez et al., 1998, Stewart and Maxwell, 1999). 5-HT and NA modulate spinal pathways selectively and differentially (Bras et al., 1989, Bras et al., 1990, Jankowska et al., 2000, Jankowska et al., 1997).

Sensory transmission to superficial and deep dorsal horn neurons is either depressed by 5-HT in rats (Garraway and Hochman, 2001, Lopez-Garcia, 1998, Lopez-Garcia and King, 1996) or, alternatively, in a smaller proportion of cases, 5-HT actually potentiates sensory transmission (El-Yassir et al., 1988).

In rats, electrical stimulation of the dorsal raphe lowered movement thresholds and this effect could be blocked *in vivo* by direct cortical application of WAY-100135, a 5-HT_{1A} antagonist, indicating that 5-HT is primarily acting through the 5-HT_{1A} receptor (Scullion et al., 2013). In a complimentary study investigating motor movements of forelimbs in rats, *in vivo* bath application of tissues with application of WAY-100135 induced action potential firing whereas the agonist 8-OH-DPAT, a 5-HT_{1A} agonist, had the opposite effect. Taken together, these results demonstrate that 5-HT, acting through 5-HT_{1A} receptors, plays an

excitatory role in motor map expression (Scullion et al., 2013). Previous studies have shown that other neuromodulators alter cortical motor map expression, including DA (Brown et al., 2011, Brown et al., 2009, Metz et al., 2004) and ACh (Conner et al., 2003, Ramanathan et al., 2009). When motor map integrity is disrupted, behavioural deficits, e.g. reaching for a desired object with the contralateral paw, are observed (Whishaw, 2000).

Neuromodulators can alter the gain of certain groups of premotor interneurons (Jankowska et al., 2000). Gain may be a result of an interaction between diffuse descending neuromodulators and highly specific local synaptic inhibitory circuits. The effect on motoneuronal excitability is so strong that even motor behaviours requiring minimal force would be virtually impossible without substantial monoaminergic drive. Because raphé output was found to increase in tandem with locomotion, motoneuronal gain may be proportional to the level of force exerted. In the rat dorsal horn, neurons descending from the rostral ventromedial medulla are the major source of serotonergic projections (Potrebic et al., 1994). The control of dendritic processes via descending monoaminergic inputs is likely to be vital for normal motor behaviour. Many bulbospinal monoaminergic systems with heterogeneous transmitter phenotypes act on a variety of spinal metabotropic receptor subtypes, suggestive of the notion that spinal neuromodulation is a highly differentiated process (see Garraway and Hochman, 2001). Thus, a key issue is that the brainstem nuclei that are the origin of 5-HT and NA inputs to the cord are highly state dependent (Heckman et al., 2008).

When 5-HT and DA are coupled in concentrations sufficient to produce a measurable motor output, a rostrocaudal gradient of excitability emerges as observed in the mouse spinal cord, putatively attributed to the differential distribution of receptors along the spinal cord (Christie and Whelan, 2005). Serotonergic and noradrenergic inputs to the spinal cord originate in the brainstem while descending dopaminergic pathways originate in the hypothalamus (Jordan et al., 2007). Modulatory actions of monoamines on spinal commissural interneurons coordinating left-right hindlimb muscle activity were investigated and the differences of these actions were found to depend upon the intrinsic properties of those interneurons rather than the patterns of

innervation by monoaminergic fibres (Hammar et al., 2004). The synaptic actions of 5-HT and NA may be exerted onto dendrites and somata of spinal interneurons rather than axon terminals, as evidenced at the ultrastructural level. However, the mechanisms underlying the effects of neuromodulators have not been fully elucidated and these transmitters may be operating at either pre- or postsynaptic sites (Maxwell et al., 2000).

1.7 Neuronal specification in sensorimotor systems

Spinal neurons serve two main functions: to relay cutaneous sensory information to higher centres in the brain and to integrate proprioceptive input and motor output. These two functional systems are partially anatomically segregated with neurons and circuits that are capable of processing cutaneous sensory input populating the dorsal horn. Comparatively, circuits involved in proprioception and motor control are situated in the ventral horn (Jessell, 2000). In the developing embryonic spinal cord, a functional shift occurs as the neurotransmitter phenotype of interneurons populating the ventral spinal cord changes. Numerous development studies have identified four class of embryonic interneurons, designated as V0, V1, V2 and V3 (see Alvarez, et al., 2005). However, little is known about their adult phenotype. Cell fates could be influenced by ambient flux encountered in the embryonic environment, i.e., ΔpH and temperature, as they further differentiate and populate the spinal cord.

The allocation of cell fate in the spinal cord depends upon two signalling systems which intersect along the rostrocaudal and dorsoventral axes of the neural tube, establishing a grid-like set of positional cues (Lumsden and Krumstauf, 1996, Pituello, 1997). The position of progenitor cells along these axes is thought to influence their fate by defining which inductive neurochemical signals, and the concentrations, to which they are exposed (Jessell, 2000). Signalling along the rostrocaudal axis of the neural tube establishes the main subdivisions of the CNS: forebrain, midbrain, brainstem and spinal cord (Lumsden and Krumstauf, 1996) and the dorsoventral signalling system has a prominent role of in establishing neuronal diversity (Pituello, 1997).

1.7.1 Group Ia, Ib and II interneurons

Interneurons are typically confined within the CNS whereas motoneurons extend beyond. First order interneurons are monosynaptically excited by sensory afferent fibres whereas second, third, and “higher order interneurons” are excited by other neurons. Finally, last order interneurons synapse onto motoneurons. Individual interneurons can actually excite at different orders simultaneously (Jankowska, 1992) so the terminology can become ambiguous. As primary afferents enter the spinal cord, fibres bifurcate and branch as either ascending or descending collaterals that descend to motor nuclei. Most primary afferent fibres from receptors in skin, subcutaneous tissue, muscle, fascia, joint capsules and viscera enter the CNS through the dorsal roots (Brown, 1981). Proprioceptors contain their own sensory receptors, termed proprioceptors, which are integral to motor control. Figure 1.2 schematically illustrates afferent recurrent inhibition.

Type Ia sensory fibres primarily respond to changes in length of muscle fibres. Ia interneurons especially tend to populate ventral lamina VII with dominant inputs from Ia afferents (Hultborn et al., 1971). They are characterised by inputs from sensory Ia muscle afferents and provide reciprocal inhibition to antagonistic motor pools (Eccles et al., 1956). Excitation of interneurons by Ia afferents from extensors (agonist) muscles evokes inhibition of flexor (antagonist) muscles and vice versa such that these interneurons mediate Ia reciprocal inhibition (Jankowska, 1992). Group Ia interneurons are modulated by Renshaw cells (Hultborn et al., 1971), which are defined as inhibitory interneurons located at the mediolateral border of the motor nuclei (Brown, 1981). In contrast to Ia interneurons, Renshaw cells do not receive direct input from primary afferents and their excitation by other interneurons is relatively limited (Jankowska, 2013). Descending tract axons and peripheral afferents may excite Ia inhibitory interneurons not only directly but also indirectly via fusimotor neurons and muscle spindle primaries (Jankowska, 1992).

Another type of proprioceptor, besides muscle spindles, are Golgi tendon organs which are innervated by group Ib sensory axons that respond to tendon stretch. Group Ib axons enter the spinal cord with extensive branching and synapse on ventral horn interneurons. Group Ib interneurons depend upon peripheral input

from a greater variety of afferents. Therefore, presynaptic inhibition is thought to be relatively more essential to controlling Ib interneurons than Ia interneurons. Presynaptic inhibition may then not only weaken but change the relative contribution of these afferents to the excitation of Ib interneurons (Jankowska, 1992). Ib fibres have collaterals that arborise widely in the intermediate region (Brown, 1981) (Figure 1.2).

Axons from secondary endings in muscle spindles are Group II afferent fibres. Group II fibres contact respond to changes in muscle fibre length and group II interneurons are found mainly in the grey matter of mid-lumbar, e.g. L4 (Cavallari et al., 1987), and lumbosacral segments and receive strong monosynaptic innervation from group II fibres (Jankowska, 1992). In the dorsal horn, group II interneurons are heterogeneous and may be either excitatory or inhibitory. First order interneurons in group II afferent pathways have been distinguished according to their anatomical location within the spinal grey matter: laminae IV-V, VI-VII, and VIII (Maxwell et al., 1997). Findings indicate that inhibitory dorsal horn group II interneurons exercise widespread inhibitory control over multiple cell types located on both sides of the spinal cord (Bannatyne et al., 2006). Monoamines were found to powerfully influence premotor interneurons monosynaptically activated by group II afferents (Bras et al., 1989, Bras et al., 1990, Jankowska et al., 2000) and although the precise mechanism of this influence is still unknown, findings demonstrate there is a morphological basis for modulatory actions as the vast majority (95%) of monoaminergic contacts were found on dendritic processes (Maxwell et al., 2000).

Neurons within laminae V - VII integrate inputs from group Ib afferents, mediating reflex actions from tendon organs, and from group II muscle spindle afferents. Patterns of reflex actions from these groups and task dependent changes in their actions, such as during locomotor tasks, are influenced by premotor interneurons integrating information from both afferent groups (Edgley and Jankowska, 1987). However, a further review of compiled evidence demonstrates that in all of these subpopulations differences between individual interneurons mediating reflex actions from group Ib afferents and/or from group II afferents are only minor, not distinctive, and they may therefore operate as

one functional population. Therefore, these neurons may be more appropriately classified as “group I/II interneurons” (Jankowska and Edgley, 2010).

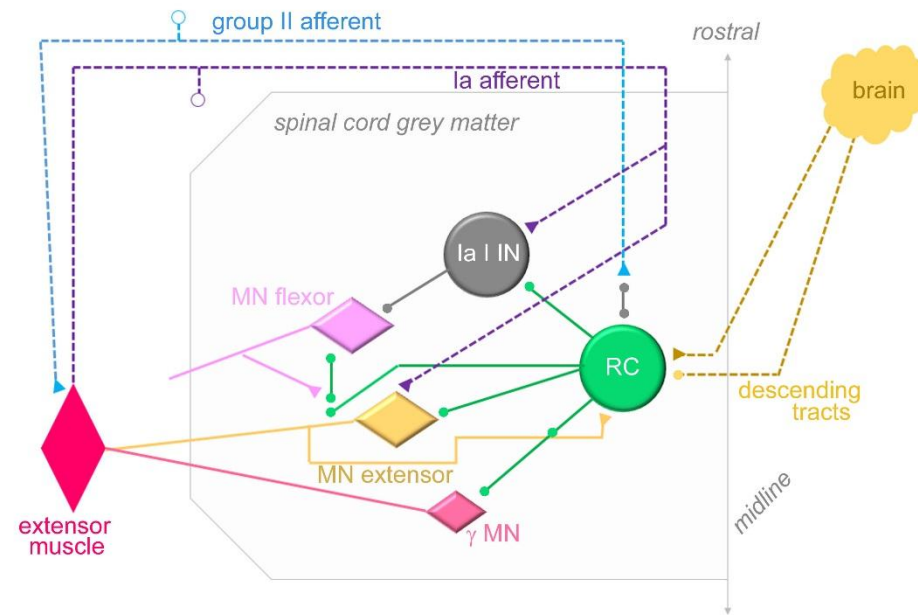


Figure 1.2 General schematic of recurrent inhibition

Excitatory synapses are represented as triangular shapes and inhibitory synapses as round dots. Renshaw cell (RC) with inhibitory axons, shown in green, is activated by a recurrent collateral from an extensor motoneuron (MN), forming a feedback loop. Ia inhibitory interneuron (Ia I IN), shown in grey, excited by Ia afferents. Gamma (γ) MN and extensor MN directly innervate extensor muscle. Descending tracts both excite and inhibit RC.

1.7.2 Commissural interneurons

Commissural interneurons (CINs) are characterised by axons crossing the midline, associated with coordinating left-right locomotion. CINs are a heterogeneous population involved in both phasic postural adjustments and rhythmic alternating movements during locomotion, swimming and scratching. In the rodent lumbar spinal cord, axonal projections of CINs are distinctly inter-segmental (ascending, descending or both) or intra-segmental (Stokke et al., 2002) where “inter” refers to between segments and “intra” is within segments. CINs are heterogeneous and the most reliably identified population are premotor lamina VII interneurons with both excitatory and inhibitory neurochemical profiles (Jankowska, 2007). An investigation of axonal projections of reticulospinal (RetS) neurons in adult cats revealed that distinct populations of CINs in intermediate zones directly excite and inhibit motoneurons located contralaterally (Bannatyne et al., 2003). Investigation of CINs in the cat spinal cord revealed that CIN subpopulations depend on intrinsic interneuronal inputs rather than on patterns of innervation by descending monoaminergic fibres. Such modulatory effects of monoamines on different populations of interneurons might permit reconfiguration of the actions of CINs according to behavioural context requiring adaptively appropriate locomotor responses (Hammar et al., 2004).

1.7.3 ChAT interneurons

At the level of the synapse, vesicular transport of ACh depends primarily on ΔpH (Wang, 2008) and muscarinic ACh receptors belong to the class of metabotropic receptors. ACh is synthesized in the cytoplasm of ChAT nerve terminals, concentrating in synaptic vesicles until release. At the spinal level, endogenous ACh is especially important for modulating sensory processing. ACh was once considered to be the only neurotransmitter released at both central and peripheral synapses of somatic motoneurons (Curtis and Ryall, 1964, Eccles et al., 1954, Windhorst, 1996) although more recent studies have challenged this idea (Herzog et al., 2004, Mentis et al., 2006, Nishimaru et al., 2005). In the spinal cord, intrinsic ACh acts as biogenic amine transmitter. In contrast to bulbospinal monoamine transmitters i.e., 5-HT, DA and NA, ACh is distinct in

that it facilitates evoked excitatory postsynaptic potentials (Garraway and Hochman, 2001). A monoclonal antibody to ChAT, the ACh synthesising enzyme, has been used to localise ChAT within neurons in ICC preparations of adult rat spinal cord (Barber, 1984).

Modulatory influences on neuronal output and behaviour are mediated by sets of ChAT interneurons that can elicit an array of postsynaptic responses. The activation of cortical ChAT systems modulates sensory threshold, states of attention and consolidation of memory (Giocomo and Hasselmo, 2007, Lawrence, 2008, Pauli and O'Reilly, 2008). Morphological and functional features of ChAT spinal neurons enable them to collect segmental information in superficial layers of the dorsal horn and modulate it over several segments (Mesnage et al., 2011). The spinal cord contains several classes of ChAT interneurons with proposed roles in sensory processing and motor output (Barber, 1984, Huang et al., 2000, Phelps et al., 1984). Insights into ChAT modulatory function have emerged through pharmacological manipulation of ChAT receptors, however, due to their widespread distribution, the link between the dynamics of ChAT microcircuitry and physiological function is not yet fully established (Wess, 2003). As a result, defining the contribution of individual classes of ChAT modulator interneurons to specific behaviours is challenging (Zagoraïou et al., 2009).

Neurons immunoreactive for ChAT have been classified and include preganglionic autonomic neurons, small dorsal horn neurons found in laminae III-V, motoneurons, partition neurons found in lamina VII, and central canal neurons in lamina X (Barber, 1984, Borges and Iversen, 1986, Houser et al., 1983, Phelps et al., 1984, Sherriff and Henderson, 1994). The ChAT plexus of dendritic processes in laminae II-III (Ribeiro-da-Silva and Cuello, 1990a) arise, at least in part, from intrinsic spinal neurons, most likely those with somata in laminae III-IV (Barber, 1984). These neurons are rare and disperse along the mediolateral axis (Mesnage et al., 2011). In lamina III, ChAT interneurons receive contacts from both myelinated and unmyelinated primary afferents and different classes of afferents target particular dendritic domains and are likely to be components of an inhibitory feedback pathway monosynaptically activated by primary afferents (Olave et al., 2002). ChAT partition cells segregate into ipsilaterally

and bilaterally projecting populations where the latter preferentially exhibit connectivity to functionally equivalent motoneuron pools (Stepien et al., 2010).

As some ChAT cells may be considered a subset of nitric oxide synthase (NOS cells), many ChAT cells are immunoreactive to neuronal nitric oxide synthase (nNOS) (Spike et al., 1993). The enzyme nicotinamide adenine dinucleotide phosphate (NADPH diaphorase) is expressed as nNOS isoform throughout the brain and spinal cord (Bredt et al., 1991b, Mizukawa et al., 1989, Valtschanoff et al., 1992, Vincent and Kimura, 1992). Specifically in the lumbar cord, NADPH diaphorase is largely restricted to GABAergic neurons in lumbar segments and this enzyme tends to coincide with neurons in which GABA coexists with glycine or ACh (Spike et al., 1993). The highest concentration of nNOS reactive cells are found in laminae II and III and around the central canal with some cells scattered through the laminae IV-VI region. In the ventral horn, nNOS immunoreactive cells can be found but motoneurons are not labelled (Valtschanoff et al., 1992). Motoneurons are known to receive prominent ChAT inputs, C boutons, from spinal interneurons. Zagoraïou et al. (2009) have shown that the transcription factor Pitx2 marks a small population of spinal ChAT interneurons, $V0_C$ neurons, which represent the sole source of C boutons. These C boutons align with postsynaptic m2 class muscarinic receptors and K^+ channels (Hellström et al., 2003, Muennich and Fyffe, 2004, Wilson et al., 2004) and these synapses exert a modulatory influence on motoneuron firing (Brownstone et al., 1992).

1.8 Neural Networks

Neural networks in the spinal cord are capable of producing rhythmic movements even when isolated from the brain and sensory inputs. These “neural oscillators” are referred to as central pattern generators (CPGs) (MacKay-Lyons, 2002). Core sets of excitatory and inhibitory spinal interneurons construct spinal motor networks (Grillner and Jessell, 2009). Command repertoires are structured before a movement begins and are sent to the muscle with the correct timing such that the entire sequence may be executed in the absence of peripheral feedback (Marsden et al., 1984). Spinal cord CPGs produce coordinated activation of flexor and extensor motoneurons during locomotion (McCrea and Rybak, 2008). At the level of the synapse,

neuromodulators can evoke changes in CPG properties, conferring flexibility (MacKay-Lyons, 2002). Sensory afferents involved in muscle and cutaneous reflexes have important regulatory functions by ensuring phase transition in locomotion and preserving balance. Sensory feedback is vital for modulation of motor outputs, but it is unclear whether sensory feedback is necessary for the development of the CPG (Kullander, 2005).

1.9 Physical properties of spinal neurons

Because the majority of synapses in the CNS are found on dendrites, the regulation of dendritic arbors is of critical importance to neural organisation (Snider, 1988). To some degree, dendritic arbors appear to be established at early developmental stages by intrinsic genetic mechanisms (Banker and Cowan, 1979, Honig and Hume, 1986, Kriegstein and Dichter, 1983). However, dendritic arborisation is also influenced by extrinsic factors, particularly neural connections (Deitch and Rubel, 1984a) and neurotrophic molecules may affect dendritic arborisation as well (Snider, 1988). The complexity and variety of dendritic processes raise difficult questions concerning the role played by neuronal geometry in shaping neural behaviour. The development of quantitative models for characterising the detailed branching patterns of dendritic trees is a major step toward providing a basis for defining the functional roles of spinal neurons (Lindsay et al., 2007). Stereological techniques provide meaningful quantitative descriptions of the geometry of three-dimensional structures from measurements that are on two-dimensional images (see Schmitz and Hof, 2005).

A common feature of reconstruction models is the use of parametric distributions to characterise morphological data (Ascoli et al., 2001, Burke et al., 1992). Historically, Ramon y Cajal (1909) described three discreet types of neurons in the substantia gelatinosa (lamina II) and later studies (Gobel, 1975, Gobel, 1978) using intracellular staining have defined four main types of neurons in the cat dorsal horn: islet, stalked, arboreal and border (Grudt and Perl, 2002). In a study involving transgenic mice expressing green fluorescent protein specifically in cholinergic interneurons, ratios of dendritic and axonal processes were found to be significantly elongated rostrocaudally as correlated to distinct

tonic and phasic firing properties such that a marked anisotropy emerged (Mesnage et al., 2011). Results from a study of mammalian autonomic ganglia related the number of axons in synaptic contact with various types of cells and the anatomical complexities of their various cell targets (Purves and Hume, 1981). Taken together, such findings raise the possibility that a function of dendrites is to regulate the number of different innervating axons. The number of different dendritic and axonal processes that innervate neurons is a major determinant of their ability to integrate information (Hume and Purves, 1981).

1.10 Scope of this research and overarching aims

Descending systems are differentially involved in sensorimotor processes associated with hindlimb movement within the spinal cord. However, the neurotransmitters used by these systems and their neuronal targets within the spinal cord is largely unknown. To trace descending systems, axon terminals were labelled by anterograde transport of CTb and the corresponding reconstructed brain injection sites for all experiments are shown in Appendices Figures 1, 2 and 3. These investigations will address each of the following overarching aims:

To identify the neurotransmitter phenotypes and distribution of axons descending from the medulla and the sensorimotor cortex that project to lower lumbar spinal segments

To identify the neurochemical content of contacts onto ChAT and ChAT::nNOS expressing interneurons targeted by descending axons

To classify these neuronal populations targeted by descending systems according to their morphology across laminar boundaries and their dendritic orientations

Chapter 2. General experimental methods

This chapter presents a detailed overview of all general experimental methods and materials used throughout this project to fulfil the principal aims. Subsequent experimental chapters will present experimental techniques specific to that investigation.

2.1 Surgical procedures and anaesthesia

All animal procedures were conducted in accordance with British Home Office regulations and the Animals Scientific Procedures Act (1986) with approval by the Glasgow University Ethics committee. Professor David Maxwell injected the CTb into the rat brains with my assistance. Prior to surgery, adult male albino Sprague Dawley rats (Harlan, Bicester, UK) were housed in groups in temperature controlled cages on a 12 hour light/dark cycle with behavioural enrichments provided and freely accessible food and water. The stereotaxic coordinates for each descending system are listed in Table 2.1. There are two methods to finding the stereotaxic coordinates of an intended injection target site, interaural and bregma. For the medullary injection sites, interaural coordinates were used. Bregma coordinates were used for the sensorimotor cortex rather than interaural because these coordinates are closer to the target. Any given injection site was found from the list of anatomical structures in the stereotaxic atlas (Paxinos and Watson, 2003) with the anterior-posterior (AP) coordinate indicated in the sagittal diagram grid (Figure 2.1). The dorsoventral (DV) and mediolateral (ML) coordinates were then determined from the corresponding coronal diagram grid.

Descending System	Target	Interaural Coordinates, mm		
		AP	DV	ML
RetST-MLF	medial longitudinal fascicle	-3.8	+1.0	+0.1
RetST-CVLM	caudal ventral lateral medulla	-4.8	-0.4	+1.8
		Bregma Coordinates, mm		
		AP	DV	ML
CST	sensorimotor cortex	-1.7	-2.0	+2.0

Table 2.1 Stereotaxic coordinates for the descending systems

Interaural coordinates are used to target the medullary sites (MLF and CVLM) and bregma coordinates are used to target the sensorimotor cortex. AP = anterior posterior; DV = dorsoventral; ML = mediolateral; mm = millimetre.

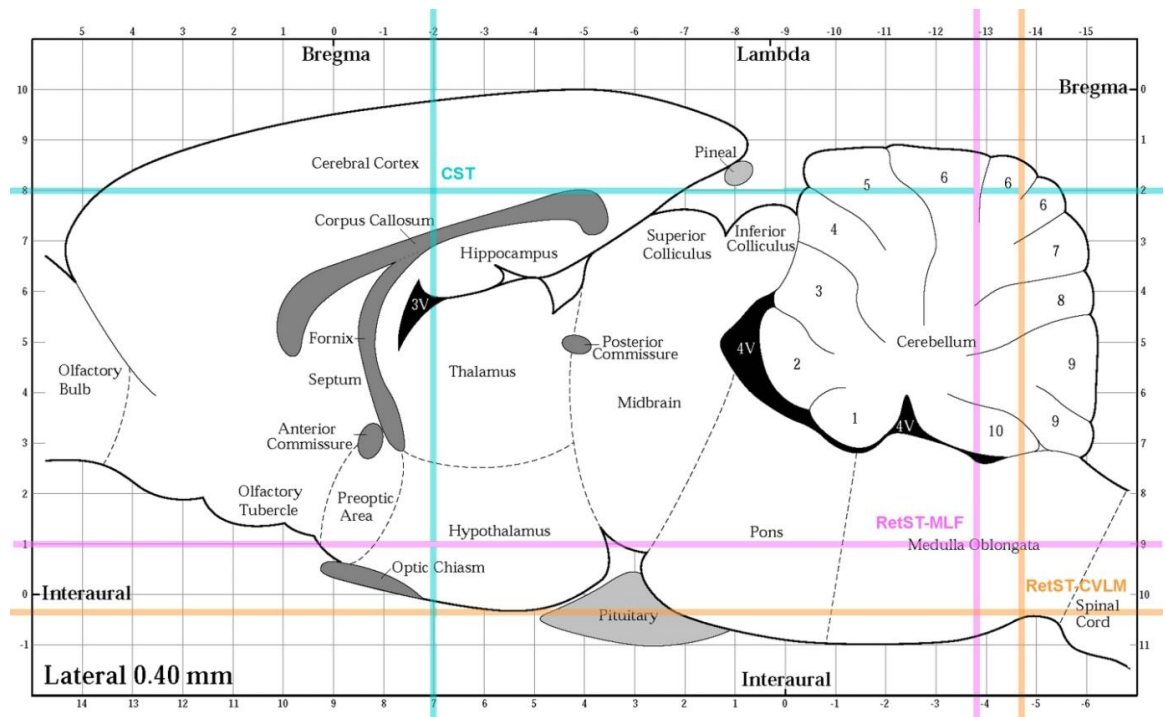


Figure 2.1 Injection sites for the descending systems in the sagittal plane

Coordinates for the CST (blue grid), medullary RetST-MLF (pink grid) and RetST-CVLM (orange grid) are indicated (mm = millimetre). Based on Paxinos and Watson, 2003.

Immediately preceding surgery, rats were weighed (250-350 grams (g)) on a balance scale (Adventurer-Pro, Ohaus) and deeply anaesthetised with an intraperitoneal injection (*ip*) of a 2:1 cocktail of the dissociative drug Ketamine (Boehringer Ingelheim Vetmedica, Inc., USA) and Xylazine (Bayer Plc., UK) at 0.1 millilitre (ml) / 100 g. Fur was shaved from the scalp (Contura Shaver, Vet Tech, UK) and the rat was transferred to the surgical theatre and placed onto a heated platform (Vet Tech Solutions LTD). Surgical instruments were autoclaved (SES Little Sister 3, Eschmann). The depth of the anaesthetic effect was gauged by the withdrawal reflex; the back paw was squeezed tightly to evoke withdrawal of the limb. If this reflex was absent, then the surgical procedure may proceed or otherwise the rat was given a supplemental dose of the injectable anaesthetic (≈ 0.1 ml *ip*). The withdrawal reflex was checked regularly throughout the procedure to assess whether further drug was necessary to ensure deep anaesthesia. For some of our stereotaxic procedures, rats were anaesthetised with gaseous isoflurane, a halogenated ether: 2-chloro-2-(difluoromethoxy)-1,1,1-trifluoro-ethane (Sigma Aldrich, UK) delivered via a compact anaesthetic trolley with a vapouriser (Vet Tech Solutions LTD). After the isoflurane was initially introduced in an anaesthetic chamber (Vet Tech Solutions LTD), a face mask was fitted to continuously administer a 2%⁺ dose scavenged using an Active Scavenging Unit (Fluo Vac System, Vet Tech Solutions).

Under strict aseptic conditions, the rat was fitted into the stereotaxic frame (World Precision Instruments, Inc.) as shown in Figure 2.2. Equidistant ear bars were inserted into the external auditory meatus such that the head may rotate freely up and down but not sideways. The head was finally secured by placing incisors into the clamped incisor bar. Sterile surgical drapes isolated the surgical area. The incision site was swabbed with ethanol and the rat's eyes were protected with a thin layer of petroleum-based eye ointment (Lacri-Lube, Allergan) and/or gauze moistened with water. The skull was then exposed with the incised skin retracted. Bregma, lambda and the sagittal suture were represented as shown in Figure 2.3.

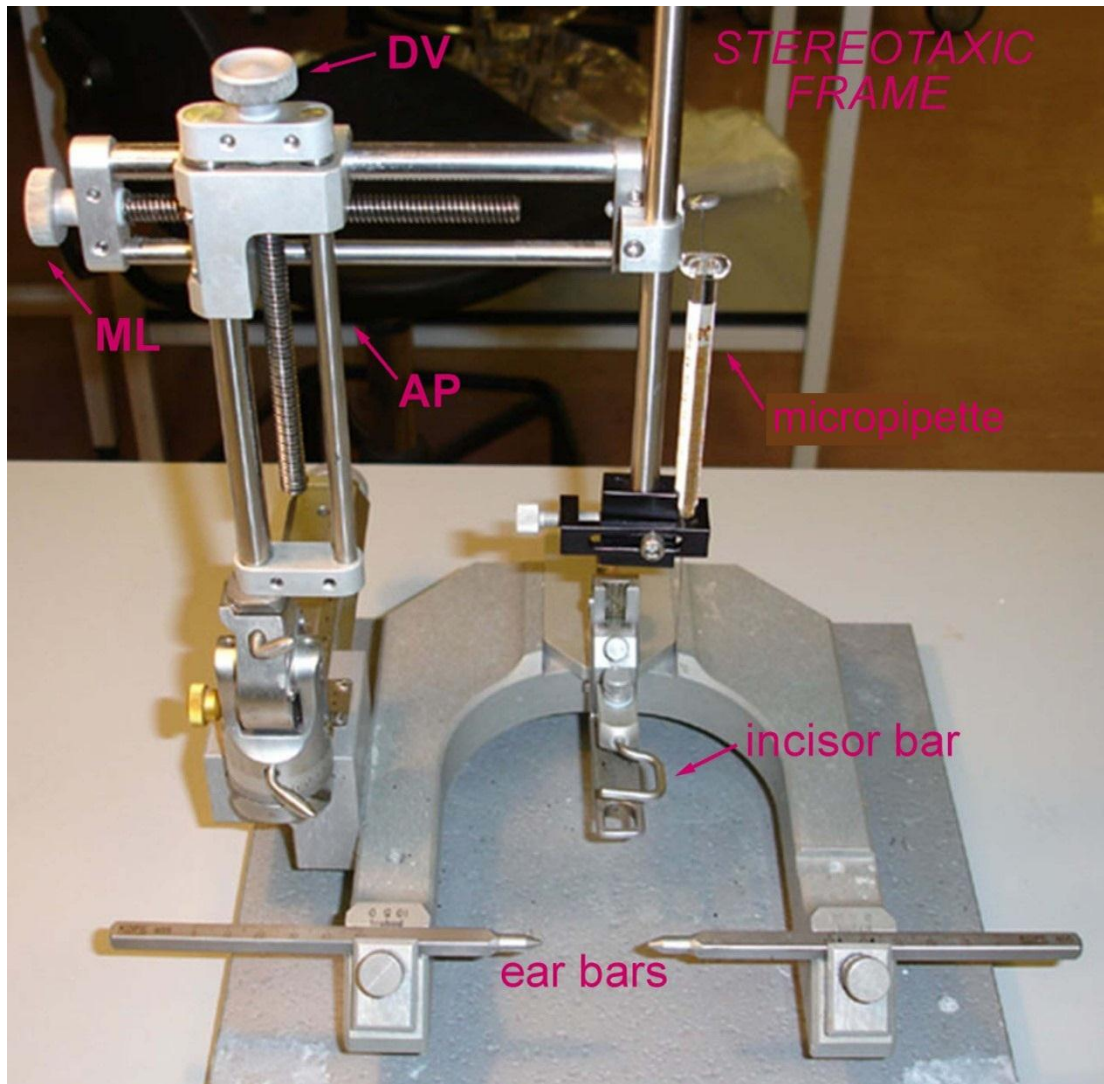


Figure 2.2 The stereotaxic frame

The labelled photographs details the stereotaxic frame. The micropipette is precisely aligned in the mediolateral (ML) and anterior-posterior (AP) direction while the rat's head is affixed with the ear and incisor bars.

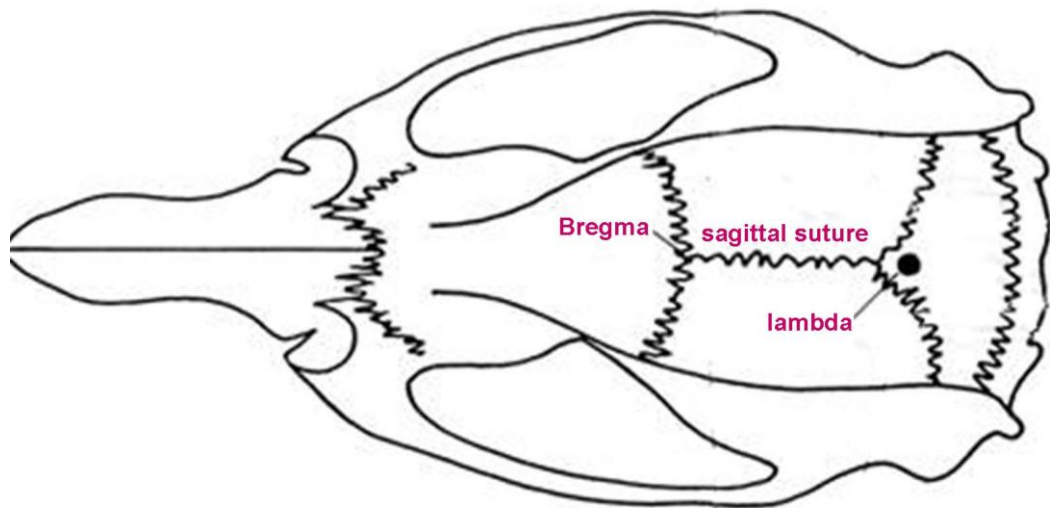


Figure 2.3 Bregma, lambda and the sagittal sutures of the rat skull

The sutures are visualised during the stereotaxic procedures. Based on Paxinos and Watson, 2003.

To zero the stereotaxic frame, the tip of the glass micropipette was aligned with the sagittal suture (or Bregma for the sensorimotor cortex injection site) and the ML reading from the Vernier scale (mm) was recorded as 'zero'. For the AP and DV coordinates, the tip of the micropipette was situated at the right ear bar with the readings each recorded as 'zero.' To calculate the target coordinates, the known stereotaxic coordinates were subtracted from these 'zero' figures. A burr hole was drilled through the skull with a dental drill (World Precision Instruments, Inc.) to accommodate the micropipette with a tapered tip diameter of approximately 20 μm . If necessary, bleeding from the skin or bone surrounding the burr hole was cauterised with a thermal cautery unit (Geiger Medical Technologies) to prevent blood from clogging the glass tip. The micropipette was filled with 1% CTb (Sigma-Aldrich Co., Poole, UK) in distilled water with a Pico injector (World Precision Instruments, Sarasota, FL, USA). For medullary injections, 200 nl of CTb was injected and 3 x 200 nl for the sensorimotor cortex injections. The micropipette was inserted into the brain and lowered to the designated DV target coordinate. CTb was pulse titrated at a rate of 1-5 pound-force per square inch, absolute (psi) using the Pico injector. The micropipette was left in place for five minutes to prevent backflow of CTb into the glass tip. The micropipette was then withdrawn and the wound was

then sutured (Coated VICRYL suture, Ethicon) and the procedure concluded. The anti-inflammatory drug, Carprofen (0.1 ml / 100 g *ip*; Pfizer) was given. Under close veterinary supervision, the rat was transferred to a recovery cage and normal exploratory behaviour was expected within minutes. Within 2-4 hours, the rat was fully recovered and food and water were freely provided.

2.2 Perfusion, dissection and tissue preparation for immunocytochemistry

After a six day postoperative survival period, rats were anaesthetised with Pentobarbitone (1 ml / 200 g *ip*; Sigma-Aldrich, UK). Professor David Maxwell performed the perfusions with my assistance. When the withdrawal reflex was absent, the rat was perfused with mammalian ringer solution immediately followed by 1L of 4% paraformaldehyde (Sigma-Aldrich, UK) in 0.1 phosphate buffer (PB). Reagents were introduced by a syringe through the left ventricle via gravity feed. The spinal cord and brain were removed and stored in bottles containing paraformaldehyde fixative solution overnight at 4°C. To cryoprotect the brain, sucrose was added to this fixative solution (3 g / 10 ml). The cortex and brainstem were cut into 100 µm coronal sections with a freezing microtome (Leitz, Wetzlar) for histological examination of the injection site. Lower lumbar spinal cord segments from L3 to L5 were cut in 60 µm transverse, parasagittal and horizontal sections with a Vibratome (Leica VT10005). Brain and cord sections were immediately dehydrated in a 1:1 solution of ethanol (EtOH) in distilled water to enhance antibody penetration. Surfactants denature proteins and for antibodies to optimally penetrate the tissue's lipid bilayer, all antibody combinations were diluted with 0.3% Triton X-100 (Sigma-Aldrich, UK) in phosphate buffer saline (plus Triton X-100 ©) (PBST). Surplus sections were stored in glycerol at -20° Celsius (C). Whole blocks of tissue were cryoprotected by overnight saturation with sucrose PB, drained, then stored in liquid nitrogen, which freezes instantly at -210°C. Formulae for common laboratory reagents used throughout this project are provided in Appendix 2 Table 1.

2.3 Identification of injection sites

Injection sites of the brain and axon terminals labelled by anterograde transport of CTb of the cord were revealed using the chromogen 3, 3'-diaminobenzidine (DAB; Sigma-Aldrich, UK). Brain sections and a few representative transverse cord sections were incubated in goat anti (α)-CTb (List Quadratech, USA) at 1:1000 for 2 days at 4°C followed by three quick rinses in phosphate buffer saline (PBS). Sections were kept free-floating during all incubations on an agitation platform (IKA Vibrax VXR Shaker). Sections were then incubated in biotinylated α -goat immunoglobulin (IgG) (Jackson ImmunoResearch, USA) at 1:500 for 4 hours at 25°C followed by three quick rinses in PBS. Sections were finally incubated in avidin horseradish peroxidase (HRP; Sigma-Aldrich, UK) at 1:1000 for 2 hours at 25°C followed by two quick rinses in PB. Finally DAB solution in PB was activated by H₂O₂ and filtered with sections immediately reacted for 10 minutes. Immunoreactive anatomical sites appeared as a rusty-brown colour. Sections were mounted on gelatinised slides and stored overnight in formalin vapour. Serial solutions of distilled water, 70% EtOH, 90% EtOH, 100% EtOH and finally a histological clearing agent (Histo-clear II, National Diagnostics, USA) dehydrated and cleared the mounted slides, which were then cover-slipped using a histological mounting medium (Histomount, National Diagnostics, USA). Sections were observed with a transmission light microscope (Nikon Eclipse E600, Surrey, UK) and digitally photographed with an AxioCam camera (Carl ZEISS, Inc., Germany) using AxioVision 4.8 software (Carl ZEISS, Inc., Germany). To determine specific anatomical structures targeted by the CTb injections, coronal templates from the stereotaxic rat brain atlas (Paxinos and Watson, 2003) were referenced. Representative photomicrographs are shown in Figure 2.4. Brain injection sites for all animals are shown in Appendix 1 Figures 1, 2 and 3.

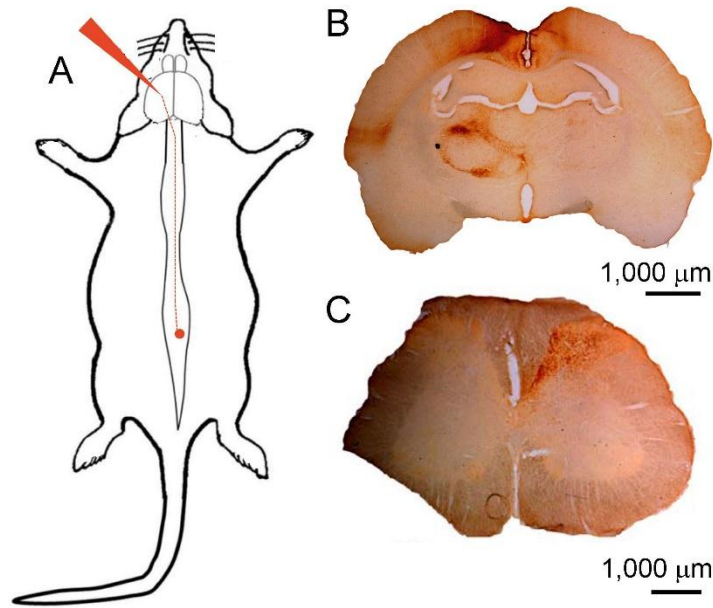


Figure 2.4 Anterograde transport of CTb labelled terminals in a lower lumbar segment

In this example, CST axons were anterogradely labelled with CTb injected into the sensorimotor cortex (A). Photomicrograph of the targeted injection site in a coronal brain section reacted with DAB (B) and transverse L3 spinal cord section showing the location of labelled axon terminations.

2.4 Orientation of immunofluorescent spinal cord tissue

To facilitate further analyses of immunofluorescent tissues, spinal cord sections must be precisely mounted onto slides with the correct orientation (Figure 2.5). Prior to cutting sections for immunofluorescence, lower lumbar segments L3, L4 and L5 spinal cord blocks were notched on the side opposite the labelled axon terminals (Figure 2.4). For blocks to be sectioned transversely, the ventral-lateral white matter was notched. For parasagittal sections, the notch was caudal-ventral. For horizontal sections, the notch was caudal-lateral. Blocks were embedded in agar (Sigma-Aldrich, UK) and then sectioned with the Vibratome.

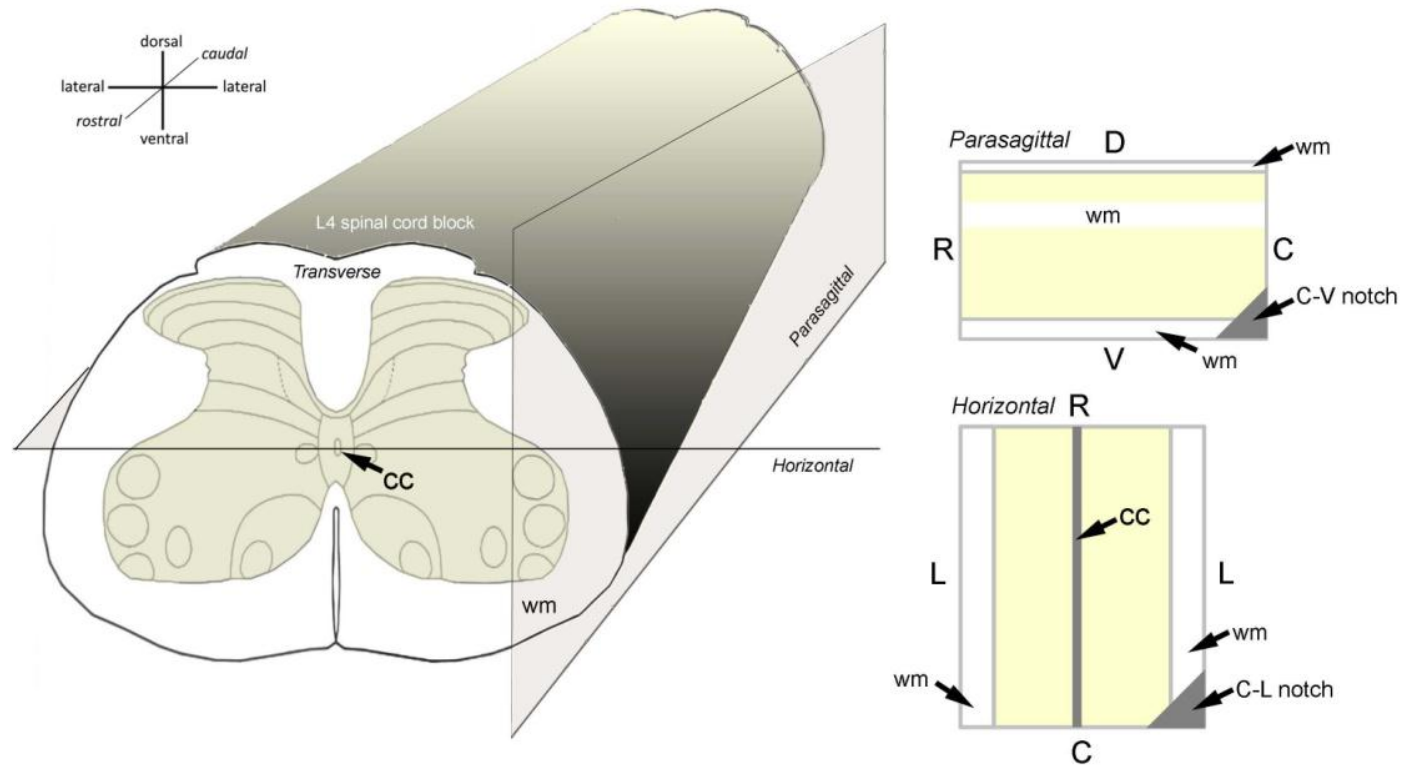


Figure 2.5 Three-dimensional spinal cord block in transverse, parasagittal and horizontal spatial planes

D = dorsal; V = ventral; R = rostral; C = caudal; L = lateral; cc = central canal; wm = white matter.

2.5 Antibody characterisation

Primary antibodies against transporters, neurotransmitters and receptors were selected to fulfil the aims of this project. I conducted all ICC experimental techniques and subsequent analyses on processed tissues. A primary antibody has a selective affinity to a target antigen already present in the tissue. Spinal cord sections were incubated in various primary antibody combinations raised in different species. Then sections were incubated in the species-specific secondary antibody combinations conjugated to various fluorophores (Figure 2.6). A secondary antibody is generally an IgG raised in donkey against the IgG belonging to the animal species of the paired primary antibody. The specificity of any given primary antibody is demonstrated by a negative control: the absence of immunoreactivity in regions of the CNS known not to contain neurons that transport the tracer. For a positive control, the antibody is tested on neurons that are known to contain the target antigen. To ensure quality control for each antibody used in this project, the supplier provided referenced information about the immunoprecipitation and immunoblotting tests to determine an antibody's specificity and optimal concentration. Information pertaining to the specificity, controls, species reactivity and application of primary antibodies used for all experiments are listed in Appendix 2 Table 2.

For all ICC experiments presented in this project, the following general techniques were followed unless otherwise indicated. Continuously agitated spinal cord sections were incubated for three days at 4°C in various primary antibody combinations then incubated overnight in secondary antibody combinations at 4°C. Sections were always rinsed in PBS three times after each incubation period. With notches aligned, sections were mounted on glass slides and cover-slipped with a glycerol based anti-fade medium (Vectashield; Vector Laboratories, Burlingame, CA, USA). For experiments using four primary antibodies, sections were sequentially reacted. The fourth primary antibody is paired with biotin bound to avidin. Biotin is a very small coenzyme (molecular weight = 244.31 g/mol) that binds specifically to avidin with a high affinity. Avidin is conjugated to a fluorophore. All secondary antibodies were supplied by Jackson ImmunoResearch, West Grove, USA, except Alexa-fluor 488 (Alexa 488) and avidin Pacific Blue (AvPB), which was supplied by Molecular Probes, Eugene,

USA. Sequentially reacted sections were then scanned twice as described in Figure 2.7.

2.6 Image acquisition and confocal microscopy

For all experiments, immunoreactions were repeated for three animals ($n = 3$). I examined all processed tissues using confocal microscopy. Terminals were counted as positive only if fully filled with a given marker in the same focal plane. Contacts were defined as being in close apposition to neuronal processes in the same focal plane with no intervening black pixels. The radii (r) and surface areas of somata were mathematically calculated based on the measured perimeter from the projected confocal image using Image J 1.43u software programme (National Institutes of Health, USA). The transcendental value of pi (π) was designated as 3.14 to approximate the radii of soma that are assumed to be spherically shaped for the purposes of these experiments. Radius (μm) = perimeter / (2π) and surface area (μm^2) = $4\pi r^2$. The number, length and surface area of dendrites was recorded directly from Neurolucida Explorer 9.14.3 software (MBF Bioscience - MicroBrightField, Inc. 1987-2010).

Immunoreactive sections were scanned with a three-colour channel laser confocal microscope (Bio-Rad, Hemel Hempstead UK) as shown in Figure 2.7, which also describes the fluorophores used throughout this project. Sections were scanned at x40 oil immersion with a zoom factor of 2 with a $0.5 \mu\text{m}$ z-separation (unless otherwise indicated in subsequent chapters). To locate specific neurons within sections, especially in the parasagittal and horizontal plane, low power images were scanned at x20 with a zoom factor of 1 with a $1-2 \mu\text{m}$ z-separation. Slightly overlapping serial scans were montaged as necessary to fully reconstruct dendritic processes. Neurons were reconstructed in three dimensions using Neurolucida 9.14.3 software (MBF Bioscience - MicroBrightField, Inc. 1987-2010). Images are displayed in single focal planes, unless otherwise indicated, with colour channels separated and adjusted using Adobe Photoshop 7.0 (1990-2000).

Data from the all experiments were gleaned from analyses based upon confocal microscopy where immunofluorescent axon terminals and their neuronal targets

were quantified. Structures forming putative appositions can be detected from a series of thin optical sections that are a fraction of a micron in depth. Therefore, it is highly probable any two structures in apposition in a single optical plane form a synaptic contact since they cannot physically lie above or below each other in that plane of focus. General image acquisition and data analyses methods are outlined in Figure 2.8.

2.7 Tissue allocation for experiments

Processed spinal cord segments L3, L4 or L5 containing anterogradely labelled axons descending from the MLF, CVLM or CST were allocated for all experiments as indicated in Appendix 2 Table 3. Surplus tissues were routinely stored and used for later experiments. A few sections from any given single agar-embedded segment could be cut in a given plane of orientation, removed from the Vibratome chuck, re-embedded in agar, and remounted in another plane such that further sections from a single segment could be cut in more than one spatial plane for use in subsequent experiments.

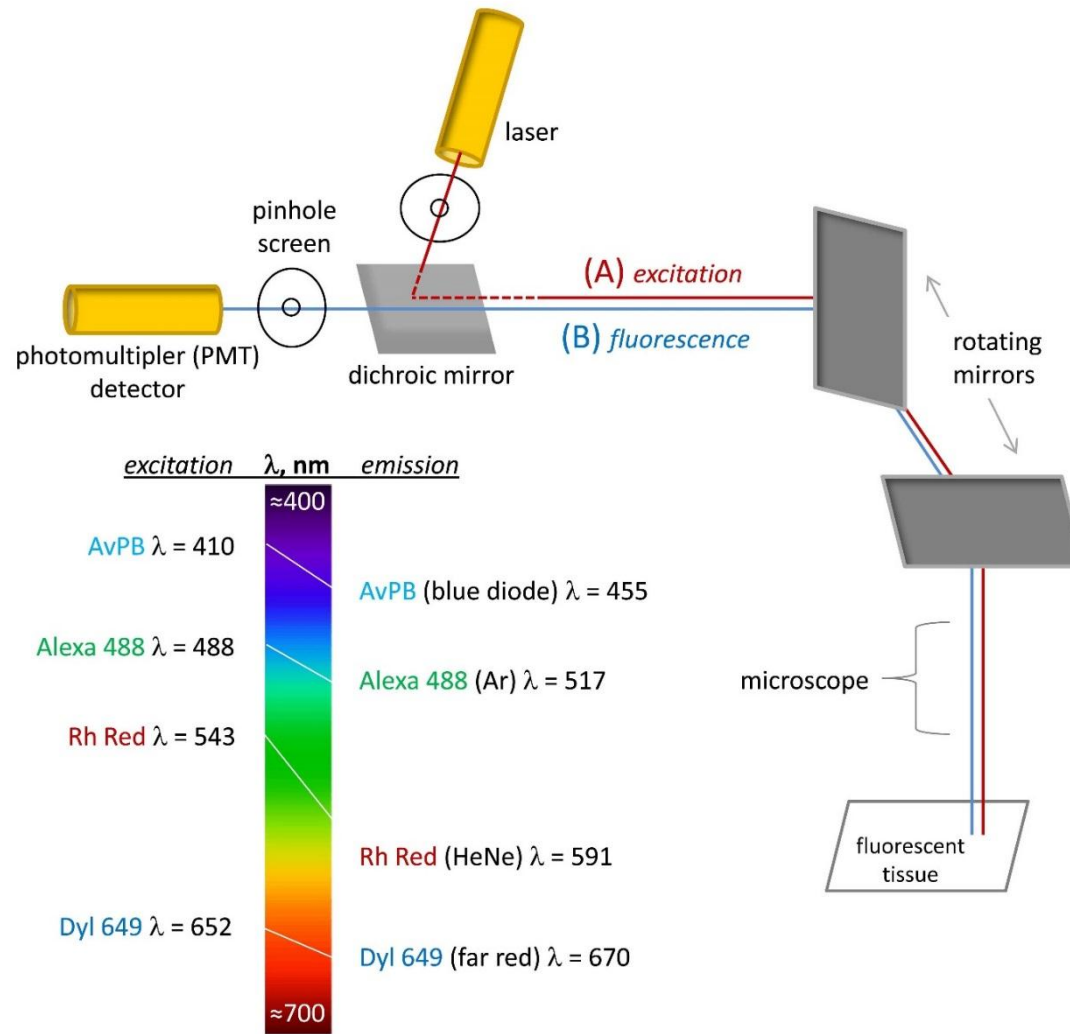
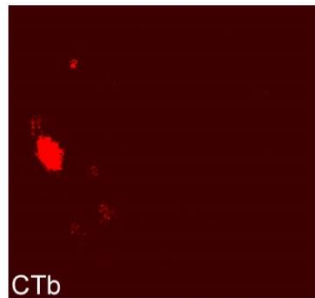


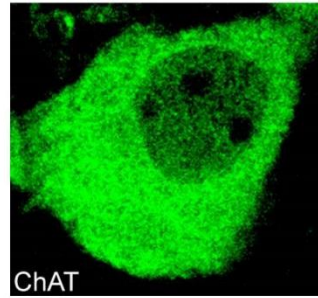
Figure 2.6 Confocal microscope instrument schematic

Highly ordered laser light is scanned across the spinal cord tissue section by rotating scanning mirrors. The tissue is illuminated axially rather than at different angles so the entire optical field is uniformly illuminated. Optical sections occur as light passes through the pinhole to the photomultiplier (PMT) detector. Excited particles in the tissue fluoresce at a given wavelength, λ (nm). Some of the excitation energy is lost as excited electrons drop to a lower shell state, finally resting as light is emitted as detected colour. The fluorescent light (B, blue line) is descanned by the same mirrors that scan the excitation light (A, red line), which then passes through the dichroic mirror and selectively through the pinhole where light not incident from the focal plane is rejected. The light passing through the pinhole is then detected by the PMT, resulting in a sharply resolved image. Fluorophores: AvPB = Avidin Pacific Blue; Alexa 488 = Alexa-fluor 488; Rh Red = Rhodamine Red; Dyl 649 = Dylight 649. AvPB is detected within the ultra-violet visible (UV vis) range. Based on Semwogerere and Weeks, 2005.

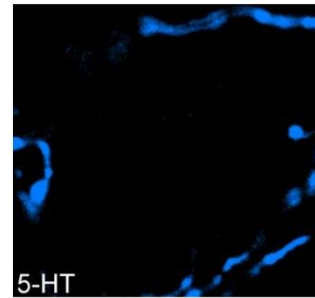
Sequential Immunoreaction



Rhodamine Red, λ 543
Anterograde labelling
of axon terminals

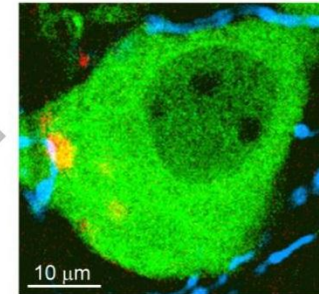


Alexa 488, λ 488
Labels cholinergic
interneuron

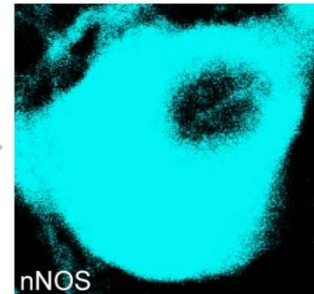


Cy5, λ 637
Labels axon
terminals

merge



re-scanned section containing ChAT cell



Biotin \rightarrow Avidin Pacific Blue
 λ 410 (pseudo-colour cyan)
Labels interneuron
ChAT⁺ / nNOS⁺

primary antibodies		species-specific secondary antibodies + fluorescent particles
mouse anti-CTb	\rightarrow	Rhodamine Red
goat anti-ChAT	\rightarrow	Alexa 488
rat anti-5-HT	\rightarrow	Cy5
rabbit anti-nNOS	\rightarrow	Biotin \rightarrow Avidin Pacific Blue

Figure 2.7 Sequential immunoreaction diagram

The diagram describes the process of triple labelling immunocytochemistry for CTb, ChAT and 5-HT and the sequential labelling of nNOS. The confocal images show how the labelling can be visualised independently in separate colour (red, green, blue) channels and merged to assess the spatial distribution of antigens in a single optical plane. To perform sequential immunocytochemistry with an additional primary antibody, nNOS, the section is re-scanned with the blue diode within the ultra-violet visible (UV vis) range. This additional nNOS labelling is revealed by AvPB, indicating the cell is positive for both ChAT and nNOS. The secondary antibody Cyanine 5 (Cy5) can be used interchangeably with Dyl 649, visualised as blue (see Figure 2.6).

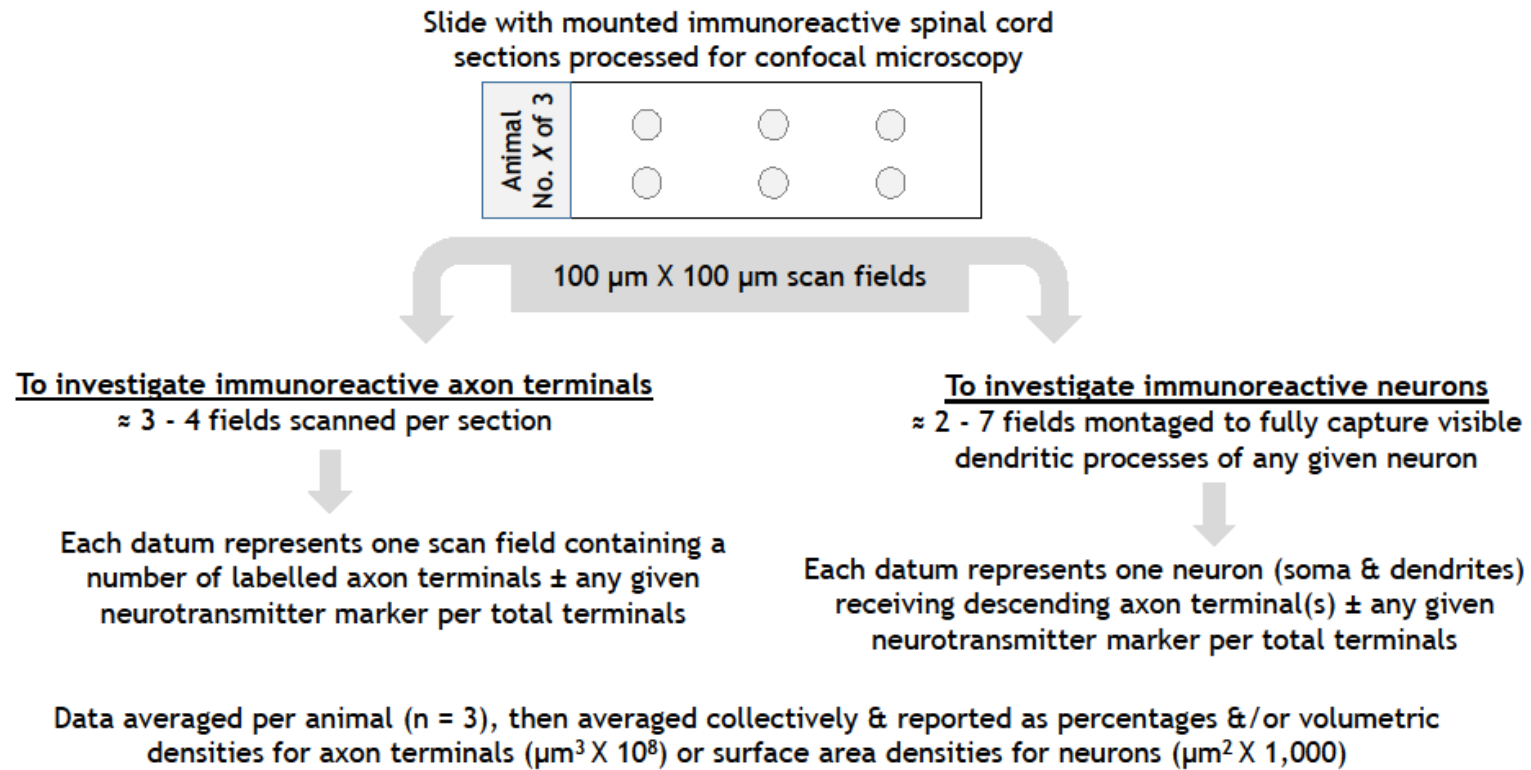


Figure 2.8 Diagram of general image acquisition and data collection methods

2.8 Statistical analyses

Statistically analysed data were presented graphically using GraphPad Prism 4 for Windows (1992-2007). To analyse the neurochemical content of descending axon terminals, datum was the whole number frequency of terminals per total CTb terminals in any given single scanned field expressed in terms of volumetric density (μm^3) at eight orders of magnitude (10^8). To analyse immunoreactive boutons onto neuronal targets, datum was the whole number frequency of contacts onto a given ChAT interneuron expressed in terms of surface density (μm^2) as outlined in Figure 2.8. For scatter plots, datum was jittered and bars graphically represent the mean. Standard error bars are displayed in all bar graphs. For all experiments the level of statistical significance was set at 95% confidence intervals ($p < 0.05$) and standard deviations are reported (\pm SD).

Before applying statistical analyses, data were tested *a priori* for normality using the D'Agostino & Pearson omnibus normality test. A Gaussian (normal) distribution is given by the function:

$$y = ae^{-\frac{(x-b)^2}{2c^2}}$$

Where a, b and c are real constants and $e \approx 2.72$ (Euler's number).

Alternatively, the Shapiro-Wilk *a priori* test for normality could have been chosen, but this test is not as robust when there are 'ties', e.g. the same numbers of labelled axon terminals containing a given transmitter. Normality tests report a p value (95% confidence interval) and the null hypothesis is that each sampled datum is from a normally distributed population. If data are normally distributed, then the question is whether a random sampling of data would deviate from the Gaussian ideal as much as the actual data does. So, if $p < 0.05$ then the data are considered to be not normally distributed and a non-parametric test is thus applied, e.g. Kruskal-Wallis, rather than parametric t-test or analysis of variance (ANOVA) test. Alternatively, to justify using the more powerful parametric tests, data could have been transformed, e.g. logarithmic transformation, but this approach would greatly increase the likelihood of making Type I errors. One-way ANOVA tests were appropriately chosen to compare three or more unmatched groups. In contrast, two-way and

three-way ANOVA tests determine the effect of two and three respective nominal predictor variables and are thus not applicable to the address the following investigations.

Although *a priori* tests are sufficient to determine whether data are normally distributed, some experimental data are displayed graphically. The premise is that the normal probability plots compares the sampled data with what is expected of normally distributed data. If the data is normal, then the probability plot assumes a pattern of linearity, $y = mx + b$ (where y and x are real constants, m is the slope and b is the y -intercept), when columnar data is numerically ordered (Figure 2.9).

Post hoc test for a linear trend to determine whether groups increase or decrease systemically or randomly. Dunn's multiple comparison *post hoc* tests accompany nonparametric tests to compare differences in the sum of ranks with significance reported as p values. Tukey's *post hoc* tests accompany parametric tests to compares every mean with every other mean.

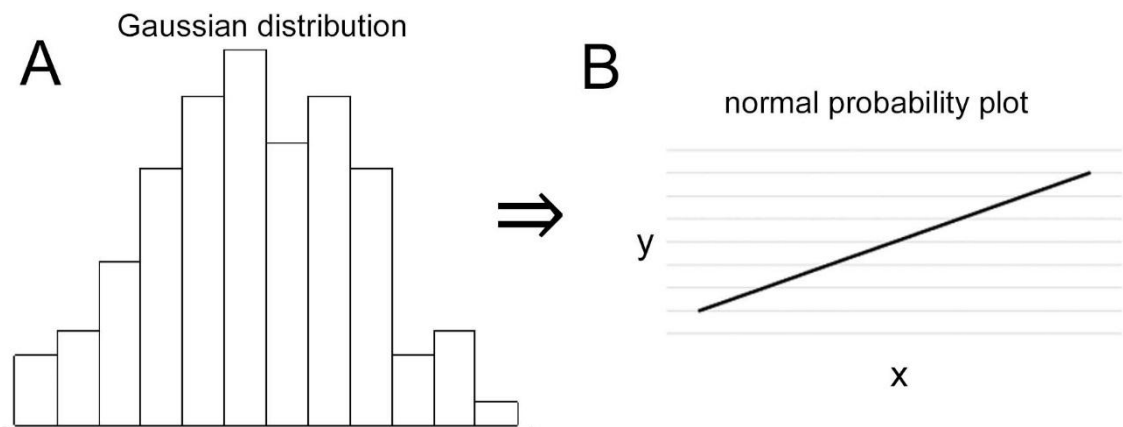


Figure 2.9 Normal probability plot

The data from an imaginary population assuming a Gaussian distribution (A) was numerically ordered (smallest to largest) and the resulting normal probability plot was linear ($y = mx + b$) with the line of best fit shown (B). For experimental data sets, *a priori* D'Agostino & Pearson omnibus normality tests determined whether data were parametric or not so that the appropriate statistical tests were chosen. To visualise *a priori* analyses, data were plotted graphically.

Chapter 3. Neurotransmitter phenotypes of medullary axonal projections within lower lumbar spinal segments

3.1 Introduction

Many descending systems are known to excite spinal neurons yet the neurotransmitter phenotypes used by these systems still are largely unknown. Although the RetS pathways are phylogenetically amongst the oldest of the descending pathways, their role in limb movement remain elusive (see Jankowska and Edgley, 2006). The independent activities of postural control and movement indicate descending pathways use separate yet closely interacting regulatory signals (Schepens and Drew, 2003) and the RetST is likely to serve a fundamental role in integrating such activities (Jankowska and Edgley, 2006). There are several components to the RetST; from Latin, “reticulated” means intricately web-like. Located in the tegmentum of the brainstem from the mesencephalon through the myelencephalon, the reticular formation represents a smooth functional transition between descending and ascending sensorimotor systems.

This study focuses on the neurotransmitter content of axon terminals descending from the MLF and CVLM. Electrophysiological studies have demonstrated that stimulation of the MLF activates many reticulospinal fibres which produce profound effects on networks involved in motor control (Edgley et al., 2004, Jankowska et al., 2003). Pharmacological, lesion and electrophysiological studies in the rat have established that the CVLM participates in many vital autonomic functions such as baroreceptive, vestibulosympathetic and somatosympathetic reflexes (Agarwal et al., 1990, Aicher et al., 1995, Jeske et al., 1993).

The systems descending from the reticular formation have been reported as having heterogeneous transmitter content. Many systems descending from the medulla are serotonergic (Bowker et al., 1981b) and diverse neurochemicals originating from the medullary raphé such as 5-HT can elicit rhythmic motor activities (Alford et al., 2003, Jordan and Schmidt, 2002a, Rossignol et al., 2002). Axons descending from the medulla may also contain other co-transmitters such as amino acids and peptides (Bowker and Abbott, 1990, Maxwell et al., 1996). There is evidence in the rat (Vetrivelan et al., 2009) and mouse (Martin et al., 2011) that spinally projecting neurons surrounding the MLF region contain VGLUT2 mRNA which is consistent with electrophysiological

evidence in cats that many medullary axons send strong excitatory signals to spinal neurons (see Achermann and Borbely, 1994, Edgley et al., 2004, Hammar et al., 2011, Jankowska et al., 2003, Wilson and Yoshida, 1969) while other medullary axons are glycinergic (Holstege and Bongers, 1991) and GABAergic (Antal et al., 1996, Holstege, 1991). There is further evidence that these inhibitory transmitters may be co-localised within the same neurons (Hossaini et al., 2012).

It is hypothesised that axons descending from the reticular formation project differentially to lower lumbar spinal cord segments and express a combination of transmitters. Because the MLF and CVLM are anatomically and functionally distinct systems, then it is hypothesised that they express different transmitters in different ratios. If these axon terminations express inhibitory transmitters, then evidence of co-localisation is expected. Descending medullary axons are hypothesised to express 5-HT. In order to investigate the neurotransmitter phenotypes of anterogradely labelled medullary axons projecting to lower lumbar segments of the spinal cord, a series of immunoreactions were conducted with subsequent analyses. The experiments addressed the following aims:

To determine the distribution of medullary axons projecting to lower lumbar spinal cord segments

To determine the neurotransmitter phenotypes of axon terminals descending from the MLF and CVLM within lower lumbar spinal cord segments

To determine the neurotransmitter phenotypes of inhibitory axon terminals from the MLF and the CVLM within lower lumbar spinal cord segments

To determine if medullary axons projecting to lower lumbar spinal cord segments contain serotonin

3.2 Methods

3.2.1 Image acquisition

For the following series of experiments, brain injection sites from a total of ten rats were visualised using DAB as a chromogen were reconstructed (Appendix 1 Figures 1 and 2). For each series of experiments (Table 3.1), images were captured from a minimum of six transverse sections per animal. Immunoreactive sections were scanned by using a 40x oil immersion lens with a zoom factor of 2 and z-separation of 0.5 μm . For each section at least three fields with a 100 μm X 100 μm scanning area were obtained from different regions of the grey matter. Using Neurolucida, a 10 x10 μm grid was superimposed over the image stacks. To avoid bias, stacks were visualised in the red channel first such that only CTb immunoreactivity was shown. Approximately one terminal per grid cell was counted (depending upon the given section) and then each counted terminal was evaluated again separately in the green and blue channels to count the other marker(s). Terminals were counted as positive only if fully filled with a given marker in the same focal plane. To accurately determine the laminar location of terminals, semi-opaque standard templates of transverse spinal cord segments (based on Molander et al. 1984) were overlaid onto scanned images as necessary. Scale bar lengths are denoted on all images. Datum was the average number of immunoreactive axon terminals containing a given neurotransmitter per total labelled terminals in any given scan field (see Figure 2.8).

3.2.2 Derivation of laminar volume

First the surface areas of each scaled bilateral laminar region for L3, L4 and L5 transverse sections was found as indicated in the conceptual model where I deconstructed laminar regions. Each spinal cord lamina is as if an area under a curve confined by dorsal and ventral boundaries, which can be theoretically conceptualised as an integral function. Cubic volumes were based on 60 μm thick sections (Figure 3.1) since sections processed for ICC were uniformly cut at 60 μm for maximum antibody penetration (see Chapter 2). Transverse templates were filled with hexagonal grids and hexagons were manually counted and summed (Figure 3.2). Hexagons straddling laminar borders were counted as

'halves' and summed accordingly. Hexagons were chosen rather than square grids because they stack optimally in curved spaces, e.g. carbon molecules, snowflakes, honeycombs: since hexagons have 120 degree angles, three can come together in corners for a total of 360 degrees (see Kepler, 1596). Datum was expressed in terms of cubic density (μm^3) at eight orders of magnitude (10^8).

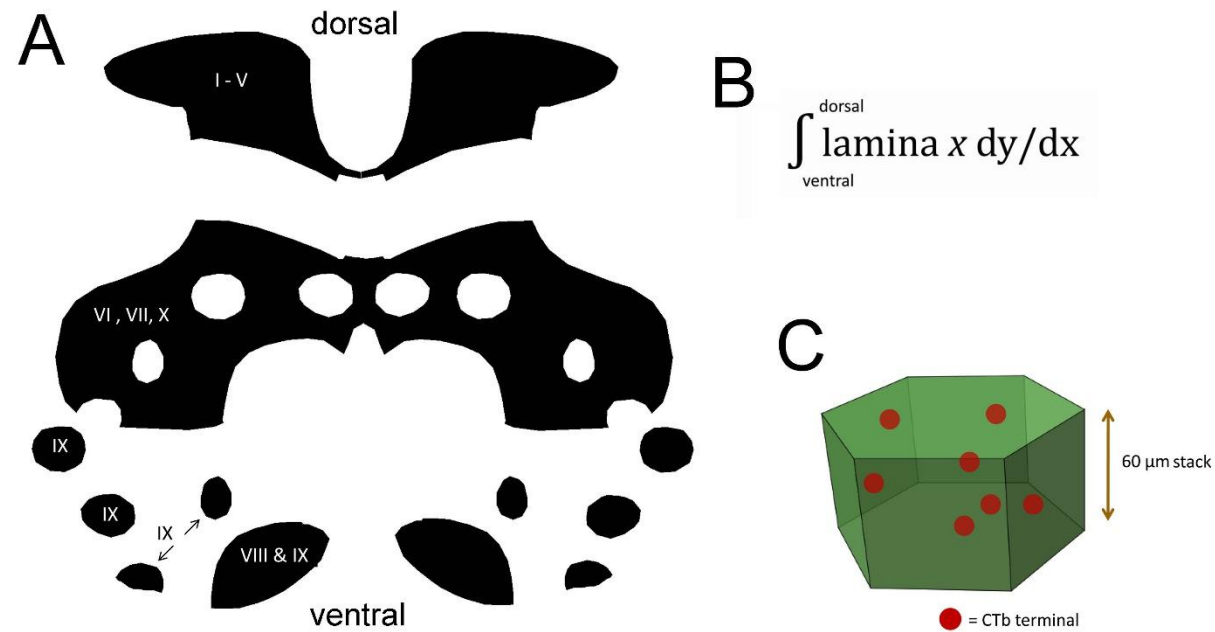
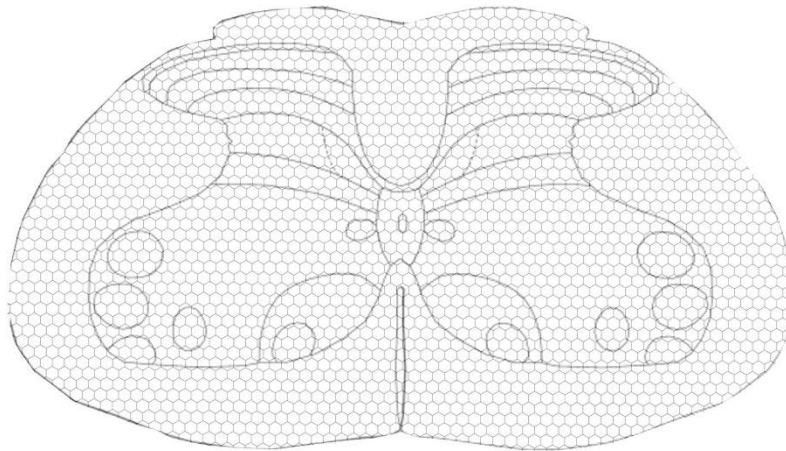


Figure 3.1. Conceptual model of bilateral laminar regions containing CTb terminals

Bilateral laminar regions of a representative L4 section (based on Molander et al., 1984) were deconstructed. For L4 segments, lamina IX regions are fully embedded within lamina VII, shown subtracted from the intermediate region (A). Any given laminar area can be conceptualised as an area within a curved space confined by dorsal and ventral laminar boundaries, as an integral (B). Labelled CTb terminals exist within three dimensional laminar volume of space, as shown in the hexagonal prism, uniformly cut at a thickness of 60 µm (C).



$$\begin{aligned} \text{volume of hexagon} \\ &= \frac{3\sqrt{3}}{2} \text{ area}^2 * 60 \mu\text{m} \end{aligned}$$

Figure 3.2. Derivation of laminar volume using hexagons

A transverse L4 section template is shown as an example (based on Molander et al., 1984). Scaled templates were filled with hexagonal grids. Hexagons were counted and summed to find the volume of L3, L4 and L5 rat spinal cord segments.

3.2.3 Statistical Analysis

Nonparametric tests necessitate that the sampled data does not assume a Gaussian (normal) distribution and data were checked *a priori* for normality. Although the Gaussian assumption accounts for the distribution of the overall population, rather than just the sampled data, the *a priori* assessed the scatter of the distribution from the following experiments. The Kruskal-Wallis test compared the medians of sampled data with Dunn's multiple comparisons test *post hoc* to test the neurotransmitter content of axons across laminar regions.

Aim	Primary antibody combinations	Concentrations	Supplier	Secondary antibodies	Concentrations	Sequential immunoreaction	Sequential secondary antibody
1	gt. CTb	1:50,000	List Biological Laboratories, Campbell CA USA	Biotinylated IgG	1:500	Avidin HRP (1:1,000)	DAB
	mo. CTb	1:250	A. Wilkström, University of Gothenburg	Rh Red	1:100		
2	g. pig VGLUT1	1:1,000	Millipore, Harlow UK	Dyl 649	1:500		
	g. pig VGLUT2	1:5,000	Millipore, Harlow UK	Dyl 649	1:500		
	rbt. VGAT	1:1,000	Synaptic Systems, Göttingen Germany	Alexa 488	1:500		
3	gt. CTb	1:50,000	List Biological Laboratories, Campbell CA USA	Rh Red	1:500		
	rbt. GlyT2	1:1,000	Millipore, Harlow UK	Alexa 488	1:500		
	mo. GAD67	1:1,000	Millipore, Harlow UK	Dyl 649	1:500		
4	mo. CTb	1:250	A. Wilkström, University of Gothenburg	Rh Red	1:100		
	g. pig VGLUT1	1:1,000	Millipore, Harlow UK	Dyl 649	1:500		
	g. pig VGLUT2	1:5,000	Millipore, Harlow UK	Dyl 649	1:500		
	rbt. VGAT	1:1,000	Synaptic Systems, Göttingen Germany	Dyl 649	1:500		
	rbt. 5-HT	1:250	Affiniti, Exeter UK	Alexa 488	1:500		

Antibodies diluted in 0.3% PBST

gt. = goat; mo. = mouse; g. pig = guinea pig; rbt. = rabbit

Table 3.1. Summary of primary and secondary antibody combination and concentrations

DAB was used as a substrate to visualise CTb staining. All secondary antibodies were raised in donkey and conjugated to Rh Red, Dyl 649 (supplied by Jackson ImmunoResearch, West Grove, USA) or Alexa 488 (supplied by Molecular Probes, Eugene, USA). Avidin HRP and DAB supplied by Sigma-Aldrich, Dorset, UK. Antibody labelling: CTb, traces myelinated axons; VGLUT1 and VGLUT2, synaptic vesicles; vesicular GABA transporter (VGAT), glycinergic and GABAergic synaptic vesicles; glycine transporter 2 (GlyT2), plasma membrane; glutamic acid decarboxylase 67 (GAD67), synaptic vesicles recognising GAD isoform with molecular weight 67 Kd; 5-HT, synaptic terminals.

3.3 Results

3.3.1 Aim 1: To determine the distribution of medullary axons projecting to lower lumbar spinal cord segments.

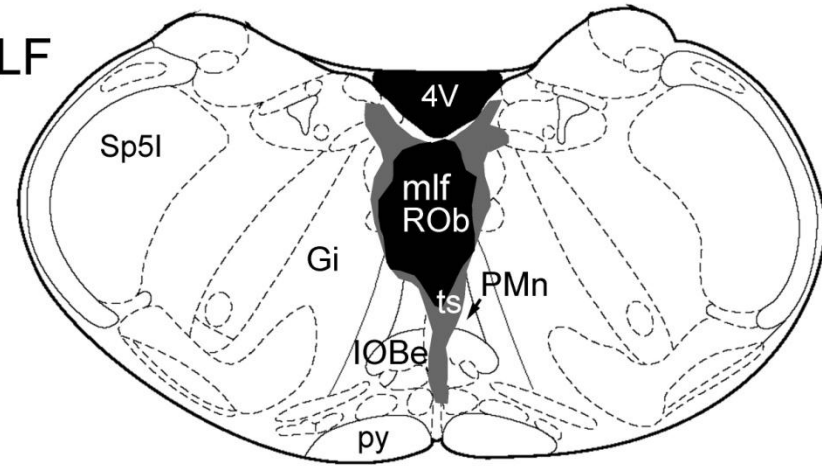
3.3.1.1 MLF and CVLM axon labelling within lumbar segments

CTb was injected into the MLF, slightly to the left of the midline (Table 2.1) to label descending axons anterogradely. The CTb tracer diffused into the raphé obscuris, paramedian reticular nucleus and tectospinal tract. A considerable number of terminals were found on both sides of the spinal cord and were distributed in the intermediate grey matter and ventral horn including motor nuclei. CTb was injected into the CVLM to label axons (Table 2.1) and the tracer also diffused into the ambiguous nucleus and solitary tract. Reconstructed brain injection sites are shown in Figure 3.3. Terminals from the CVLM were principally found ipsilateral to the injection site and were distributed in the intermediate grey matter and ventral horn including motor nuclei. For both systems, a few terminals were found in the white matter. Axons projecting from these descending systems are shown in Figures 3.4 and 3.5. These systems were found to project differently to spinal laminae as hypothesised.

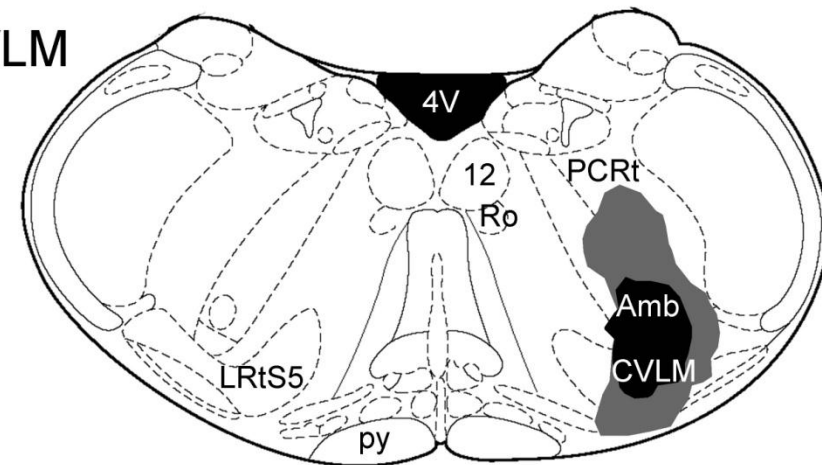
The mathematically derived volumes of grey and white matter laminar regions for L3, L4 and L5 sections were expressed in scientific notation. Most laminae were found to be six orders of magnitude in volume. Lamina VII volumes were an order of magnitude greater except in the L5 segment and lamina X had the smallest volume at 5 orders of magnitude. The L4 segment at the hindlimb enlargement has the greatest total volume and L5 the least (Table 3.2).



MLF



CVLM



1000 μ m

Figure 3.3. Brain reconstructions for MLF and CVLM injection sites

Exemplary reconstructions of the CTb injection sites labelling the MLF and CVLM. The inner black shaded areas represent the core of the injection site and the grey shaded areas represent the maximum diffusion of CTb within the brain. 100 µm thick coronal sections reacted with DAB to reveal the tracer are shown on the left with corresponding drawings on the right. Template drawings are from Paxinos and Watson (1997). For the MLF injection site, the CTb tracer labelled the MLF (medial longitudinal fasciculus), ROb (raphé obscurus nucleus) and ts (tectospinal tract) with other anatomical sites included for contextual reference, including the 4V (4th ventricle), Gi (granular insular cortex), IOBe (inferior olive beta subnucleus), PMn (paramedian reticular nucleus), py (pyramidal tract) and Sp5I (spinal trigeminal nucleus, interpolar part). For the CVLM injection site, the CTb tracer labelled the CVLM (caudal ventral lateral medulla), Amb (ambiguus nucleus) with diffusion into the LRtS5 (lateral reticular nucleus, subtrigeminal part) with other anatomical sites included for contextual reference, including 12 (cerebellar lobule 12), PCRt (parvicellular reticular nucleus) and Ro (raphé obscurus). Brain reconstructions from all experiments are shown in Appendix 1 Figures 2 and 3.

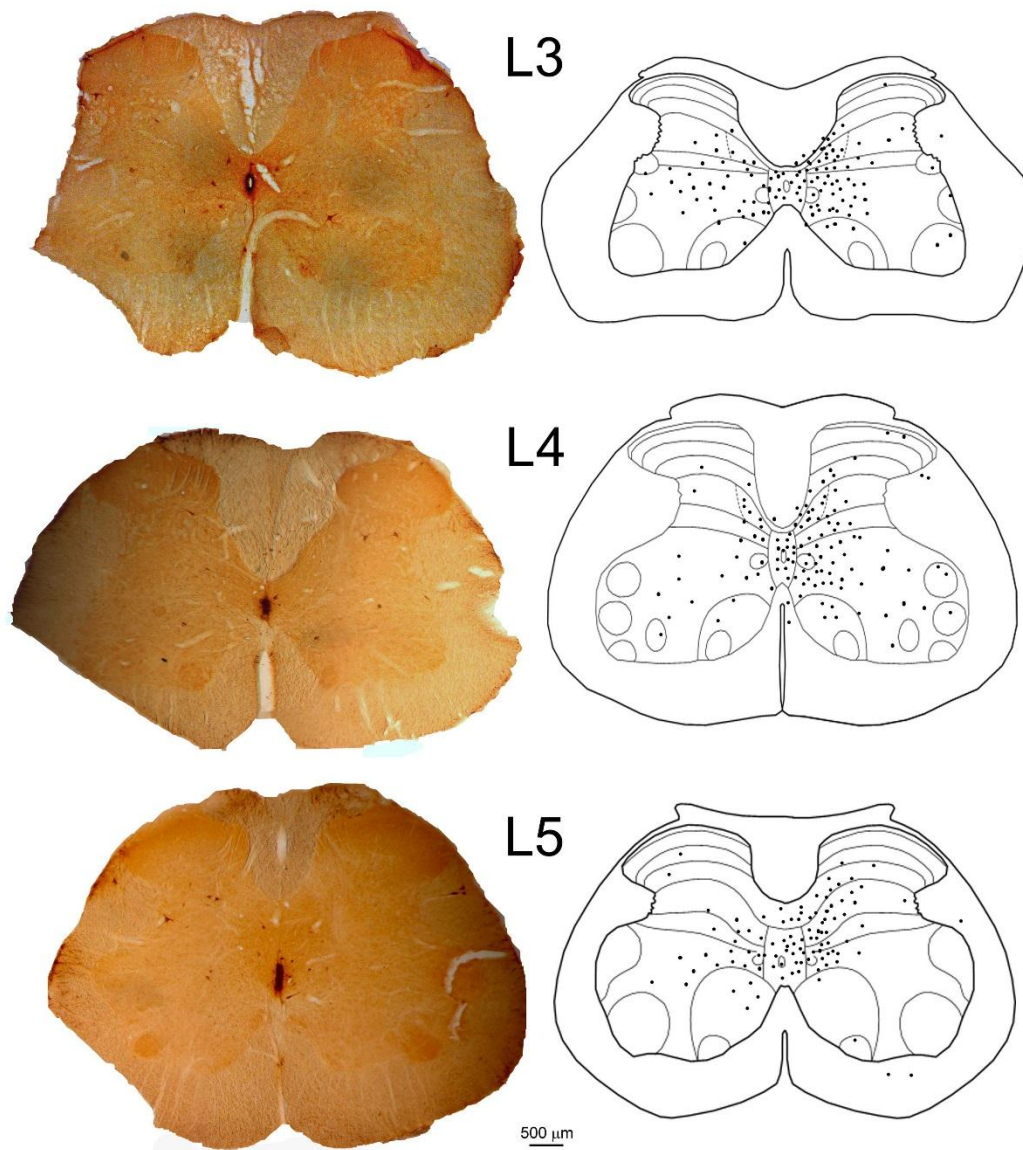


Figure 3.4. Distribution of labelled terminals from the MLF

Labelled terminals in the lumbar cord were revealed with DAB shown on the left. The notch is contralateral relative to the injection site. The drawings on the right show the distribution of terminals superimposed onto standard L3, L4 and L5 transverse sections (based on Molander et al., 1984). Terminals were plotted from 60 µm thick sections.

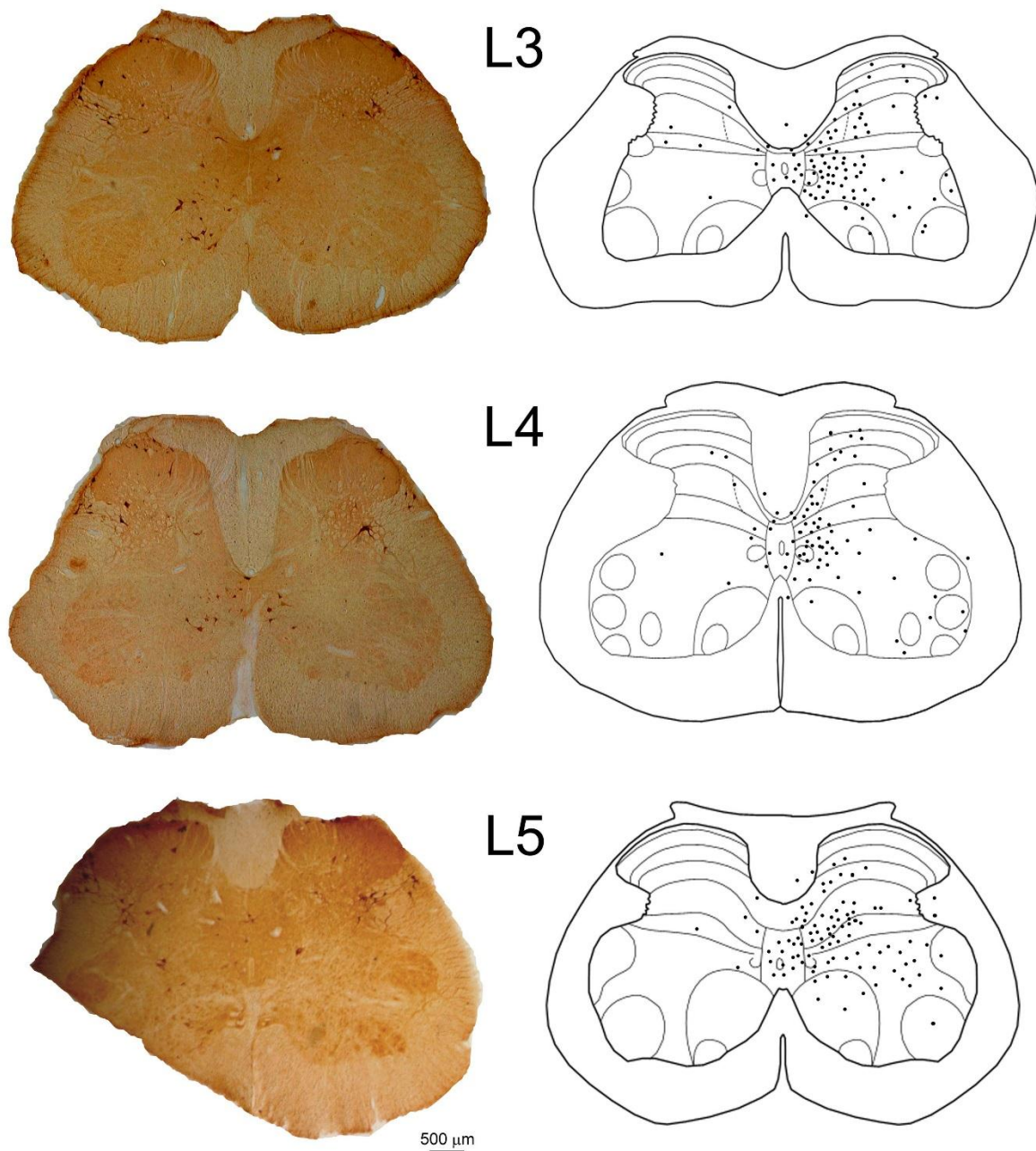


Figure 3.5. Distribution of labelled terminals from the CVLM

Labelled terminals in the lumbar cord were revealed with DAB shown on the left. The notch is contralateral relative to the injection site. The drawings on the right show the distribution of terminals superimposed onto standard L3, L4 and L5 transverse sections (based on Molander et al., 1984). Terminals were plotted from 60 μm thick sections.

	L3	L4	L5
laminae	volume, μm^3	volume, μm^3	volume, μm^3
I & II	2.027×10^6	3.424×10^6	2.703×10^6
III	1.532×10^6	2.612×10^6	1.757×10^6
IV	2.433×10^6	2.973×10^6	3.018×10^6
V	4.325×10^6	3.513×10^6	3.919×10^6
dorsal sum	1.032×10^7	1.252×10^7	1.140×10^7
VI	2.027×10^6	2.612×10^6	2.027×10^6
VII	1.361×10^7	2.144×10^7	9.100×10^6
X	9.461×10^5	9.911×10^5	1.306×10^6
intermediate sum	1.658×10^7	2.505×10^7	1.243×10^7
VIII	2.613×10^6	3.694×10^6	5.181×10^6
IX	4.775×10^6	4.730×10^6	5.316×10^6
ventral sum	7.338×10^6	8.424×10^6	1.050×10^7
white matter	4.055×10^7	4.735×10^7	2.424×10^7
grey matter	3.428×10^7	4.600×10^7	3.433×10^7
total sum	7.483×10^7	9.334×10^7	5.857×10^7

Table 3.2. Laminar volumes for L3, L4 and L5 lumbar spinal segments

Laminar volumes for L3, L4 and L5 lumbar segmental sections cut at 60 μm thickness were derived and reported as dorsal, intermediate and ventral grey matter laminar regions expressed in terms of scientific notation. The total volume of the grey matter and the white matter are reported for each segment. The superficial dorsal horn's narrow laminae I and II densities were combined. The L4 segment has the greatest volume, corresponding to the hindlimb enlargement, and the L5 segment has the least volume as it tapers caudally towards the sacral segments.

3.3.2 Aim 2: To determine the neurotransmitter phenotypes of axon terminals descending from the MLF and CVLM within lower lumbar spinal cord segments

To investigate the neurochemical properties of glutamatergic terminals descending from the MLF and CVLM, sections were reacted with a combination of antibodies against CTb, VGLUT1 and VGLUT2 (Table 3.1). A total of 361 axon terminals from the MLF ($n = 3$) and 2881 axon terminals from the CVLM ($n = 3$) within the grey matter were analysed. From the MLF population, terminals containing VGLUT2 had an average density of 4.72 per $\mu\text{m}^3 \cdot 10^8$ (± 1.62) with negligible expression of VGLUT1. From the CVLM population, terminals containing VGLUT2 had an average volumetric density of 3.93 per $\mu\text{m}^3 \cdot 10^8$ (± 0.11) while terminals containing VGLUT1 had a nearly negligible density of 0.02 per $\mu\text{m}^3 \cdot 10^8$ (± 0.01) (Appendix 3 Table 1).

To investigate excitatory and inhibitory MLF and CVLM axons, sections were reacted with a combination of antibodies against CTb, VGAT and a mixture of VGLUT1 and VGLUT2 raised in the same species (g. pig) such that these two VGLUT antibodies reacted with the same secondary antibody (Table 3.1). Throughout this present investigation, this antibody mixture will be denoted as [VGLUT1 + VGLUT2]. A total of 745 axon terminals from the MLF ($n = 3$) and 1,619 axon terminals from the CVLM ($n = 3$) within the grey matter were sampled. From the MLF population, terminals containing [VGLUT1 + VGLUT2] had an average density of 5.38 per $\mu\text{m}^3 \cdot 10^8$ (± 0.75) and terminals containing VGAT had an average density of 1.90 per $\mu\text{m}^3 \cdot 10^8$ (± 0.57). From the CVLM population, terminals containing [VGLUT1 + VGLUT2] had an average density of 5.34 per $\mu\text{m}^3 \cdot 10^8$ (± 0.63) and terminals containing VGAT had an average density of 1.96 per $\mu\text{m}^3 \cdot 10^8$ (± 0.36) (Appendix 3 Table 2). Immunofluorescent confocal microscope images from these reactions are shown Figures 3.6 and 3.7.

The *a priori* D'Agostino & Pearson omnibus normality test indicated that the data did not assume a normal distribution and the distribution is shown as a histogram plot. Consequently, nonparametric tests were consequently applied (Figure 3.8). As hypothesised, descending MLF and CVLM axons express a heterogeneous

combination of neurotransmitters, however the neurochemical content of axons descending from these two distinct medullary anatomical sites were found to not significantly differ (Figure 3.9).

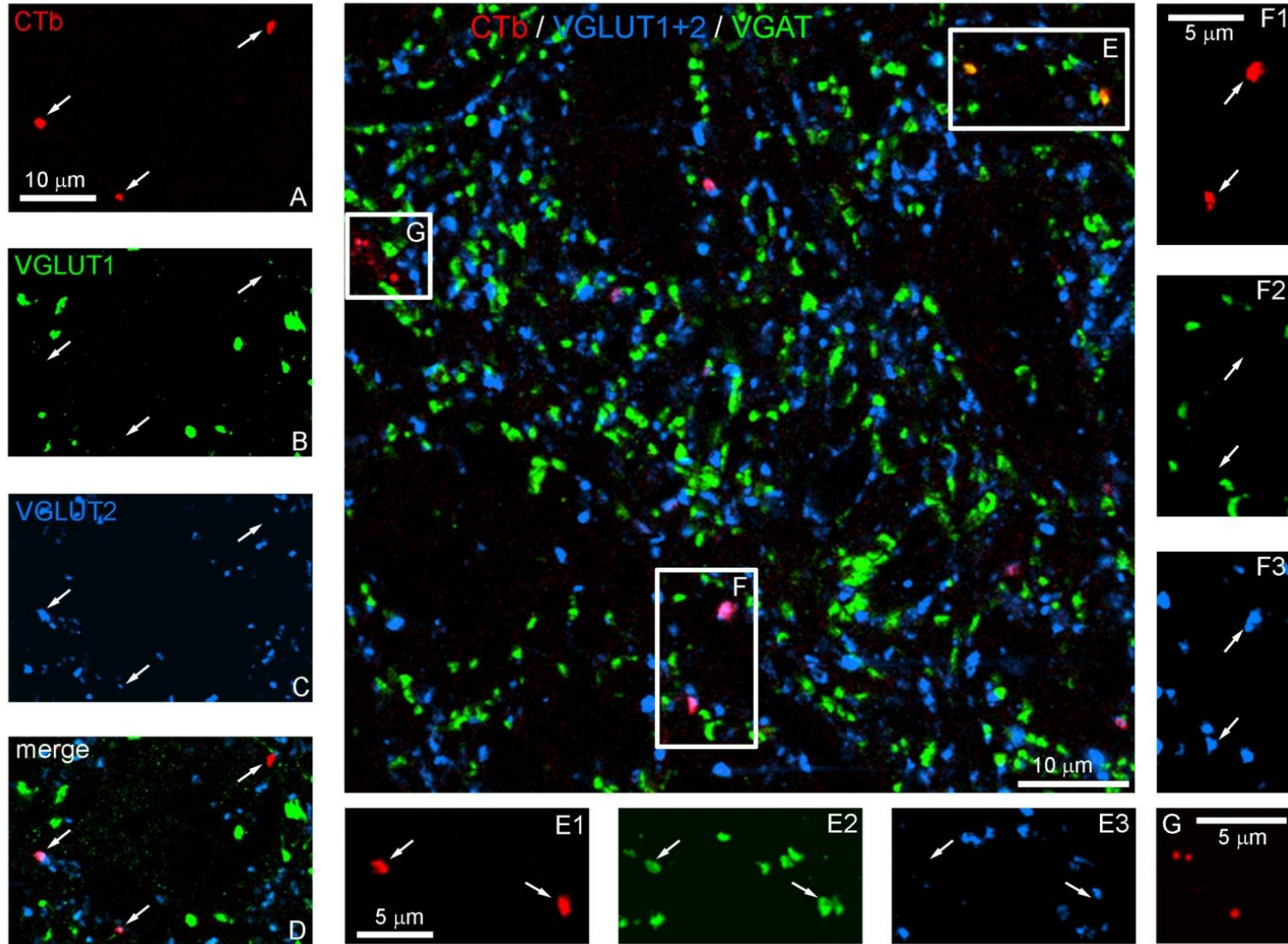


Figure 3.6. Immunocytochemistry of MLF terminals

In single optical planes, immunoreactive CTb terminals (A) were negative for VGLUT1 (B) and positive for VGLUT2 (C) as shown in magenta in the merged image (D). Inset box E shows CTb terminals (E1) positive for VGAT (E2) and negative for [VGLUT1+VGLUT2]. Inset box F shows CTb terminals (F1) negative for VGAT (F2) and positive for [VGLUT1+VGLUT2] (F3). Inset box G shows CTb terminals negative for both markers.

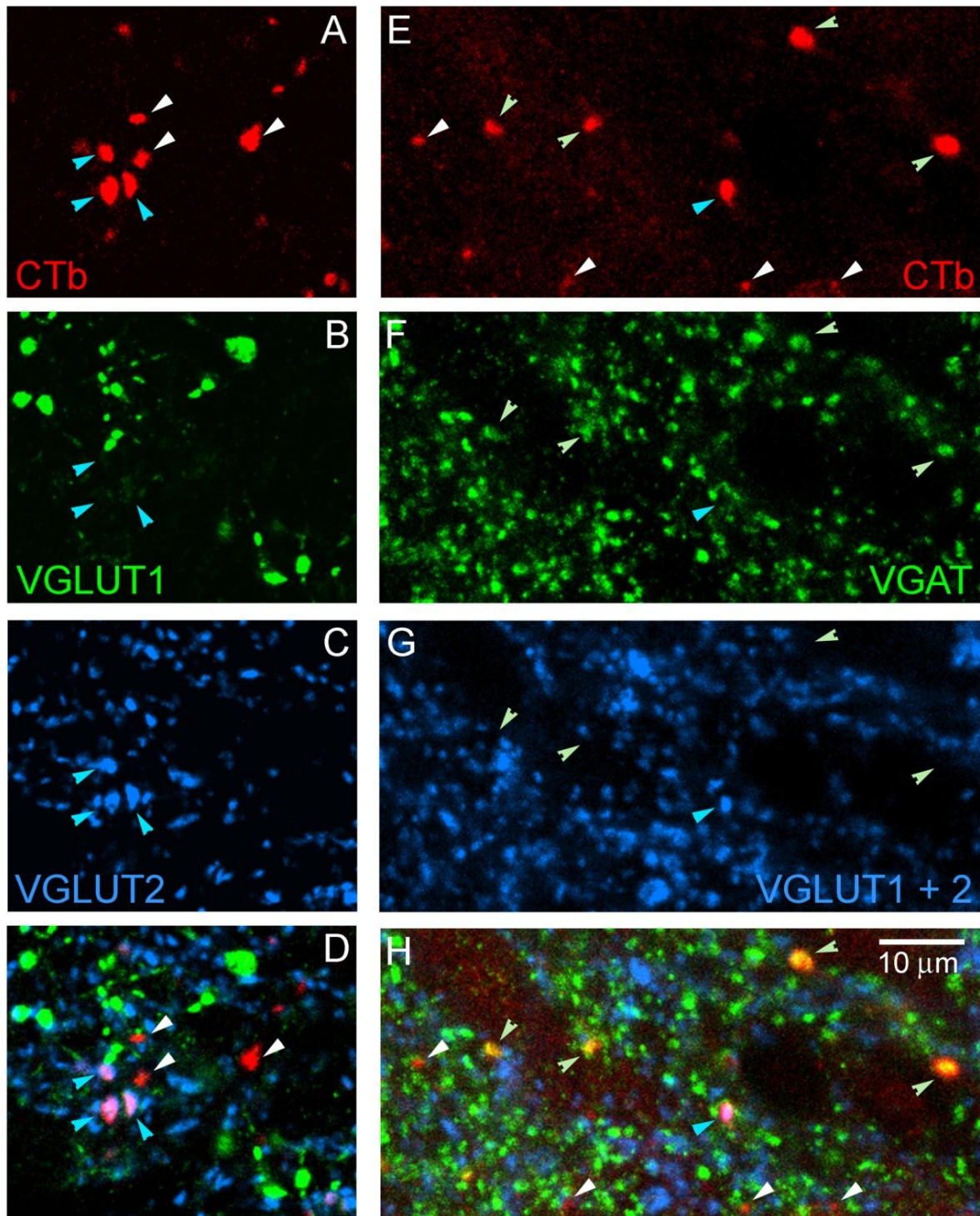


Figure 3.7. Immunocytochemistry of CVLM terminals

In single optical planes, immunoreactive CTb terminals (A) are negative for VGLUT1 (B) and positive for VGLUT2 denoted by blue pointers (C) as shown in the merged image (D). CTb terminals (E) are positive for VGAT denoted by green pointers (F) and positive for [VGLUT1+VGLUT2] denoted by blue pointers (G) as shown in the merged image (H). For all panels, negative CTb terminals are denoted by white pointers.

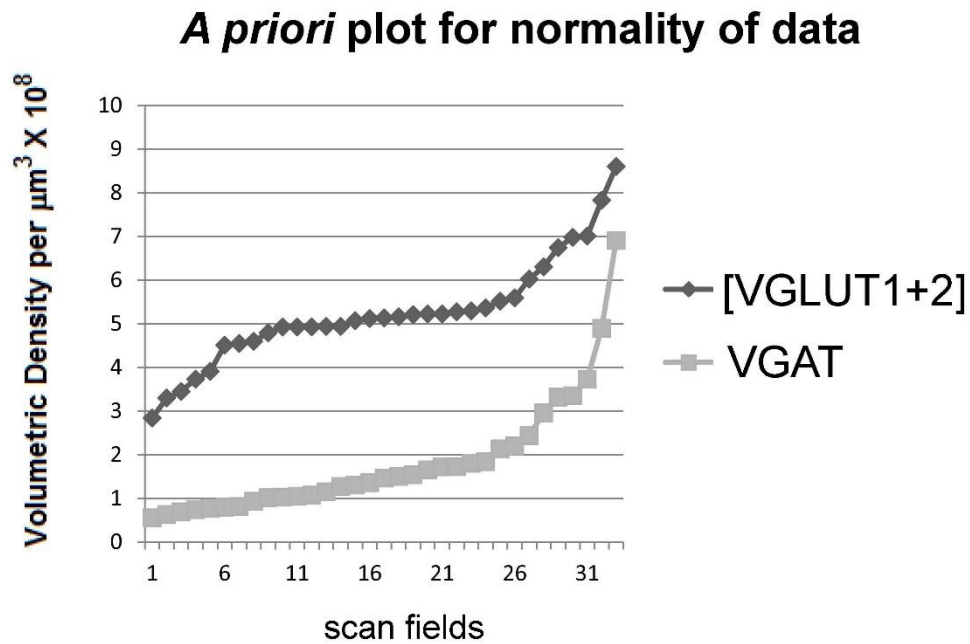


Figure 3.8. Example of an *a priori* histogram plot

This histogram shows that the data does not assume a Gaussian distribution as confirmed by the *a priori* D'Agostino & Pearson omnibus normality test. Therefore nonparametric tests were applied to analyse data from experiments. For normally distributed data, the distribution would be linear ($y = mx + b$). Normality was tested for all experimental data and this example shows the distribution of the volumetric densities of axon terminals within a $100 \mu\text{m} \times 100 \mu\text{m}$ scan field immunoreactive to VGLUT2 ($n = \text{three animals}$) and VGAT ($n = \text{three animals}$).

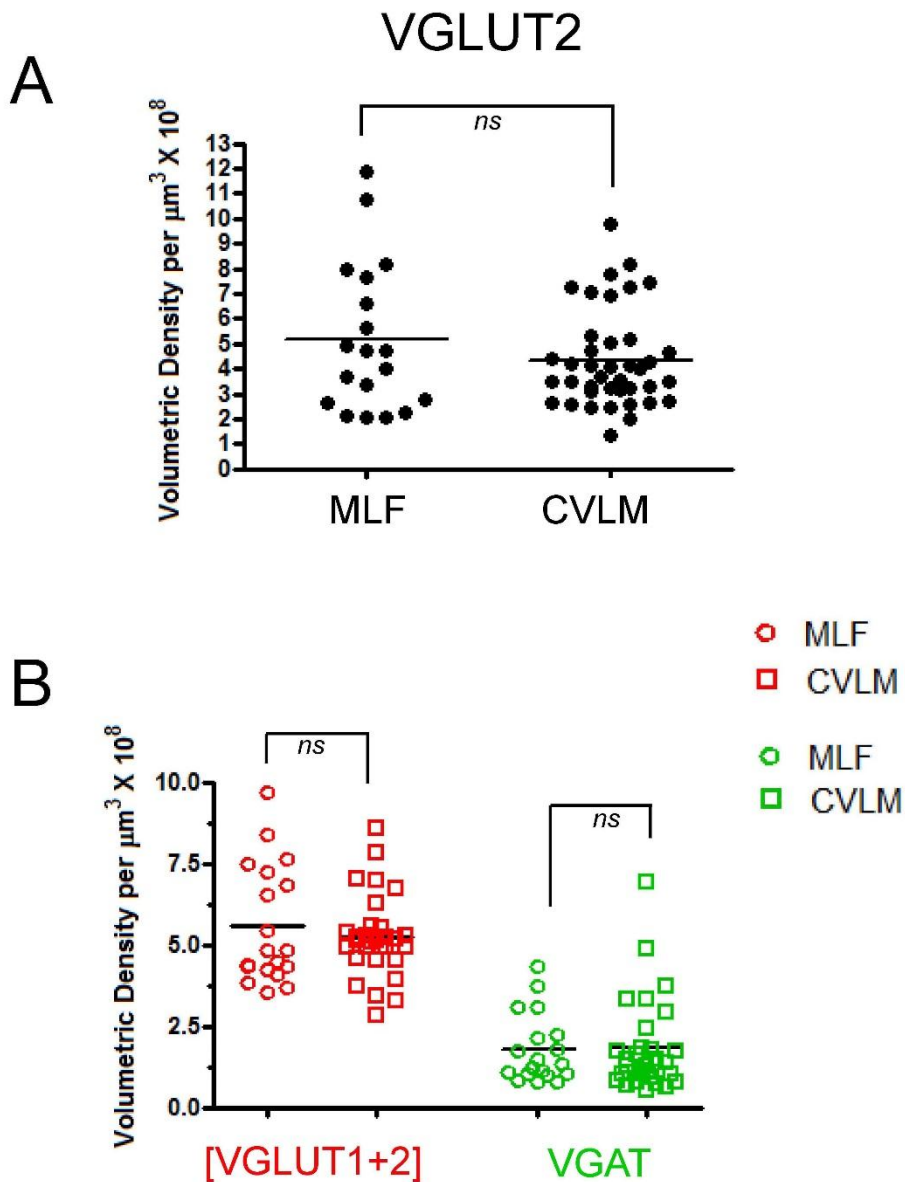


Figure 3.9. Volumetric density comparison of MLF and CVLM terminal transmitter content

Kruskal-Wallis tests compared the median densities of glutamatergic axons (A) in all examined laminae; the populations did not differ. The median density of excitatory and inhibitory axons (B) did not differ ($p > 0.05$). Each datum represents one $100 \mu\text{m} \times 100 \mu\text{m}$ scan field containing an averaged number of labelled axon terminals containing the given transmitter per total terminals. Scatter plot bars represent the mean. $N = 3$ animals. (A) MLF, 361 terminals examined; CVLM, 2881 terminals examined (B) MLF, 745 terminals examined; CVLM, 1619 terminals examined.

3.3.2.1 Laminar density comparison of excitatory and inhibitory axon terminals projecting from the MLF and CVLM

The grey matter density of medullary axons was found to be lesser in intermediate laminae VI, VII and X for both VGLUT2 and VGAT as compared to the laminae examined more dorsally. The transmitter ratio of axonal populations was most evident in the ventral horn with excitatory densities greater for MLF axons and inhibitory densities greater for CVLM axons. In dorsal laminae I-V, CVLM axons exhibited the greatest densities of both transmitters. These anatomically distinct axonal populations were not significantly different in terms of their transmitter density across laminar boundaries (Figure 3.10).

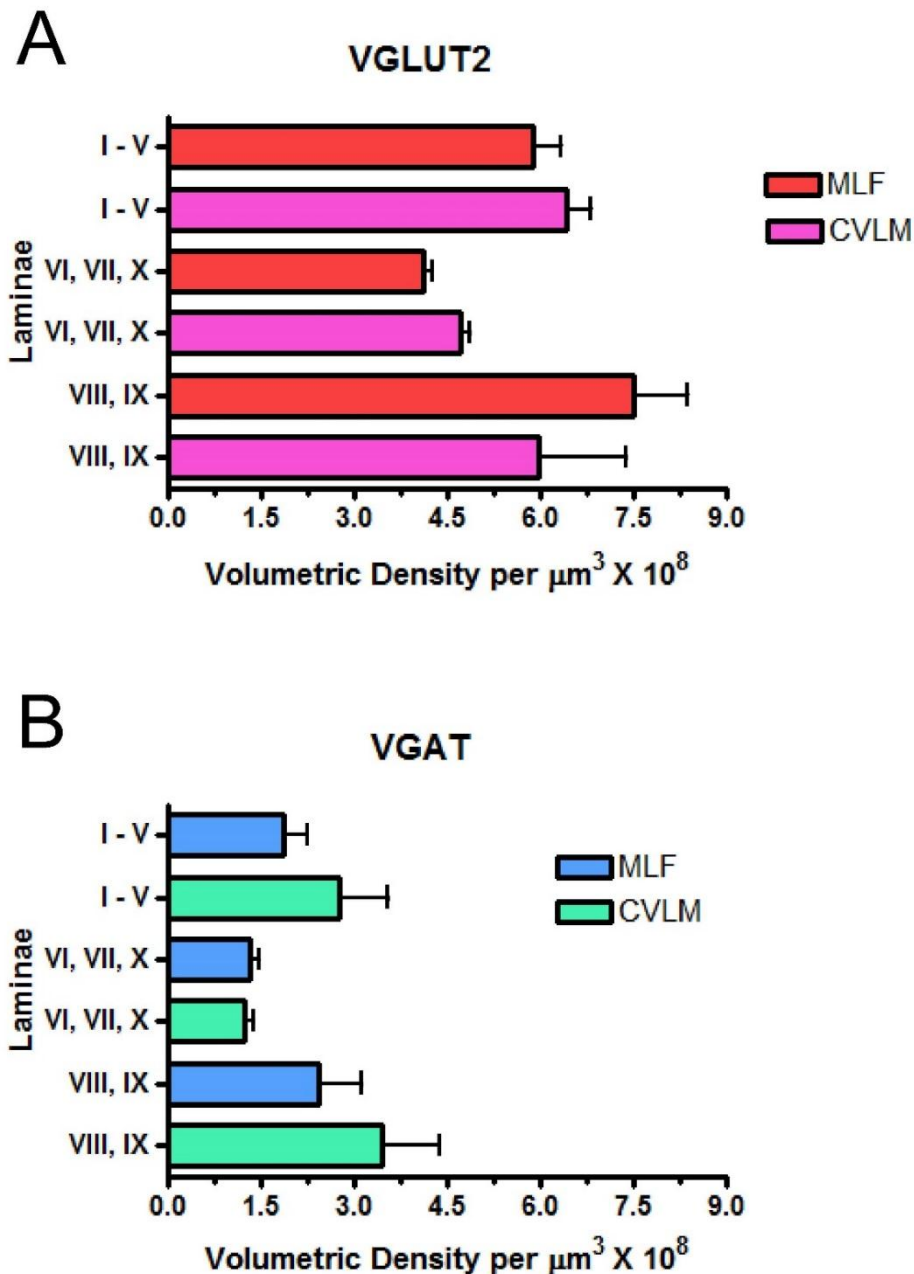


Figure 3.10. Laminar densities of excitatory and inhibitory medullary axon terminals

Kruskal-Wallis tests compared the median densities of axonal populations containing VGLUT2 (A) and VGAT (B) across laminar boundaries ($p > 0.05$). MLF and CVLM populations containing VGLUT2 and VGAT did not differ significantly. Medullary axons were predominantly excitatory (A) with lesser expression of inhibitory amino acids (B). Each coloured bar represents 100 $\mu\text{m} \times 100 \mu\text{m}$ scan fields containing an averaged number of labelled axon terminals containing the given transmitter per total terminals within the indicated laminar region. Standard error bars shown. $N = 3$ animals. (A) MLF, 361 terminals examined; CVLM, 2881 terminals examined (B) MLF, 745 terminals examined; CVLM, 1619 terminals examined.

3.3.3 Aim 3: To determine the neurotransmitter phenotypes of inhibitory axon terminals from the MLF and the CVLM within lower lumbar spinal cord segments

Sections were reacted with a combination of antibodies against CTb, GlyT2 and GAD67 (Table 3.1). From the MLF population, a total of 2,421 immunoreactive axon terminals were analysed ($n = 3$) and 3,923 terminals ($n = 3$) from the CVLM population. From the MLF population, terminals containing GlyT2 had an average density of 2.17 per $\mu\text{m}^3 \cdot 10^8$ (± 0.85) and 3.30 per $\mu\text{m}^3 \cdot 10^8$ (± 0.55) from the CVLM population. From the MLF population, terminals containing GAD67 had an average density of 2.96 per $\mu\text{m}^3 \cdot 10^8$ (± 2.34) and 2.07 per $\mu\text{m}^3 \cdot 10^8$ (± 0.32) from the CVLM population. A few CTb terminals were found to be double labelled for both GlyT2 and GAD67. Double labelled MLF axons had an average density of 0.51 per $\mu\text{m}^3 \cdot 10^8$ (± 0.34) and double labelled CVLM axons had an average density of 0.68 per $\mu\text{m}^3 \cdot 10^8$ (± 0.06) (Appendix 3 Table 3). Immunofluorescent confocal microscope images from these reactions are shown in Figure 3.11. The volumetric densities of these populations did not differ significantly (Figures 3.12). As hypothesised, MLF and CVLM axons do express inhibitory transmitters and although there is evidence of co-localisation, this expression is comparatively limited.

CTb / GlyT2 / GAD67

MLF = A - D

CVLM = E - H

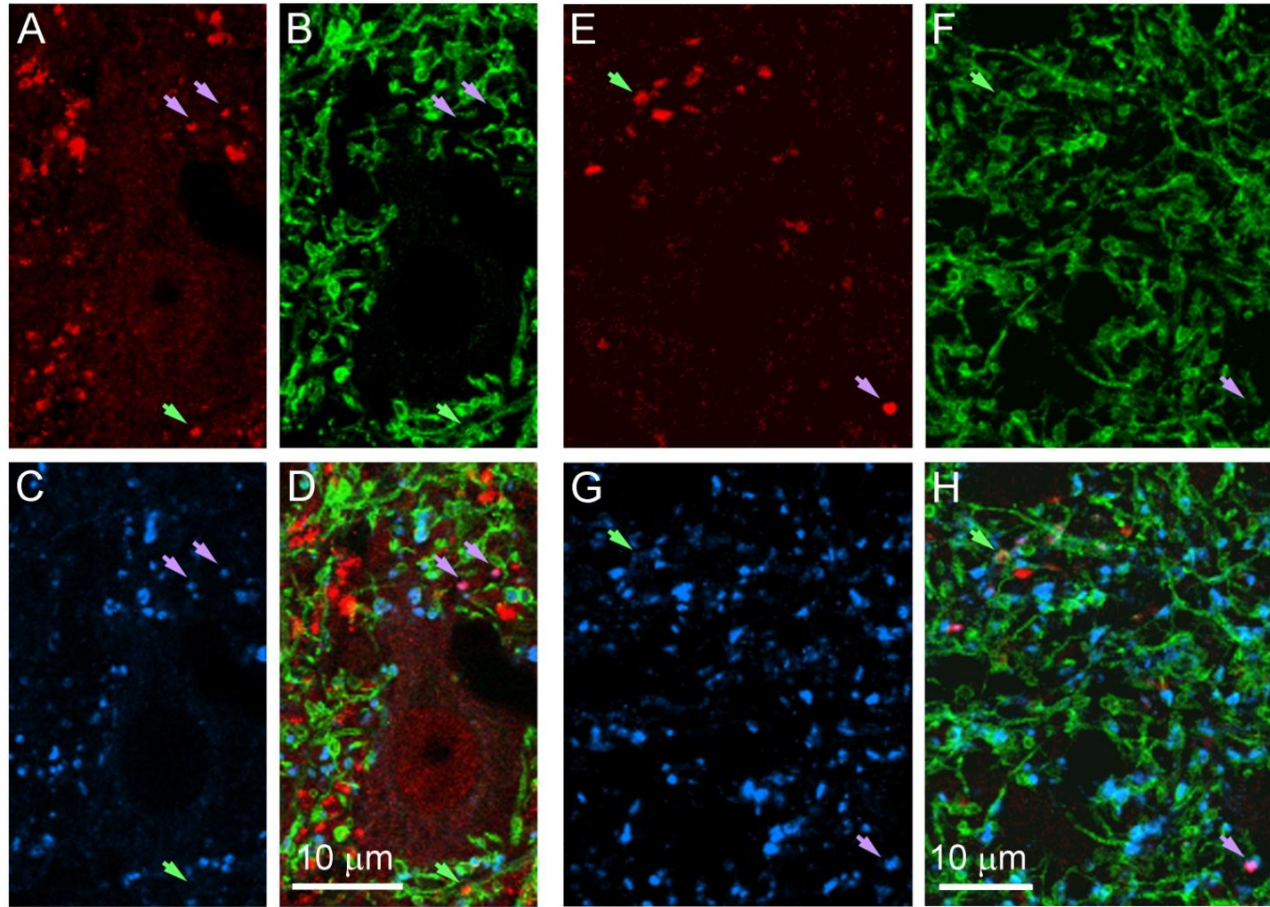


Figure 3.11. Immunocytochemistry of inhibitory axons

In single optical planes, immunoreactive CTb terminals from the MLF (A) and CVLM (E) are positive for GlyT2 (B, F) and GAD67 (C, G) as indicated by green and lavender arrows, respectively, in the merged images (D, H) as shown in single optical planes. Immunoreactivity for GlyT2 typically surrounds boutons as the transporter is found in the plasma membrane rather than in the cytoplasm.

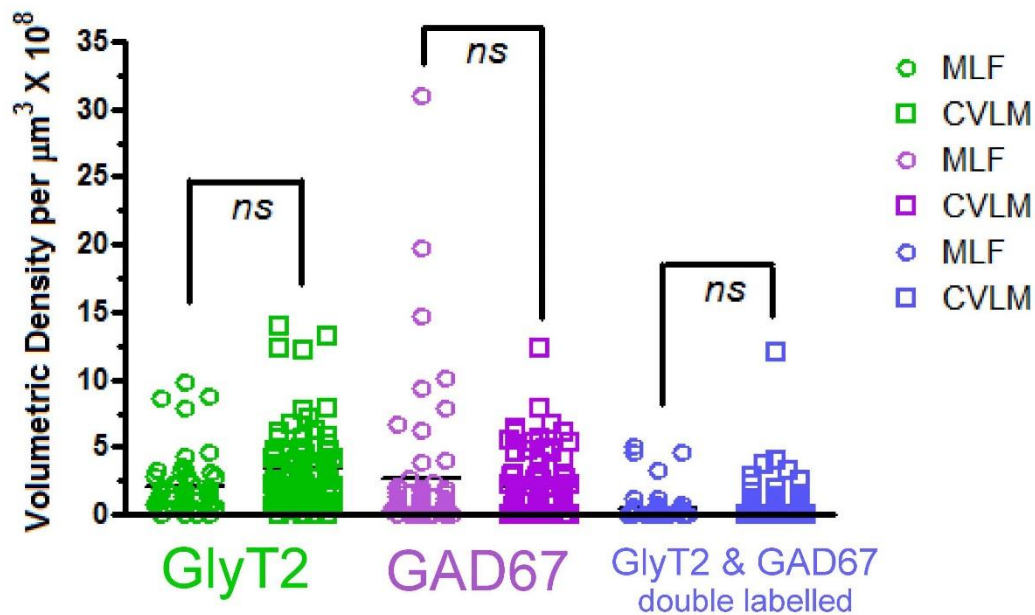


Figure 3.12. Scatter plot comparison of glycine and GABA volumetric densities from MLF and CVLM axonal populations

The volumetric density of inhibitory axon terminals from the MLF (circles) and CVLM (squares) did not significantly differ. Comparatively few axons were double labelled for both inhibitory amino acids. Kruskal-Wallis with Dunn's multiple comparison *post hoc* compared medians ($p > 0.05$). Each datum represents one $100 \mu\text{m} \times 100 \mu\text{m}$ scan field containing an averaged number of labelled axon terminals containing the given transmitter per total terminals. Scatter plot bars represent the mean. $N = 3$ animals. MLF, 2421 terminals examined; CVLM, 3923 terminals examined.

3.3.3.1 Laminar comparison of axon terminals containing glycine and GABA projecting from the MLF and CVLM

Although the inhibitory transmitters of these distinct medullary pathways do not significantly differ, there were differences found across laminar boundaries. The volumetric density of glycinergic and GABAergic axons projecting from the MLF and CVLM were investigated in defined medial and lateral laminar regions (Figure 3.13). The density of glycinergic terminals were more evenly distributed across laminar boundaries in the MLF population as compared to the CVLM population,

where the lamina X density especially differed from dorsal regions (Figure 3.14). The greatest density of GABAergic terminals from the MLF was found in lamina X, but this effect was less pronounced for the CVLM population (Figure 3.15). The density of axons containing both inhibitory amino acids was most apparent in laminae VI and VII for both descending pathways with a considerable density also in lamina X (Figure 3.16).

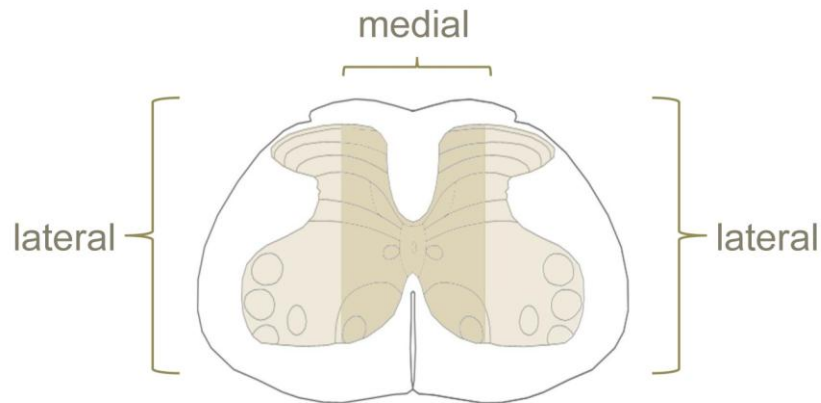


Figure 3.13. Transverse medial and lateral regions

Spinal L4 section shown as an example (based on Molander et al., 1984). The medial region is shaded darker with lateral regions shown in paler beige.

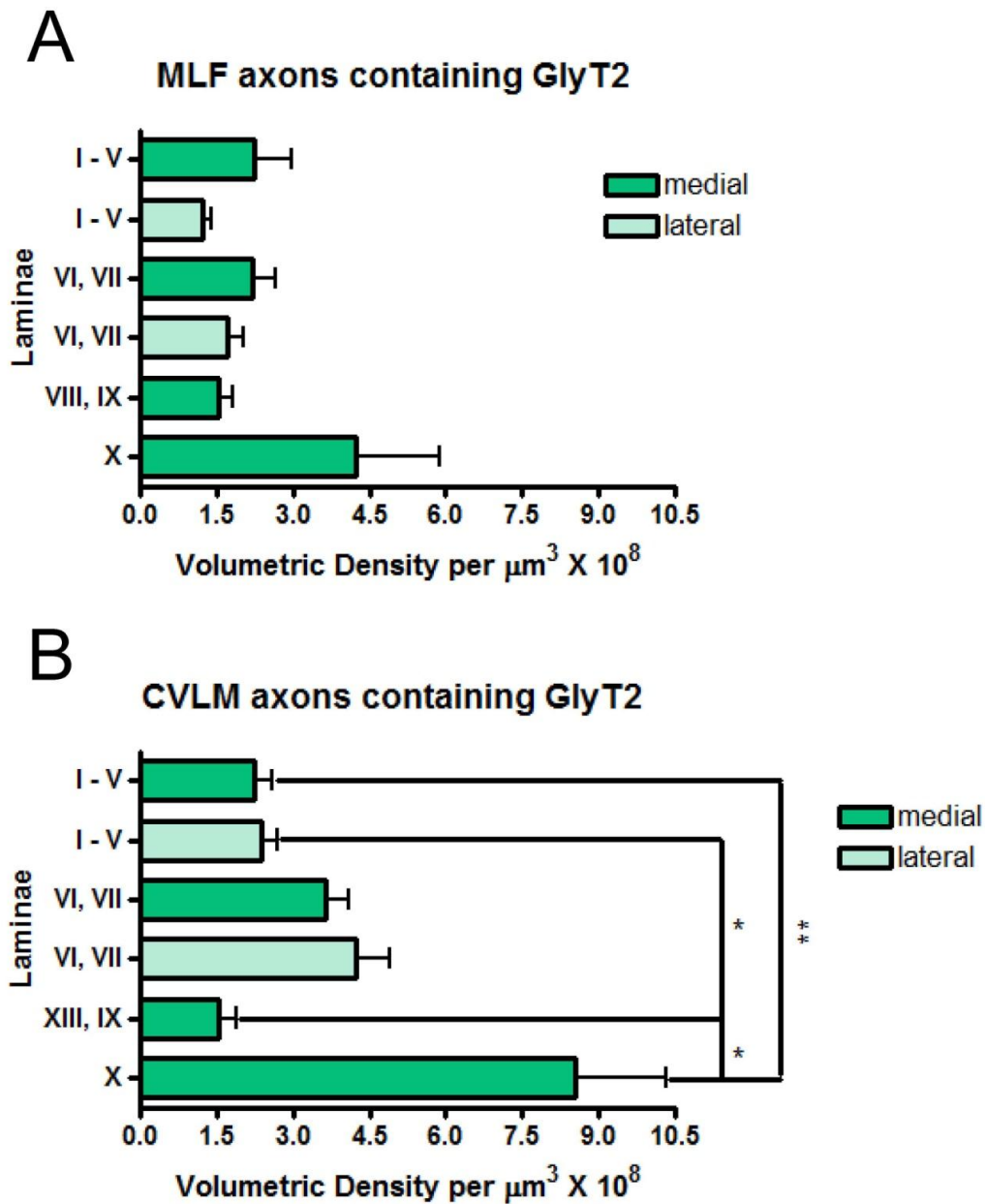


Figure 3.14. Volumetric densities of glycinergic axons from the MLF and CVLM across laminae

Kruskal-Wallis with Dunn's multiple comparison *post hoc* compared medians (* $p < 0.05$, ** $p < 0.01$) of axons from the MLF (A) and CVLM (B). Axons in lamina X were comparatively rich in GlyT2, and significantly for the CVLM population. Each green bar represents 100 $\mu\text{m} \times 100 \mu\text{m}$ scan fields containing an averaged number of labelled axon terminals containing GlyT2 per total terminals within the indicated laminar region. Standard error bars shown. N = 3 animals. (A) MLF, 2421 terminals examined (B) CVLM, 3923 terminals examined.

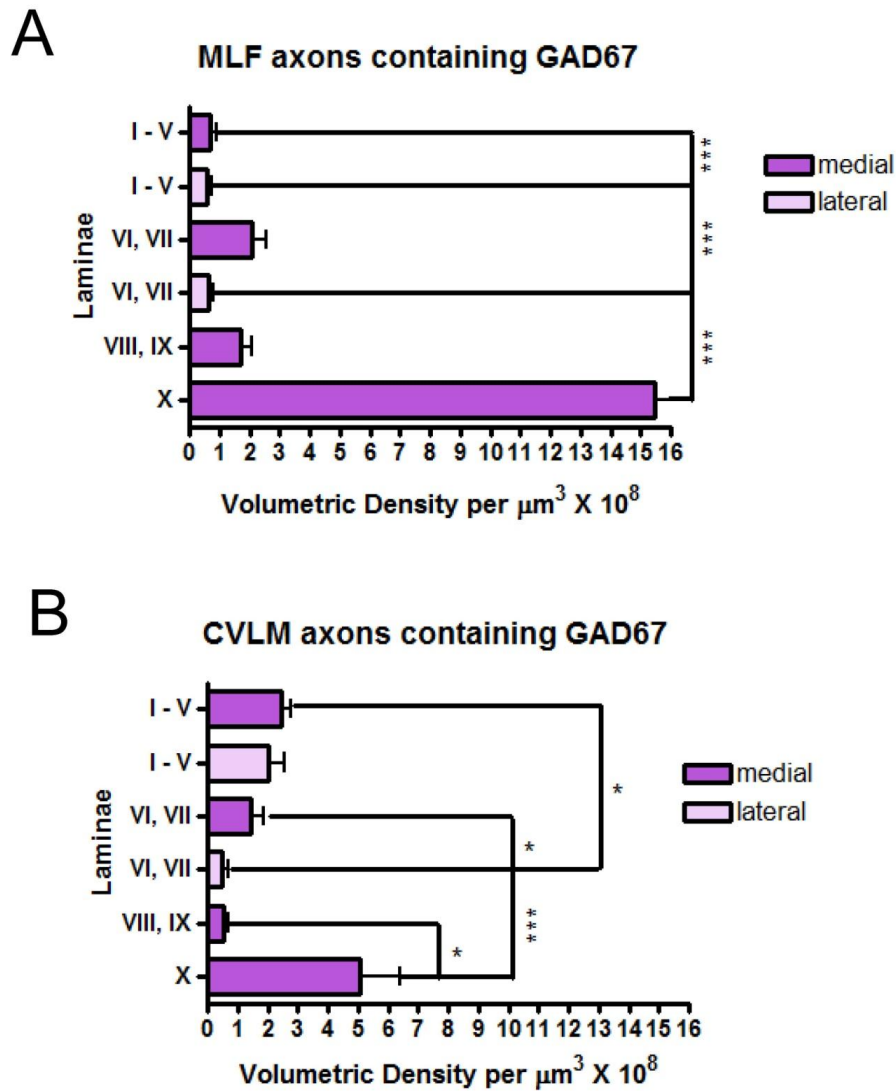


Figure 3.15. Volumetric densities of GABAergic axons from the MLF and CVLM across laminae

Kruskal-Wallis with Dunn's multiple comparison *post hoc* compared medians (* $p < 0.05$, *** $p < 0.001$) of axons from the MLF (A) and CVLM (B). Axons in lamina X were comparatively significantly rich in GABA for both descending system populations. Each purple bar represents 100 $\mu\text{m} \times 100 \mu\text{m}$ scan fields containing an averaged number of labelled axon terminals containing GABA per total terminals within the indicated laminar region. Standard error bars shown. N = 3 animals. (A) MLF, 2421 terminals examined (B) CVLM, 3923 terminals examined.

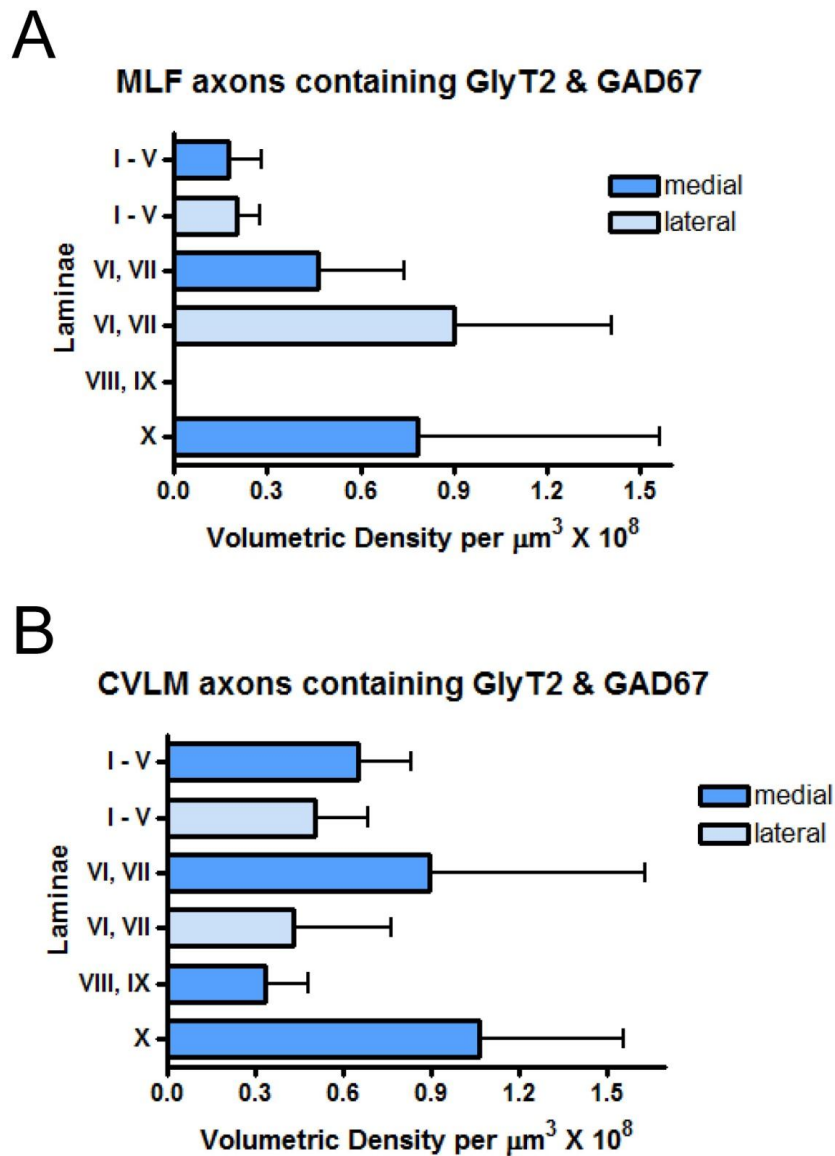


Figure 3.16. Volumetric densities of axons from the MLF and CVLM containing both inhibitory amino acids across laminae

Kruskal-Wallis with Dunn's multiple comparison *post hoc* compared medians ($p > 0.05$) of axons from the MLF (A) and CVLM (B). Lamina X axonal populations for both descending systems were comparatively rich in amino acids although differences across laminar boundaries were not significant. There was considerably variability of inhibitory axonal densities in intermediate laminae VI and VII. Each blue bar represents $100 \mu\text{m} \times 100 \mu\text{m}$ scan fields containing an averaged number of labelled axon terminals doubled labelled for both GlyT2 and GAD67 per total terminals within the indicated laminar region. Standard error bars shown. $N = 3$ animals. (A) MLF, 2421 terminals examined (B) CVLM, 3923 terminals examined.

3.3.4 Aim 4: To determine if medullary axons projecting to lower lumbar spinal cord segments contain serotonin

To determine if medullary axon terminals contained 5-HT, in two separate immunoreactions from three animals, sections with terminals from MLF were reacted with a combination of antibodies against CTb, [VGLUT1+VGLUT2] and 5-HT and further sections were reacted with CTb, VGAT and 5-HT (Table 3.1). A total of 80 immunofluorescent terminals were examined with no evidence of the presence of 5-HT in terminals (Figure 3.17). Further, sections with terminals from the CVLM from one animal were reacted with antibodies against CTb and 5-HT. All examined terminals were negative for 5-HT (Figure 3.18). Although medullary axons were hypothesised to express 5-HT, these terminals were uniformly non-reactive to antibody against 5-HT.

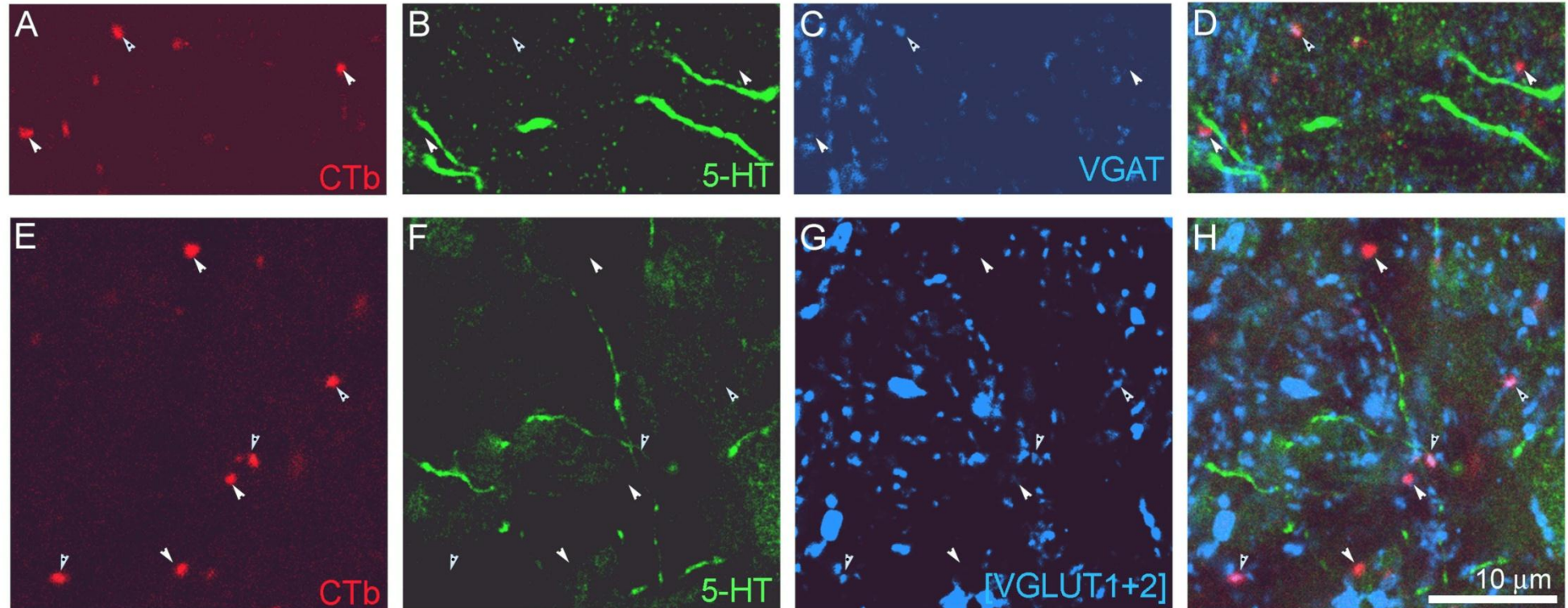


Figure 3.17. Immunofluorescent axons from the MLF and serotonin

Immunoreactive CTb terminals (A & E, red) from the MLF were reacted with antibodies against 5-HT (B & F, green) and VGAT (C, blue) and a mixture of VGLUT1+VGLUT2 (G, blue) denoted by black-dotted pointers. Negative CTb terminals were denoted by white pointers. All terminals were negative for 5-HT as shown in merged panels (D & H) in single optical planes.

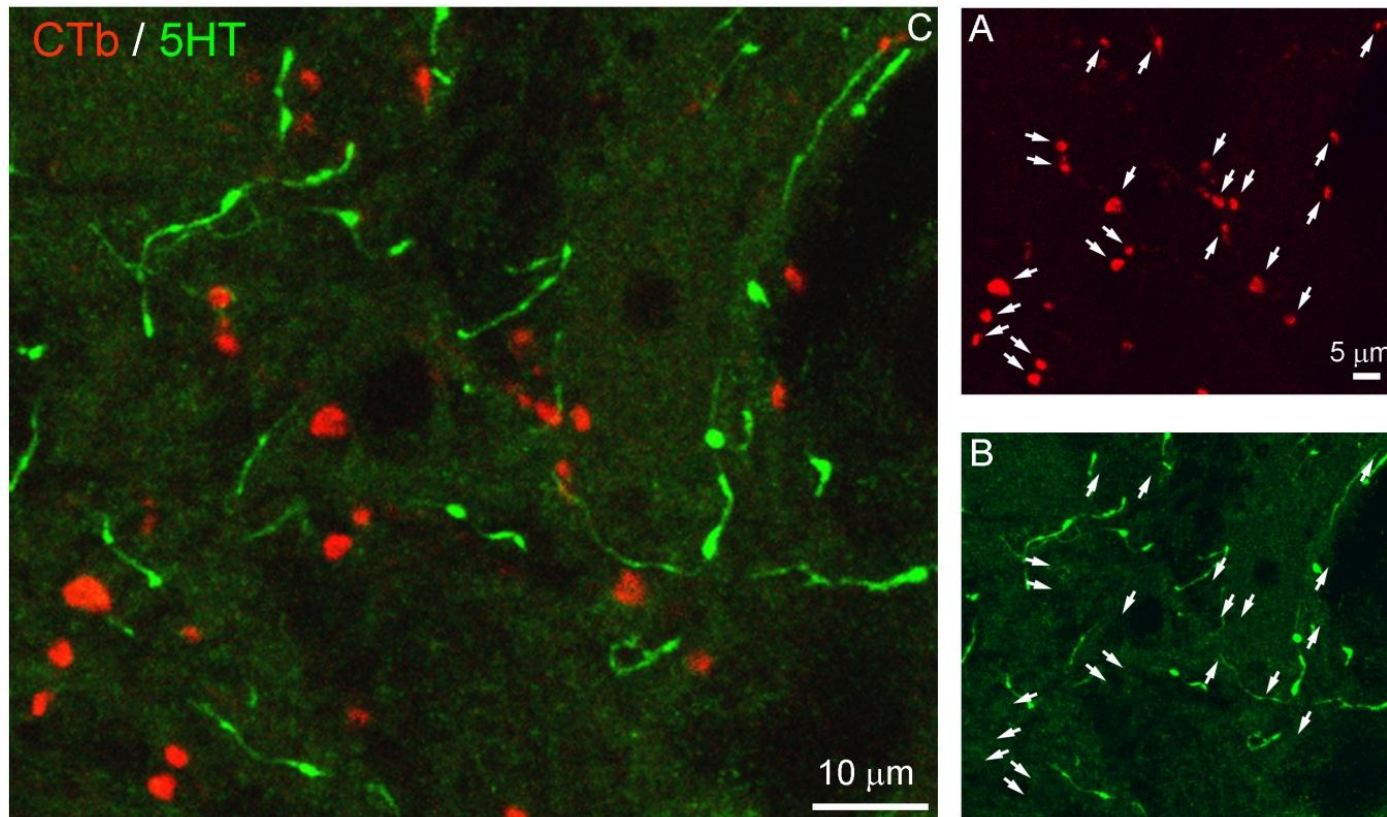


Figure 3.18. Immunofluorescent axons from the CVLM and serotonin

Immunoreactive CTb terminals from the CVLM (A) were reacted with 5-HT (B) and all terminals were negative for 5-HT as shown in the merged panel (C) in single optical planes.

3.4 Discussion

3.4.1 Qualitative summary

The series of complimentary immunoreactions elucidated the heterogeneous neurotransmitter phenotypes of axons descending from the MLF and CVLM. Taken together, expressed in percentiles, these investigations revealed that MLF axons were 61% (± 7.0) glutamatergic via VGLUT2 compared to 65% (± 7.7) from the CVLM population although the grey matter from the MLF population was very slightly denser in laminar volume. VGAT was contained in 21% (± 6.1) of MLF axons and 23% (± 2.1) of CVLM axons (see Appendix 3 Table 2). Therefore, approximately 17% of MLF axon and 12% of CVLM axons were not immunoreactive to the tested antibodies, and they were not serotonergic. Results indicate that the different functional properties of the anatomically distinct MLF and CVLM axons are achieved using by using the same neurotransmitters and in the same proportions. Summarised finding are represented qualitatively in Figure 3.19.

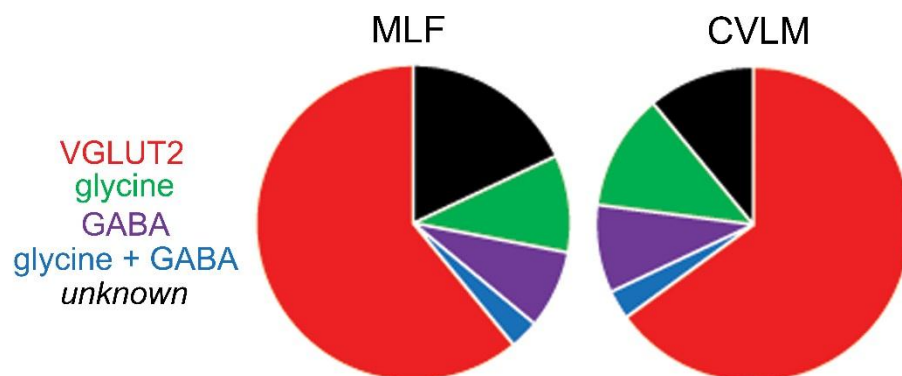


Figure 3.19. Qualitative summary of medullary axon neurochemicals

Percentiles of neurotransmitters in MLF and CVLM axonal populations.

3.4.2 Labelling of descending systems

CTb has been used extensively as a retrograde tracer but is also sequestered by cells and axons (Chen and Aston-Jones, 1995) such that CTb may be transported anterogradely as well as retrogradely (Ericson and Blomqvist, 1988). As with other tracers, CTb may be taken up by axons of passage in the CNS (Chen and Aston-Jones, 1995) and therefore the possibility that this tracer has contaminated axons derived from cell sources beyond the intended target area of injection cannot be excluded. This may be especially likely with MLF injections since fibres from the VST (Nyberg-Hansen and Mascitti, 1964, Wilson and Peterson, 1978) and the tectospinal tract (Petras, 1967) also descend into this region although medial VST axons in rat terminate in the cervical dorsal horn (Bankoul and Neuhuber, 1992). So a consideration for MLF injections is that, in addition to RetS axons, spinoreticular cells were also labelled retrogradely and their collateral axons may have contaminated these findings. However, another study using a very sensitive method for revealing CTb reported that retrogradely transported CTb is detected in cell bodies and proximal dendrites but not in axons or fibre bundles (Angelucci et al., 1996).

3.4.3 Identification of neurotransmitter phenotypes

The discovery of VGLUT1 and VGLUT2 and the production of specific antibodies against them have been proven to be a reliable method for identifying axon terminals that contain glutamate. ICC localisation of glutamate, glutaminase, or the expression of reuptake transporters for excitatory amino acids has been used to reliably identify glutamatergic axons projecting to the spinal cord (Alvarez et al., 2004, Oliveira et al., 2003, Persson et al., 2006, Todd et al., 2003, Varoqui et al., 2002). In the spinal cord, most large diameter myelinated primary afferent axons contain VGLUT1 whereas terminals of spinal interneurons contain VGLUT2 (Todd et al., 2003, Varoqui et al., 2002). Although this information indicates the source of excitatory terminals in the spinal cord, further studies have found that other descending axons contain VGLUT1 and VGLUT2 (Du Beau et al., 2012). Based upon extensive electrophysiological findings in the cat, most descending systems are known to monosynaptically excite their target spinal neurons (see (Jankowska, 1992, Jankowska and Edgley, 2010).

The introduction of antibodies against VGAT provides a reliable method for identifying inhibitory axon terminals since this transporter is found in both glycinergic and GABAergic boutons (Chaudhry et al., 1998). Colocalisation of glycine and GABA has been reported for many spinal interneurons and especially in the dorsal horn (Todd and Spike, 1993). The results from this study indicate that most inhibitory axons from both the MLF and CVLM are either purely glycinergic or GABAergic. However, another study using fluorescent *in situ* hybridization techniques found many spinally projecting neurons in the ventromedial medulla contain mRNAs for both GlyT2 and GAD67 (Hossaini et al., 2012). GAD exists as two isoforms with molecular masses of 65 and 67 kDa (GAD65 and GAD67, respectively), which are encoded by independent genes (Erlander et al., 1991). While both isoforms are present in most GABAergic neurons in the rat CNS, GAD65 appears to specifically target membranes and nerve endings, whereas GAD67 is more extensively distributed in cells (Feldblum et al., 1995, Mackie et al., 2003). Both forms synthesise GABA, but GAD67 might preferentially synthesise cytoplasmic GABA (Soghomonian and Martin, 1998).

Descending inhibitory mechanisms predominantly function via inhibitory interneurons (Lundberg, 1982). Collective studies suggest that glycinergic neurons in the ventral medial medulla may mediate motor atonia during REM sleep (Hajnik et al., 2000, Holmes and Jones, 1994, Lai and Siegel, 1988, Lai and Siegel, 1992, Morales et al., 2006, Schenkel and Siegel, 1989, Siegel et al., 1991) although recent studies in rats have challenged this idea (Lu et al., 2000) as normal REM atonia has been reported after lesioning the medial medulla in rats (Lu et al., 2008).

The MLF injection sites included the raphé obscuris which is known to project to the intermediate grey matter and the ventral horn (Bowker et al., 1981b) yet none of the labelled axons contained 5-HT. The most plausible explanation is that most raphé spinal axons are unmyelinated (Westlund et al., 1992) and therefore may not sequester the CTb tracer. However, cells containing 5-HT have successfully been retrogradely traced with CTb (Tanaka et al., 2006) so this discrepancy may be due specifically to the anterograde transport of CTb.

A proportion of RetS axons were not labelled by the markers used in this study (Figure 3.19). Possible explanations are that these terminals contain another transmitter not tested for or they are glutamatergic as unmyelinated primary afferents expressing neither VGLUT1 nor VGLUT2 (Todd et al., 2003). These terminals plausibly may contain VGLUT3, a transporter present in raphé spinal axons that project to sympathetic regions of the spinal cord (Nakamura et al., 2005a).

The inhibitory actions of the RetST in nociceptive pathways associated with the discrimination of painful stimuli are well documented (Fields and Basbaum, 1978) and many of these systems use monoaminergic transmitters which are known to depress peripheral inputs to many premotor interneurons (Dougherty et al., 2005) and may play a role in sculpting motor movements. So as the neurochemical profiles of neurons from these reticular components overlap, their diverse functional roles may be indistinct too (see Mason, 2001). Most actions of descending systems are mediated via interneurons (Jankowska, 1992) and these systems are crucial in the selection of motor patterns by influencing interneuronal activities.

Chapter 4. Axon terminals descending from the sensorimotor cortex and their neuronal targets in lower lumbar spinal cord segments

4.1 Introduction

Phylogenetically advanced species must have sophisticated motor pathways linking supraspinal motor centres with the spinal cord. Unlike brainstem motor pathways which are well developed at birth, the CS pathway is not (Kudo et al., 1993, Martin et al., 1980). Each cortical neuron is uniquely receptive with a bias towards the somatosensory modality (Houk et al., 1993) which indicates that a variety of sensorimotor combinations are represented in the motor cortex initiating appropriate limb movements (Houk, 1989). The motor cortex may function to select specific motor commands by filtering sensory information discriminately and also by coordinating the activities of other descending systems related to the control of distal and proximal muscles (Canedo, 1997). Compared to other descending pathways, the CST is highly collateralised which accounts for why the CST can mediate more fractionated types of movements that characterise distal extremities (Kuypers, 1981). Although the CST is classically considered a crossed pathway, ipsilateral projections in the lumbosacral enlargement are considered potentially significant in terms of understanding the repercussions of cortical or spinal lesions (see Jankowska and Edgley, 2006).

The vertebrate CNS is exposed to a continual barrage of afferent impulses from various sensory organs such that overall information-processing capabilities are exceeded. The central control of information flow in peripheral afferents seems to play an important role in generating integrated movements and the processing of sensory information, including nociceptive information. CS axons descending to the dorsal horn are an important source of presynaptic inhibition of primary afferent fibres (Canedo, 1997, Wall and Lidierth, 1997) and the CST may allow gating or filtering of sensory afferent input associated with volitional motor commands (Lemon, 2008). Sensory neurotransmission from primary afferents onto spinal neurons appears to be principally mediated by glutamate. For this reason, considerable attention has been directed to the identification of glutamatergic markers in the spinal cord, especially in relation to sensory afferents. While both VGLUT1 and VGLUT2 have been reported to be contained in terminals of glutamatergic neurons and in the spinal cord, only large diameter primary afferents contain VGLUT1 (Alvarez et al., 2004, Oliveira et al., 2003, Persson et al., 2006, Todd et al., 2003).

The synaptic interconnections between afferent fibres and their interneuronal targets in the dorsal horn of the rat are complex (Rudomin and Schmidt, 1999). In terms of motor behaviour, excitatory and inhibitory interneurons that are activated by primary afferents clearly play different roles (Aggelopoulos et al., 1996, Holmqvist and Lundberg, 1959, Holmqvist and Lundberg, 1961) and a fundamental goal is to characterise their neuronal targets, input properties and morphologies. The spinal cord contains several classes of ChAT interneurons with proposed roles in sensory processing and motor output (Barber, 1984, Huang et al., 2000, Phelps et al., 1984). Spinal circuits dedicated to the control of motor output are constructed from a complex array of interneuron subtypes (Bannatyne et al., 2009, Jankowska, 2001) that derive from cardinal progenitor domains (Goulding, 2009, Jessell, 2000), implying that a single progenitor domain gives rise to multiple subclasses of adult interneurons (Zagoraïou et al., 2009). The activation of cortical systems expressing ChAT modulate sensory thresholds, states of attention and the consolidation of memory (Giocomo and Hasselmo, 2007, Lawrence, 2008, Pauli and O'Reilly, 2008). Within the spinal cord, innervation by ChAT is apparently intrinsic rather than derived from the brain (Sherriff et al., 1991) or from the periphery (Barber, 1984).

Spinal interneurons are currently classified according to their synaptic inputs as well as their ability to modulate motoneuron firing (Jankowska, 1992). Therefore, the mechanisms that select specific synaptic inputs onto interneurons are of key interest. Adult interneurons may acquire their pattern of connectivity by the loss or weakening and/or the gain or strengthening of specific synaptic inputs during development (Mentis et al., 2006). The pruning of synaptic inputs plays important roles in shaping adult connectivity in many parts of the CNS (Crepel et al., 1976, Katz and Crowley, 2002, Katz and Shatz, 1996, Kim and Kandler, 2003, Shatz, 1983) yet the mechanisms determining these patterns of synaptic connections onto spinal interneurons are uncertain (Mentis et al., 2006). Because of the enormous diversity in distinct presynaptic neuronal subtypes and the fact that cell bodies can be distantly located from their interconnected neurons, investigating the organisation of overall connectivity patterns can be a challenging task (Stepien et al., 2010).

Neurons and circuits that process cutaneous sensory input are concentrated in the dorsal horn whereas circuits involved in proprioception and motor control are largely confined ventrally. How spinal neurons are allocated in the cord is dependent on signalling systems that intersect along the rostrocaudal and dorsoventral axes, establishing a grid-like set of positional cues (Jessell, 2000). Signalling along the rostrocaudal axis establishes the main subdivisions of the CNS (Jessell, 2000, Lumsden and Krumstauf, 1996). Anatomical evidence indicates that neurons extend their dendrites to allow for potential synaptic connections (Stepanyants and Chklovskii, 2005) and it is proposed that dendrites and axons are ideally matched to anatomically maximize connections to their potential connection partners (Cuntz, 2012) and theoretical predictions from optimality criteria are congruent with this idea (Wen and Chklovskii, 2008). For dendritic and axonal processes, wiring principles and branching patterns are certainly intertwined (Chklovskii and Koulakov, 2004, Cuntz et al., 2007, Wen and Chklovskii, 2008). Further, branching patterns can actually be predicted (Cuntz et al., 2010) such that a direct link between specific patterns of synaptic connectivity to the corresponding dendritic tree emerges (Cuntz, 2012) although the diverse factors that determine the number of axons innervating any single neuron are largely unknown (Purves and Hume, 1981). To some degree, dendritic processes appear to be specified at early development stages (Banker and Cowan, 1979, Honig and Hume, 1986, Kriegstein and Dichter, 1983) although dendritic processes are influenced too by extrinsic factors, especially neural connections (Benes et al., 1977, Deitch and Rubel, 1984b, Sumner and Watson, 1971).

It is hypothesised that axons from the sensorimotor cortex will express VGLUT1 and terminate dorsally in lower lumbar spinal cord segments. CST axons are expected to contact ChAT interneurons, principally in dorsal laminae. The orientation of ChAT dendrites is hypothesised to correlate to their input densities. In order to investigate descending sensorimotor axons in the cord and their neuronal targets, a series of immunoreactions were conducted with subsequent analyses. The following experiments addressed the following aims:

To determine the distribution of anterogradely labelled axon terminals descending from the sensorimotor cortex within lower lumbar spinal cord segments

To identify the neurotransmitter phenotype of CST axons in lower lumbar segments

To investigate immunoreactive contacts onto ChAT interneurons receiving input from the CST across laminar boundaries

To classify ChAT interneurons dendritic orientations as related to their contact densities

4.2 Methods

4.2.1 Image acquisition and analyses

For the following series of experiments, spinal cord tissue from nine rats receiving CTb injections into the sensorimotor cortex were processed for analyses (Appendices 1 Figure 3). The neurotransmitter content of CST axons was established using ICC techniques with subsequent confocal microscopy and analyses. Laboratory techniques, image acquisition and statistical analyses were congruent with methods as outlined in Chapters 2 and 3.

For the analyses of interneuronal targets of the CST, datum was the number of immunoreactive terminals per mean contact surface density ($1,000 \mu\text{m}^2$) across defined spinal laminar regions. To represent the horizontally stacked laminae in the transverse plane, bar graphs are displayed horizontally while bar graphs from the experiment conducted in the parasagittal plane are represented vertically. To analyse findings, the *a priori* D'Agostino & Pearson omnibus normality test revealed that experimental data did not assume a Gaussian distribution. Therefore the nonparametric Kruskal-Wallis test compared medians of sampled data with Dunn's multiple comparison's *post hoc* to test the differences between the neurochemical content of boutons contacting interneurons across laminar

boundaries in the transverse and parasagittal plane with significance reported as p values.

Because ChAT dendrites tended to be orientated rostrocaudally within spinal segments, some dendritic processes were not fully visualised so neuronal reconstructions in the transverse plane were considered partial. To fully reconstruct interneurons in the parasagittal plane, approximately two to seven slightly overlapping scan fields were montaged as necessary to reveal branching dendrites. To conceptually visualise the orientation of interneurons within the spinal cord grey matter, Image J was used to freely rotate and translocate any given cell process about the X (rostrocaudal), Y (dorsoventral) and Z (mediolateral) axes in the parasagittal plane (Figure 4.1).

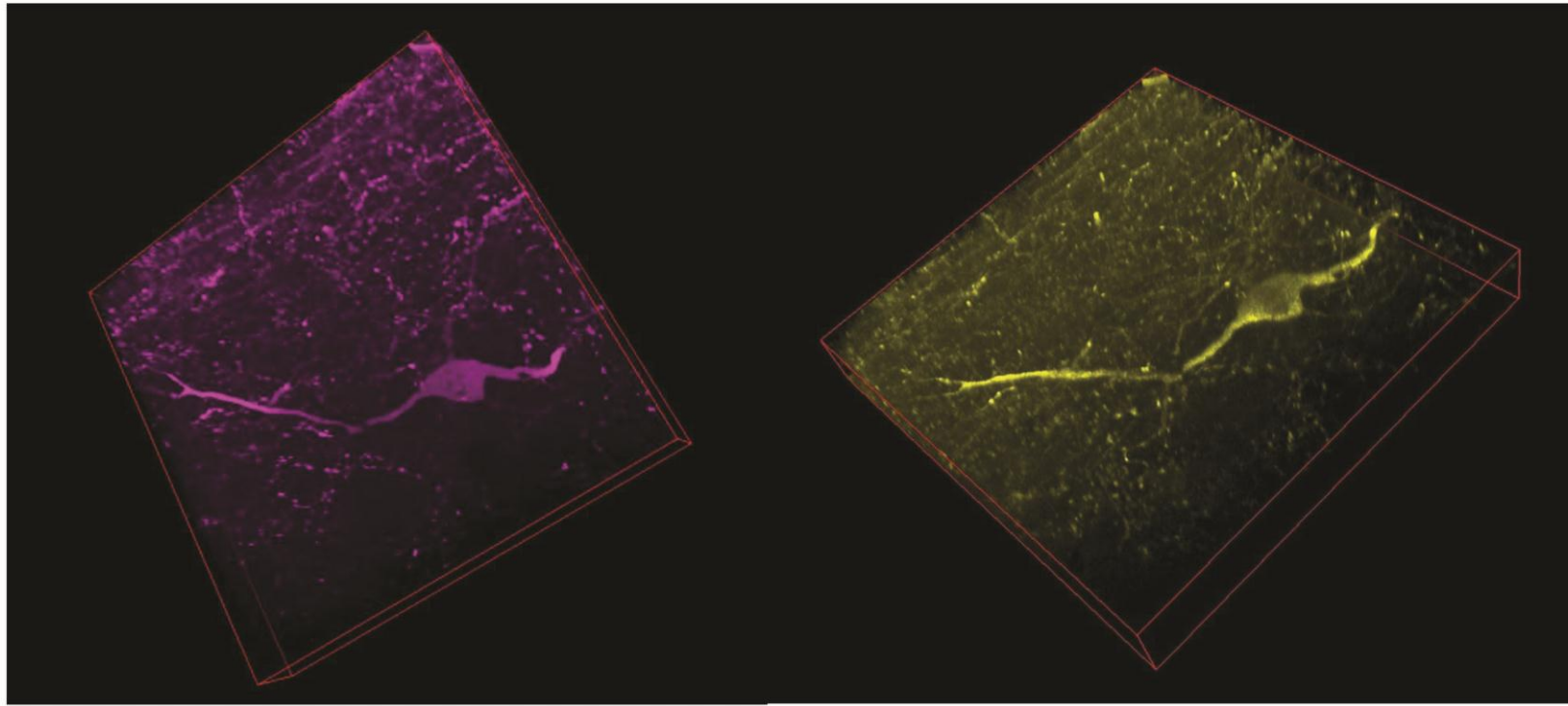


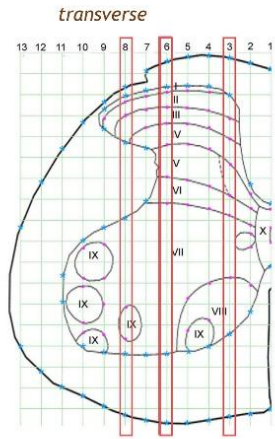
Figure 4.1 ChAT interneuron conceptually visualised in spinal cord grey matter

To conceptually explore any given ChAT interneuron in a single optical field, Image J was used to freely rotate and translocate any cell process about the X, Y and Z axes. Shown in different pseudo colours for contrast. For analyses, several scan fields ($\approx 2 - 7$) were montaged to fully reveal dendritic processes in the parasagittal plane.

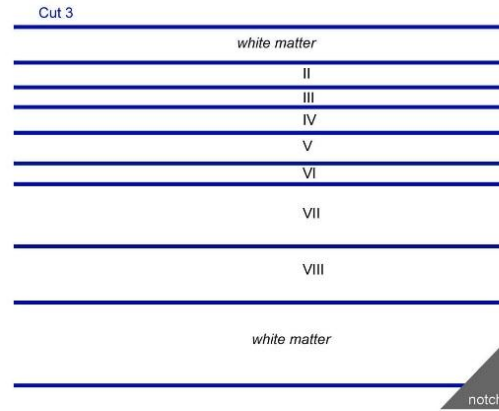
4.2.2 Laminar boundaries in the parasagittal plane

Standard transverse templates based upon Molander's scheme are conventionally used to accurately locate neurons within spinal cord laminae of rat. Transverse templates are advantageous since they can be applied uniformly and consistently to all sections within a given lumbar segment since the spinal cord is shaped as an elliptical tube (see Figure 2.5). Conversely, for parasagittally sectioned segments, each cut section is different and there was no applicable consensual template and thus laminar boundaries were undefined. Based upon standard transverse templates, I derived laminar boundary maps for L3, L4 and L5 segments cut in the parasagittal plane at 120 μm increments and intermediate 60 μm increments can be readily inferred as well. A square grid was superimposed over standard transverse template. Scaled 'cuts' at 120 μm increments represent how the segment is sectioned from the midline (central canal), which lies flat against the Vibratome chuck. Coordinates were plotted along the vertical axes corresponding to the transverse laminar boundaries and then extrapolated into the parasagittal plane as horizontal lines. To accurately determine the laminar location of interneurons, these parasagittal templates served as 'maps' of the scanned images and scaled semi-opaque templates were overlaid onto scanned images as necessary (Figure 4.2).

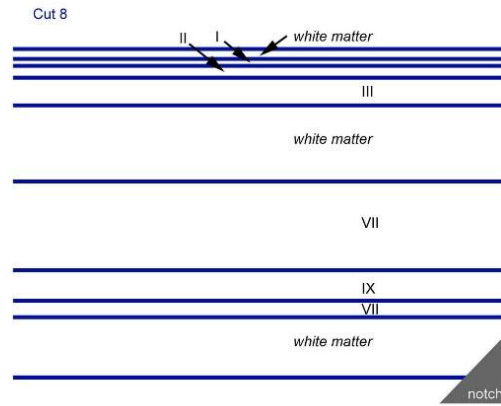
A



B



D



C

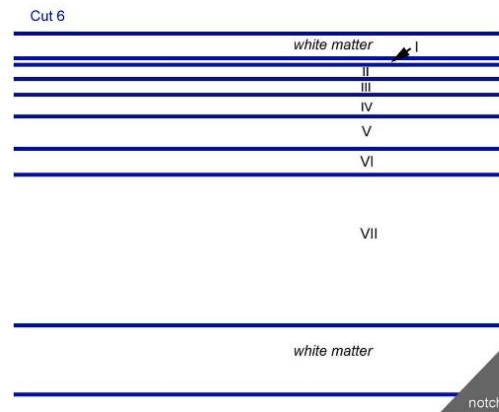


Figure 4.2 Laminar boundary maps in the parasagittal plane

An exemplary L4 transverse template hemisphere (based on Molander et al., 1984) is shown (A) with a superimposed square grid at 120 μm increments designated as 'cuts' such that Cut 1 is 120 μm from the midline, Cut 2 is 240 μm and so on. As an example of the established laminar maps, Cuts 3, 6 and 8 are highlighted (red narrow vertical rectangles) with the plotted transverse coordinates extrapolated into the parasagittal plane as shown in B, C and D, respectively, shown as blue horizontal lines. Sections were notched caudal-ventrally, indicated by the corner grey triangles, to accurately orientate the sections mounted onto slides. Note that Cut 8 (D) approaching the lateral edge of the cord, for example, is comprised of a sizable proportion of white matter surrounded by lamina III dorsally and lamina VII ventrally on this mounted section.

4.2.3 Stereological techniques to examine neuronal targets

Stereological analyses were performed on ChAT interneuron reconstructions exported from Neuroexplorer using Image J. Dendritic branching patterns of ChAT interneurons were assessed as XY Ratios in the parasagittal plane. A rectangle was drawn around each scaled neuron to exactly and entirely encompass all dendritic branches where the X axis was the rostrocaudal dimension and the Y axis was the dorsoventral dimension. For any imaginary neuron in the parasagittal plane, if the X and Y axes were equal such that all dendritic branches were fully contained within a square, then the dimensionless XY Ratio was one. By definition, rostrocaudally orientated neurons had an XY Ratio greater than one and dorsoventrally orientated neurons had an XY Ratio less than one (Figure 4.3).

To describe the orientation of dendritic branching relative to the soma in the parasagittal plane, the geometric centres of both the entire interneuron and the soma were located. Connecting these two centres established a vector with four direction possibilities: dorsocaudal, dorsorostral, ventrorostral or ventrocaudal. That is, dendrites were determined to be predominantly situated towards a given anatomical direction (Figure 4.4).

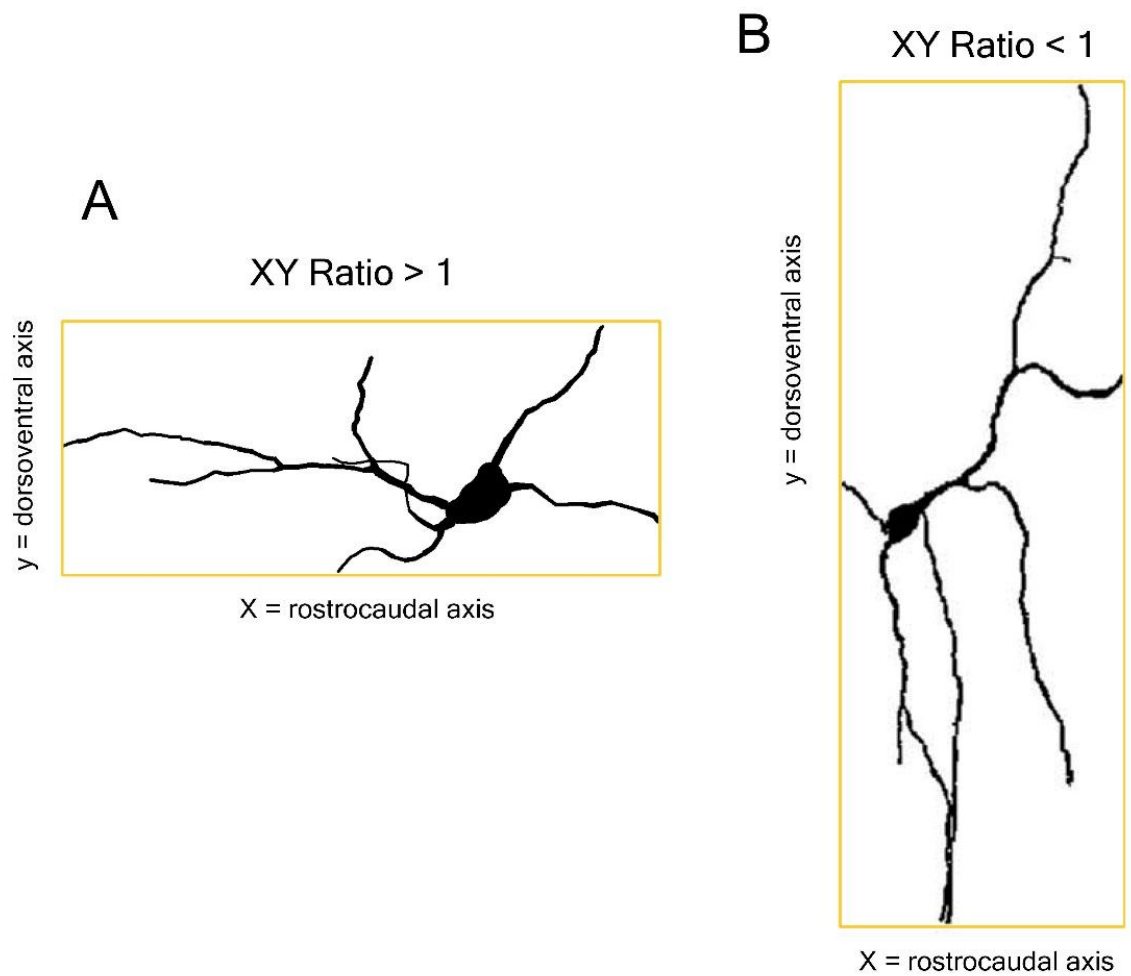


Figure 4.3 Derivation of XY Ratios

For any imaginary neuron in the parasagittal plane, rostrocaudally orientated neurons have a dimensionless XY Ratio greater than one (A) and dorsoventrally orientated neurons have an XY Ratio less than one (B).

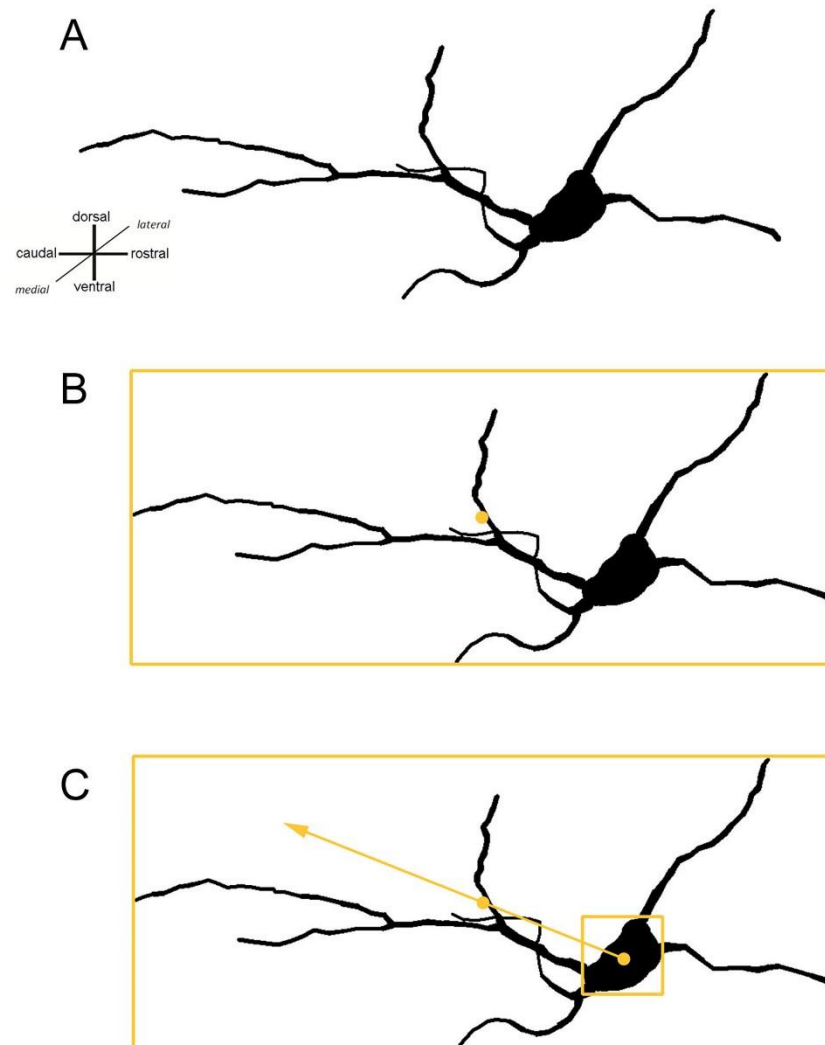


Figure 4.4 Dendritic orientation in the parasagittal plane

To find the dendritic orientation for any imaginary neuron in the parasagittal plane (A), all dendritic branches were encompassed within a rectangle and the geometric centre of neuronal processes was located as indicated by the gold dot (B) and similarly for the soma (C). By connecting these two centres, there are four possible anatomical directions: dorsocaudal, dorsorostral, ventrorostral or ventrocaudal. The dendritic orientation of this neuron is dorsocaudal as indicated by the vector arrow (C). That is, dendrites were predominantly situated towards the dorsocaudal axis relative to the soma in this example.

Aim	Primary antibody combinations	Concentrations	Supplier	Secondary antibodies	Concentrations	Sequential immunoreaction	Sequential secondary antibody
1	gt. CTb	1:50,000	List Biological Laboratories, Campbell CA USA	Biotinylated IgG	1:500	Avidin HRP (1:1,000)	DAB
	mo. CTb	1:250	A. Wilkström, University of Gothenburg	Rh Red	1:100		
2	rbt. VGLUT1	1:5,000	Millipore, Harlow UK	Alexa 488	1:500		
	g. pig VGLUT2	1:5,000	Millipore, Harlow UK	Dyl 649	1:500		
	mo. CTb	1:250	A. Wilkström, University of Gothenburg	Rh Red	1:100		
2	g. pig VGLUT1	1:1,000	Millipore, Harlow UK	Dyl 649	1:500		
	g. pig VGLUT2	1:5,000	Millipore, Harlow UK	Dyl 649	1:500		
	rbt. VGAT	1:1,000	Synaptic Systems, Göttingen Germany	Alexa 488	1:500		
	mo. CTb	1:250	A. Wilkström, University of Gothenburg	Rh Red	1:100		
3	g. pig VGLUT1	1:1,000	Millipore, Harlow UK	Dyl 649	1:500		
	gt. ChAT	1:100	Millipore, Harlow UK	Alexa 488	1:500		

Antibodies diluted in 0.3% PBST

gt. = goat; mo. = mouse; rbt. = rabbit; g. pig = guinea pig

Table 4.1 Summary of primary and secondary antibody combination and concentrations

DAB was used as a substrate to CTb visualise staining. All secondary antibodies were raised in donkey and conjugated to biotin, Rh Red, Dyl 649 (supplied by Jackson ImmunoResearch, West Grove, USA) or Alexa 488 (supplied by Molecular Probes, Eugene, USA). Avidin HRP and DAB supplied by Sigma-Alrich, Dorset, UK. Antibody labelling: CTb, traces myelinated axons; VGLUT1 and VGLUT2, synaptic vesicles; VGAT, glycinergic and GABAergic synaptic vesicles; ChAT, cholinergic neuronal processes.

4.3 Results

4.3.1 Aim 1: To determine the distribution of axon terminals descending from the sensorimotor cortex within lower lumbar spinal cord segments

Injection sites to label the CST targeted the primary and secondary motor cortex and the adjacent primary sensory cortex (Figure 4.5). Labelled terminals in the grey matter of the lumbar spinal cord were most numerous in dorsal laminae I - VI contralateral to the injection site and were especially concentrated medially near lamina IV. Fewer terminals were present in lamina VII and only rarely were found in the ventral horn. Occasionally very sparse terminations were found within the ipsilateral intermediate grey matter (Figure 4.6). The predominantly dorsal location of labelled CST axons in spinal laminae is congruent with the hypothesis although a considerable number of terminals were found to populate intermediate laminar regions also.

4.3.1.1 Location of cholinergic neurons in the transverse plane

Input properties of populations of ChAT interneurons analysed in the following experiments included small dorsal horn neurons especially located in the laminae III - V region, partition neurons in the lamina VII region and central canal neurons within lamina X (Figure 4.7).

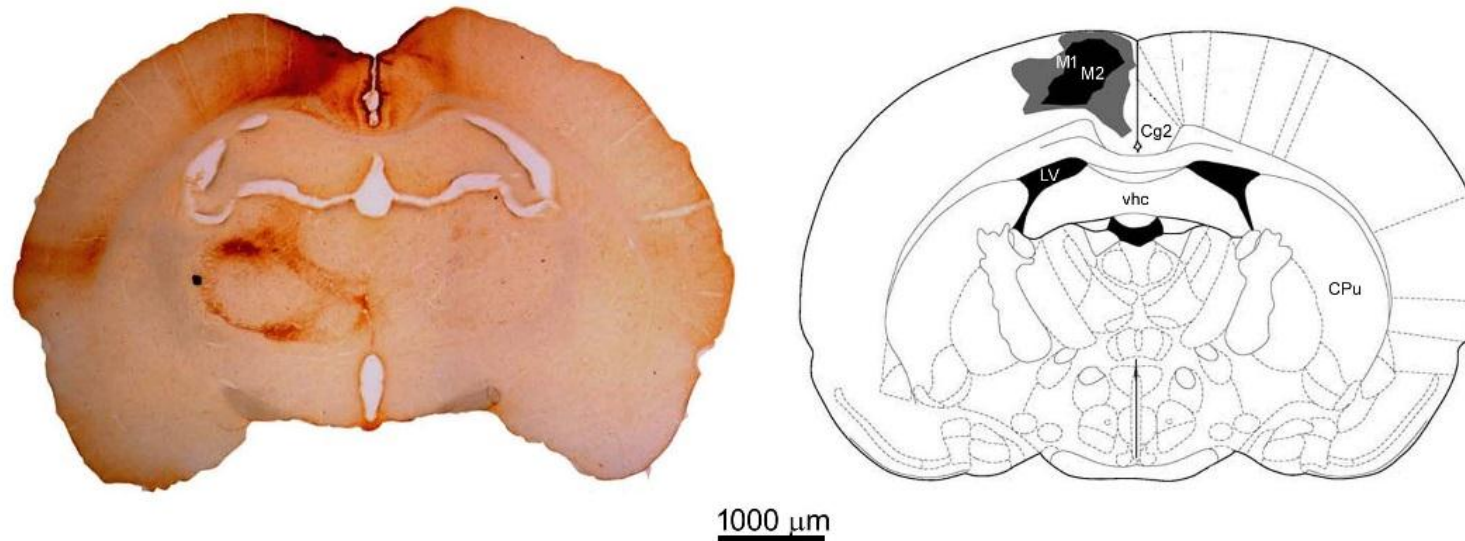


Figure 4.5 Brain reconstruction for CST injection site

Exemplary reconstruction of the CTb injection site labelling the CST. The inner black shaded area represents the core of the injection site and the grey shaded area represents the maximum diffusion of CTb within the brain. 100 μm deep coronal sections reacted with DAB to reveal the tracer is shown on the left with the corresponding drawing on the right. Template drawings are from Paxinos and Watson (1997). The CTb tracer labelled the M1 (primary motor cortex) and M2 (secondary motor cortex) with other anatomical sites included for contextual reference, including the Cg2 (cingulate cortex 2), LV (lateral ventricle), vhc (ventral hippocampal commissure) and CPu (caudate putamen, striatum). The sensorimotor cortex was labelled also (not shown in this section). Brain reconstructions from all experiments are shown in Appendix 1 Figure 3.

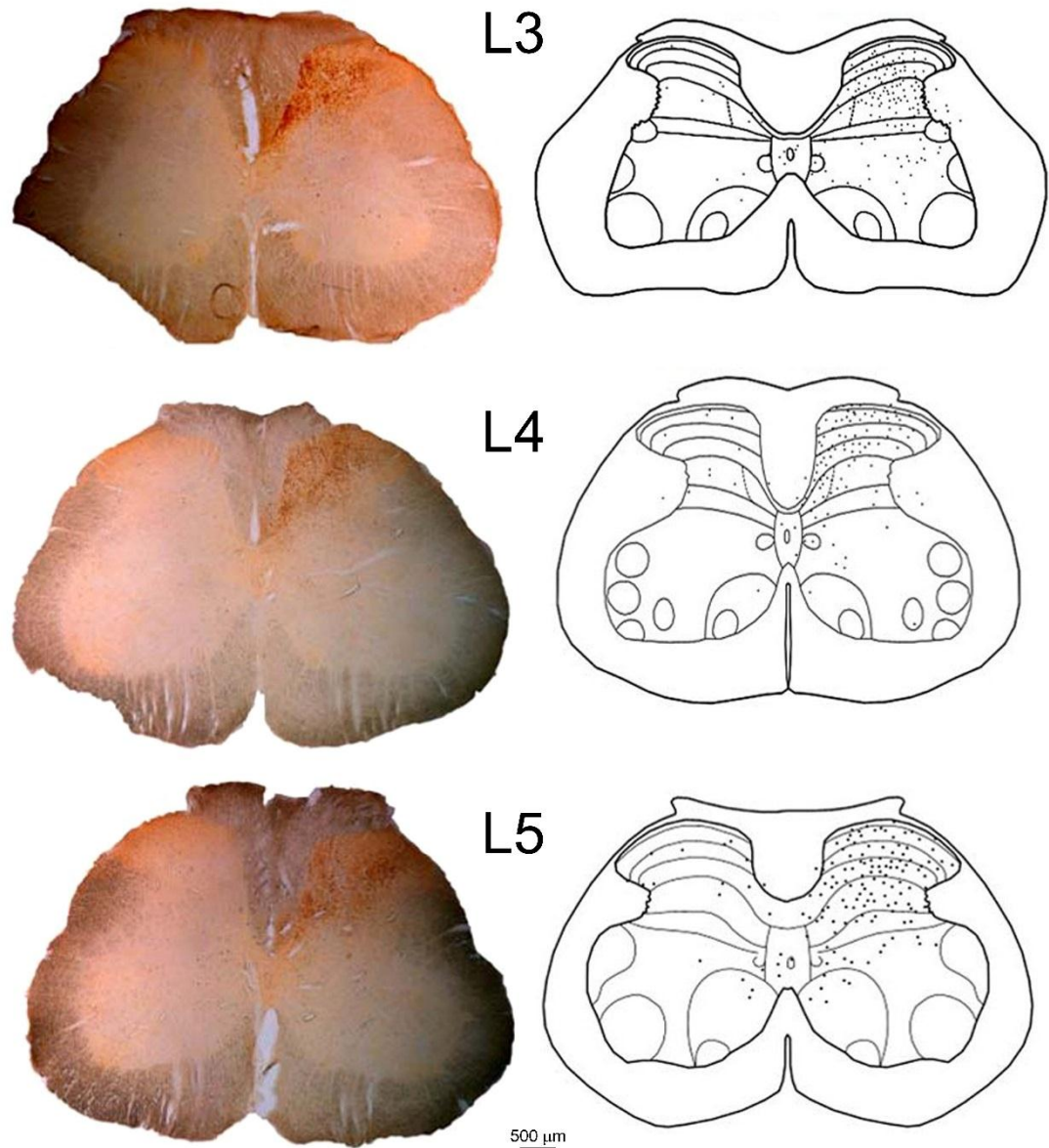


Figure 4.6 Distribution of labelled terminals from the CST

Labelled terminals in the lumbar cord were revealed with DAB shown on the left. The notch is ipsilateral relative to the injection site (notch not visible in L5 section). The drawings on the right show the distribution of terminals superimposed onto standard L3, L4 and L5 transverse sections (based on Molander et al., 1984). Terminals were plotted from 60 µm thick sections.

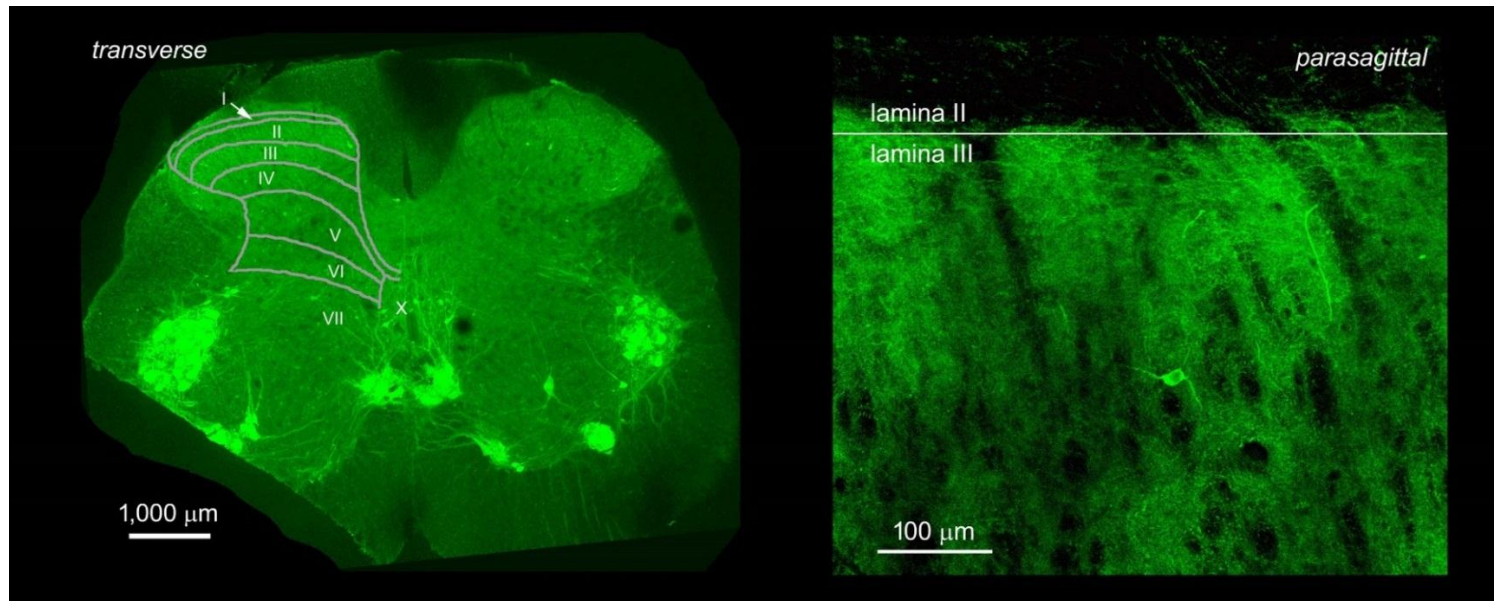


Figure 4.7 ChAT neurons revealed in an L4 transverse and parasagittal section

Confocal microscopy images of neurons immunoreactive to antibody against ChAT (green) revealed in a low-power L4 transverse (left) and parasagittal section (right) scaled at an order of magnitude difference. A standard transverse template (based on Molander's scheme) was superimposed onto the transverse image with laminae I - VII and X boundaries demarcated. A laminar map was superimposed onto the parasagittal image with the laminae II / III boundary demarcated by the horizontal line. Lamina II corresponds to the substantia gelatinosa layer which appears slightly translucent and the dense plexus of ChAT dendrites are visible in lamina III (parasagittal plane). Note that the somata of motoneurons in the ventral horn (transverse plane) were considerably larger than other immunoreactive somata. The transverse section is ventrally notched (far left-hand side).

4.3.2 Aim 2. To identify the neurotransmitter phenotype of CST axons in lower lumbar segments

To investigate the neurochemical properties of glutamatergic terminals descending from the CST, sections from three animals were reacted with a combination of antibodies against CTb, VGLUT1 and VGLUT2 (Table 4.1). A total of 1227 axon terminals from the CST within the grey matter of lower lumbar segments were analysed. Congruent with the hypothesis, VGLUT1 was contained in 98.99% (± 0.18) of labelled axons with a negligible VGLUT2 content of 1.01% (± 0.18) as shown (Appendix 4 Table 1).

To verify that CST axons were not immunoreactive to VGAT, section from three animals were reacted with a combination of antibodies against CTb, VGAT and a mixture of VGLUT1 and VGLUT2 raised in the same species (g. pig) such that these two antibodies reacted with the same secondary antibody (Table 4.1). Throughout this chapter, this antibody mixture will be denoted as [VGLUT1 + VGLUT2]. A total of 881 axons from the CST within the grey matter of lower lumbar segments were analysed. [VGLUT1 + VGLUT2] was contained in 100% of labelled axon with no VGAT present as shown (Appendix 4 Table 2). Immunofluorescent confocal microscope images from these reactions are shown (Figure 4.8).

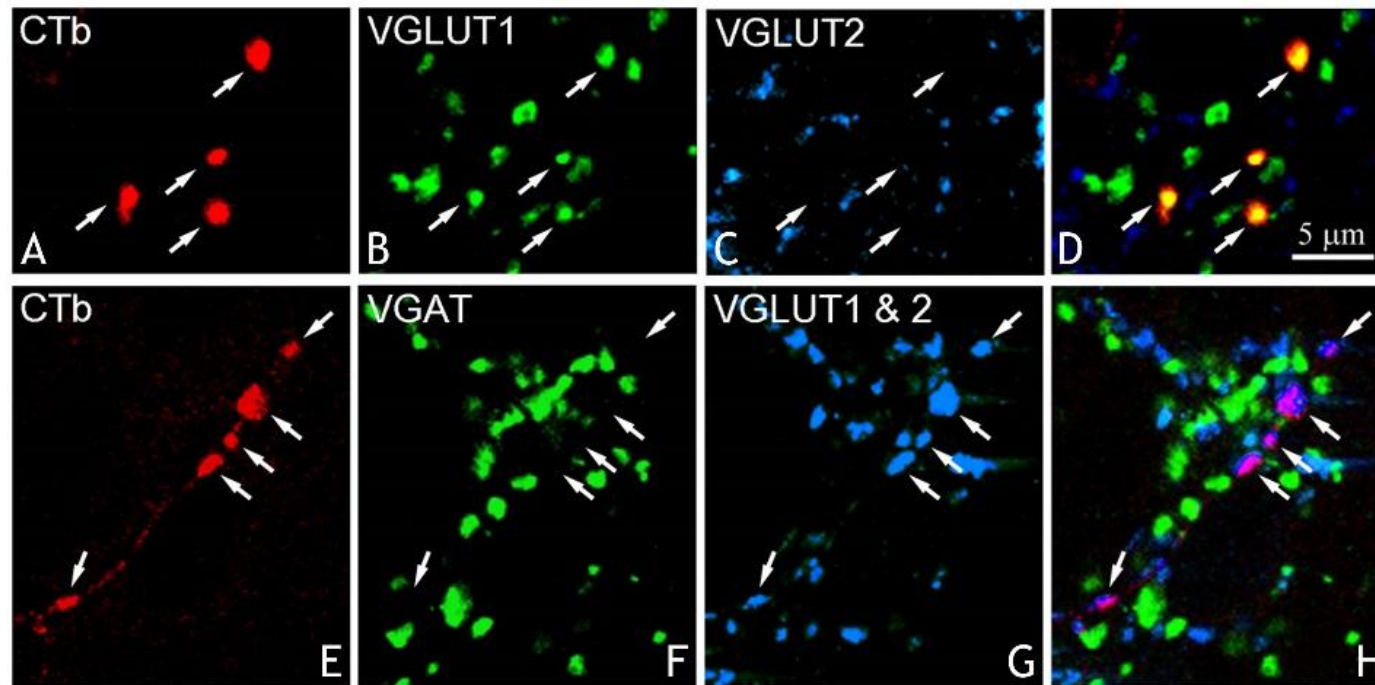


Figure 4.8 Immunoreactive CST axon terminals

In single optical planes, immunoreactive CTb terminals (A) were positive for VGLUT1 (B) and negative for VGLUT2 (C) as shown in yellow in the merged image (D). Immunoreactive CTb terminals (E) were negative for VGAT (F) and positive for combined VGLUT1 and VGLUT2 (G) as shown in magenta in the merged panel (H). Note that all labelled terminals are glutamatergic.

4.3.3 Aim 3: To investigate immunoreactive contacts onto ChAT interneurons receiving input from the CST across laminar boundaries

4.3.3.1 Transverse plane

To investigate the neurochemical properties of contacts onto reconstructed interneurons, transverse sections from three animals were reacted with a combination of antibodies against CTb, VGLUT1 and ChAT (Table 4.1). A total of 63 reconstructed cells in the grey matter of lower lumbar segments were examined (Appendix 4 Tables 3, 4, and 5). There were sparse descending inputs from the sensorimotor cortex onto ChAT interneurons in the dorsal horn and fewer in the intermediate laminae. A representative image from confocal microscopy is shown (Figure 4.9).

The two sources of inputs onto ChAT interneurons were reported as total VGLUT1 contacts and then CTb contacts containing VGLUT1 (CTb⁺VGLUT1). ChAT interneurons were classified according to their laminar location and were reported accordingly to their surface densities. ChAT interneurons received more CST contacts in dorsal laminae I - V than those in the intermediate laminae VI, VII and X (Figure 4.10).

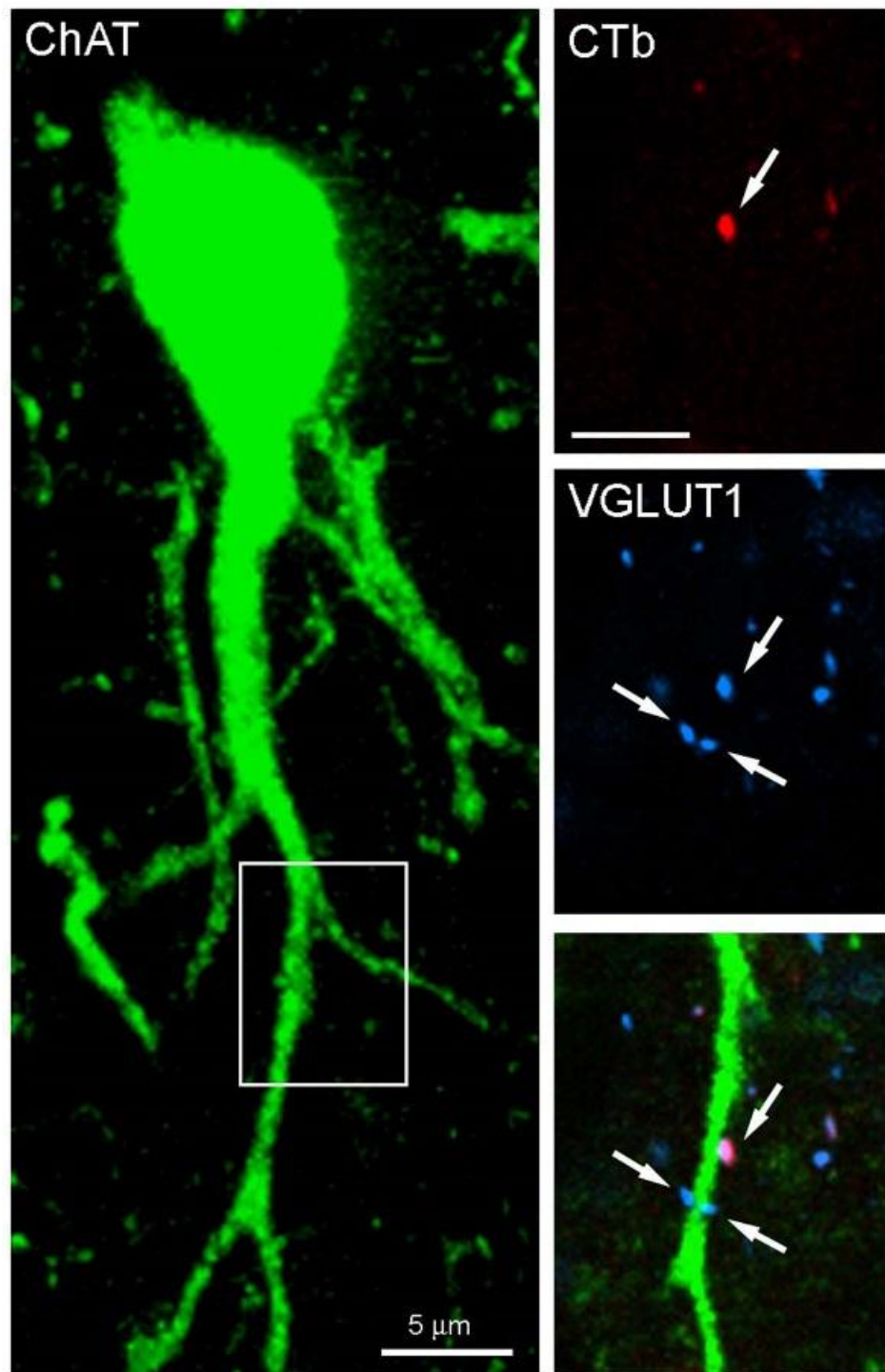


Figure 4.9 CST inputs onto ChAT interneuron in the transverse plane

Cholinergic interneuron (green) in lamina X from a transverse section shown as a projected image. From the inset box, the right-hand side vertical panel detail in separate colour channels shows a dendrite receiving a VGLUT1⁺CTb contact (magenta) and two more distal VGLUT1 contacts (blue). All scale bars = 5 μm.

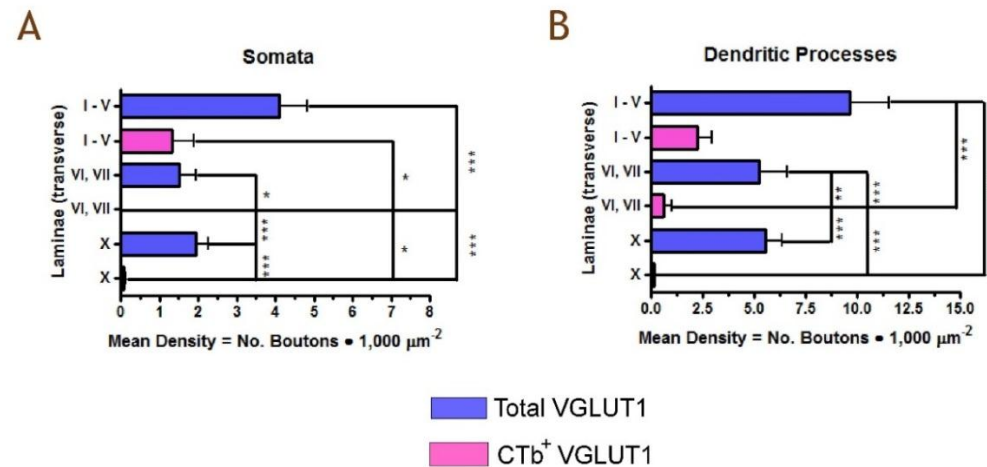


Figure 4.10 Neuronal densities of ChAT interneurons receiving CST input across transverse laminar boundaries

Cholinergic interneurons were classified according to their laminar location. Each coloured bar represents mean densities of interneurons populating dorsal and intermediate laminae as indicated along the Y axes, standard error bars shown. In the transverse plane, horizontal bars represent the horizontally stacked laminae based upon Molander's scheme. Somata (A) and dendritic processes (B) in the dorsal horn received more CST contacts (magenta bars) than those in intermediate laminae and all processes received VGLUT1 contacts (blue bars). Lamina X received sparse innervation from the CST but VGLUT1 densities were significantly greater than in intermediate laminae. Kruskal-Wallis with Dunn's multiple comparison's *post hoc* (* $p < 0.05$, ** $p < 0.01$, *** $p < 0.001$). $N = 3$ animals. Laminae I-V (15 cells): somata, 54 total VGLUT1 contacts and 37 CTb⁺VGLUT1 contacts; dendrites, 74 total VGLUT1 contacts and 58 CTb⁺VGLUT1 contacts. Laminae VI-VII (17 cells): somata, 32 total VGLUT1 contacts and 0 CTb⁺VGLUT1 contacts; dendrites, 43 total VGLUT1 contacts and 4 CTb⁺VGLUT1 contacts. Laminae X (32 cells): somata, 64 total VGLUT1 contacts and 3 CTb⁺VGLUT1 contacts; dendrites, 70 total VGLUT1 contacts and 3 CTb⁺VGLUT1 contacts.

4.3.3.2 Parasagittal plane

To further investigate the neurochemical properties of contacts onto reconstructed interneurons in the parasagittal plane, the same antibody combination (Table 4.1) was performed on tissue from three animals with labelled CST axons. Dendritic processes from this experiment were fully visualised for reconstruction with slightly greater sampling in intermediate zones and therefore slightly larger somatic radii are reported. From this experiment, a total of 35 fully reconstructed cells in the grey matter of lower lumbar segments were examined (Appendix 4 Tables 6, 7, and 8) and a representative confocal microscopy image is shown with an accompanying reconstruction (Figure 4.11).

ChAT interneurons received more CST contacts dorsally but unlike dendritic processes investigated in the transverse plane, there were slightly more inputs found on interneurons in intermediate laminae VI, VII and X. To compare results between the transverse and parasagittal experiments, the axes representing mean densities are scaled identically for dendritic processes and then for the soma (Figures 4.12).

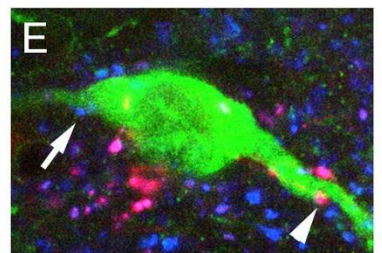
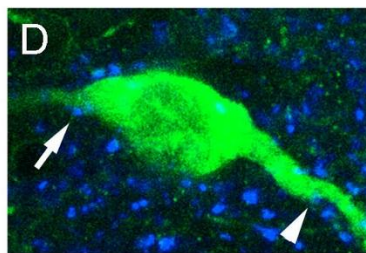
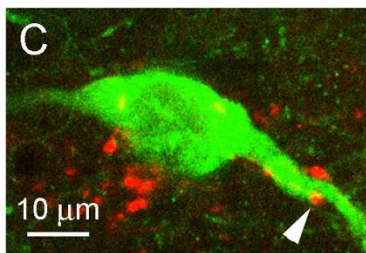
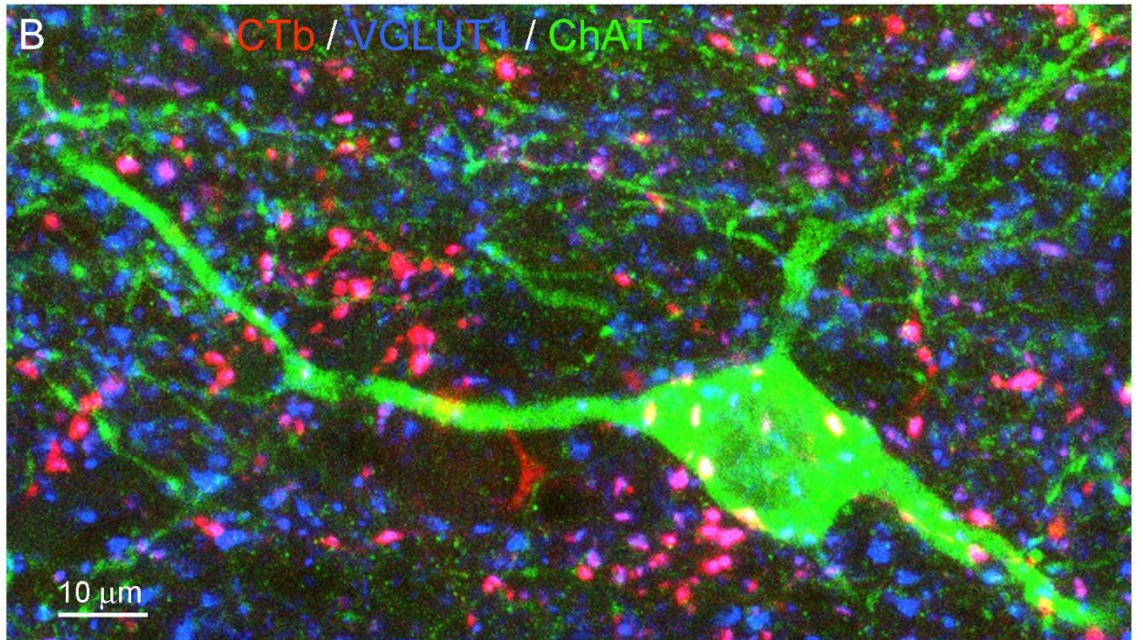
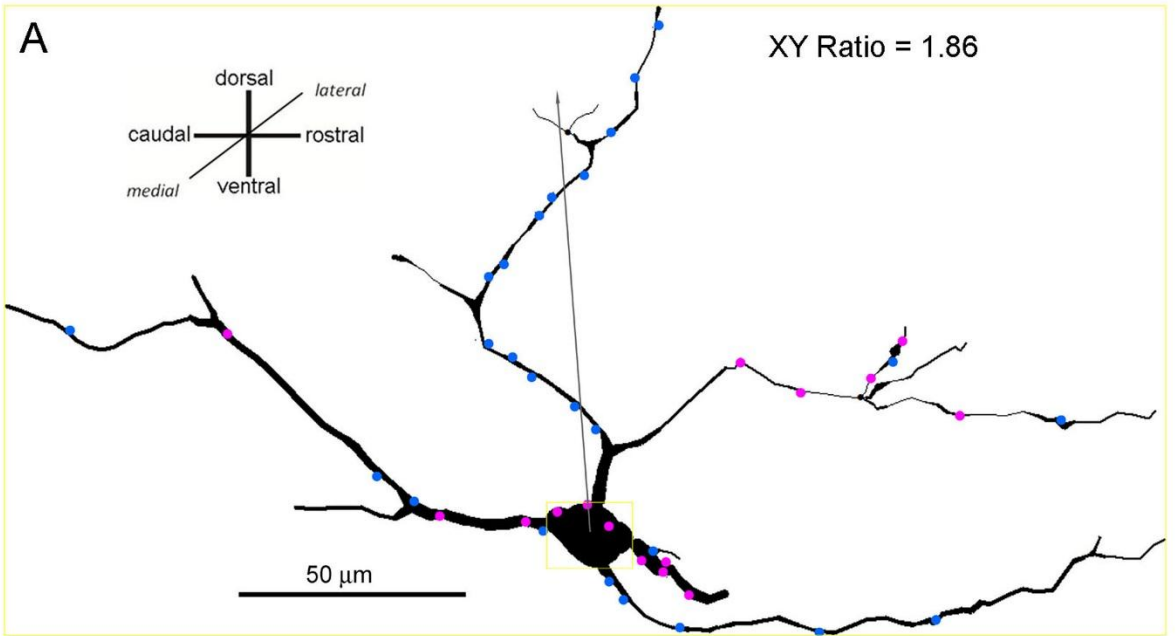


Figure 4.11 ChAT interneuron in laminae III / IV of an L4 spinal segment in the parasagittal plane

Three dimensional reconstruction in the parasagittal plane (A) with VGLUT1⁺CTb boutons (magenta) and VGLU1 boutons (blue) shown. The dimensionless XY Ratio relates the linear rostrocaudal (X) and dorsoventral (Y) parameters. The grey vector arrow denotes the dorsocaudal orientation, derived from the soma's geometric centre to the interneuron's geometric centre. Projected confocal microscope image (B) showing the neurochemical properties of the ChAT interneuron (green) receiving inputs descending from the CST (red) enriched with VGLUT1 (blue). In single optical planes, inset boxes show a CTb labelled terminal (C) and a VGLUT1 bouton (D). The merged image (E) shows this CTb marker coinciding with VGLUT1 (magenta) in three colour channels.

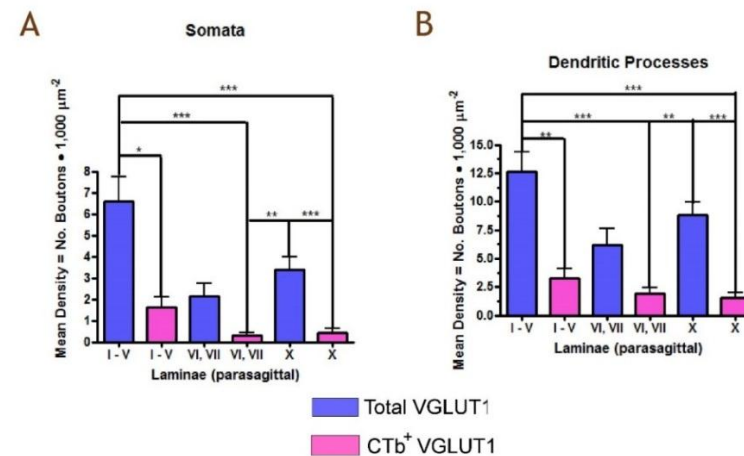


Figure 4.12 Neuronal densities of ChAT interneurons receiving CST input across parasagittal laminar boundaries

ChAT interneurons were classified according to their laminar location. Each coloured bar represents mean densities of interneuronal populations found in dorsal and intermediate laminae, standard error bars shown. In the parasagittal plane, vertical bars represent the stacked laminae based upon Molander's scheme. Somata (A) and dendritic processes (B) in the dorsal horn received more CST contacts (magenta bars) than those in intermediate laminae and all processes received VGLUT1 contacts (blue bars). The CST targeted dendritic processes (B) in intermediate laminae and near the central canal rather than somata (A) with significantly greater contact densities. Kruskal-Wallis with Dunn's multiple comparison's *post hoc* (* $p < 0.05$, ** $p < 0.01$, *** $p < 0.001$). $N = 3$ animals. Laminae I-V (12 cells): somata, 78 total VGLUT1 contacts and 19 CTb⁺VGLUT1 contacts; dendrites, 222 total VGLUT1 contacts and 48 CTb⁺VGLUT1 contacts. Laminae VI-VII (9 cells): somata, 33 total VGLUT1 contacts and 5 CTb⁺VGLUT1 contacts; dendrites, 95 total VGLUT1 contacts and 30 CTb⁺VGLUT1 contacts. Laminae X (14 cells): somata, 64 total VGLUT1 contacts and 7 CTb⁺VGLUT1 contacts; dendrites, 160 total VGLUT1 contacts and 23 CTb⁺VGLUT1 contacts.

4.3.4 Aim 4: Classification of ChAT dendritic orientations as related to their contact densities

To investigate the relationship of neuronal geometry to contact densities, reconstructed ChAT interneurons were classified according to their predominant dendritic orientation indicated by resultant vectors (Figures 4.13, 4.14 and 4.15). The population of dorsoventral cells (XY Ratio < 1) having dendrites situated mostly dorsocaudally from their soma had greater total mean combined contact density from VGLUT1 and VGLUT1⁺CTb (2.94 per 1,000 $\mu\text{m}^2 \pm 0.83$). In comparison, dorsorostrally orientated cells had just slightly lesser mean densities (1.76 per 1,000 $\mu\text{m}^2 \pm 0.64$). Ventrorostrally orientated cells (1.10 per 1,000 $\mu\text{m}^2 \pm 0.39$) and dendrites situated predominantly ventrocaudally had the fewest mean contact densities (0.94 per 1,000 $\mu\text{m}^2 \pm 0.17$) (Appendix 4 Table 9).

For the population of rostrocaudal cells (XY Ratio > 1) with dendrites situated mostly dorsocaudally from their soma had the greatest total mean combined contact densities from VGLUT1 and VGLUT1⁺CTb (1.65 per 1,000 $\mu\text{m}^2 \pm 0.78$). Dorsorostrally orientated cells had just slightly lower mean densities (1.36 per 1,000 $\mu\text{m}^2 \pm 0.48$), then ventrocaudally orientated cells (0.93 per 1,000 $\mu\text{m}^2 \pm 0.47$) and dendrites situated predominantly ventrorostrally had the least mean contact densities (0.84 per 1,000 $\mu\text{m}^2 \pm 0.64$) (Appendix 4 Table 9). While the mean contact densities of these stereologically defined populations did not statistically differ significantly, a qualitative pattern was apparent upholding the hypothesis that the geometric orientation of dendritic arbors relates to input density (Figure 4.15).

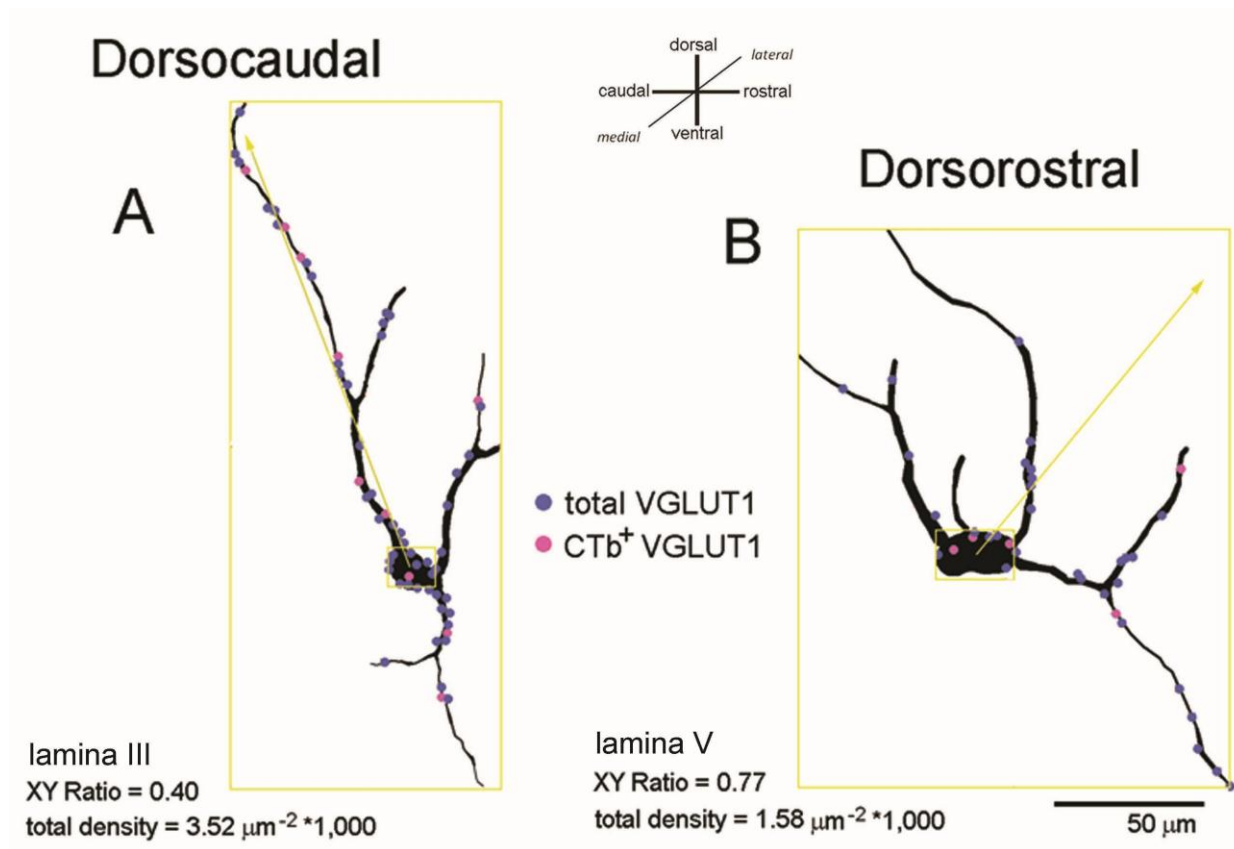


Figure 4.13 Dendritic orientations of reconstructed ChAT interneurons in the parasagittal plane, Part I (Dorsal)

Three dimensional reconstruction of ChAT interneurons in the parasagittal plane with VGLU1 boutons (blue) and VGLUT1⁺CTb boutons (magenta). Dimensionless XY Ratios and total contact densities with laminar locations are reported. To describe how dendritic branches were predominantly situated relative to their soma, there were four possible directional orientations (dorsocaudal, dorsorostral ventrocaudal, ventrorostral). Dorsocaudal (A) and dorsorostral (B) orientations are denoted by gold vector arrows.

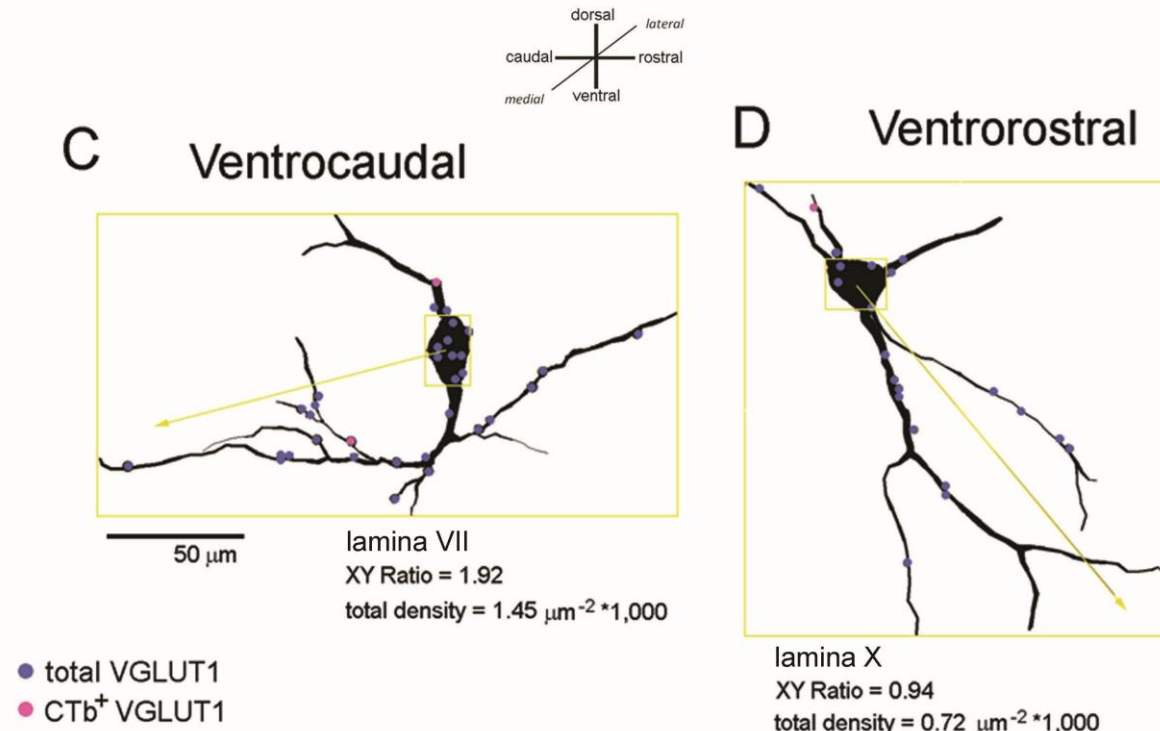


Figure 4.14 Dendritic orientations of reconstructed ChAT interneurons in the parasagittal plane, Part II (Ventral)

Three dimensional reconstruction of ChAT interneurons in the parasagittal plane with VGLU1 boutons (blue) and VGLUT1⁺CTb boutons (magenta). Dimensionless XY Ratios and total contact densities with laminar locations are reported. To describe how dendritic branches were predominantly situated relative to their soma, there were four possible directional orientations (dorsocaudal, dorsorostral ventrocaudal, ventrorostral). Ventrocaudal (C) and ventrorostral (D) orientations are denoted by gold vector arrows.

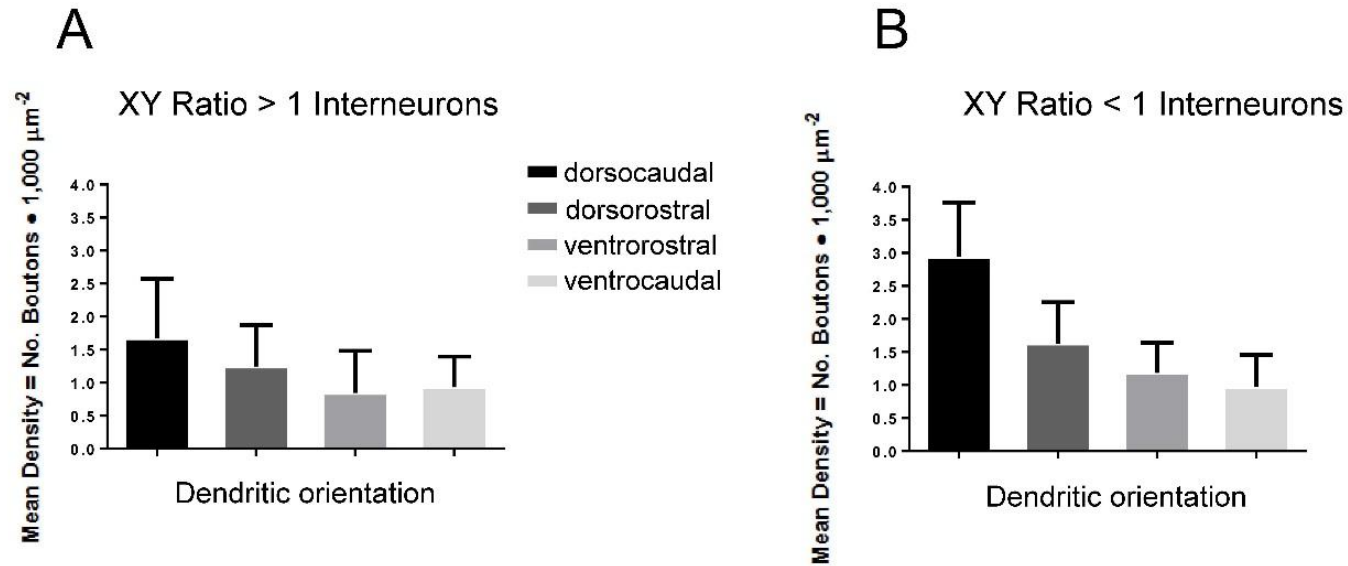


Figure 4.15 Dendritic orientations relative to total contact density in the parasagittal plane

Two populations of ChAT interneurons (XY Ratio > 1, A or XY Ratio < 1, B) were further classified according to the predominant orientation of their dendritic branches. Interneurons having dendrites that branched predominantly dorsocaudally (black bars) had greater total mean contact densities while ventrorostrally and ventrocaudally dendritic arbors were lesser (paler grey bars). This relationship was not statistically significant but qualitatively consistent for both populations (A, B). Kruskal-Wallis with Dunn's multiple comparison's *post hoc* ($ns > 0.05$) for $n = 3$ animals. Standard error bars shown.

4.4 Discussion

4.4.1 Distribution of excitatory descending sensorimotor axons

The greatest density of anterogradely labelled CST terminals was in the dorsal horn contralateral to the injection site, especially in laminae III - VI. While this dorsal pattern of CST axon terminations was hypothesised, there were sparse terminations found in the intermediate zone also, with considerably less in the ventral horn. These findings are consistent with reports from similar studies (Antal, 1984, Brown, 1971, Casale et al., 1988, Valtschanoff et al., 1993). Numerous projections to the superficial dorsal horn were also found, which is also consistent with previous observations (Casale et al., 1988). In rats the principal crossed component descends within the dorsal region of the dorsal white columns (Brosamle and Schwab, 1997, Liang et al., 1991), propagating numerous collateral branches terminating in the dorsal horn and intermediate zone grey matter. Observations from this study show the dorsal column region was strongly labelled with the CTb tracer.

Findings from this ICC study demonstrates that the descending CST is homogeneously excitatory via VGLUT1 as hypothesised. A negligible few labelled terminals contained VGLUT2 and no terminals contained VGAT. Consistent with observations from this study, VGLUT1 is known to be most abundant in laminae III - IV and medial lamina V. The distribution pattern of axons containing VGLUT1 supports the idea that this transporter is responsible for glutamatergic uptake from cutaneous and muscle mechanoreceptors synapses (Alvarez et al., 2004). Alvarez et al. (2004) reports that the interpretation of immunopositive boutons is complicated because of the existence of significant metabolic pools of glutamate and glutaminase that are unrelated to neurotransmission (De Biasi and Rustioni, 1990, Storm-Mathisen et al., 1995). However, synaptic terminals of spinal sensory afferents are strongly immunoreactive for glutamate, which suggests a glutamatergic function (Broman, 1993, De Biasi and Rustioni, 1988, De Biasi and Rustioni, 1990, Valtschanoff et al., 1994). VGLUT1 mRNA is also highly expressed in the deep layers of the cerebral cortex where CST neurons are

located (Fremeau Jr et al., 2001, Ni et al., 1994). Then, the CST is an important source of small VGLUT1 varicosities (Persson et al., 2006).

4.4.2 Neuronal targets of descending sensorimotor axon terminals

Results from the present ICC study provided insights into the distribution of primary afferents and CST fibres contacting ChAT interneurons. The dorsal horn population were all richly innervated by VGLUT1, the transporter associated with large diameter myelinated primary afferents (Todd et al., 2003, Varoqui et al., 2002). While the greatest VGLUT1 densities were found in dorsal horn interneurons, the lamina X population notably received considerable VGLUT1 input as well. Across laminar boundaries, VGLUT1 contact densities varied considerably less than did densities from the CST. Descending CST axons sparsely contacted the population surrounding lamina X central canal cluster cells. Data from earlier studies have indicated that primary sensory afferent fibres excite ChAT interneurons and that ACh released by axon terminals of these interneurons modulates sensory information via both pre- and postsynaptic mechanisms (Ribeiro-da-Silva and Cuello, 1990a).

ChAT interneurons are likely components of an inhibitory feedback pathway monosynaptically activated by primary afferents (Olave et al., 2002) and findings from the present study suggest that the CST acts through ChAT interneurons to influence the processing of incoming sensory information. Further, based upon comprehensive findings from electrophysiological investigations in the cat, the monosynaptic action of most descending systems onto their spinal target neurons is excitatory (Jankowska, 1992). The classical form of presynaptic inhibition is associated with primary afferent depolarisation, which is mediated by inhibitory interneurons that form axo-axonic synapses with terminals of primary afferent axons (Rudomin and Schmidt, 1999). Schmidt and collaborator have shown that some pathways mediating primary afferent depolarisation are modality specific. Such findings suggest that the ensuing presynaptic inhibition could play an important role in sensory discrimination by eliminating surplus excitation (Jänig et al., 1967, Rudomin and Schmidt, 1999). The pharmacological action of powerful seizure-inducing GABA receptor antagonists, gabazine, picrotoxin, and bicuculline, can radically alter primary afferent stimulation (Game and Lodge,

1975). Lesions of the CST cause a breakdown in fine sensorimotor control, which implies a deterioration not only in motor function, but also in mechanisms of sensory feedback (Lemon and Griffiths, 2005).

Consistent with findings from the present study, numerous ChAT interneurons are known to populate the superficial dorsal horn, particularly lamina III (Barber, 1984, Borges and Iversen, 1986, Kimura et al., 1981, Phelps et al., 1984). Dendrites are dense in lamina III with fibres and terminals concentrated slightly deeper in laminae III - V (Phelps et al., 1984, Phelps et al., 1988). There is little evidence to suggest that ACh itself is a primary afferent transmitter (Gwyn and Flumerfelt, 1971, Karczmar et al., 1980) since, for instance, spinal cord transection or neonatal capsaicin negligibly effects the expression of ChAT in the dorsal horn (Holzer-Petsche et al., 1986). Although some descending systems can have direct actions on motoneurons (Lemon, 2008) most of their actions are mediated through interneurons (Jankowska, 1992).

Olave and others (2002) investigated the input of unmyelinated primary afferents onto ChAT interneurons by injecting the transganglionic tract tracer *Bandeiraea simplicifolia* isolectin b4 (IB4) into the sciatic nerve in rat. IB4 labels unmyelinated afferent fibres (Finkelstein et al., 1974, Ganser et al., 1983, Goldstein and Winter, 1999, Scott et al., 1990, Trojanowski et al., 1982) by binding predominantly to a subgroup of unmyelinated non-peptidergic primary afferents (Silverman and Kruger, 1990). Primary afferents which bind IB4 formed contacts with ChAT interneurons and axons labelled with IB4 were found to form an obvious plexus in lamina II. Many axons labelled with IB4 are likely to respond to noxious stimuli (Fang et al., 2000) and ChAT cells are known to not possess the substance P receptor (Naim et al., 1997). These findings are congruent with observations that peptidergic afferents form sparse appositions with ChAT cells (Olave et al., 2002).

Some of the inputs to lamina X central canal cluster cells may be derived from primary afferents, since early Golgi studies (Scheibel and Scheibel, 1969) have shown that primary afferent fibres terminate among neurons in lamina X (Barber, 1984). Further, the results of physiological studies indicate that neurons in this region respond with a short latency to action potentials in modality specific cutaneous afferents (Honda and Perl, 1981). Descending CS

fibres play an important role in the selection of sensorimotor patterns via populations of interneurons. While the CST was hypothesised to contact ChAT interneurons, and principally in dorsal laminae, the implications of this systems role in innervating premotor and central canal cluster cells is interesting as sensory inputs may be inextricably linked to motor systems.

4.4.3 Stereologically classified interneuronal populations

Because earlier descriptions of ChAT interneurons mention a preferential rostrocaudal orientation of dendritic arbors (Barber, 1984), immunoreactive tissue containing labelled ChAT interneurons were cut in the parasagittal plane to better reveal dendritic processes for reconstruction and analyses.

Alternatively, horizontal sections would suffice to not compromise dendritic arbors. In the parasagittal plane, interneurons with extensively truncated dendrites were excluded from analyses although inevitably some dendritic branches were not fully revealed in montages of multiple scans. A consideration too is that bending of the superficial layers of the spinal cord may distort the interpretation of the orientation of the dendritic arbor (Cordero-Erausquin et al., 2009). However, very few interneurons from the superficial dorsal horn were included in this study. Findings from this study indicate that the predominant dendritic orientation may be related to the mean contact density of populations of ChAT interneurons, suggesting that the inherent geometry may predict the frequency of primary afferent inputs. In sum, dendritic arbors located predominantly dorsally and/or caudally relative to their soma tended to have greater inputs.

Mesnager et al. (2011) observed that the somata of ChAT interneurons located in lamina III had dendritic processes that were significantly asymmetrical and that the preferentially dorsally directed processes displayed an extensive rostrocaudal spread in lamina II interneurons (Yasaka et al., 2010), which accounts for how such a sparse population of neurons can be a major contributor to the dense lamina III ChAT plexus. The orientation of dendritic arbors is proven to be an important distinguishing feature and between neurons, the orientation of dendritic arborisation patterns varies systematically (Grudt and

Perl, 2002) yet the mechanism determining these patterns of synaptic connections onto spinal interneurons are uncertain (Mentis et al., 2006). Analysis of connectivity between ChAT partition cells and motoneurons have revealed that the existence of ipsilaterally and bilaterally projecting populations, both with widespread rostrocaudal segmental origin, and the latter with preferential connectivity to equivalent motoneurons bilaterally (Stepien et al., 2010).

The present study has demonstrated heterogeneous dendritic branching patterns across laminar regions. A proposed function of dendritic processes is to integrate neurochemical information (Hume and Purves, 1981). Based upon previous comparative studies of dendritic complexity in neonatal and adult ganglion neurons (Purves and Hume, 1981), the matching of neuronal geometric properties and innervation patterns occur postnatally (Hume and Purves, 1981). During development, descending CST terminals compete with each other for synaptic space on spinal neurons and more active terminals are competitively able to secure more synaptic space. Such early synaptic activity may be attributed to the refinement of CS connections (Martin, 2005), even before adaptive motor behaviours are expressed (Lawrence and Hopkins, 1976, Martin, 1985).

Chapter 5. Targets of the descending reticulospinal pathways

5.1 Introduction

Distinct populations of spinal neurons with specific functions can be identified based on their common features of transmitter/receptor expression patterns, morphology, connectivity and their membrane properties. Many medullary raphé neurons receive convergent inputs related to multiple spinal systems, which suggests they may serve compound functions (Mason, 2001). In lower lumbar spinal segments, populations of descending RetS axon terminations are known to be a neurochemically heterogeneous; the majority of axons express VGLUT2 while a smaller proportion express VGAT (Du Beau et al., 2012).

Modulatory influences on neuronal output and locomotion are mediated by sets of ChAT interneurons that elicit a diverse array of postsynaptic responses (Zagoraïou et al., 2009) yet the neurochemical properties of descending systems targeting these cell populations remain largely unknown. Among the identified groups of ChAT interneurons (Barber, 1984) that show especially strong ChAT immunoreactivity are central canal cluster cells populating lamina X and partition cells in the intermediate zone that extends medially from lamina X towards the lateral edges of the grey matter (see Barber, 1984).

Many ChAT interneurons in the rat spinal cord are known to contain NOS (Spike et al., 1993). The enzyme NADPH diaphorase, which is known to be present in the brain (Thomas and Pearse, 1964) and many spinal neurons, is considered to correspond to NOS and several histochemical studies have mapped the distribution of these neurons (Bredt et al., 1991a, Mizukawa et al., 1989, Valtschanoff et al., 1992, Vincent and Kimura, 1992). The neuronal form of nitric oxide, nNOS, is the enzyme responsible for synthesis of gaseous nitric oxide by neurons (see Tricoire and Tania, 2012). Pharmacological studies suggest that NOS may be involved in transmission in sympathetic ganglia (Briggs, 1992) and also in somatosensory processing (Haley et al., 1992, Kitto et al., 1992, Meller et al., 1992a, Meller et al., 1992b, Moore et al., 1991).

Brainstem neurons implicated in the initiation of locomotion include serotonergic, dopaminergic, noradrenergic, and glutamatergic neurons which give rise to descending tracts (Jordan et al., 2007). Endogenous 5-HT contributes to the development of spinal locomotor circuits (Branchereau et al.,

2002, Cazalets et al., 2000, Pflieger et al., 2002). Besides these long-term trophic effects, further studies have shown that monoamines can elicit rhythmic spinal cord activity with a locomotor-like pattern (Alford et al., 2003, Jordan and Schmidt, 2002b, Rossignol et al., 2002). 5-HT is considered to be a pivotal modulator of spinal motor networks. By engaging diverse 5-HT receptor subtypes at both the pre- and postsynapse, locomotor rhythm is effectively stabilised (Grillner and Jessell, 2009). Data from studies of neonatal mouse preparations suggest that activation of dopaminergic receptors, either by endogenous DA or by 5-HT, contributes to the effectiveness of 5-HT induced locomotor-like activity (Madriaga et al., 2004) and such findings are consistent with the proposal that release of multiple monoamines, i.e., 5-HT, DA and NA, can evoke and/or modulate coordinated locomotion (Jordan and Schmidt, 2002b).

Most, if not all, DA terminals in the spinal cord are thought to arise from the A11 cell group of the hypothalamus (Björklund and Skagerberg, 1979, Qu et al., 2006, Skagerberg and Lindvall, 1985) yet the role of these A11 cell groups in the initiation of locomotion has not been explicitly tested (Jordan et al., 2007). Adrenaline is released by the adrenal medulla and NA is then synthesised from DA by DBH, binding to adrenergic receptors (Creese and Iversen, 1975). In subcortical regions, ChAT interneurons regulate the output of dopaminergic pathways implicated in sensorimotor learning, action selection and reward (Joshua et al., 2008, Maskos et al., 2005, Mena-Segovia et al., 2008, Wang et al., 2006). The pharmacological receptor subtypes mediating the actions of NA and 5-HT are notable. Findings from intracellular recordings in the rat spinal cord suggest that NA may inhibit nociceptive input by increasing the potassium conductance of neurons (North and Yoshimura, 1984). NA and 5-HT released by descending monoaminergic neurons may differ in the potency with which they depress transmission from afferents to different functional types of neurons. This depression may involve different membrane receptors at different locations (Bras et al., 1990). In the dorsal horn (Lu and Perl, 2007), intermediate zone and ventral horn, transmission of NA may be depressed principally through activation of the α_2 adrenergic receptor (Bras et al., 1990). However, evidence from pharmacological studies indicate that the excitatory effects of NA may occur through activation of the α_1 adrenergic receptor (Lu and Perl, 2007).

In the spinal cord, DA can also elicit locomotor-like activity in isolated neonatal preparations (Jiang et al., 1999, Kiehn and Kjaerulff, 1996, Madriaga et al., 2004, Whelan, 1996) although specific dopaminergic neurons that give rise to a descending pathway involved in the initiation of locomotion have not been identified (Jordan et al., 2007). Because the activity of the motor output system is controlled by the cohort of premotor neurons, the last-order neurons establishing direct synaptic connections, understanding the connectivity rules of defined premotor interneurons to functionally distinct motoneurons is essential for understanding how the motor output system is organised (Stepien et al., 2010).

It is hypothesised that axons descending from the MLF and CVLM will contact ChAT interneurons and with different input densities across laminar boundaries in lower lumbar spinal segments. At least some ChAT interneurons are expected to express nNOS in intermediate zones and these cells are hypothesised to receive input from 5-HT and NA. MLF axons are hypothesised to contact ChAT interneurons bilaterally across intermediate laminar boundaries as visualised in the horizontal plane. In order to investigate the neuronal targets of descending axons labelled anterogradely from the RetST CVLM and MLF and the role of monoamines within the spinal cord, a series of immunoreactions were conducted with subsequent analyses. The experiments addressed the following aims:

To identify the neurochemical content of contacts onto ChAT interneurons from descending CVLM axons across laminar boundaries in the transverse plane

To investigate the contacts onto intermediate zone interneurons innervated by the MLF in the horizontal plane

To determine the relationship of ChAT::nNOS interneurons in laminae VI, VII and X with 5-HT

To qualitatively compare ChAT interneurons receiving modulatory input from monoamines in the parasagittal plane

5.2 Methods

5.2.1 Image acquisition and analyses

For the following series of experiments, spinal cord tissue from four rats receiving CTb injections into the CVLM and three rats receiving CTb injections into the MLF were processed for analyses (Appendix 1 Figures 1 and 2). Additionally, processed tissue was used from one naïve Sprague Dawley rat with no injection site (Table 5.1). Medullary axons contacting spinal neurons were traced anterogradely using CTb and their neurotransmitter content was established using ICC techniques. Laboratory techniques, image acquisition and statistical analyses were consistent with methods as outlined in previous Chapters 2, 3, and 4. The distribution of the experimental data was determined by the *a priori* D'Agostino & Pearson omnibus normality test so that the appropriate statistical analyses were chosen.

To represent the horizontally stacked laminae in the transverse plane, bar graphs are displayed horizontally while bar graphs from the experiment conducted in the horizontal plane are represented vertically. Scholl analyses was used as a method to investigate the morphology of interneurons using NeuroLucida software. For any interneuron, the total diameter in μm units was found by drawing an outer concentric circle or 'shell' that encompassed the length of all dendritic processes. An inner shell was then drawn at half this calculated diameter to delineate proximal (inner) and distal (outer) dendritic locations. Immunoreactive contacts were counted as proximal or distal depending on whether they were situated inside or outside of this inner concentric shell.

To investigate the relationship between interneurons immunoreactive to ChAT and nNOS, sections were scanned using a different confocal microscopy method such that interneurons immunoreactive to ChAT fluoresced at 488 nm (green) and nNOS interneurons fluoresced at 410 nm and emitted at 455 nm (blue) within the ultra-violet visible (UV vis) range. Interneurons expressing both ChAT and nNOS, designated as ChAT::nNOS interneurons, were detected at both

wavelengths within the same focal planes and soma and proximal dendrites assumed the same shape (see Figures 2.6 and 2.7). A series of confocal microscopy scans were taken at low-power (x20) with a zoom factor of 1 with a 2 μm z-separation and immunoreactive interneurons within scan fields were counted using Neuroludica software. A 20x20 μm grid was superimposed over the image stacks. To avoid bias stacks were visualised in the green channel first such that only ChAT immunoreactivity was shown. Approximately one soma per grid cell was counted (depending upon the given scan field) and then each counted soma was evaluated again separately in the blue channel to assess whether the given soma also expressed nNOS. To accurately determine the laminar location of soma, semi-opaque standard templates of transverse spinal cord segments (based on Molander et al., 1984) were overlaid onto scanned images as necessary.

5.2.2 Laminar boundaries in the horizontal plane

To determine the laminar location of spinal neurons, accurate laminar maps are necessary. Standard transverse templates based upon Molander's scheme are advantageous since they can be consistently applied to all sections within a given lumbar segment. Like tissues sectioned parasagittally (see Chapter 4), laminar boundaries in the horizontal plane were undefined since each cut section is different and there was no consensual template. Based upon standard transverse templates, I derived laminar boundary maps for L3, L4 and L5 segments cut in the horizontal plane at 120 μm increments where intermediate 60 μm increments can be readily interpolated as well. A square grid was superimposed over standard transverse templates. Scaled 'cuts' at 120 μm increments represent how the segment is sectioned from the most superficial dorsal horn as the Vibratome blade then progressively cuts in the ventral direction towards the chuck (see Chapter 2). Coordinates were plotted along the horizontal axes corresponding to the transverse laminar boundaries and then extrapolated into the horizontal plane as vertical lines. These horizontal templates served as 'maps' of the scanned images and scaled semi-opaque templates were overlaid onto scaled as necessary. Unlike the parasagittal laminar maps, I observed that several laminar boundaries were not as clearly delineated. That is, some cuts straddled borders diagonally and were comprised of more than one lamina and/or layers of white matter (Figure 5.1).

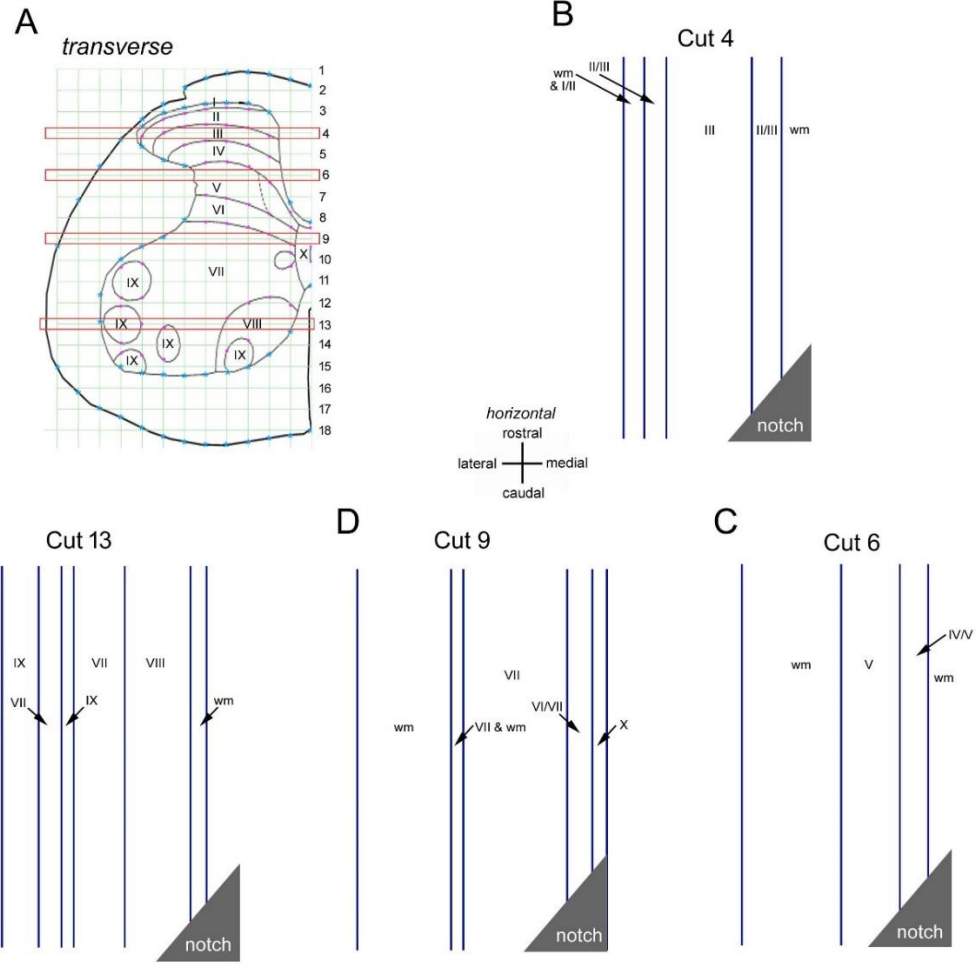


Figure 5.1 Laminar boundaries in the horizontal plane

An exemplary L4 transverse template hemisphere (based on Molander et al., 1984) is shown (A) with a superimposed square grid at 120 μm increments designated as 'cuts' such that that Cut 1 is 120 μm from the most superficial dorsal white matter, progressing ventrally. For the following study, tissue sections examined in the horizontal plane were bilateral and only sections from intermediate zone laminae were collected; the figure shown is bilateral to illustrate the horizontal plane. As an example of the established laminar maps, Cuts 4, 6, 9 and 13 are highlighted (red narrow horizontal rectangles), with the plotted horizontal coordinates extrapolated into the horizontal plane as shown in B, C, D and E, respectively, shown as blue vertical lines. Sections were notched caudally, indicated by the corner grey triangles, to accurately orientate the sections mounted onto slides. Note that a few of the horizontal cuts contained 'mixed' laminae (B and D); for instance the lateral edge of Cut 4 (B) contains both white matter (wm) and laminae I / II within one 120 μm cut increment.

Aim	Primary antibody combinations		Supplier	Secondary antibodies		Sequential immunoreaction
		Concentrations			Concentrations	
1	mo. CTb	1:250	A. Wilkström, University of Gothenburg	Rh Red	1:100	
	rbt. VGLUT2	1:1,000	Synaptic Systems, Göttingen Germany	Dyl 649	1:500	
	gt. ChAT	1:100	Millipore, Harlow UK	Alexa 488	1:500	
1	mo. CTb	1:250	A. Wilkström, University of Gothenburg	Rh Red	1:100	
	rbt. VGAT	1:1,000	Synaptic Systems, Göttingen Germany	Dyl 649	1:500	
	gt. ChAT	1:100	Millipore, Harlow UK	Alexa 488	1:500	
2, 3	mo. CTb	1:250	A. Wilkström, University of Gothenburg	Rh Red	1:100	
	rat 5-HT	1:100	Affiniti, Exeter UK	Cy5	1:500	
	gt. ChAT	1:100	Millipore, Harlow UK	Alexa 488	1:500	
	rbt. nNOS	1:5,000	Millipore, Harlow UK	Biotinylated IgG	1:500	AvPB (1:1,000)
4	rbt. 5-HT	1:250	Affiniti, Exeter UK	Rh Red	1:100	
	mo. DBH	1:500	Millipore, Harlow UK	Dyl 649	1:500	
	gt. ChAT	1:100	Millipore, Harlow UK	Alexa 488	1:500	

Antibodies diluted in 0.3% PBST

mo. = mouse; rbt. = rabbit; gt. = goat

Table 5.1 Summary of primary and secondary antibody combinations and concentration

All secondary antibodies were raised in donkey and conjugated to biotin, Rh Red, Dyl 649, Cy5 (supplied by Jackson ImmunoResearch, West Grove, USA) AvPB, or Alexa 488 (supplied by Molecular Probes, Eugene, USA). Antibody labelling: CTb, traces myelinated axons; VGLUT1 and VGLUT2, synaptic vesicles; VGAT, glycinergic and GABAergic synaptic vesicles; 5-HT, synaptic terminals; ChAT, cholinergic neuronal processes; nNOS, neuronal processes containing nitric oxide synthase; DBH, axons that synthesise NA.

5.3 Results

5.3.1 Aim 1: To identify the neurochemical content of contacts onto ChAT interneurons from descending CVLM axons across laminar boundaries in the transverse plane

CTb was injected into the CVLM of three animals to anterogradely label descending axon terminals in lower lumbar spinal segments sectioned transversely (see Figures 3.3 and 3.5). To investigate the excitatory neurochemical properties of labelled CVLM axons targeting reconstructed interneurons, sections were reacted with a combination of antibodies against CTb, VGLUT2 and ChAT and a total of 57 reconstructed cells in the grey matter of lower lumbar segments were examined (Appendix 5 Tables 1, 2 and 3). Similarly, to investigate inhibitory CVLM axonal targets, transverse sections from three animals were reacted with a CTb, VGAT and ChAT and a total of 61 reconstructed cells were examined. Populations of interneurons were classified according to their location within laminae III-V, VI-VII and X (Appendix 5 Tables 4, 5 and 6). ChAT interneurons were morphologically classified as mediolateral (XY Ratio > 1) or dorsoventral (XY Ratio < 1) according to the elongation of their dendritic branches within spinal laminae (see Figure 4.3). Confocal microscopy images are shown from both experiments (Figures 5.2 and 5.3). The *a priori* D'Agostino & Pearson omnibus normality test indicated that data did not assume a normal distribution and therefore the Kruskal-Wallis with Dunn's multiple comparisons *post hoc* to compare medians.

The majority of descending CVLM axons targeting ChAT interneurons contained VGLUT2. ChAT interneurons receiving excitatory CVLM inputs were found predominantly in laminae VI and VII. Descending glutamatergic CVLM axons preferentially targeted mediolaterally orientated interneurons in all laminae except in lamina X where the densities of dorsoventrally orientated dendritic processes were significantly greater (Figure 5.4). ChAT interneurons receiving inhibitory CVLM inputs were found predominantly in dorsal laminae III, IV and V. However, a considerable portion of mediolaterally orientated dendritic processes near the central canal received inhibitory input and densities were significantly greater than those found in intermediate laminae VI and VII (Figure

5.5). To compare the morphology of CVLM boutons onto ChAT interneurons, Sholl analyses compared mean dendritic densities from these experiments. Significantly, excitatory CVLM boutons containing VGLUT2 were situated on distal dendrites while inhibitory CVLM boutons containing VGAT tended to target proximal dendrites. Glutamatergic CVLM boutons showed the greatest range of target sites onto distal dendrites (Figure 5.6).

As hypothesised, descending CVLM axons did contact ChAT interneurons with considerable variation in input densities across laminar boundaries, with only minor differences between mediolaterally or dorsoventrally orientated interneurons. In particular, lamina X was found to be richly innervated by both excitatory and inhibitory immunoreactive CVLM fibres.

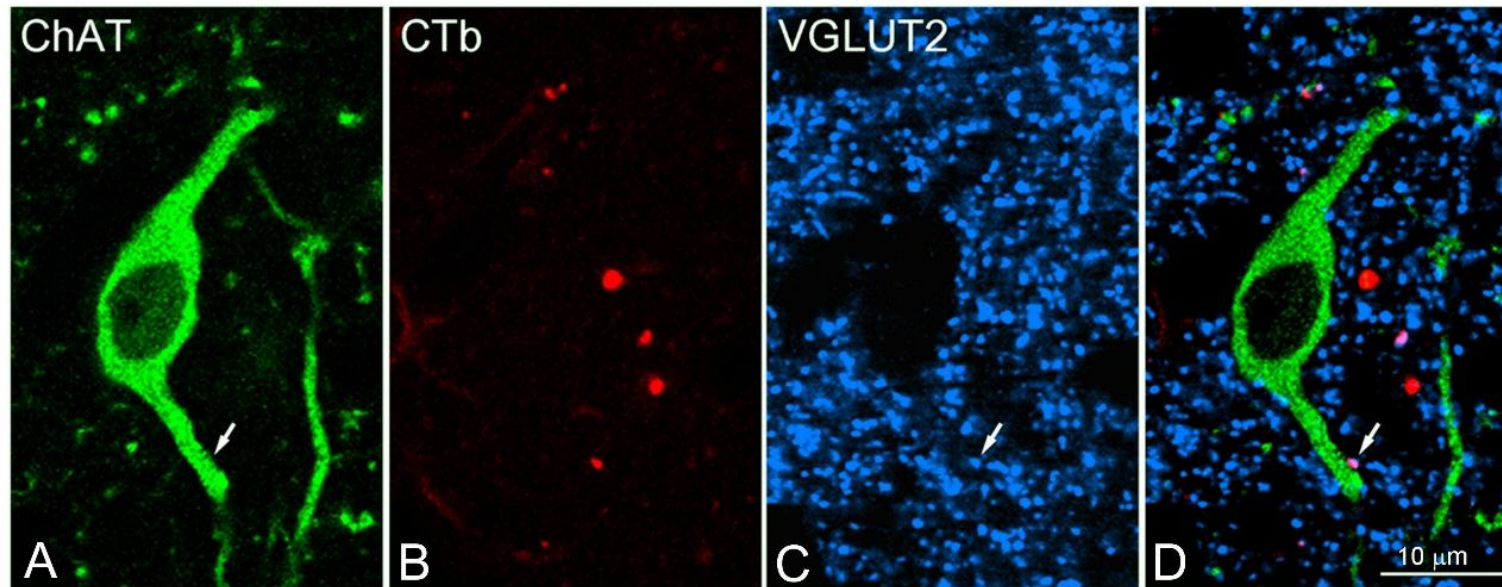


Figure 5.2 ChAT interneuron in lamina VII receiving excitatory CVLM input

Confocal microscopy image of an interneuron immunoreactive to ChAT (A) in a single optical plane. The proximal dendrite (arrow) received descending CVLM input (B) enriched with VGLUT2 (C) as revealed in the merged image (D) denoted by the arrow.

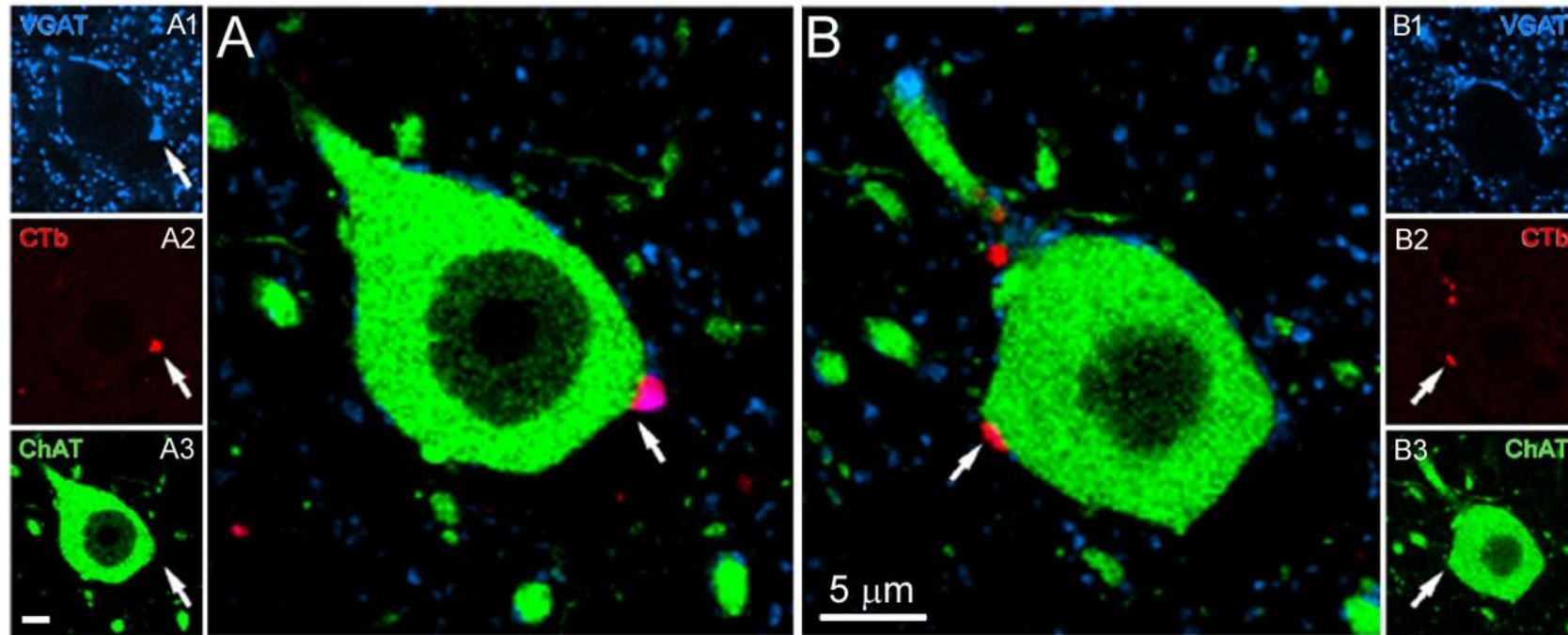


Figure 5.3 ChAT soma receiving inhibitory CVLM input

Confocal microscopy image of a soma immunoreactive to ChAT in lamina X shown in two separate single optical fields (A3 and B3). This soma received both CVLM input enriched with VGAT (A) and a CVLM bouton negative for VGAT (B) as shown in separate colour channels (A1, A2, B1 and B2). All scale bars = 5 μm .

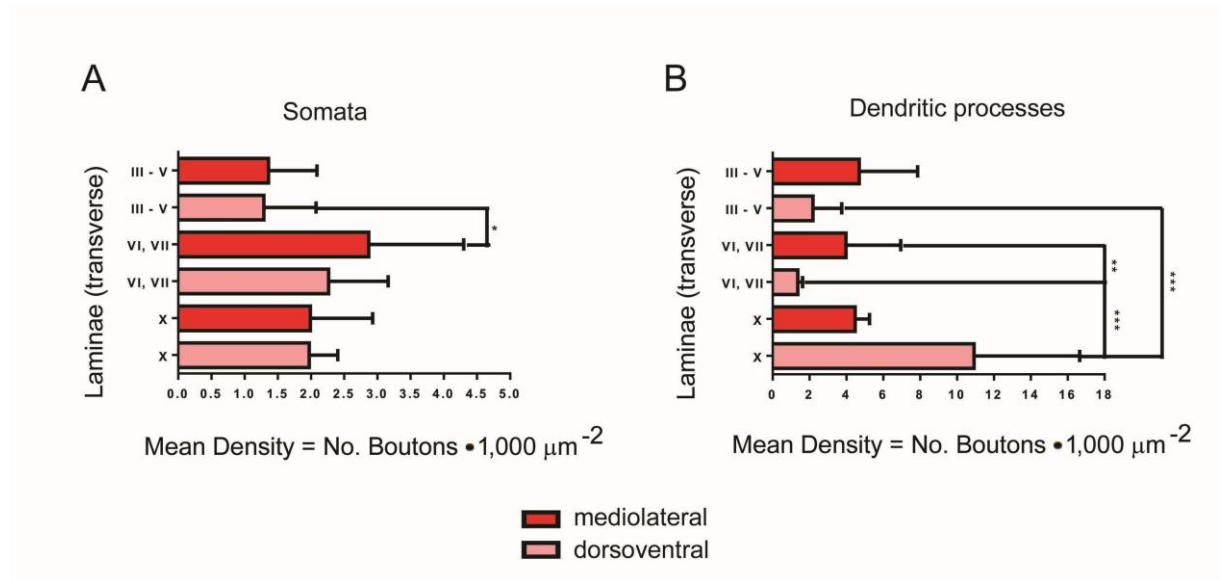


Figure 5.4 Neuronal densities of morphologically defined ChAT interneurons receiving CVLM boutons containing VGLUT2 across transverse laminar boundaries

Cholinergic interneurons were classified according to their morphology in the transverse plane. Each coloured bar represents mean densities of interneurons populating the given laminar region with standard error bars shown. The somata of mediolaterally orientated interneurons (XY Ratio > 1) had significantly greater excitatory densities in the intermediate zone (A). CVLM axons containing VGLUT2 preferentially targeted mediolaterally orientated interneurons in all laminae except lamina X where dorsoventrally orientated dendritic processes (XY Ratio < 1) had significantly greater densities (B). Kruskal-Wallis with Dunn's multiple comparisons *post hoc* (* $p < 0.05$, ** $p < 0.01$, *** $p < 0.001$). N = 3 animals. Laminae III - V (20 cells). somata (A): 42 total CTb contacts, 27 VGLUT2⁺CTb contacts; dendrites (B): 104 total CTb contacts, 65 VGLUT2⁺CTb contacts. Laminae VI-VII (17 cells). somata (A): 120 total CTb contacts, 92 VGLUT2⁺CTb contacts; dendrites (B): 209 total CTb contacts, 112 VGLUT2⁺CTb contacts. Laminae X (20 cells). somata (A): 93 total CTb contacts, 72 VGLUT2⁺CTb contacts; dendrites (B): 167 total CTb contacts, 103 VGLUT2⁺CTb contacts.

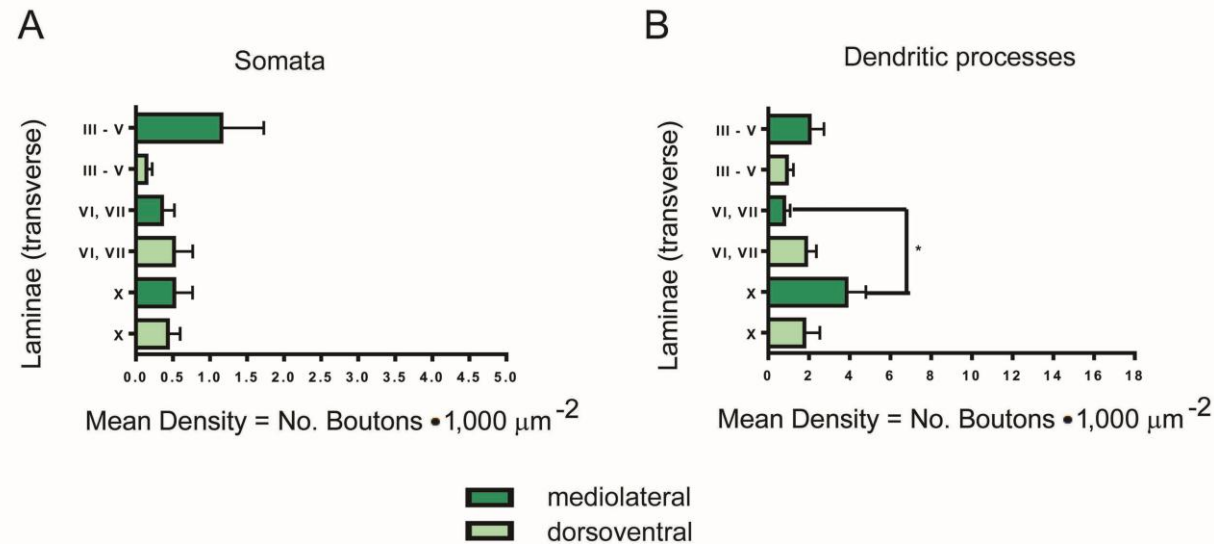


Figure 5.5 Neuronal densities of morphologically defined ChAT interneurons receiving CVLM boutons containing VGAT across transverse laminar boundaries

Cholinergic interneurons were classified according to their morphology in the transverse plane. Each green bar represents mean densities of interneurons populating the given laminar region with standard error bars shown. The somata of mediolaterally orientated interneurons (XY Ratio > 1) had greater inhibitory densities in dorsal laminae III - V (A). CVLM axons containing VGAT preferentially targeted mediolaterally orientated dendritic processes in lamina X with significantly greater inhibitory densities (B). Kruskal-Wallis with Dunn's multiple comparisons *post hoc* (* $p < 0.05$). N = 3 animals. Laminae III - V (19 cells). somata (A): 52 total CTb contacts, 13 VGAT⁺CTb contacts; dendrites (B): 122 total CTb contacts, 35 VGAT⁺CTb contacts. Laminae VI-VII (24 cells). somata (A): 45 total CTb contacts, 13 VGAT⁺CTb contacts; dendrites (B): 120 total CTb contacts, 45 VGAT⁺CTb contacts. Laminae X (18 cells). somata (A): 38 total CTb contacts, 9 VGAT⁺CTb contacts; dendrites (B): 96 total CTb contacts, 45 VGAT⁺CTb contacts.

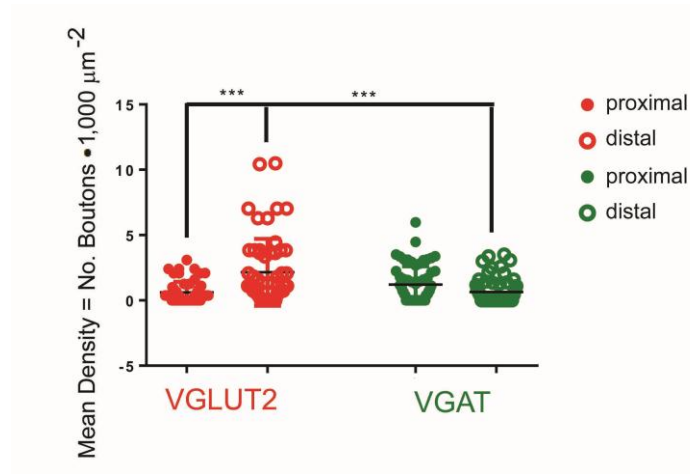


Figure 5.6 Dendritic densities of ChAT interneurons classified according to distance of immunoreactive CVLM boutons from soma

Sholl analyses compared the mean dendritic densities of all examined ChAT interneurons receiving excitatory (red) and inhibitory (green) CVLM inputs. A concentric circle or 'shell' encompassed all dendritic processes and those that were situated within the inner half were designated as proximal and those outside the shell were distal. CVLM boutons containing VGLUT2 were situated significantly further distally (open circles) while boutons containing VGAT were found proximally (closed circles), closer to somata, as described in the methods. There were significant morphological differences between dendrites receiving excitatory and inhibitory CVLM inputs. Kruskal-Wallis with Dunn's multiple comparison's *post hoc* (***) $p < 0.001$; $n = 57$ interneurons for VGLUT2 experiment and $n = 61$ interneurons for VGAT experiment). Scatter plot bars represent the means.

5.3.2 Aim 2: To investigate neuromodulation of intermediate zone interneurons innervated by the MLF in the horizontal plane

CTb was injected into the MLF of three animals to anterogradely label descending axon terminals in lower lumbar spinal segments (see Figures 3.3 and 3.4) sectioned horizontally. To investigate the interneurons targeted by labelled MLF axons and their serotonergic inputs, sections were reacted with a combination of antibodies against CTb, 5-HT, ChAT and nNOS (Table 5.1). Immunoreactive sections were first scanned in the red, blue and green channels to detect CTb, 5-HT and ChAT, respectively. Then sections were re-scanned such that the nNOS signal was detected in the UV vis range (as described in the methods section). Processes specifically in intermediate laminae VI, VII and lamina X populations were scanned for analyses. In the laminae VI - VII population, 17 ChAT interneurons were fully reconstructed and 38.10% (± 20.62) of these cells also expressed nNOS. In the lamina X population, 15 ChAT interneurons were reconstructed and 90.48% (± 16.50) of these cells also expressed nNOS. These cells were designated as ChAT::nNOS (Appendix 5 Tables 7 and 8). The *a priori* D'Agostino & Pearson omnibus normality test indicated that data were distributed normally and therefore the ANOVA with Tukey's *post hoc* compared means.

While none of the descending MLF axon terminals targeting these interneurons contained 5-HT (see Chapter 3), 5-HT boutons did form contacts onto these interneurons as hypothesised. A representative confocal microscopy image (Figure 5.7) and an interneuron reconstructed in three dimensions are shown (Figure 5.8). The average densities of ChAT interneurons were classified according to their positive or negative expression of nNOS. All interneurons received slightly greater input from 5-HT than from descending MLF axons. The densities of ChAT and ChAT::nNOS populations did not significantly differ in terms of their inputs sources as indicated by the scatter plot (Figure 5.9).

The input properties relating the densities of ChAT and ChAT::nNOS interneuronal populations were examined in the laminae VI-VII intermediate

zone and lamina X surrounding the central canal. The densities of ChAT::nNOS population received significantly greater serotonergic input than from MLF axons and this relationship was similar across laminar boundaries (Figure 5.10).

As a considerable number of labelled MLF axons terminate bilaterally (see Figure 3.4), the contact densities of contralaterally and ipsilaterally located ChAT and ChAT::nNOS interneurons targeted by the MLF and receiving input from 5-HT were compared in laminae VI, VII and X. The inputs from both MLF axons and 5-HT were found to be very similar for the contralateral and ipsilateral populations (Figure 5.11). This finding confirms that MLF axons target ChAT interneurons bilaterally, as indicated by diffusion of CTb surrounding the injection site. Addressing the hypothesis, some of the examined ChAT interneurons expressed nNOS in these laminar regions. However, their neurochemical profiles were not significant in terms of inputs received from the MLF or from 5-HT.

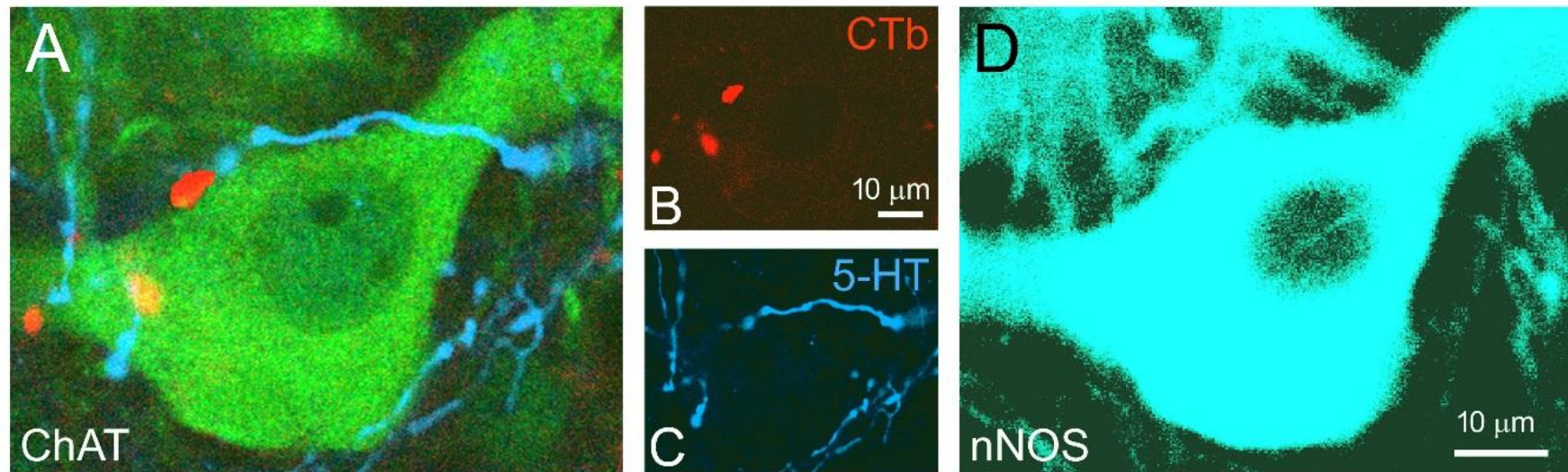


Figure 5.7 ChAT::nNOS interneuron receiving input from the MLF and 5-HT

Confocal microscopy image of a soma immunoreactive to ChAT (A) and nNOS (D) in lamina X shown in a single optical section. This soma received input from the MLF as indicated by the CTb marker in the red channel (B) and from 5-HT shown in the blue channel (C). MLF axons did not contain 5-HT.

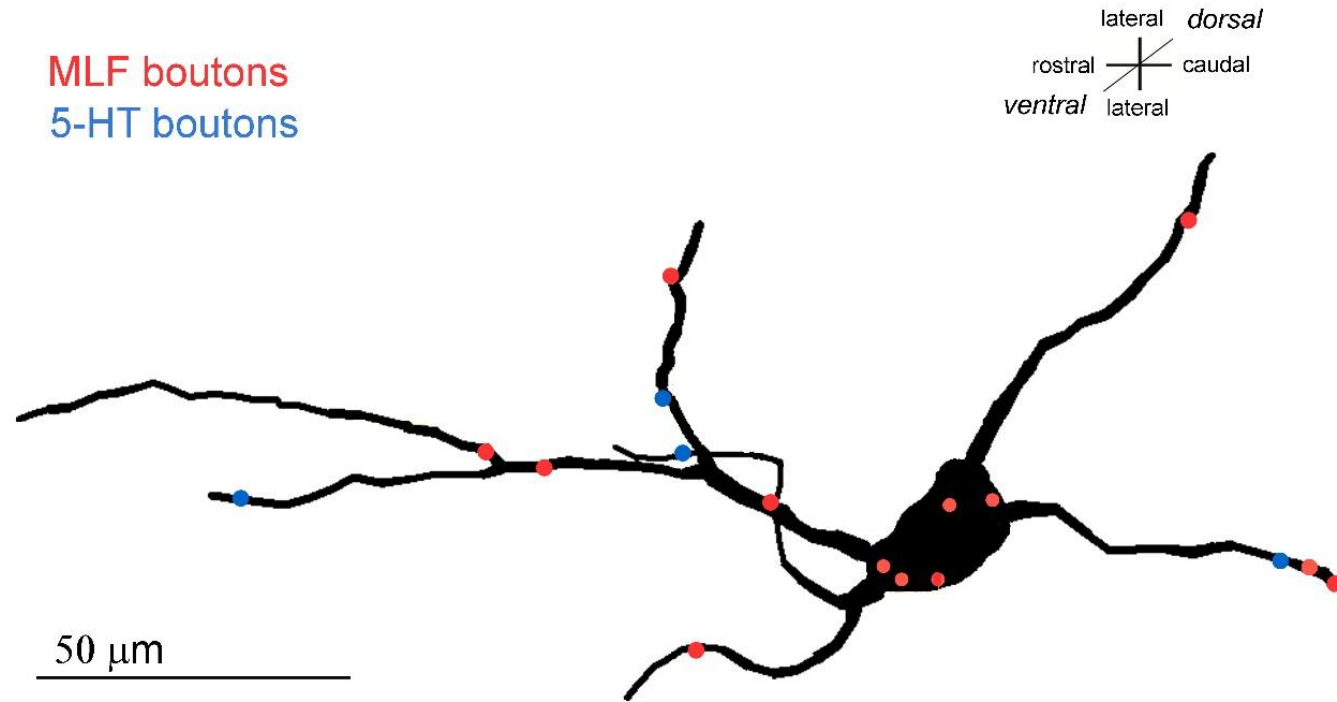


Figure 5.8 ChAT interneuron receiving input from the MLF and 5-HT

Three dimensional reconstruction of a ChAT interneuron in the horizontal plane receiving input from descending MLF axons (red) and from 5-HT (blue). This exemplary interneuron is orientated rostrocaudally within the grey matter of laminae VI of an L4 segment.

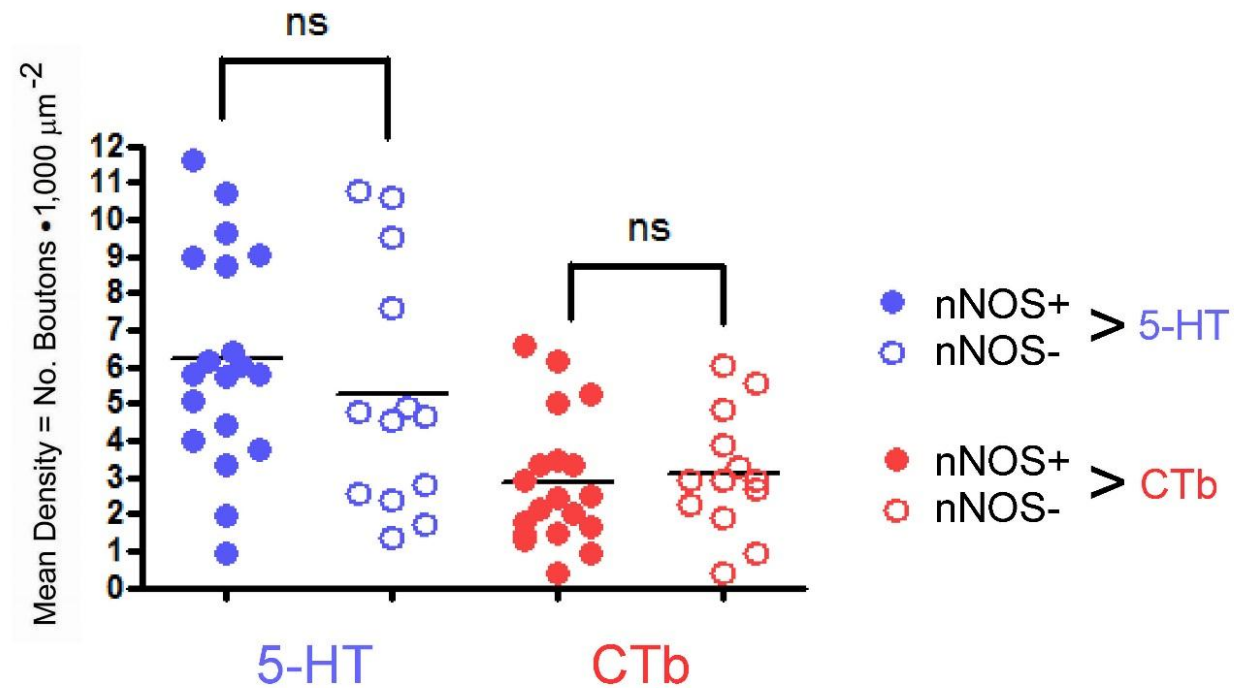


Figure 5.9 Density comparison nNOS::ChAT interneurons receiving input from the MLF and 5-HT

The contact densities of ChAT and ChAT::nNOS interneurons in the intermediate zone and near the central canal did not significantly differ and interneurons received greater input from 5-HT than from descending MLF axons. Each datum represents a cell and bars represent the mean ($n = 3$ animals). One-way ANOVA with Tukey's *post hoc* ($p > 0.05$). $N = 3$ animals.

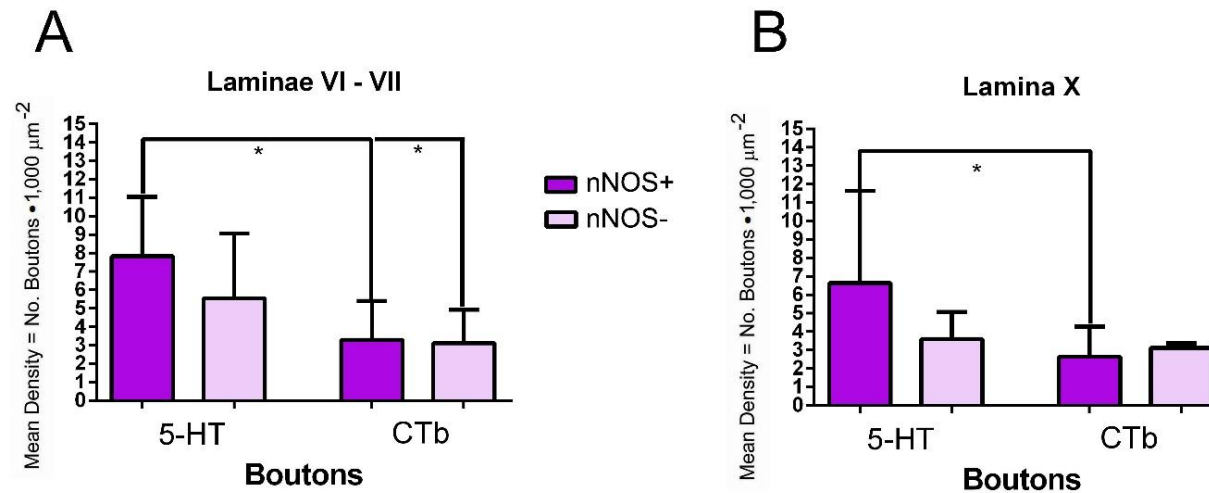


Figure 5.10 Relationship of ChAT and ChAT::nNOS interneuronal populations receiving input from the MLF and 5-HT across intermediate laminar boundaries in the horizontal plane

The nNOS::ChAT population of interneurons receiving input from 5-HT (purple) and from the MLF (lavender) had greater densities in both laminae VI and VII (A) and near the central canal (B). Each coloured bar represents mean densities of interneurons populating the given laminar region with standard error bars shown. The densities of populations receiving input from 5-HT differed significantly from those innervated by the MLF in these intermediate zones. Each datum represents a cell ($n = 3$ animals). One-way ANOVA with Tukey's *post hoc* (* $p < 0.05$). $N = 3$ animals. Laminae VI-VII (17 cells (38.10% ChAT::nNOS)). Somata: 61 5-HT contacts, 37 CTb contacts. Dendritic: 200 5-HT contacts, 79 CTb contacts. Lamina X (15 cells (90.48% ChAT::nNOS)). Somata: 33 5-HT contacts, 27 CTb contacts. Dendritic: 112 5-HT contacts, 49 CTb contacts.

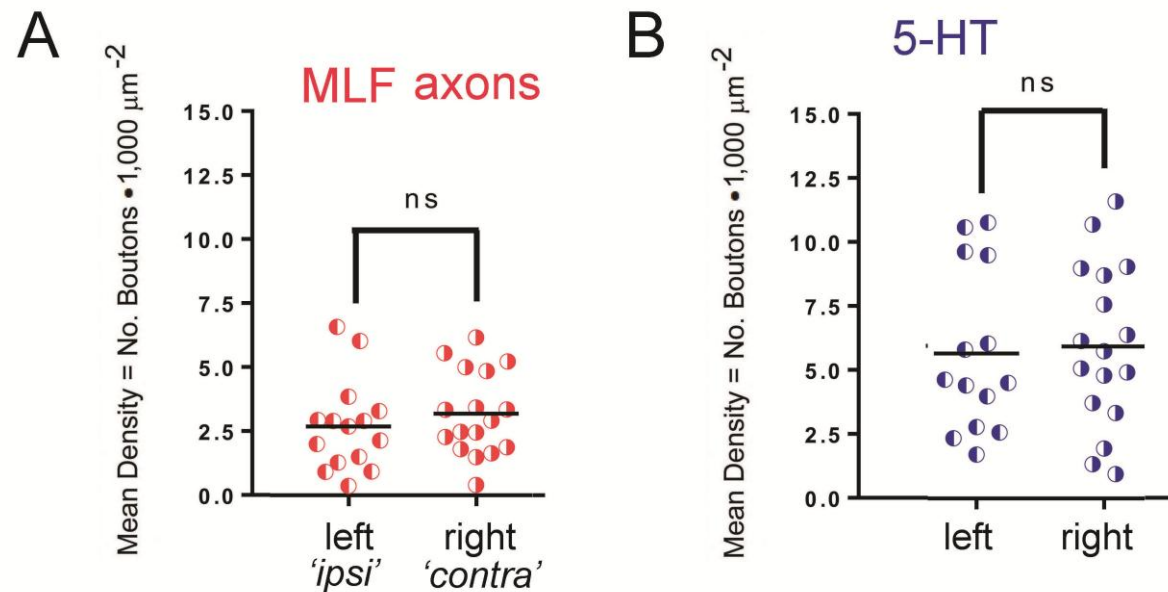


Figure 5.11 Bilateral comparison of densities of interneurons targeted by 5-HT and descending MLF axons

The injection site was targeted slightly to the left of the midline by +0.1 mm (Appendix 5 Figure 1) such that labelled MLF axons terminating on the right side of the cord were considered to be contralateral (contra) while terminations on the left side were ipsilateral (ipsi) (A). To investigate the targets of the MLF (red), the densities of both ChAT and ChAT::nNOS intermediate zone interneurons were compared (A) as well as their inputs from 5-HT (blue) (B). The densities of these populations, divided by the midline, did not differ significantly. Each datum represents a cell and bars represent the mean ($n = 3$ animals). One-way ANOVA with Tukey's *post hoc* ($p > 0.05$).

5.3.3 Aim 3: To determine the relationship of ChAT::nNOS interneurons in laminae VI, VII and X

To investigate the relationship between interneurons expressing ChAT, nNOS and/or ChAT::nNOS in laminae VI, VII and X, transverse sections from three animals receiving CTb injections in the MLF were reacted with the same antibody combination against CTb, 5-HT, ChAT and nNOS. However, the immunoreactive expression of MLF axons and 5-HT was not the focus of this present aim. Although the CTb tracer signal was present, it was not detected using this particular confocal microscopy method. The ANOVA with Tukey's *post hoc* compared means.

In laminae VI and VII, 80 total immunoreactive interneurons were counted with 27.74% (± 3.64) expressing ChAT, 38.70% (± 4.15) expressing nNOS and 33.56% (± 7.51) expressing both markers. In lamina X, 105 total immunoreactive interneurons were counted with 17.70% (± 3.83) expressing ChAT, 42.72% (± 2.30) expressing nNOS and 39.58% (± 3.75) expressing both markers (Appendix 5 Table 9). Low-power confocal microscopy scans revealed the relationship of these interneurons and 5-HT was revealed also (Figure 5.12). Interneurons expressing nNOS were the most prevalent population in these laminar regions with a considerable portion immunoreactive to both markers (Figure 5.13).

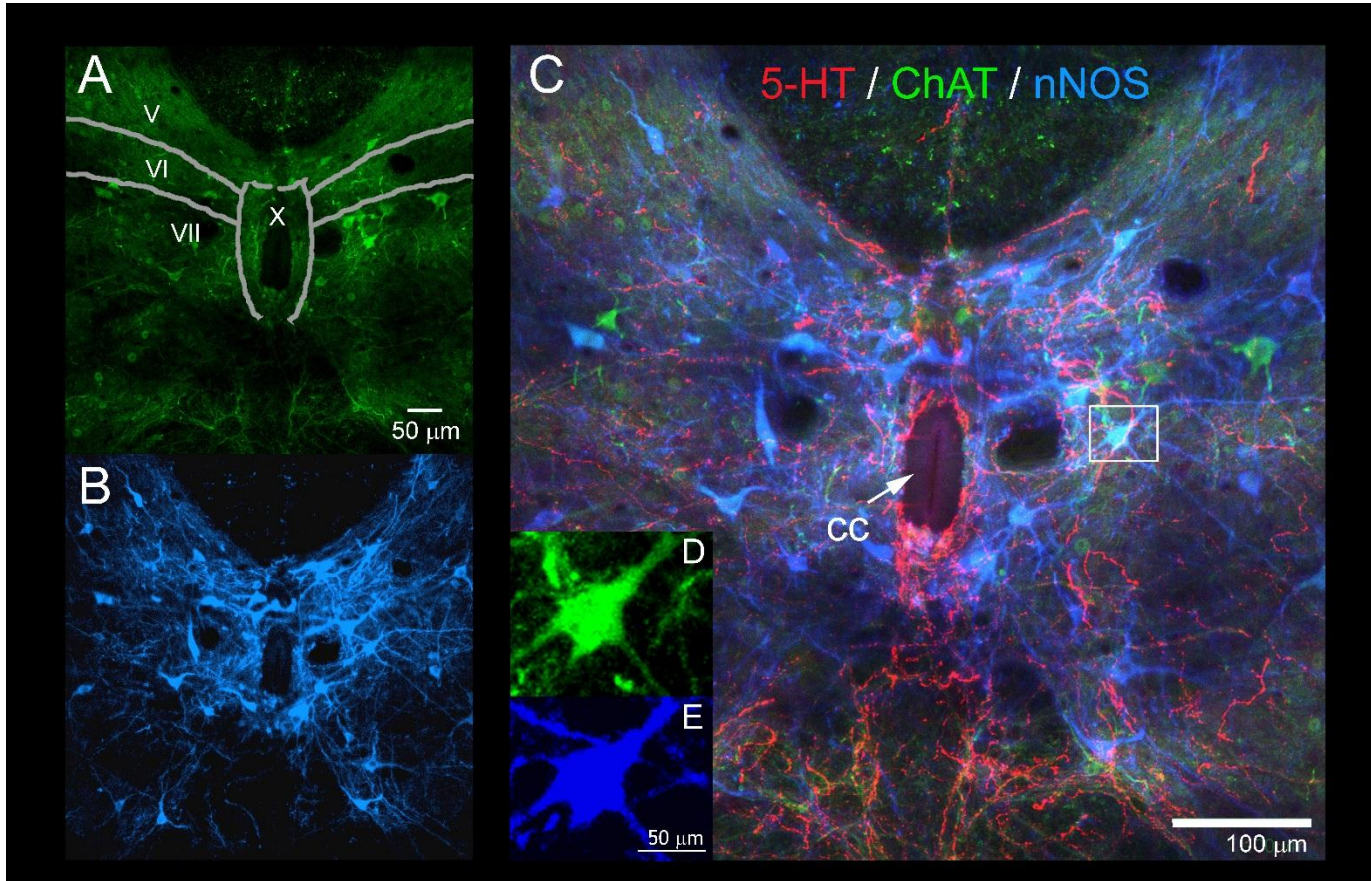


Figure 5.12 Relationship of ChAT::nNOS immunoreactive interneurons in the intermediate zone with 5-HT

Projected low-power confocal microscopy image of intermediate zone regions containing ChAT interneurons visualised in the green channel. (A) L4 transverse section with laminar boundaries indicated by a superimposed standard template based upon Molander's scheme. (B) nNOS cells are visualised in the blue channel. The merged image reveals ChAT (green), nNOS (blue) ChAT::nNOS (cyan) cell populations (C) and 5-HT immunoreactivity is visualised in the red channel, especially present near the central canal (cc). The ChAT::nNOS cell shown in the inset box (C) is immunoreactive to both ChAT (D) and nNOS (E) as visualised in separate colour channels. While the CTb tracer is present, it is not visible using this particular confocal microscopy method. Immunofluorescence is shown in pseudo-colours. Note that 5-HT is present in all laminar regions.

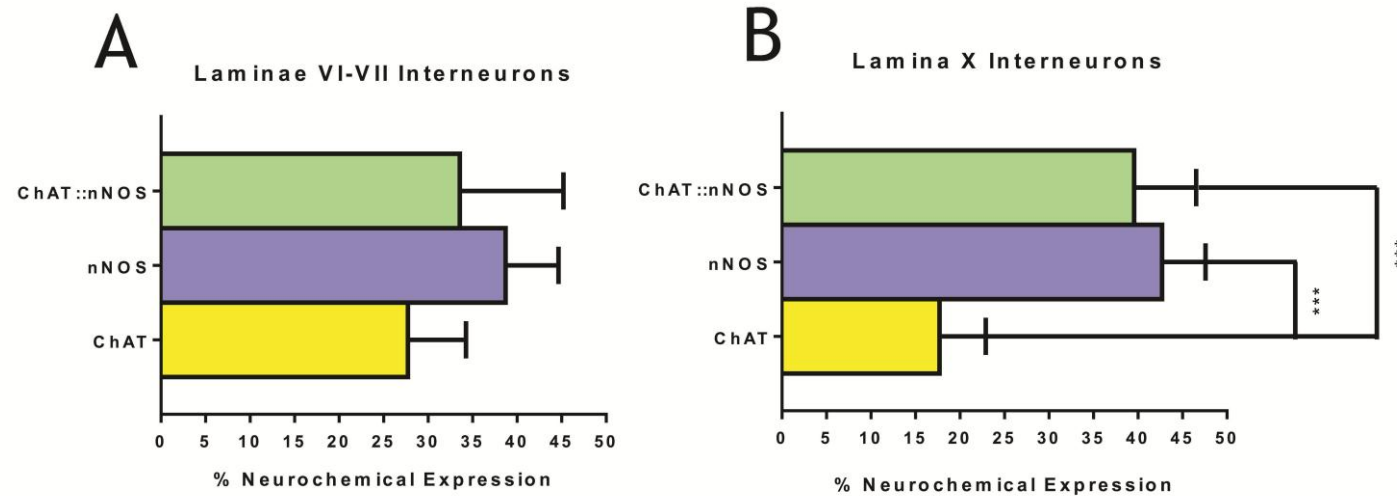


Figure 5.13 The relationship of ChAT, nNOS and ChAT::nNOS expressing interneurons in laminae VI - VII and X

Immunoreactive interneurons in laminae VI - VII (A) and lamina X (B) were counted. The majority of interneurons expressed nNOS (blue) and in the lamina X populations, the number of these cells differed significantly from those cells expressing ChAT::nNOS (green) and ChAT (yellow). ChAT interneurons were found less frequently in both laminar populations. One-way ANOVA with Tukey's *post hoc* for $n = 3$ animals (** $p < 0.001$). Standard error bars shown. Laminae VI-VII: 80 total cells (27.74% ChAT, 38.7% nNOS, 33.56% ChAT::nNOS). Lamina X: 105 total cells (17.70% ChAT, 42.72% nNOS, 39.58% ChAT::nNOS).

5.3.4 Aim 4: To qualitatively compare ChAT interneurons in naïve rat tissue receiving modulatory input from monoamines in the parasagittal plane

To qualitatively investigate modulatory inputs onto ChAT interneurons from 5-HT and axons expressing DBH in the parasagittal plane, tissue from one L3 spinal segment of naïve rat (one animal) was sectioned parasagittally. DBH recognised axons that synthesise NA, an enzyme that converts DA to NA. ChAT interneurons were fully reconstructed and five cells were fully reconstructed in the laminae VI-VII region and five cells were fully reconstructed in the lamina X region (Appendix 5 Table 10). Representative confocal microscopy images are shown (Figures 5.14 and 5.15).

Noradrenergic boutons contacted ChAT interneurons as hypothesised. In the laminae VI-VII population, there were greater input densities from 5-HT than from DBH, and the lamina X population showed greater input densities from DBH onto somata while 5-HT input densities were greater onto dendrites. Sholl analysis revealed only slight qualitative differences between the proximal and distal dendrites receiving monoaminergic inputs (Figure 5.16).

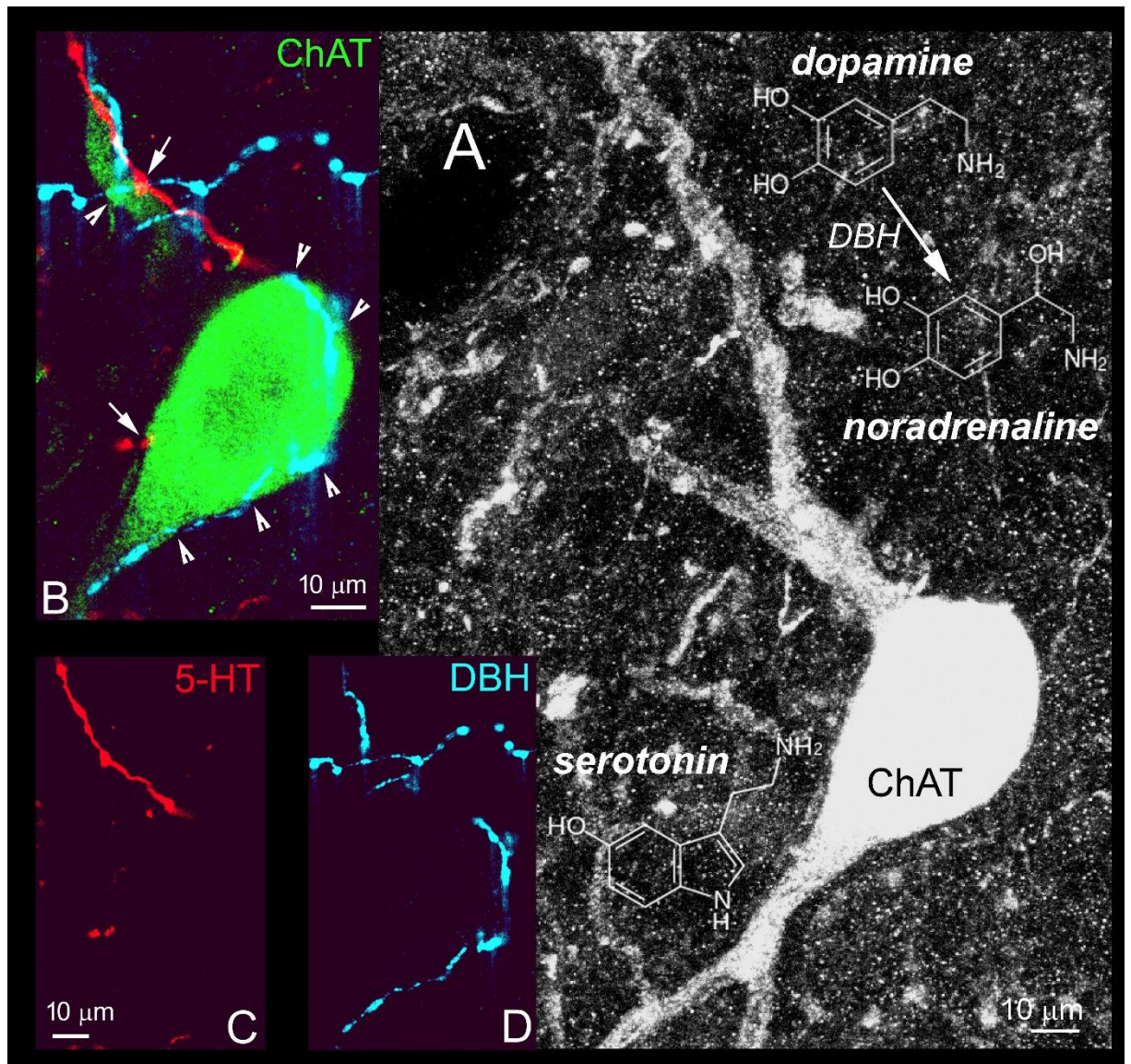


Figure 5.14 Neuromodulation of a ChAT interneuron

An immunoreactive ChAT interneuron in naïve rat tissue was revealed in a single channel projected confocal microscopy 'raw' image in lamina IV of an L4 segment sectioned parasagittally (A). Both monoamines (chemical structures, A) contacted this soma and proximal dendrite with 5-HT boutons denoted by arrows and DBH boutons denoted by arrowheads in a single optical field (B). 5-HT (C) and DBH (D) are shown in separate colour channels in single optical fields. DBH converts DA to NA by addition of a hydroxyl group within synaptic vesicles (A).

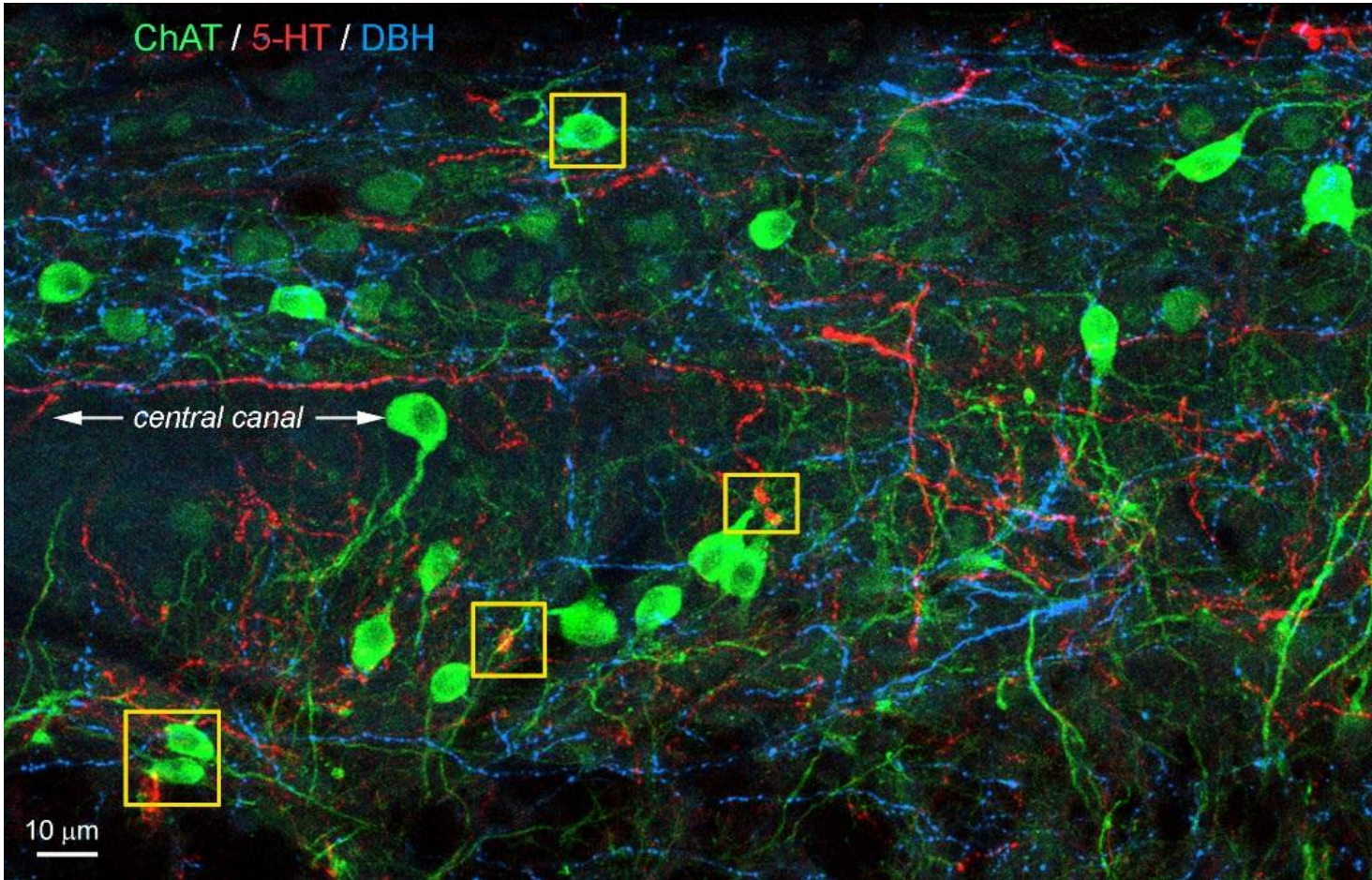


Figure 5.15 ChAT interneurons neuromodulated by 5-HT and NA near the central canal

Projected low-power confocal microscopy image of immunoreactive ChAT interneurons distributed about the central canal as indicated. Yellow inset boxes indicate regions of interest as both 5-HT and DBH marker were found to contact interneurons. Not that the central canal is visualised horizontally in the parasagittal plane.

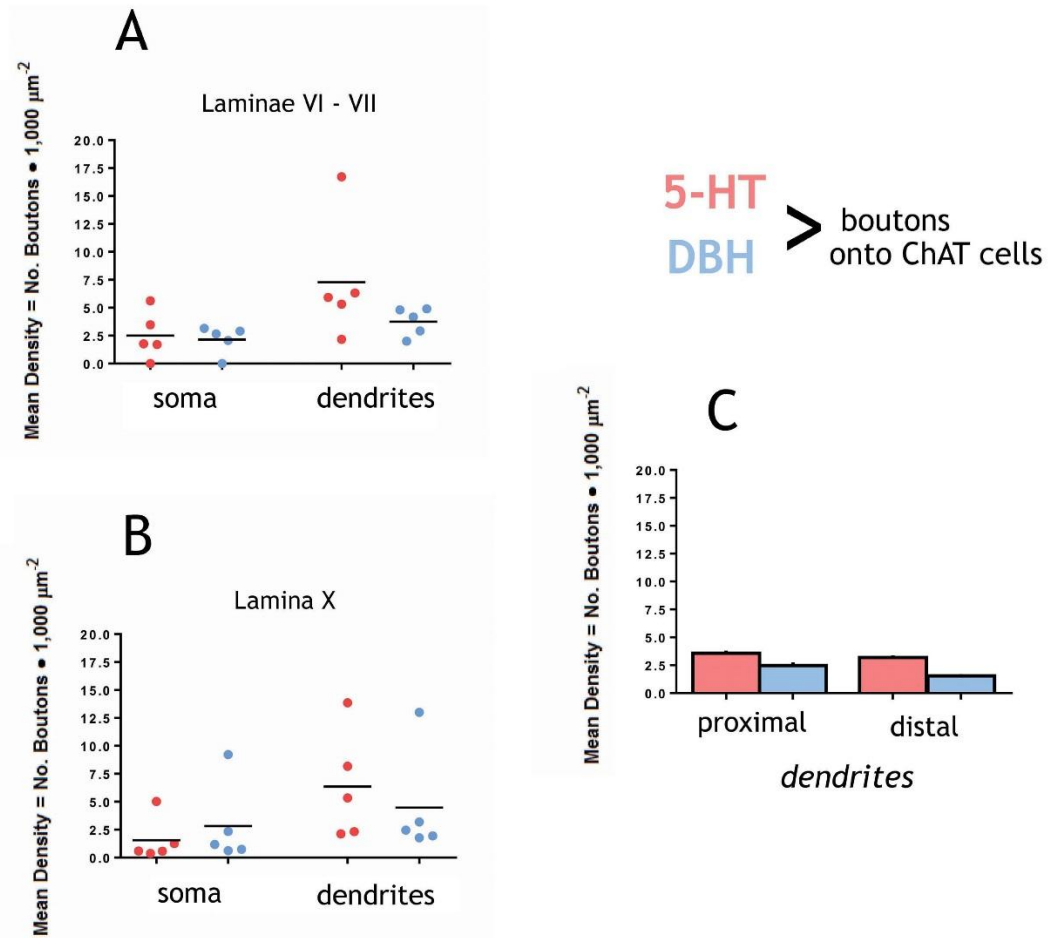


Figure 5.16 Density comparison of ChAT interneurons in the parasagittal plane receiving modulatory input from monoamines

Monoaminergic boutons contacted ChAT interneurons in naïve rat tissue. Each datum represents a ChAT interneuron. There were greater input densities from 5-HT than from DBH in the laminae VI-VII population (A). In the lamina X population, somatic densities were slightly greater for DBH while 5-HT inputs were greater onto dendrites (B) with scatter plot bars representing the standard mean. A concentric circle or 'shell' encompassed all dendritic processes and those that were situated within the inner half were designated as proximal and those outside the shell were distal. Inputs onto proximal and distal dendritic processes from 5-HT and DBH were similarly distributed with slightly greater expression of 5-HT as revealed by Sholl analysis (C) ($n = 1$ animal, no injection site). Laminae VI-VII: 5 cells examined; Lamina X: 5 cells examined.

5.4 Discussion

5.4.1 Excitatory and inhibitory CVLM inputs onto ChAT interneurons across laminar boundaries in the transverse plane

Analyses of data from this anterograde tract tracing and immunohistochemical study has provided insights into the distribution of descending excitatory and inhibitory CVLM input onto populations of ChAT interneurons. Antibody against VGAT detected both glycinergic and GABAergic boutons. Overall, ChAT interneurons had greater contacts densities from VGLUT2 positive CVLM axon terminals than from VGAT positive terminals. Within the spinal cord, coordination between neurons is controlled principally by the interaction between glutamate and glycine (Brodin and Grillner, 1985a, Brodin and Grillner, 1985b, Dale, 1985, Dale et al., 1986, Dale and Roberts, 1985, Grillner and Wallen, 1980). The CVLM is likely to sculpt motor activity using both excitatory and inhibitory transmitters in tandem. In terms of the overall neural networks underlying the rhythmic patterns of locomotion, neurons need a source of excitation, which may be intrinsic to the neuron or may come from neurons external to the network (Alford et al., 2003). In generating any motor output, inhibitory synaptic transmission and inhibitory interneurons are crucial for coordinating antagonistic muscles of each joint (Baldissera et al., 1981), especially controlling temporal and spatial activation patterns of limbs on both sides of the body. Thus, inhibition is essential for controlling the speed and stability of the locomotor rhythm (Nishimaru and Kakizaki, 2009).

In contrast to densities of VGLUT2 positive CVLM boutons on proximal dendrites, there was considerable variability of distally located VGLUT2 positive CVLM boutons. A methodological consideration may be that dendritic arbors were not fully visualised, especially for mediolaterally orientated cells in transverse sections. The dendritic distribution of VGAT positive CVLM boutons was comparatively uniform. An interesting finding was the significantly greater CVLM input onto lamina X central canal cells, both excitatory and inhibitory. The area surrounding the central canal emerged as a region of interest. Pertinent to this

laminar region and the adjacent intermediate zone, Renshaw cells act as premotor inhibitory interneurons that are excited by motoneuron axon collaterals before they leave the spinal cord (Jankowska, 2013) via the activation of nicotinic receptors (Alvarez and Fyffe, 2007, Willis, 1971). Dendritic processes of Renshaw cells have been uniquely characterised as having a high density of proximal inhibitory synapses (Alvarez and Fyffe, 2007).

All intermediate zone interneurons are regarded as intersegmental neurons that may span a few segments but do not extend beyond lumbar segments. Further, all of the subpopulations of intermediate zone interneurons included interneurons innervated by group I and II afferents (Jankowska and Edgley, 2010). In the intermediate zone, group Ia interneurons located in the grey matter of lamina VII were originally considered merely to serve as relays to change the type of transmitter from excitatory (in synapses made by peripheral afferents) to inhibitory (glycine) but Ia interneurons also function as premotoneuron integration centres (Jankowska, 2013) by relaying sensory reflex inputs to motoneurons (Hultborn et al., 1971, Jankowska, 1992, Wang, 2008, Windhorst, 2007). As these interneuronal groups have now been more appropriately classified collectively as group I/II interneurons (Jankowska and Edgley, 2010), results from the present study indicate that these groups are targeting premotor interneurons using VGLUT2 and VGAT.

The neuronal orientation, mediolateral or dorsoventral, within any given laminar region was not significant in terms of contact densities. However, differences in glutamatergic and inhibitory densities between laminar regions were apparent. Interestingly, all laminar regions contained mediolaterally and dorsoventrally orientated interneurons, suggestive of the inherent morphological diversity of ChAT interneurons. In terms of the hypothesis, considerable variation of contact densities were observed throughout spinal laminae and this result was seemingly irrespective of morphological parameters, indicative of the complexity of instantiated interneurons. A recent comparative study of intermediate zone excitatory and inhibitory interneurons in the cat spinal cord found no discernable pattern regarding the location or the extent of dendritic arbors. However, major morphological differences were found in their axonal projections; excitatory interneurons projected either ipsilaterally, bilaterally or

contralaterally while inhibitory interneurons projected exclusively ipsilaterally and this finding was confirmed by electrophysiological data (Bannatyne et al., 2009). In sum, individual partition cells receiving descending input from the CVLM having divergent morphological patterns may be recruited selectively to modulate pools of motoneurons with specificity, executing behaviourally appropriate motor tasks requiring alternation of extensor burst amplitudes (see Zagoraïou et al., 2009, Stepien et al., 2010).

5.4.2 Serotonergic inputs onto interneurons in laminae VI, VII and X innervated by the MLF

MLF axons were labelled anterogradely and this ICC study provided insights into descending MLF inputs onto populations of ChAT and ChAT::nNOS interneurons in laminae VI, VII and X in the horizontal plane. The inherent orientation of ChAT dendrites may be better accommodated in tissues sectioned horizontally and/or parasagittally rather than transversely. However, horizontal sections can be disadvantageous since the hemispheres can separate while cutting, especially sections from the superficial dorsal or deep ventral horn. Because I was investigating interneurons in the grey matter of intermediate zones near the central canal, horizontal sections were ideal since this region is contiguous. Horizontal sections allowed for bilateral examination of the cord, which is pertinent considering that MLF axons are known to be distributed bilaterally (Du Beau et al., 2012). Labelled MLF axons projecting to the right (contralateral) and left (ipsilateral) sides of the cord relative to the injection site were found to target cells nearly equally, as might be expected since the MLF injection site was targeted very close to the midline (mediolateral = +0.1mm). Contact densities from both sources were similar across laminar regions with the ChAT::nNOS populations receiving statistically insignificantly greater serotonergic modulation. This finding confirms that the CTb tracer diffused across the midline to label descending MLF axons. Other studies have reported that serotonergic fibres have been found in all laminae of the cord and at all rostrocaudal levels, as in the rat (Jones and Light, 1990), which fits the concept that the serotonergic systems exert an overarching modulatory role on both sensory and motor functions (Mason and Leung, 1996, White et al., 1996).

A recent confocal microscopy study investigating intracellularly labelled CINs found that the number and pattern of contacts from serotonergic and noradrenergic fibres were very similar (Hammar et al., 2004). Such findings suggest that the differences in the modulatory actions of monoamines, and the subsequent changes in the recruitment of morphological subpopulations in various behavioural situations, depends upon the intrinsic properties of the interneurons rather than on the pattern of innervation by monoamines. Monoamines contacting group II premotor interneurons may be strategically positioned to influence primary afferent inputs, as both occur predominantly on dendritic processes (Maxwell and Riddell, 1999). Descending monoaminergic systems were observed to have similar actions on excitatory and inhibitory group II pathways (Jankowska et al., 1993, Schomburg and Steffens, 1988), which is consistent with findings of similar density and patterns of distribution of contacts onto populations of premotor interneurons (Maxwell et al., 2000).

5.4.3 The relationship of ChAT::nNOS interneurons in laminae VI, VII and X with 5-HT

Analysis of immunoreactive interneurons expressing ChAT and nNOS in intermediate zones and surrounding the central canal characterised the role of premotor interneurons. The majority of cells expressed nNOS and neurochemical expressions were similar across laminar boundaries. Lamina X provides a ChAT relay between the dorsal, intermediate and ventral grey matter (Borges and Iversen, 1986). Many peptides are present within lamina X (Gibson et al., 1981) and some ChAT neurons could be peptidergic (Borges and Iversen, 1986), which may serve regulatory functions for ChAT neurons in other laminar regions (Butcher and Woolf, 1982). Previous studies have found that ChAT partition cells that do not express nNOS likely give rise to C boutons on motoneurons. C boutons regulate the excitability of motoneurons via m2 muscarinic receptors (see Miles et al., 2007) and muscarinoreceptive neurons are known to provide a sustained monosynaptic bilateral excitation to RetS neurons (Smetana et al., 2010). The transcription factor Pitx2 marks a small cluster of spinal ChAT interneurons, VO_c neurons, which are the sole source of C boutons synapses onto spinal motoneurons (Zagoraïou et al., 2009). The biophysical

processes of VOc neurons, e.g. slow tonic firing and large afterhyperpolarising potentials, are typical of ChAT and monoaminergic modulatory neurons (Bennett et al., 2000, Li and Bayliss, 1998, Masuko et al., 1986) and their connectivity suggests that they participate in the spinal premotor network devoted to the modulation of motor output (Zagoraiou et al., 2009).

5.4.4 Qualitative comparison of ChAT interneurons in naïve rat tissue receiving modulatory input from monoamines

Immunoreactive ChAT interneurons from naïve tissue that received no tract tracer injection were reconstructed in intermediate zones and lamina X. Monoaminergic boutons contacted these cell populations, with great inputs from 5-HT than DBH, although there was an outlying cell having an exceptionally high serotonergic dendritic density (16.73 per 1,000 μm^2) as compared to the mean (7.29 per 1,000 $\mu\text{m}^2 \pm 5.52$). Data were not statistically analysed since one animal was used for this particular experiment.

Catecholaminergic and serotonergic regions of the CNS are largely heterogeneous with respect to their synaptic connections as demonstrated in studies in the rat. In the intermediate and ventral horn in cat, NA and 5-HT released in tandem by descending monoaminergic neurons were found to differ in the potency with which they depress transmission from incoming afferents yet this effect was not apparent in the dorsal horn (Bras et al., 1989).

Immunoreactive fibres for tyrosine hydroxylase, the enzyme involved in the synthesis of catecholamine neurotransmitters (see Kumer et al., 1996), have been found in all spinal laminae, and might represent noradrenergic, adrenergic and/or dopaminergic fibres (VanderHorst and Ulfhake, 2006). NA can prevent spinal interneurons from responding to nerve impulses from muscle spindle afferents while having no effect on transmission from primary afferents to the very same neuron (Jankowska, 2013). Dopaminergic receptors can contribute to 5-HT evoked rhythmogenesis in networks of spinal neurons (Madriaga et al., 2004). A pharmacological study revealed that low concentrations of 5-HT ($< 10 \mu\text{M}$) combined with DA can produce a stable locomotor rhythm in rats and mice (Jiang et al., 1999, Sqalli-Houssaini et al., 1993, Whelan et al., 2000). At higher

concentrations (10 - 100 μM), 5-HT alone can activate spinal locomotor circuits. Taken together, data suggest that high concentrations of 5-HT may be cross-reacting and activating DA receptors, specifically D_1 and D_2 receptor families (Madriaga et al., 2004). Further, different DA receptors may be found in different laminar locations within the rat spinal cord (van Dijken et al., 1996). Such findings add credence to the idea that catecholaminergic and serotonergic signalling pathways interact to produce locomotion (Madriaga et al., 2004).

Concluding Remarks

The present investigation revealed the heterogeneous neurochemical profile of medullary axonal projections in lower lumbar segments. While the MLF and CVLM are anatomically and functionally distinct, they were found to use the same transporters, principally VGLUT2 (61% and 65%, respectively), and in statistically the same proportions. Rarely a RetST terminal was observed to contain both VGLUT1 and VGLUT2. Colocalisation of these two transporters is frequently observed in the developing CNS (see Nakamura et al., 2005) but occurs only occasionally in the adult (Hioki et al., 2003). While the significance of this observation is not clear, colocalisation may possibly confer special functional properties on these synapses (Todd et al., 2003). An alternative explanation is that it may be a residual developmental phenomenon (Hioki et al., 2003). In the rodent brain, extensive expression of VGLUT2 is already evident at birth in contrast to VGLUT1. In many regions of the CNS, VGLUT2 is down-regulated in parallel with an increase in VGLUT1 expression (Boulland et al., 2004, Fremeau et al., 2004). A plausible speculation is that patterns of primary afferents in adult rats may be reflecting development changes of axonal connectivity as the cortical “motor map” forms. Results from the present study have revealed that virtually all axons descending from the CST were found to contain VGLUT1 (Du Beau et al., 2012).

MLF and CVLM axons were immunoreactive to VGAT (21% and 23%, respectively), accounting for the expression of GlyT2 (9.05% and 12.51%, respectively) and GAD67 (7.54% and 8.67%, respectively) with only a minor proportion of terminals expressing both inhibitory amino acids (2.15% and 2.91%, respectively). During REM sleep, the balance between GABAergic and serotonergic fibres descending from the lower brainstem shifts where serotonergic fibres are inactive (Holstege, 1991, Siegel, 1989). Alternatively, findings from electrophysiological recordings in cat motoneurons showing that projections mediating muscle atonia are glycinergic (Soja et al., 1987) is congruent with more recent collective studies implicating the activation of glycinergic neurons in the ventromedial medulla during this oneiric state (see Holstege, 1991). Taken together, the presumed glycinergic part of this system may be especially active during REM sleep whereas the GABAergic part would be active during other states of sleep and wakefulness (Holstege, 1991). In addition to active inhibition by glycine and GABA, dysfacilitation of serotonergic and noradrenergic transmission has been

demonstrated in the depression of motoneuronal activity during REM sleep (Fenik et al., 2004). In sum, the hypothesis that the generation and maintenance of REM atonia are under the influence of many cell groups and neurotransmitters is likely (see Siegel, 1989). To quantify the reciprocal relationship of these inhibitory amino acids and their role in the motor atonia, a further approach would be to investigate the spinal neuronal targets of inhibitory axons descending from the ventromedial medulla. There is ultrastructural evidence that glycine and GABA may act as cotransmitters within the spinal cord. Gephyrin, a scaffolding protein associated with inhibitory synapses, can differentiate between glycine and GABA at postsynaptic release sites (Todd et al., 2006).

Findings from the present investigation have revealed that a proportion of labelled MLF and CVLM axons (17% and 12%, respectively) were not immunoreactive to the tested antibodies and none of the labelled axons contained 5-HT, as plausibly explained by the fact that most raphé spinal axons are unmyelinated (Westlund et al., 1992) and consequently may not sequester CTb. These unidentified axons may be glutamatergic as unmyelinated primary afferents (Todd et al., 2003) or possibly may contain VGLUT3, as discussed in Chapter 3. Controversy exists regarding the proportions of serotonergic medullary raphé and ventromedial reticular cells that project to the spinal cord (see Mason, 2001). These discrepancies are likely due to differences in the anatomical regions studied and in the transport efficiency of the various retrograde tracers used. Regardless of the precise numbers, there is no doubt that the descending projection from the medullary raphé and ventromedial reticular nuclei includes serotonergic and nonserotonergic neurons, both of which are likely to be of functional significance in the spinal cord (Mason, 2001).

Neuroanatomical studies have used the transganglionic tract tracer IB4 to label unmyelinated afferent fibres (Finkelstein et al., 1974, Ganser et al., 1983, Goldstein and Winter, 1999, Scott et al., 1990, Trojanowski et al., 1982) and this marker could be useful in identifying the unknown neurotransmitter phenotype(s) used by medullary axons from the neurochemically and anatomically diverse reticular formation.

The present investigation revealed that ChAT interneurons were richly innervated by CST axons expressing VGLUT1, especially in the dorsal horn. The dorsal horn ChAT plexus, as observed in previous studies, is localised in lamina III (Barber et al., 1984) and/or lamina II (Olave et al., 2002). Since these ChAT processes interact with central terminals of primary afferents, then they are likely controlling the entry of sensory information (Ribeiro-da-Silva and Cuello, 1990b). In sum, the ChAT dorsal plexus seems to be fundamental to the modulatory effects of ACh on sensory transmissions. Because dendrites of ChAT interneurons are better rendered in spinal parasagittal sections in the rat (Barber, 1984, Olave et al., 2002), classical transverse sections may have overlooked the extent of these dendritic branching patterns. Three-dimensional reconstructions of ChAT neurons have demonstrated a unique morphological signature with a significantly asymmetrical orientation of dendritic processes (Mesnage et al., 2011). The present study has revealed a uniform pattern of greater afferent inputs onto cells with dorsally situated dendritic processes. In terms of stereology, anatomical evidence demonstrates that neurons send out their dendrites to maximise connections to their potential connection partners (Stepanyants and Chklovskii, 2005) and theoretical predictions are based upon such connectivity principles.

In terms of functional implications, there is accumulating evidence suggesting that impairments of the CST due to injury is not restricted to contralateral movement as ipsilateral movement may be affected too (see Lemon 2008 review Pg. 197). Based upon such evidence, neurons in the intact hemisphere may be involved with the recovery of motor function (Jankowska and Edgley, 2006b) although there is no consensus about these mechanism (Cauraugh and Summers, 2005, Chen et al., 2002, Hallet, 2001, Serrian et al., 2004). Axonal sprouting may be considered part of a general rewiring of cortical connections that explain, at least in part, functional recovery after spinal cord injury (Bareyre et al, 2004). An important consideration is that descending pathways function as part of an overarching network rather than as separate controllers of the spinal cord. As Edgerton has written, “the spinal cord functions as part of the brain, not as its servant” (see Jankowska and Edgley 2006).

The postsynaptic properties of neurons targeted by the CST could be further investigated by immunoreaction with parvalbumin, a slow Ca^{2+} buffer associated with regulation of short-term synaptic plasticity (Caillard et al., 2000). In the spinal cord, specific cell types and their connectivity patterns have been distinguished by their expression of different calcium binding proteins (Anelli and Heckman, 2005). Spinal interneurons that express parvalbumin receive inputs from myelinated primary afferents and are a likely source of the inhibitory inputs that selectively regulate non-noxious tactile inputs (Hughes et al., 2012). An important goal is to understand the role of the CST in gating sensory afferent inputs and how it might function to rescind unnecessary reafference.

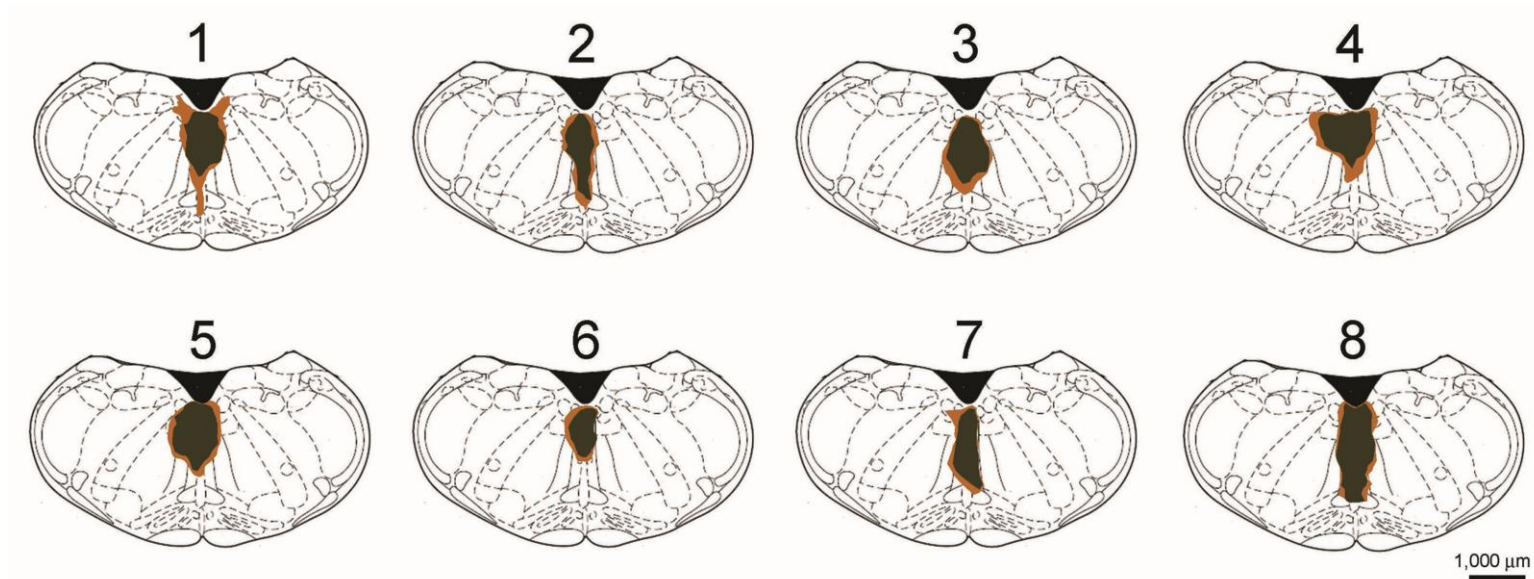
Descending motor commands that produce specific motor patterns may be coupled to both brainstem monoaminergic nuclei, e.g. the emotional descending system, and to reciprocal inhibitory interneurons in the spinal cord (see Heckman, 2008). The present investigation has provided insights into the neurochemical properties of medullary axons targeting ChAT and ChAT::nNOS interneurons, particularly medial partition cells and central canal cell populations receiving monoaminergic inputs. ChAT interneurons in these regions that lack nNOS are candidate sources of C boutons onto motoneurons that regulate excitability via m2 muscarinic receptors (Zagoraïou et al., 2009). Sherrington (1906) has referred to motoneurons as “the final common pathway.” Multiple central and peripheral influences coalesce into the motoneuron activations that produce adaptably appropriate motor behaviours (Wolpaw, 2010). Descending monoaminergic systems confer overall behavioural flexibility by modulating spinal reflexes (Jankowska and Edgley, 2010). A key problem is that the descending projections are highly diffuse; the monoaminergic system is not organised in the specific fashion that characterises other systems, e.g. the CST (Bjorklund, 1982). Diffuse neuromodulation could plausibly provide the appropriate overall level of motor pool excitability and specific spinal inhibitory pathways could be used to specifically focus this excitability.

While the present investigations focus on properties of individual neurons, findings have implications for understanding networks of neurons with broad application. When commissural muscarinic terminals originating from lamina X

interneurons and intermediate zone partition cells are activated, short-term potentiation of glutamatergic inputs to motoneurons are induced. This short-term potentiation is occluded in the presence of the muscarinic antagonist atropine (Bertrand and Cazalets, 2011), an anti-cholinergic alkaloid. The present investigations have elucidated the role of ChAT interneurons in the spinal motor systems in these specific laminar regions. Interactions between ChAT and glutamatergic neurotransmitter systems have been shown to influence numerous forms of synaptic plasticity throughout the CNS (see Martella et al., 2009). Experimental models based on spinal cord reflexes facilitate the study of the gradual plasticity that makes possible most rapid learning phenomena. These models reveal principles that may apply to learning and memory throughout the CNS. Additionally, they offer new approaches to guiding activity-dependent plasticity so as to restore functions lost to spinal cord injury, trauma or disease (Wolpaw, 2010).

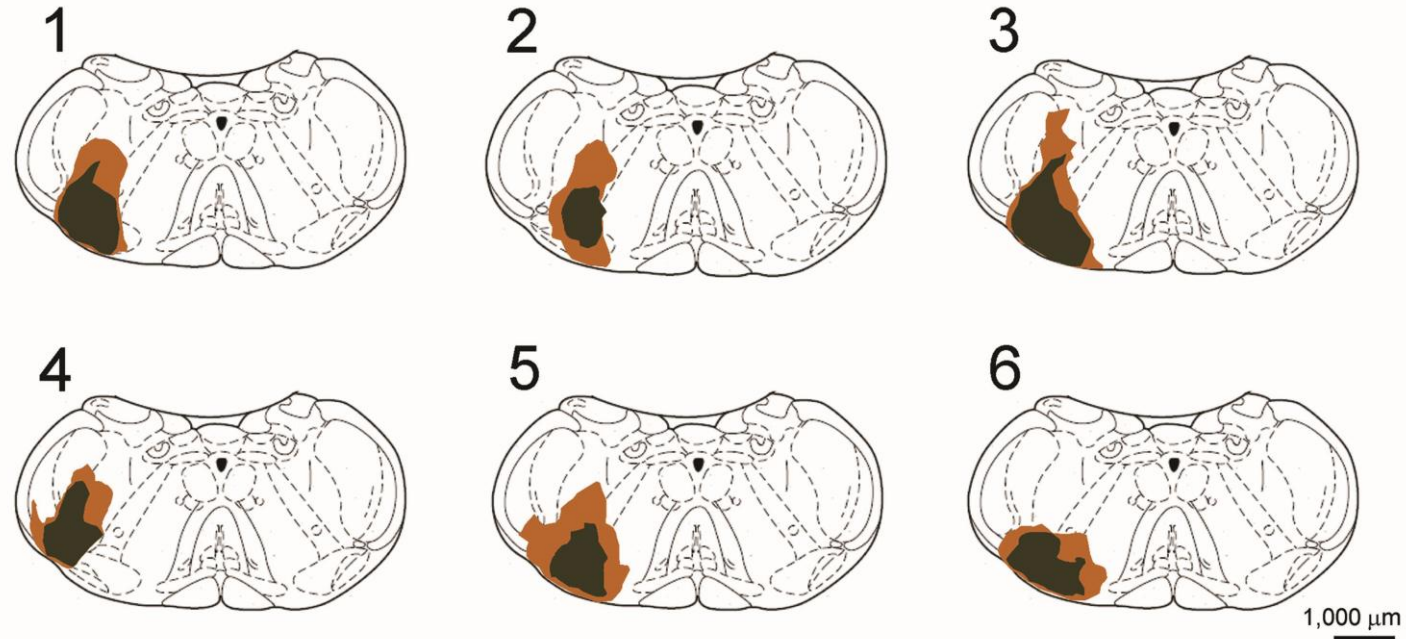
Individual neurons are adaptive and synaptic strength may vary in response to central modulation or sensory input (see Alford et al., 2003). Many interneurons targeted by descending systems are tempered by multisensory inputs arising from various afferent sensory signals and different muscles (see Jankowska and Edgley, 2010). Activity in the developing CST and the sensory consequences, which are inextricably linked to movement, shape the termination topography, morphology, and possibly spinal circuits more generally (see Martin, 2005). Cumulative findings have further implications for isolating and redirecting spinal sensory signals. For instance, haptics exploits the sense of afferent touch arising from mechanical signals such as the movement of limbs, contact force and torque. Haptic perception can now be feasibly investigated in novel ways. Mechanical stimulation can be used to enhance volitional remote control of robotic devices, e.g. prosthetics (see Robles-De-La-Torre, 2008), to interface patterns of rhythmic locomotion in concert with supraspinal commands.

Appendices for Chapter 1: Brain reconstructions for all experiments



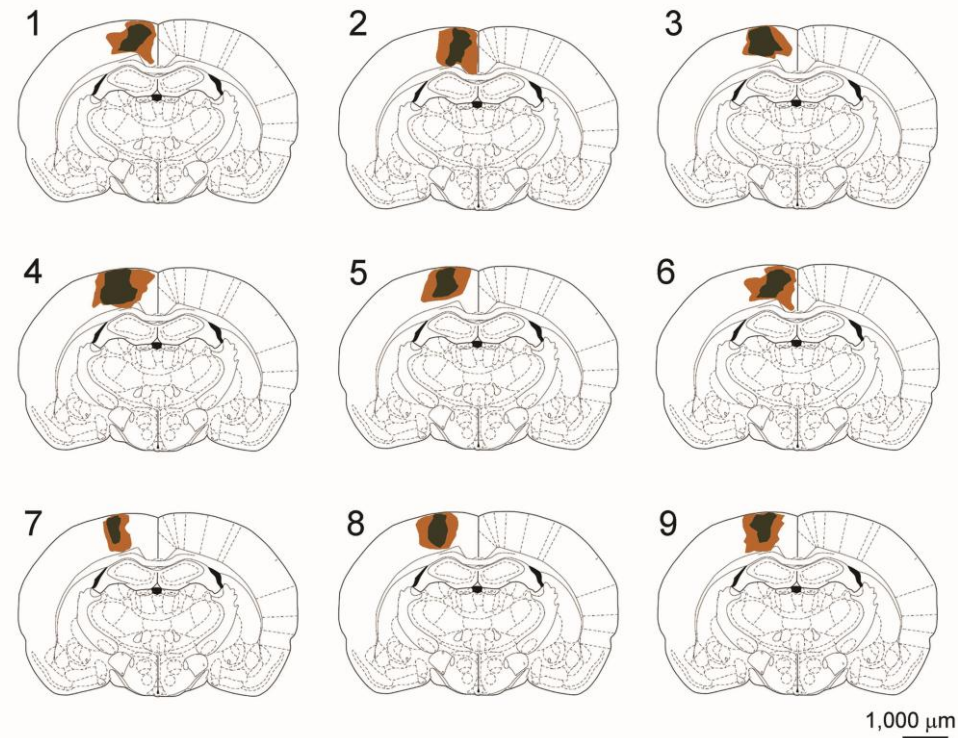
Appendix 1 Figure 1 Brain reconstructions for all MLF brain injection sites

100 μm thick coronal sections were reacted with DAB to reveal the CTb tracer labelling the MLF. To identify the labelled anatomical regions, template drawings from Paxinos and Watson (1997) were superimposed onto scaled photomicrographs. The cerebellum is not shown. The inner darker brown area depicts the core of the injection site and the outer brown area depicts the maximum diffusion of CTb within the brain. During the surgical procedures, the glass micropipette was positioned into the left side of the brain very near the midline (mediolateral = + 0.1). Labelled anatomical regions are shown and described in Chapter 3 and surgical procedures are described in Chapter 2. Animal numbers are designated (1 - 8) for all experiments.



Appendix 1 Figure 2 Brain reconstructions for all CVLM brain injection sites

100 μm thick coronal sections were reacted with DAB to reveal the CTb tracer labelling the CVLM. To identify the labelled anatomical regions, template drawings from Paxinos and Watson (1997) were superimposed onto scaled photomicrographs. The cerebellum is not shown. The inner darker brown area depicts the core of the injection site and the outer brown area depicts the maximum diffusion of CTb within the brain. During the surgical procedures, the glass micropipette was positioned into the left side of the brain. Labelled anatomical regions are shown and described in Chapter 3 and surgical procedures are described in Chapter 2. Animal numbers are designated (1 - 6) for all experiments.



Appendix 1 Figure 3 Brain reconstructions for all sensorimotor cortex brain injection sites

100 μm thick coronal sections were reacted with DAB to reveal the CTb tracer labelling the CST. To identify the labelled anatomical regions, template drawings from Paxinos and Watson (1997) were superimposed onto scaled photomicrographs. The inner darker brown area depicts the core of the injection site and the outer brown area depicts the maximum diffusion of CTb within the brain. During the surgical procedures, the glass micropipette was positioned into the left side of the brain. Labelled anatomical regions are shown and described in Chapter 4 and surgical procedures are described in Chapter 2. Animal numbers are designated (1 - 9) for all experiments.

Appendices for Chapter 2: Laboratory reagents

Appendix 2 Table 1 Formulae for common laboratory reagents

To prepare 4 L of 0.1 M phosphate buffer (PB) stock solution:

37.4 g of $\text{NaH}_2\text{PO}_4 \cdot 2\text{H}_2\text{O}$ in 1200 ml H_2O

84.9 g Na_2HPO_4 in 3000 ml H_2O

Distilled water is added to bring the total volume to 4 L with buffered pH 7.4

To prepare 0.3 M phosphate buffer saline solution (PBS):

100 ml of 0.2 M PB in 1900 distilled water plus 36 g NaCl

Sucrose PB: 30 g sucrose in PB

PBST: 0.3% Triton X-100 in PB

Ringer solution:

Contains $\text{CaCl}_2 + \text{KCl} + \text{NaCl} + \text{NaHCO}_3 + \text{glucose}$ in PB, buffered to pH 7.4

To prepare 1L of 4% paraformaldehyde fixative solution:

40 g paraformaldehyde

400 ml distilled H_2O at $\approx 68^\circ\text{C}$

500 ml 0.2 PB

NaOH, to raise pH (few drops)

Solution is cooled and then filtered with enough distilled water added to bring the total volume to 1 L with pH adjusted as necessary

$$\text{pH} = -\log [\text{H}^+]$$

C = Celsius; g = grams; L = litres; log = logarithmic, base 10; ml = millilitre; M = molar (moles per litre).

Appendix 2 Table 2 Primary antibody characterisation

The following summarised information regarding antibody specificity, controls, species reactivity, and application is provided as per suppliers' data information as referenced in Tables 3.1, 4.1 and 5.1 in Chapters 3, 4 and 5, respectively.

5-HT Labels synaptic terminals containing 5-HT. This antibody was quality control tested using standard immunocytochemistry (ICC) methods. This antiserum demonstrates positive labelling of rat hypothalamus, raphé nuclei and spinal cord using indirect immunofluorescent and AvHRP techniques.

ChAT Labels cells by catalysing the reversible synthesis of ACh from acetyl coenzyme and choline at ChAT synapses. The specificity of ChAT is shown by ChAT neurons in the brain and spinal cord. Positive controls include the presence of immunostaining in human placenta lysates, rat forebrain/rostral hypothalamus. For quality assurance, this antiserum is routinely evaluated by Western blots on mouse brain lysates.

CTb Traces myelinated axons possessing the GM1 ganglioside, retrogradely and anterogradely. The specificity of antibody against CTb is demonstrated by the lack of staining in regions of the CNS that did not contain neurons that had transported the tracer and by the presence of immunostaining in neurons known to project to the injection sites.

DBH Recognises the enzyme DBH that is present in axons that synthesise NA. This antiserum reacts with a single band on Western blots of bovine adrenal homogenates. For positive controls, this antibody stains only cells known to contain DBH, such as sympathetic neurons, adrenal medullary cells and central adrenergic neurons.

GAD67 Labels synaptic vesicles recognising glutamic acid decarboxylase isoform 67. To ensure specificity, this antiserum was found to react with 67kDa isoform of GAD67 of rat, mouse and human origins. Quality assurance was evaluated by immunohistochemistry by SK-N-SH cell lysate (human neuroblastoma cell line).

GlyT2 Labels the plasma membrane. To ensure specificity, this antiserum was tested on tissue sections from the CNS and the staining pattern corresponds to the pattern described using *in situ* hybridisation with probes to GlyT2 mRNA.

nNOS Labels cells producing nitric oxide. The specificity of this antibody is shown by immunoreactivity with nNOS in the human brain and this sequence is highly conserved in rat and mouse as well. Antibody binding is neutralised in Western blot by pre-adsorption with the immunogen peptide.

VGAT This antibody is specific for VGAT (molecular weight 57 kDa) and antiserum specificity is assured by Western blot on rat retina lysates. The immunogen peptide shows no significant homology with other known proteins.

VGLUT1 This antibody is specific for VGLUT1 (molecular weight 62 kDa) localised in synaptic vesicles exhibiting excitatory features. Antiserum specificity is assured by ICC on tissue sections from the rat CNS corresponding to the pattern described using other antisera to VGLUT1.

VGLUT2 This antibody is specific for VGLUT2 (molecular weight 52 kDa) localised in synaptic vesicles exhibiting excitatory features. Antiserum specificity is assured by Western blots on rat brain lysate.

Appendix 2 Table 3 Allocation of processed spinal cord tissue containing anterograde labelled axons (and naïve tissue) for all experiments

		Animal Numbers (L3, L4, L5 segments)																								
		MLF								CVLM						CST									naïve	
Chapter	Aim	1	2	3	4	5	6	7	8	1	2	3	4	5	6	1	2	3	4	5	6	7	8	9	(1)	
3	1	x	x	x	x	x	x	x	x	x	x	x	x	x	x											
	2	x	x	x						x	x	x														
	3	x	x	x						x	x	x														
	4	x	x		x					x	x	x														
4	1															x	x	x	x	x	x	x	x	x	x	
	2															x	x	x								
	3																		x	x	x	x	x	x	x	
	4																						x	x	x	
5	1									x			x	x	x											
	2				x		x	x	x																	
	3						x	x	x																	
	4																									x

Spinal segments L3, L4, and L4 were used interchangeably for experiments. Surplus processed tissues were often stored frozen for later experiments. Any given segment could be cut in more than one plane of orientation by re-positioning it on the Vibratome chuck. Tissues contained anterogradely labelled axon terminals as indicated (MLF, CVLM and CST). Tissue from a rat receiving no CTb injection (naïve tissue) was used for one experiment.

Appendices for Chapter 3: Data tables

Appendix 3 Table 1 Glutamatergic axon terminals from the MLF and CVLM

MLF							
Animal No.	Ave. Total No. CTb Terminals	Ave. % VGLUT1/CTb	Ave. % VGLUT2/CTb	Ave. % VGLUT1&VGLUT2/CTb 'double-label'	Ave. VGLUT1/CTb volumetric density, $\mu\text{m}^3 \times 10^8$	Ave. VGLUT2/CTb volumetric density, $\mu\text{m}^3 \times 10^8$	Ave. VGLUT1&VGLUT2/CTb volumetric density, $\mu\text{m}^3 \times 10^8$ 'double-label'
1	58	0	59.34	0	0	4.74	0
2	153	0	68.92	0	0	3.09	0
3	150	0	53.30	0	0	6.33	0
Sum/Ave	361	0	60.52	0	0	4.72	0
\pm SD	-	-	7.88	-	-	1.62	-
CVLM							
1	1042	0.38	64.59	0.38	0.02	3.89	0.02
2	903	1.44	63.34	0.11	0.09	3.85	0.01
3	936	0.64	58.65	0.32	0.04	4.06	0.02
Sum/Ave.	2881	0.82	62.20	0.27	0.05	3.93	0.02
\pm SD	-	0.55	3.13	0.14	0.03	0.11	0.01
Ave. = average; No. = number; SD = standard deviation							

The number of immunoreactive MLF and CVLM axon terminals containing VGLUT1 and VGLUT2 from scan fields were summed and expressed in terms of volumetric density based upon the laminar volumes for L3, L4 and/or L5 segments in the transverse plane.

Appendix 3 Table 2 Excitatory and inhibitory axon terminals from the MLF and CVLM

MLF					
Animal No.	Ave. Total No. CTb Terminals	Ave. % [VGLUT1+VGLUT2] /CTb	Ave. % VGAT/CTb	Ave. [VGLUT1+VGLUT2]/CTb volumetric density, $\mu\text{m}^3 \times 10^8$	Ave. VGAT/CTb volumetric density, $\mu\text{m}^3 \times 10^8$
1	246	57.07	22.65	4.91	1.95
2	122	57.32	26.86	4.99	2.45
3	377	69.31	14.84	6.24	1.30
Sum/Average	745	61.23	21.45	5.38	1.90
\pm SD	-	7.00	6.10	0.75	0.57
CVLM					
1	334	65.37	23.13	6.02	2.13
2	997	72.34	20.47	5.21	1.54
3	288	57.01	24.71	4.79	2.20
Sum/Average	1619	64.91	22.77	5.34	1.96
\pm SD	-	7.68	2.15	0.63	0.36
Ave. = average; No. = number; SD = standard deviation					

The number of immunoreactive MLF and CVLM axon terminals containing [VGLUT1+VGLUT2] and VGAT from scan fields were summed and expressed in terms of volumetric density based upon the laminar volumes for L3, L4 and/or L5 segments in the transverse plane.

Appendix 3 Table 3 Inhibitory axon terminals from the MLF and CVLM

MLF							
Animal No.	Ave. Total No. CTb Terminals	Ave. % GlyT2/CTb	Ave. % GAD67/CTb	Ave. % GlyT2+GAD67/CTb 'double-label'	Ave. GlyT2/CTb volumetric density, $\mu\text{m}^3 \times 10^8$	Ave. GAD67/CTb, volumetric density, $\mu\text{m}^3 \times 10^8$	Ave. GlyT2+GAD67/CTb, volumetric density, $\mu\text{m}^3 \times 10^8$ 'double-label'
1	516	12.31	9.92	3.58	3.15	5.23	0.70
2	528	6.04	9.73	2.24	1.69	3.08	0.70
3	1377	8.80	2.97	00.65	1.66	0.57	0.12
Sum/Ave.	2421	9.05	7.54	2.15	2.17	2.96	0.51
\pm SD	-	3.14	3.96	1.47	0.85	2.34	0.34
CVLM							
1	1220	11.30	8.85	2.77	3.07	2.27	0.69
2	1818	12.11	8.33	2.02	3.93	2.24	0.61
3	885	14.13	8.83	3.92	2.89	1.71	0.73
Sum/Ave.	3923	12.51	8.67	2.91	3.30	2.07	0.68
\pm SD	-	1.46	0.29	0.96	0.55	0.32	0.06
Ave. = average; No. = number; SD = standard deviation							

The number of immunoreactive MLF and CVLM axon terminals containing GlyT2 and GAD67 from scan fields were summed and expressed in terms of volumetric density based upon the laminar volumes for L3, L4 and/or L5 segments in the transverse plane.

Appendices for Chapter 4: Data tables

Appendix 4 Table 1 CST axon terminals immunoreacted with antibodies against VGLUT1 and VGLUT2

Animal No. (CST)	Ave. Total No. CTb Terminals	Ave. No. VGLUT1/CTb Terminals	Ave. No. VGLUT2/CTb Terminals	Ave. %VGLUT1/CT b Terminals	Ave. %VGLUT2/CT b Terminals
1	330	326	4	98.79	1.21
2	577	572	5	99.13	0.87
3	320	317	3	99.06	0.94
Sums/Ave	1227	1215	12	98.99	1.01
.					
\pm SD	145.58	144.70	1.00	0.18	0.18
Ave. = average; No. = number; SD = standard deviation					

Immunoreactive axon terminals from the sensorimotor cortex containing VGLUT1 and VGLUT2 from scan fields were summed and expressed as percentages for L3, L4 and/or L5 segments in the transverse plane.

Appendix 4 Table 2 CST axon terminals immunoreacted with antibodies against VGLUT1, VGLUT2 and VGAT

Animal No. (CST)	Ave. Total No. CTb Terminals	Ave. No. [VGLUT1+VGLUT2] / CTb Terminals	Ave. No. VGAT/CTb Terminals	Ave. %[VGLUT1+VGLUT2]/ CTb Terminals	Ave. % VGAT/CTb Terminals
1	409	409	0	100	0
2	196	196	0	100	0
3	276	276	0	100	0
Sums/Ave	881	881	0	100	0
.					
± SD	107.59	107.59	-	-	-
Ave. = average; No. = number; SD = standard deviation					

Immunoreactive axon terminals from the sensorimotor cortex containing [VGLUT1 + VGLUT2] and not VGAT from scan fields were summed and expressed as percentages for L3, L4 and/or L5 segments in the transverse plane.

Appendix 4 Table 3 Immunoreactive boutons onto laminae I- V ChAT interneurons targeted by the CST in the transverse plane

LAMINAE I - V TRANSVERSE									
					Density = No. Boutons • 1,000 μm^{-2}				
SOMATIC									
Animal No. (CST)	No. Cells	Ave. No. CTb+VGLUT1 Contacts	Ave. Total No. VGLUT1 Contacts	Ave. Radii μm			Ave. CTb+VGLUT1 Contacts	Ave. Total VGLUT1 Contacts	
4	5	8	17	9.13			1.57	5.23	
5	3	8	9	8.23			2.56	5.28	
6	7	21	28	8.34			0.67	2.83	
Sum/Ave	15	37	54	8.58			1.60	4.45	
\pm SD	-	7.51	9.54	0.47			0.95	1.40	
DENDRITIC									
Animal No. (CST)	No. Cells	Ave. No. CTb+VGLUT1 Contacts	Ave. Total No. VGLUT1 Contacts	Ave. No. Dendrites	Ave. Length μm			Ave. CTb+VGLUT1 Contacts	Ave. Total VGLUT1 Contacts
4	5	12	18	2.80	134.20			2.73	4.93
5	3	4	4	2.33	43.23			3.73	3.73
6	7	42	52	2.29	116.33			2.24	15.58
Sum/Ave	15	58	74	2.47	97.92			2.47	8.08
\pm SD	-	20.03	24.68	0.28	48.20			0.28	6.53
Ave. = average; No. = number; SD = standard deviation									

VGLUT1⁺CTb and VGLUT1 contacts onto ChAT interneurons were expressed in terms of surface area densities.

Appendix 4 Table 4 Immunoreactive boutons onto laminae VI - VII ChAT interneurons targeted by the CST in the transverse plane

LAMINAE VI - VII TRANSVERSE							
						Density = No. Boutons • 1,000 μm^{-2}	
SOMATIC							
Animal No. (CST)	No. Cells	Ave. No. CTb ⁺ VGLUT1 Contacts	Ave. Total No. VGLUT1 Contacts	Ave. Radii μm		Ave. CTb ⁺ VGLUT1 Contacts	Ave. Total VGLUT1 Contacts
4	8	0	11	7.79		0	1.92
5	4	0	9	10.40		0	1.54
6	5	0	12	13.07		0	0.89
Sum/Ave	17	0	32	10.42		0	1.45
\pm SD	-	-	1.53	2.64		-	0.52
DENDRITIC							
Animal No. (CST)	No. Cells	Ave. No. CTb ⁺ VGLUT1 Contacts	Ave. Total No. VGLUT1 Contacts	Ave. No. Dendrites	Ave. Length μm	Ave. CTb ⁺ VGLUT1 Contacts	Ave. Total VGLUT1 Contacts
4	8	3	17	2.38	62.48	1.21	5.26
5	4	0	13	2.50	88.28	0.00	8.41
6	5	1	13	2.40	99.40	0.15	2.69
Sum/Ave	17	4	43	2.43	81.72	0.45	5.46
\pm SD	-	1.53	2.31	0.07	18.51	0.66	2.86
Ave. = average; No. = number; SD = standard deviation							

VGLUT1⁺CTb and VGLUT1 contacts onto ChAT interneurons were expressed in terms of surface area densities.

Appendix 4 Table 5 Immunoreactive boutons onto lamina X ChAT interneurons targeted by the CST in the transverse plane

LAMINA X TRANSVERSE							
						Density = No. Boutons • 1,000 μm^{-2}	
SOMATIC							
Animal No. (CST)	No. Cells	Ave. No. CTb ⁺ VGLUT1 Contacts	Ave. Total No. VGLUT1 Contacts	Ave. Radii μm		Ave. CTb ⁺ VGLUT1 Contacts	Ave. Total VGLUT1 Contacts
4	14	0	19	7.98		0	1.75
5	10	2	24	8.88		0.20	2.31
6	8	1	21	10.63		0.10	1.87
Count/Sum/Ave	32	3	64	9.16		0.10	1.98
\pm SD	-	1.00	2.52	1.35		0.10	0.29
DENDRITIC							
Animal No. (CST)	No. Cells	Ave. No. CTb ⁺ VGLUT1 Contacts	Ave. Total No. VGLUT1 Contacts	Ave. No. Dendrites	Ave. Length μm	Ave. CTb ⁺ VGLUT1 Contacts	Ave. Total VGLUT1 Contacts
4		1	34	2.00	87.22	0.07	4.78
5		1	21	1.90	59.77	0.26	7.89
6		1	15	3.00	94.24	0.10	3.91
Count/Sum/Ave		3	70	2.30	80.41	0.14	5.53
\pm SD		0.00	9.71	0.61	18.22	0.10	2.09
Ave. = average; No. = number; SD = standard deviation							

VGLUT1⁺CTb and VGLUT1contacts onto ChAT interneurons were expressed in terms of surface area densities.

Appendix 4 Table 6 Immunoreactive boutons onto laminae I - V ChAT interneurons targeted by the CST in the parasagittal plane

LAMINAE I - V PARASAGITTAL							
						Density = No. Boutons • 1,000 μm^{-2}	
SOMATIC							
Animal No. (CST)	No. Cells	Ave. No. CTb ⁺ VGLUT1 Contacts	Ave. Total No. VGLUT1 Contacts	Ave. Radii μm		Ave. CTb ⁺ VGLUT1 Contacts	Ave. Total VGLUT1 Contacts
7	2	7	12	11.92		2.22	3.99
8	5	5	21	8.26		1.80	5.24
9	5	7	45	9.51		1.21	9.29
Count/Sum/Ave	12	19	78	9.90		1.74	6.17
\pm SD	-	1.15	17.06	1.86		0.51	2.27
DENDRITIC							
Animal No. (CST)	No. Cells	Ave. No. CTb ⁺ VGLUT1 Contacts	Ave. Total No. VGLUT1 Contacts	Ave. No. Dendrites	Ave. Length μm	Ave. CTb ⁺ VGLUT1 Contacts	Ave. Total VGLUT1 Contacts
7	2	14	37	4.50	582.00	3.26	9.25
8	5	12	66	2.20	290.04	1.79	8.51
9	5	22	119	2.80	261.96	4.72	18.13
Count/Sum/Ave	12	48	222	3.17	378.00	3.26	11.96
\pm SD	-	5.29	41.58	1.19	177.23	1.46	5.35
Ave. = average; No. = number; SD = standard deviation							

VGLUT1⁺CTb and VGLUT1contacts onto ChAT interneurons were expressed in terms of surface area densities.

Appendix 4 Table 7 Immunoreactive boutons onto laminae VI - VII ChAT interneurons targeted by the CST in the parasagittal plane

LAMINAE VI - VII PARASAGITTAL							
						Density = No. Boutons • 1,000 μm^{-2}	
SOMATIC							
Animal No. (CST)	No. Cells	Ave. No. CTb ⁺ VGLUT1 Contacts	Ave. Total No. VGLUT1 Contacts	Ave. Radii μm		Ave. CTb ⁺ VGLUT1 Contacts	Ave. Total VGLUT1 Contacts
7	3	1	9	9.53		0.40	2.94
8	4	2	9	13.18		0.17	1.00
9	2	2	15	13.72		0.42	3.19
Count/Sum/Ave	9	5	33	12.14		0.33	2.38
\pm SD	-	0.58	3.46	2.28		0.14	1.20
DENDRITIC							
Animal No. (CST)	No. Cells	Ave. No. CTb ⁺ VGLUT1 Contacts	Ave. Total No. VGLUT1 Contacts	Ave. No. Dendrites	Ave. Length μm	Ave. CTb ⁺ VGLUT1 Contacts	Ave. Total VGLUT1 Contacts
7	3	13	39	2.67	304.70	2.89	9.05
8	4	13	41	3.75	376.20	1.68	5.03
9	2	4	15	2.00	239.00	1.07	4.25
Count/Sum/Ave	9	30	95	2.81	306.63	1.88	6.11
\pm SD	-	5.20	14.47	0.88	68.62	0.93	2.58
Ave. = average; No. = number; SD = standard deviation							

VGLUT1⁺CTb and VGLUT1 contacts onto ChAT interneurons were expressed in terms of surface area densities.

Appendix 4 Table 8 Immunoreactive boutons onto lamina X ChAT interneurons targeted by the CST in the parasagittal plane

LAMINA X PARASAGITTAL							
						Density = No. Boutons • 1,000 μm^{-2}	
SOMATIC							
Animal No. (CST)	No. Cells	Ave. No. CTb ⁺ VGLUT1 Contacts	Ave. Total No. VGLUT1 Contacts	Ave. Radii μm		Ave. CTb ⁺ VGLUT1 Contacts	Ave. Total VGLUT1 Contacts
7	9	7	41	9.80		0.64	3.75
8	3	0	12	11.54		0.00	2.42
9	2	0	11	11.86		0.00	3.26
Count/Sum/Ave	14	7	64	11.07		0.21	3.15
\pm SD	-	4.04	17.04	1.11		0.37	0.67
DENDRITIC							
Animal No. (CST)	No. Cells	Ave. No. CTb ⁺ VGLUT1 Contacts	Ave. Total No. VGLUT1 Contacts	Ave. No. Dendrites	Ave. Length μm	Ave. CTb ⁺ VGLUT1 Contacts	Ave. Total VGLUT1 Contacts
7	9	18	99	2.78	280.21	1.97	9.40
8	3	3	39	3.33	381.97	0.70	8.60
9	2	2	22	2.50	288.15	0.70	6.77
Count/Sum/Ave	14	23	160	2.87	316.78	1.12	8.26
\pm SD	-	8.96	40.45	0.42	56.60	0.73	1.35
Ave. = average; No. = number; SD = standard deviation							

VGLUT1⁺CTb and VGLUT1contacts onto ChAT interneurons were expressed in terms of surface area densities.

Appendix 4 Table 9 Densities of ChAT dorsoventral and rostrocaudal interneurons related to dendritic orientations

XY Ratio < 1 (DV) Orientation, Parasagittal				
Total VGLUT1 and VGLUT1 ⁺ CTb contact density = No. Boutons • 1,000 μm^{-2}				
Animal No. (CST)	Dorsocauda I	Dorsorostral	Ventrorostral	Ventrocaudal
7	2.35	2.48	0.72	0.78
8	3.52	1.23	1.50	0.91
9	-	1.58	1.10	1.13
Averages	2.94	1.76	1.10	0.94
\pm SD	0.83	0.64	0.39	0.17
XY Ratio > 1 (RC) Orientation, Parasagittal				
Total VGLUT1 and VGLUT1 ⁺ CTb contact density = No. Boutons • 1,000 μm^{-2}				
Animal No. (CST)	Dorsocauda I	Dorsorostral	Ventrorostral	Ventrocaudal
7	1.55	1.02	1.58	0.79
8	1.24	1.91	0.48	1.45
9	2.17	1.16	0.47	0.55
Averages	1.65	1.36	0.84	0.93
\pm SD	0.78	0.48	0.64	0.47
Ave. = average; No. = number; SD = standard deviation				

The VGLUT1⁺CTb and VGLUT1 contact densities of dorsoventral (DV) ChAT interneurons (XY Ratio < 1) and rostrocaudal (RC) ChAT interneurons (XY Ratio > 1) across I-VII and X laminar boundaries were classified according to their dendritic orientation.

Appendices for Chapter 5: Data tables

Appendix 5 Table 1 Glutamatergic contacts onto laminae III - V ChAT interneurons targeted by the CVLM in the transverse plane

LAMINAE III - V TRANSVERSE								
						Density = No. Boutons • 1,000 μm^{-2}		
SOMATIC								
Animal No. (CVLM)	No. Cells	%ML Cells	Ave. No. VGLUT2 ⁺ CTb Contacts	Ave. Total No. CTb Contacts	Ave. Radii μm		Ave. VGLUT2 ⁺ CTb Contacts	Ave. Total CTb Boutons
1	4	100.00	7	2	9.36		1.34	2.64
4	10	80.00	9	15	7.26		1.47	2.41
5	6	66.67	11	15	12.68		1.06	1.36
Count/Sum/Ave	20	82.22	27	42	9.77		1.29	2.13
\pm SD		16.78	2.00	1.73	2.72		0.21	0.68
DENDRITIC								
Animal No. (CVLM)	No. Cells	% ML Cells	Ave. No. VGLUT2 ⁺ CTb Contacts	Ave. Total No. CTb Contacts	Ave. No. Dendrites	Ave. Length μm	Ave. VGLUT2 ⁺ CTb Contacts	Ave. Total CTb Contacts
1	4	100.00	8	17	3.00	141.15	1.59	3.51
4	10	80.00	42	57	2.50	153.96	5.39	7.48
5	6	66.67	15	30	4.17	250.55	1.42	2.42
Count/Sum/Ave	20	82.22	65	104	3.22	181.89	2.80	4.47
\pm SD		16.78	17.95	20.40	0.86	59.81	2.25	2.66
Ave. = average; No. = number; SD = standard deviation								

CTb contacts containing VGLUT2 onto mediolateral (ML) and dorsoventral ChAT interneurons were expressed in terms of surface area densities.

Appendix 5 Table 2 Glutamatergic contacts onto laminae VI - VII ChAT interneurons targeted by the CVLM in the transverse plane

LAMINAE VI - VII TRANSVERSE									
							Density = No. Boutons • 1,000 μm^{-2}		
SOMATIC									
Animal No. (CVLM)	No. Cells	%ML Cells	Ave. No. VGLUT2 ⁺ CTb Contacts	Ave. Total No. CTb Contacts	Ave. Radii μm	Ave. VGLUT2 ⁺ CTb Contacts		Ave. Total CTb Boutons	
1	9	66.67	52	68	13.26	2.79		3.78	
4	3	66.67	19	22	13.22	2.95		3.66	
5	5	60.00	21	30	14.05	1.64		2.68	
Count/Sum/Ave	17	64.44	92	120	13.51	2.46		3.37	
\pm SD		3.85	18.50	24.58	0.47	0.71		0.60	
DENDRITIC									
Animal No. (CVLM)	No. Cells	%ML Cells	Ave. No. VGLUT2 ⁺ CTb Contacts	Ave. Total No. CTb Contacts	Ave. No. Dendrites	Ave. Length μm	Ave. VGLUT2 ⁺ CTb Contacts		Ave. Total CTb Contacts
1	9	66.67	62	118	3.44	245.80	3.70		7.08
4	3	66.67	16	25	3.67	247.77	2.17		3.31
5	5	60.00	34	66	3.20	293.48	2.41		4.72
Count/Sum/Ave	17	64.44	112	209	3.44	262.35	2.76		5.04
\pm SD		3.85	23.18	46.61	0.23	26.98	0.82		1.90
Ave. = average; No. = number; SD = standard deviation									

CTb contacts containing VGLUT2 onto mediolateral (ML) and dorsoventral ChAT interneurons were expressed in terms of surface area densities.

Appendix 5 Table 3 Glutamatergic contacts onto lamina X ChAT interneurons targeted by the CVLM in the transverse plane

LAMINAE X TRANSVERSE								
						Density = No. Boutons • 1,000 μm^{-2}		
SOMATIC								
Animal No. (CVLM)	No. Cells	%ML Cells	Ave. No. VGLUT2 ⁺ CTb Contacts	Ave. Total No. CTb Contacts	Ave. Radii μm	Ave. VGLUT2 ⁺ CTb Contacts	Ave. Total CTb Boutons	
1	4	25.00	8	18	10.65	1.30	3.08	
4	6	66.67	24	26	12.59	2.01	2.41	
5	10	20.00	40	49	12.02	2.24	2.99	
Count/Sum/Ave	20	37.22	72	93	11.75	1.85	2.83	
\pm SD		25.62	16.00	16.09	1.00	0.49	0.36	
DENDRITIC								
Animal No. (CVLM)	No. Cells	%ML Cells	Ave. No. VGLUT2 ⁺ CTb Contacts	Ave. Total No. CTb Contacts	Ave. No. Dendrites	Ave. Length μm	Ave. VGLUT2 ⁺ CTb Contacts	Ave. Total CTb Contacts
1	4	25.00	21	28	3.25	126.50	7.60	10.43
4	6	66.67	40	46	2.33	166.43	7.86	9.09
5	10	20.00	69	93	3.30	159.70	9.58	12.28
Count/Sum/Ave	20	37.22	130	167	2.96	150.88	8.34	10.60
\pm SD		25.62	24.17	33.56	0.54	21.38	1.08	1.60

Ave. = average; No. = number; SD = standard deviation

CTb contacts containing VGLUT2 onto mediolateral (ML) and dorsoventral ChAT interneurons were expressed in terms of surface area densities.

Appendix 5 Table 4 Inhibitory contacts onto laminae III - V ChAT interneurons targeted by the CVLM in the transverse plane

LAMINAE III - V TRANSVERSE								
						Density = No. Boutons • 1,000 μm^{-2}		
SOMATIC								
Animal No. (CVLM)	No. Cells	%ML Cells	Ave. No. VGAT ⁺ CTb Contacts	Ave. Total No. CTb Contacts	Ave. Radii μm		Ave. VGAT ⁺ CTb Contacts	Ave. Total CTb Boutons
6	7	57.14	6	25	9.85		0.84	3.63
1	9	44.44	7	22	11.63		0.66	1.76
5	3	66.67	0	5	14.49		0.00	0.60
Count/Sum/Ave	19	56.08	13	52	11.99		0.50	2.00
\pm SD		11.15	3.79	10.79	2.34		0.44	1.53
DENDRITIC								
Animal No. (CVLM)	No. Cells	%ML Cells	Ave. No. VGAT ⁺ CTb Contacts	Ave. Total No. CTb Contacts	Ave. No. Dendrites	Ave. Length μm	Ave. VGAT ⁺ CTb Contacts	Ave. Total CTb Contacts
6	7	57.14	9	61	2.57	227.76	1.27	5.61
1	9	44.44	19	47	2.67	142.13	1.67	4.16
5	3	66.67	7	14	3.00	168.83	1.22	2.72
Count/Sum/Ave	19	56.08	35	122	2.75	179.57	1.38	4.16
\pm SD		11.15	6.43	24.13	0.23	43.81	0.25	1.45
Ave. = average; No. = number; SD = standard deviation								

CTb contacts containing VGAT onto mediolateral (ML) and dorsoventral ChAT interneurons were expressed in terms of surface area densities.

Appendix 5 Table 5 Inhibitory contacts onto laminae VI - VII ChAT interneurons targeted by the CVLM in the transverse plane

LAMINAE VI - VII TRANSVERSE								
						Density = No. Boutons • 1,000 μm^{-2}		
SOMATIC								
Animal No. (CVLM)	No. Cells	%ML Cells	Ave. No. VGAT ⁺ CTb Contacts	Ave. Total No. CTb Contacts	Ave. Radii μm		Ave. VGAT ⁺ CTb Contacts	Ave. Total CTb Boutons
6	11	27.28	4	18	13.21		0.19	0.78
1	5	40.00	4	13	11.02		0.65	1.95
5	8	12.50	5	14	9.49		0.52	1.46
Count/Sum/Ave	24	26.59	13	45	11.24		0.45	1.40
\pm SD		13.76	0.58	2.65	1.87		0.24	0.59
DENDRITIC								
Animal No.	No. Cells	%ML Cells	Ave. No. VGAT ⁺ CTb Contacts	Ave. Total No. CTb Contacts	Ave. No. Dendrites	Ave. Length μm	Ave. VGAT ⁺ CTb Contacts	Ave. Total CTb Contacts
6	11	27.28	12	58	4.00	294.02	0.60	2.57
1	5	40.00	16	34	2.00	195.16	1.68	4.00
5	8	12.50	14	28	1.88	60.36	1.29	5.49
Count/Sum/Ave	24	26.59	45	120	2.63	183.18	1.19	4.02
\pm SD		13.76	2.65	15.87	1.19	117.29	0.54	1.46

Ave. = average; No. = number; SD = standard deviation

CTb contacts containing VGAT onto mediolateral (ML) and dorsoventral ChAT interneurons were expressed in terms of surface area densities.

Appendix 5 Table 6 Inhibitory contacts onto lamina X ChAT interneurons targeted by the CVLM in the transverse plane

LAMINAE X TRANSVERSE								
						Density = No. Boutons • 1,000 μm^{-2}		
SOMATIC								
Animal No. (CVLM)	No. Cells	%ML Cells	Ave. No. VGAT ⁺ CTb Contacts	Ave. Total No. CTb Contacts	Ave. Radii μm		Ave. VGAT ⁺ CTb Contacts	Ave. Total CTb Boutons
6	3	80.10	3	3	11.28		0.55	0.55
1	9	70.22	4	20	9.92		0.44	2.03
5	6	62.21	2	15	9.68		0.50	2.19
Count/Sum/Ave	18	70.84	9	38	10.29		0.50	1.59
\pm SD		8.96	1.00	8.74	0.86		0.05	0.90
DENDRITIC								
Animal No.	No. Cells	%ML Cells	Ave. No. VGAT ⁺ CTb Contacts	Ave. Total No. CTb Contacts	Ave. No. Dendrites	Ave. Length μm	Ave. VGAT ⁺ CTb Contacts	Ave. Total CTb Contacts
6	3	80.10	7	12	4.33	188.57	2.12	3.80
1	9	70.22	33	53	3.22	179.87	3.99	6.28
5	6	62.21	5	31	2.33	106.23	1.05	6.82
Count/Sum/Ave	18	70.84	45	96	3.30	158.22	2.39	5.64
\pm SD		8.96	15.62	20.52	1.00	45.23	1.49	1.61
Ave. = average; No. = number; SD = standard deviation								

CTb contacts containing VGAT onto mediolateral (ML) and dorsoventral ChAT interneurons were expressed in terms of surface area densities.

Appendix 5 Table 7 Laminae VI - VII ChAT interneurons targeted by the MLF and 5-HT in the horizontal plane

MLF LAMINAE VI-VII HORIZONTAL									
							Density = No. Boutons • 1,000 μm^{-2}		
SOMATIC									
Animal No. (MLF)	No. ChAT Cells	%contra- lateral cells	%ChAT cells nNOS ⁺	No. CTb Contacts	No. 5-HT Contacts	Ave. Radii μm	Ave. Density CTb Contacts	Ave. Density 5- HT Contacts	
6	7	42.86	14.29	14	7	12.93	1.00	0.40	
7	4	75.00	50.00	4	17	10.63	0.68	3.07	
8	6	33.33	50.00	19	37	12.09	1.01	2.56	
Count/Sum/Ave	17	50.40	38.10	37	61	12.18	0.89	2.01	
\pm SD	-	21.83	20.62	7.64	15.28	1.35	0.19	1.42	
DENDRITIC									
Animal No. (MLF)	No. ChAT Cells	%contra- lateral cells	%ChAT cells nNOS ⁺	No. CTb Contacts	No. 5-HT Contacts	Ave. No. Dendrites	Ave. Length μm	Ave. Density CTb Contacts	Ave. Density 5- HT Contacts
6	7	42.86	14.29	34	42	3.86	372.41	2.16	2.65
7	4	75.00	50.00	13	33	2.25	266.33	1.84	4.70
8	6	33.33	50.00	32	125	2.67	322.72	2.36	6.68
Count/Sum/Ave	17	50.40	38.10	79	200	2.92	320.49	2.12	4.68
\pm SD	-	21.83	20.62	11.59	50.72	0.83	53.08	0.26	2.01
Ave. = average; No. = number; SD = standard deviation									

CTb contacts and 5-HT contacts onto ChAT interneurons located in bilaterally intermediate zones were expressed in terms of surface area densities. Interneurons classified as contralateral were located opposite to the MLF brain injection site.

Appendix 5 Table 8 Lamina X ChAT interneurons targeted by the MLF and 5-HT in the horizontal plane

LAMINAE X HORIZONTAL									
							Density = No. Boutons • 1,000 μm^{-2}		
SOMATIC									
Animal No. (MLF)	No. ChAT Cells	%contra- lateral cells	%ChAT cells nNOS ⁺	No. CTb Contacts	No. 5-HT Contacts	Ave. Radii μm	Ave. Density CTb Contacts	Ave. Density 5- HT Contacts	
6	3	66.67	100	10	7	11.14	2.25	1.75	
7	5	80.00	100	7	13	13.47	0.65	1.40	
8	7	42.86	71.43	10	13	13.12	0.72	0.77	
Count/Sum/Ave	15	63.17	90.48	27	33	12.58	1.20	1.31	
\pm SD	-	18.82	16.50	1.73	3.46	1.26	0.90	0.50	
DENDRITIC									
Animal No. (MLF)	No. ChAT Cells	%contra- lateral cells	%ChAT cells nNOS ⁺	No. CTb Contacts	No. 5-HT Contacts	Ave. No. Dendrites	Ave. Length μm	Ave. Density CTb Contacts	Ave. Density 5- HT Contacts
6	3	66.67	100	4	17	3.67	285.10	0.74	3.75
7	5	80.00	100	23	37	2.40	194.44	2.93	5.82
8	7	42.86	71.43	22	58	2.43	259.21	1.26	5.08
Count/Sum/Ave	15	63.17	90.48	49	112	2.83	246.25	1.64	4.88
\pm SD	-	18.82	16.50	10.69	20.50	0.72	46.70	1.14	1.05
Ave. = average; No. = number; SD = standard deviation									

CTb contacts and 5-HT contacts onto ChAT interneurons located bilaterally in lamina X were expressed in terms of surface area densities. Interneurons classified as contralateral were located opposite to the MLF brain injection site.

Appendix 5 Table 9 The relationship of ChAT, nNOS and ChAT::nNOS interneurons in laminae VI, VII and X in the transverse plane

Laminae VI - VII				
Animal No. (MLF)	Ave. Total cells counted	% ChAT cells	% nNOS cells	% ChAT::nNOS cells
6	24	23.61	35.12	41.29
7	26	30.46	43.25	26.30
8	30	29.32	37.74	33.11
Sum/Ave	80	27.74	38.70	33.56
± SD	-	3.64	4.15	7.51
Lamina X				
6	30	21.86	42.75	35.40
7	38	16.95	40.41	42.65
8	37	14.31	45.00	40.70
Sum/Ave	105	17.70	42.72	39.58
± SD	-	3.83	2.30	3.75
Ave. = average; No. = number; SD = standard deviation				

Interneurons immunoreactive to ChAT, nNOS and ChAT::nNOS were counted and expressed in terms of percentages.

Appendix 5 Table 10 Monoaminergic contacts onto ChAT interneurons in laminae VI, VII and X in the parasagittal plane

PARSAGITTAL												
		Somatic					Dendritic					
					Density = No. Boutons X 1,000 μm^{-2}						Density = No. Boutons X 1,000 μm^{-2}	
<i>Naïve tissue</i>	No. Cells	Ave. No. 5-HT Boutons	Ave. No. DBH Boutons	Ave. Radii, μm	Ave. Density 5-HT Boutons	Ave. Density DBH Boutons	Ave. No. 5-HT Boutons	Ave. No. DBH Boutons	Ave. No. Dendrites	Ave. Length, μm	Ave. Density 5-HT Boutons	Ave. Density DBH Boutons
Laminae VI/VII Sums/Ave	5	41	28	14.44	2.51	2.15	95	64	3.00	282.69	7.29	3.76
\pm SD		7.01	3.97	3.25	2.13	1.27	11.02	10.31	0.71	201.02	5.52	1.26
Lamina X Sums/Ave	5	17	31	12.79	1.56	2.82	29	18	3.00	163.26	6.37	4.47
\pm SD		4.83	8.90	1.39	1.96	3.64	2.86	1.34	1.00	62.00	4.86	4.80

5-HT and DBH contacts onto ChAT interneurons were expressed in terms of were expressed in terms of surface area densities. Immunoreactive tissue was from one naïve rat with no tract tracing injection.

List of references

- ACHERMANN, P. & BORBELY, A. A. 1994. Simulation of daytime vigilance by the additive interaction of a homeostatic and a circadian process. *Biol. Cybern.*, 71, 115-121.
- AGARWAL, S. K., GELSEMA, A. J. & CALARESU, F. R. 1990. Inhibition of rostral VLM by baroreceptor activation is relayed through caudal VLM. *Am J Physiol* 258, 1271-1278.
- AGGELOPOULOS, N. C., BURTON, M. J., CLARKE, R. W. & EDGLEY, S. A. 1996. Characterization of a descending system that enables crossed group II inhibitory reflex pathways in the cat spinal cord. *J Neurosci*, 16, 723-729.
- AICHER, S. A., KURUCZ, O. S., REIS, D. J. & MILNER, T. A. 1995. Nucleus tractus solitarius efferent terminals synapse on neurons in the caudal ventrolateral medulla that project to the rostral ventrolateral medulla. *Brain Research*, 693, 51-63.
- AIHARA, Y., MASHIMA, H., ONDA, H., HISANO, S., KASUYA, H., HORI, T., YAMADA, S., TOMURA, H., YAMADA, Y., INOUE, I., KOJIMA, I. & TAKEDA, J. 2000. Molecular Cloning of a Novel Brain-Type Na⁺-Dependent Inorganic Phosphate Cotransporter. *Journal of Neurochemistry*, 74, 2622-2625.
- ALFORD, S., SCHWARTZ, E. & DI PRISCO, G. V. 2003. The Pharmacology of Vertebrate Spinal Central Pattern Generators. *The Neuroscientist*, 9, 217-228.
- ALVAREZ, F. J. & FYFFE, R. E. W. 2007. The continuing case for the Renshaw cell. *The Journal of Physiology*, 584, 31-45.
- ALVAREZ, F. J., PEARSON, J. C., HARRINGTON, D., DEWEY, D., TORBECK, L. & FYFFE, R. E. W. 1998. Distribution of 5-hydroxytryptamine-immunoreactive boutons on α -motoneurons in the lumbar spinal cord of adult cats. *The Journal of Comparative Neurology*, 393, 69-83.
- ALVAREZ, F. J., VILLALBA, R. M., ZERDA, R. & SCHNEIDER, S. P. 2004. Vesicular glutamate transporters in the spinal cord, with special reference to sensory primary afferent synapses. *The Journal of Comparative Neurology*, 472, 257-280.
- AMILHON, B., LEPICARD, E., RENOIR, T., MONGEAU, R., POPA, D., POIREL, O., MIOT, S., GRAS, C., GARDIER, A., GALLEGU, J., HAMON, M., LANFUMEY, L., GASNIER, B., GIROS, B. & EL MESTIKAWY, S. 2010. VGLUT3 (Vesicular Glutamate Transporter Type 3) Contribution to the Regulation of Serotonergic Transmission and Anxiety. *Journal of Neuroscience*, 306, 2198-2210.

- ANELLI, R. & HECKMAN, C. J. 2005. The calcium binding proteins calbindin, parvalbumin, and calretinin have specific patterns of expression in the gray matter of cat spinal cord. *Journal of Neurocytology*, 34, 369-385.
- ANGELUCCI, A., CLASCÁ, F. & SUR, M. 1996. Anterograde axonal tracing with the subunit B of cholera toxin: a highly sensitive immunohistochemical protocol for revealing fine axonal morphology in adult and neonatal brains. *Journal of Neuroscience Methods*, 65, 101-112.
- ANTAL, M. 1984. Termination areas of corticobulbar and corticospinal fibres in the rat. *J Hirnforsch* 25, 647-659.
- ANTAL, M., PETKÓ, M., POLGÁR, E., HEIZMANN, C. W. & STORM-MATHISEN, J. 1996. Direct evidence of an extensive GABAergic innervation of the spinal dorsal horn by fibres descending from the rostral ventromedial medulla. *Neuroscience*, 73, 509-518.
- ARMAND, J. 1982. The origin, course and terminations of cortico- spinal fibers in various mammals. *Prog Brain Res*, 57, 329-360.
- ASCOLI, G. A., KRISHMAR, S. J., NASUTO, S. L. & SENFT, S. L. 2001. Generation, description and storage of dendritic morphology data. *Philos. Trans. R. Soc. (Lond)*, 2001, 1131.
- BALDISSERA, F., HULTBORN, H. & ILLERT, M. 1981. Integration in spinal neuronal systems. In: BROODS, V. (ed.) *Handbook of Physiology, The Nervous System*, 2. Bethesda, MD: American Physiological Society.
- BANKER, G. A. & COWAN, W. M. 1979. Further observation on hippocampal neurons in dispersed cell culture. *J Comp Neurol*, 187, 469-494.
- BANKOUL, S. & NEUHUBER, W. L. 1992. A direct projection from the medial vestibular nucleus to the cervical spinal dorsal horn of the rat, as demonstrated by anterograde and retrograde tracing. *Anat. Embryol.*, 185, 77-85.
- BANNATYNE, B. A., EDGLEY, S. A., HAMMAR, I., JANKOWSKA, E. & MAXWELL, D. J. 2003. Networks of inhibitory and excitatory commissural interneurons mediating crossed reticulospinal actions. *European Journal of Neuroscience*, 18, 2273-2284.
- BANNATYNE, B. A., EDGLEY, S. A., HAMMAR, I., JANKOWSKA, E. & MAXWELL, D. J. 2006. Differential Projections of Excitatory and Inhibitory Dorsal Horn Interneurons Relaying Information from Group II Muscle Afferents in the Cat Spinal Cord. *The Journal of Neuroscience*, 26, 2871-2880.
- BANNATYNE, B. A., LIU, T. T., HAMMAR, I., STECINA, K., JANKOWSKA, E. & MAXWELL, D. J. 2009. Excitatory and inhibitory intermediate zone interneurons in pathways from feline group I and II afferents: differences in axonal projections and input. *The Journal of Physiology*, 587, 379-399.
- BARBER, R. P., PHELPS, P.E., HOUSER, C.R., CRAWFORD, G.D., SALVATERRA, P.M., VAUGH, J.E. 1984. The morphology and distribution of neurons containing choline acetyltransferase in the adult rat spinal cord: an immunocytochemical study. *J Comp Neurol*, 229, 329-346.

- BAREYRE, F. M., HAUDENSCHILD, B. & SCHWAB, M. E. 2002. Long-lasting sprouting and gene expression changes induced by the monoclonal antibody IN-1 in the adult spinal cord. *J. Neurosci.*, 22, 7097-7110.
- BASBAUM, A. I., CLANTON, C. H. & FIELDS, H. L. 1978. Three bulbospinal pathways from the rostral medulla of the cat: An autoradiographic study of pain modulating systems. *J Comp Neurol*, 178, 209-224.
- BELLOCCHIO, E. E., REIMER, R. J., FREMEAU, R. T. & EDWARDS, R. H. 2000. Uptake of Glutamate into Synaptic Vesicles by an Inorganic Phosphate Transporter. *Science*, 289, 957-960.
- BENES, F. M., PARKS, T. N. & RUBEL, E. W. 1977. Rapid dendritic atrophy following deafferentation: An EM morphometric analysis. *Brain Research*, 122, 1-13.
- BENNETT, B. D., CALLAWAY, J. C. & WILSON, C. J. 2000. Intrinsic Membrane Properties Underlying Spontaneous Tonic Firing in Neostriatal Cholinergic Interneurons. *The Journal of Neuroscience*, 20, 8493-8503.
- BERTRAND, S. S. & CAZALETS, J. R. 2011. Cholinergic partition cells and lamina X neurons induce a muscarinic-dependent short-term potentiation of commissural glutamatergic inputs in lumbar motoneurons. *Frontiers in Neural Circuits*, 5, 1-15.
- BJÖRKLUND, A. & SKAGERBERG, G. 1979. Evidence for a major spinal cord projection from the diencephalic A11 dopamine cell group in the rat using transmitter-specific fluorescent retrograde tracing. *Brain Research*, 177, 170-175.
- BJÖRKLUND, A., SKAGERBERG, G. 1982. Descending monoaminergic projections to the spinal cord. In *Brain Stem Control of Spinal Mechanisms*. Elsevier Biomedical Press, Amsterdam, 55-88.
- BORGES, L. F. & IVERSEN, S. D. 1986. Topography of choline acetyltransferase Immunoreactive Neurons and fibers in the rat spinal cord. *Brain Research*, 362, 140-148.
- BOULLAND, J.-L., QURESHI, T., SEAL, R. P., RAFIKI, A., GUNDERSEN, V., BERGERSEN, L. H., FREMEAU, R. T., EDWARDS, R. H., STORM-MATHISEN, J. & CHAUDHRY, F. A. 2004. Expression of the vesicular glutamate transporters during development indicates the widespread corelease of multiple neurotransmitters. *The Journal of Comparative Neurology*, 480, 264-280.
- BOWKER, R. M. & ABBOTT, L. C. 1990. Quantitative re-evaluation of descending serotonergic and non-serotonergic projections from the medulla of the rodent: evidence for extensive co-existence of serotonin and peptides in the same spinally projecting neurons, but not from the nucleus raphe magnus. *Brain Research*, 512, 15-25.
- BOWKER, R. M., STEINBUSCH, H. W. & COULTER, J. D. 1981a. Serotonergic and peptidergic projections to the spinal cord demonstrated by a combined retrograde HRP histochemical and immunocytochemical staining method. *Brain Res*, 211, 412-417.

- BOWKER, R. M., WESTLUND, K. N. & COULTER, J. D. 1981b. Origins of serotonergic projections to the spinal cord in rat: An immunocytochemical-retrograde transport study. *Brain Research*, 226, 187-199.
- BOWKER, R. M., WESTLUND, K. N. & COULTER, J. D. 1982. Origins of serotonergic projections to the lumbar spinal cord in the monkey using a combined retrograde transport and immunocytochemical technique. *Brain Res*, 9, 271-278.
- BRANCHEREAU, P., CHAPRON, J. & MAYRAND, P. 2002. Descending 5-hydroxytryptamine raphe inputs repress the expression of serotonergic neurons and slow the maturation of inhibitory systems in mouse embryonic spinal cord. *J Neurosci*, 22, 2598-2606.
- BRAS, H., CAVALLARI, P., JANKOWSKA, E. & D., M. 1989b. Comparison of effects of monoamines on transmission in spinal pathways from group I and II muscle afferents in the cat. *Exp Brain Res*, 76, 27-37.
- BRAS, H., JANKOWSKA, E., NOGA, B. R. & SKOOG, B. 1990. Comparison of effects of various types of NA and 5-HT agonists on transmission from group II muscle afferents in the cat. *Eur J Neurosci*, 2, 1029-1039.
- BREDT, D. S., GLATT, C. E., HWANG, P. M., FOTUHI, M., DAWSON, T. M. & SNYDER, S. H. 1991. Nitric oxide synthase protein and mRNA are discretely localized in neuronal populations of mammalian central nervous systems together with NADPH diaphorase. *Neuron*, 7, 615-624.
- BREDT, D. S., GLATT, C. E., HWANG, P. M., FOTUHI, M., DAWSON, T. M. & SNYDER, S. H. 1991b. Nitric oxide synthase protein and mRNA are discretely localized in neuronal populations of the mammalian CNS together with NADPH diaphorase. *Neuron*, 7, 615-624.
- BRIGGS, C. A. 1992. Potentiation of nicotinic transmission in the rat superior cervical sympathetic ganglion: Effects of cyclic GMP and nitric oxide generators. *Brain Res*, 573, 139-146.
- BRODIN, L. & GRILLNER, S. 1985a. The role of putative excitatory amino acid neurotransmitters in the initiation of locomotion in the lamprey spinal cord. II. The effects of amino acid uptake inhibitors. *Brain Research*, 360, 149-158.
- BRODIN, L. & GRILLNER, S. 1985b. The role of putative excitatory amino acid neurotransmitters in the initiation of locomotion in the lamprey spinal cord. I. The effects of excitatory amino acid antagonists. *Brain Research*, 360, 139-148.
- BRODIN, L., GRILLNER, S., DUBUC, R., OHTA, Y., KASICKI, S. & HOKFELT, T. 1988. Reticulospinal neurons in lamprey: transmitters, synaptic interactions and their role during locomotion. *Arch Ital Biol*, 126, 317-345.
- BROMAN, J. 1993. Neurotransmitters in subcortical somatosensory pathways. *Anat Embryol (Berl)*, 189, 181-214.
- BROSAMLE, C. & SCHWAB, M. E. 1997. Cells of origin, course, and termination patterns of the ventral, uncrossed component of the mature rat corticospinal tract. *J Comp Neurol*, 386, 293-303.

- BROWN, A. G. 1981. Organization in the Spinal Cord, The anatomy and physiology of identified neurones, Berlin Heidelberg New York, Springer-Verlag.
- BROWN, A. R., ANTLE, M. C., HU, B. & TESKEY, G. C. 2011. High frequency stimulation of the subthalamic nucleus acutely rescues motor deficits and neocortical movement representations following 6-hydroxydopamine administration in rats. *Experimental Neurology*, 231, 82-90.
- BROWN, A. R., HU, B., ANTLE, M. C. & TESKEY, G. C. 2009. Neocortical movement representations are reduced and reorganized following bilateral intrastriatal 6-hydroxydopamine infusion and dopamine type-2 receptor antagonism. *Experimental Neurology*, 220, 162-170.
- BROWN, L. T. 1971. Projections and termination of the corticospinal tract in rodents. *Exp Brain Res*, 13, 432-450.
- BROWNSTONE, R. M., JORDAN, L. M., SHEFCHYK, S. J., NOGA, B. R. & KRIELLAARS, D. J. 1992. On the regulation of repetitive firing in lumbar motoneurons during fictive locomotion in the cat. *Exp Brain Res*, 90, 441-455.
- BUCHANAN, J. T. & GRILLNER, S. 1991. 5-Hydroxytryptamine depresses reticulospinal excitatory postsynaptic potentials in motoneurons of the lamprey. *Neuroscience Letters*, 122, 71-74.
- BURKE, R. E., MARKS, W. B. & ULFHAKE, B. 1992. A parsimonious description of motoneuron dendritic morphology using computer simulation. *J Neurosci*, 12, 2403.
- BUTCHER, L. L. & WOOLF, N. J. 1982. Cholinergic and serotonergic systems in the brain and spinal cord: anatomic organization, role in intercellular communication processes, and interactive mechanisms. *Prog Brain Res*, 55, 1-40.
- CAILLARD, O., MORENO, H., SCHWALLER, B., LLANO, I., CELIO, M.R. & MARTY, A. 2000. Role of the calcium-binding protein parvalbumin in short-term synaptic plasticity. *Proc Natl Acad Sci U S A*, 97 (24), 13372-7.
- CANEDO, A. 1997. Primary motor cortex influences on the descending and ascending systems. *Prog Neurobiol*, 51, 287-335.
- CASALE, E. J., LIGHT, A. R. & RUSTIONI, A. 1988. Direct projection of the corticospinal tract to the superficial laminae of the spinal cord in the rat. *The Journal of Comparative Neurology*, 278, 275-286.
- CAURAUGH, J. H. & SUMMERS, J. J. 2005. Neural plasticity and bilateral movements: a rehabilitation approach for chronic stroke. *Prog Neurobiol*, 75, 309-320.
- CAVALLARI, P., EDGLEY, S. A. & JANKOWSKA, E. 1987. Post-synaptic actions of midlumbar interneurons on motoneurons of hind-limb muscles in the cat. *The Journal of Physiology*, 389, 675-689.
- CAZALETS, J.-R., GARDETTE, M. & HILAIRE, G. 2000. Locomotor Network Maturation Is Transiently Delayed in the MAOA-Deficient Mouse. *Journal of Neurophysiology*, 83, 2468-2470.

- CHAUDHRY, F. A., REIMER, R. J., BELLOCCHIO, E. E., DANBOLT, N. C., OSEN, K. K., EDWARDS, R. H. & STORM-MATHISEN, J. 1998. The Vesicular GABA Transporter, VGAT, Localizes to Synaptic Vesicles in Sets of Glycinergic as Well as GABAergic Neurons. *The Journal of Neuroscience*, 18, 9733-9750.
- CHEN, R., COHEN, L. G. & HALLETT, M. 2002. Nervous system reorganization following injury. *Neuroscience* 111, 761-773.
- CHEN, S. & ASTON-JONES, G. 1995. Evidence that cholera toxin B subunit (CTb) can be avidly taken up and transported by fibers of passage. *Brain Research*, 674, 107-111.
- CHKLOVSKII, D. & KOULAKOV, A. 2004. Maps in the brain: what can we learn from them? *Annu Rev Neurosci*, 27, 369 - 392.
- CHRISTIE, K. J. & WHELAN, P. J. 2005. Monoaminergic establishment of rostrocaudal gradients of rhythmicity in the neonatal mouse spinal cord. *Journal of Neurophysiology*, 94, 1554-1564.
- CONNER, J. M., CULBERSON, A., PACKOWSKI, C., CHIBA, A. A. & TUSZYNSKI, M. H. 2003. Lesions of the Basal Forebrain Cholinergic System Impair Task Acquisition and Abolish Cortical Plasticity Associated with Motor Skill Learning. *Neuron*, 38, 819-829.
- CORDERO-ERAUSQUIN, M., ALLARD, S., DOLIQUE, T., BACHAND, K., RIBEIRO-DASILVA, A. & DE KONINCK, Y. 2009. Dorsal horn neurons presynaptic to lamina I spino-parabrachial neurons revealed by transynaptic labelling. *J Comp Neurol*, 517, 601-615.
- COULTER, J. D., BOWKER, R. M., WISE, S. P., MURRAY, C. I., CASTIGLIONI, A. J. & WESTLUND, K. N. 1979. Cortical, tectal and medullary descending pathways to the cervical spinal cord. *Prog Brain Res*, 50, 263-274.
- COUTEAUX, R. & PECOT-DECHAVASSINE, M. 1970. Synaptic vesicles and pouches at the level of "active zones" of the neuromuscular junction. *C R Acad Sci Hebd Seances Acad Sci D*, 271, 2346-2349.
- CREESE, I. & IVERSEN, S. D. 1975. The pharmacological and anatomical substrates of the amphetamine response in the rat. *Brain Research*, 83, 419-436.
- CREPEL, F., MARIANI, J. & DELHAYE-BOUCHAUD, N. 1976. Evidence for a multiple innervation of Purkinje cells by climbing fibers in the immature rabbit cerebellum. *J Neurobiol*, 7, 567-578.
- CUNTZ, H. 2012. The dendritic density field of a cortical pyramidal cell. *Frontiers in Neuroanatomy*, 6.
- CUNTZ, H., BORST, A. & SEGEV, I. 2007. Optimization principles of dendritic structure. *Theoretical Biology and Medical Modelling*, 4, 21.
- CUNTZ, H., FORSTNER, F., BORST, A. & HÄUSSER, M. 2010. One Rule to Grow Them All: A General Theory of Neuronal Branching and Its Practical Application. *PLoS Comput Biol*, 6, e1000877.

- CURFS, M. H. J. M., GRIBNAU, A. A. M. & DEDEREN, P. J. W. C. 1996. Direct cortico-motoneuronal synaptic contacts are present in the adult rat cervical spinal cord and are first established at postnatal day 7. *Neuroscience Letters*, 205, 123-126.
- CURTIS, D. R. & RYALL, R. W. 1964. Nicotinic and muscarinic receptors of Renshaw cells. *Nature*, 87, 652-653.
- CURTIS, D. R., HOSLI, L. & JOHNSTON 1981. A pharmacological study of the depression of spinal neurones by glycine and related amino acids. *Exp Brain Res*, 6, 1-18.
- DALE, N. & KUENZI, F. M. 1997. Ion channels and the control of swimming in the *Xenopus* embryo. *Progress in Neurobiology*, 53, 729-756.
- DALE, N. & ROBERTS, A. 1984. Excitatory amino acid receptors in *Xenopus* embryo spinal cord and their role in the activation of swimming. *J Physiol*, 348, 527-543.
- DALE, N. & ROBERTS, A. 1985. Dual-component amino-acid-mediated synaptic potentials: excitatory drive for swimming in *Xenopus* embryos. *J Physiol*, 363, 35-59.
- DALE, N. 1985. Reciprocal inhibitory interneurons in the *Xenopus* embryo spinal cord. *The Journal of Physiology*, 363, 61-70.
- DALE, N. 1986. Excitatory synaptic drive for swimming mediated by amino acid receptors in the lamprey. *Prog Neurobiol*, 53, 729-756.
- DALE, N., OTTERSON, O. P., ROBERTS, A. & STORM-MATHISEN, J. 1986. Inhibitory neurones of a motor pattern generator in *Xenopus* revealed by antibodies to glycine. *Nature*, 324.
- DE BIASI, S. & RUSTIONI, A. 1988. Glutamate and substance P coexist in primary afferent terminals in the superficial laminae of spinal cord. *Proceedings of the National Academy of Sciences*, 85, 7820-7824.
- DE BIASI, S. & RUSTIONI, A. 1990. Ultrastructural immunocytochemical localization of excitatory amino acids in the somatosensory system. *Journal of Histochemistry & Cytochemistry*, 38, 1745-54.
- DEITCH, J. S. & RUBEL, E. W. 1984a. Afferent influences on brain stem auditory nuclei of the chicken: the course and specificity of dendritic atrophy following deafferentation. *J Comp Neurol*, 229.
- DEITCH, J. S. & RUBEL, E. W. 1984b. Afferent influences on brain stem auditory nuclei of the chicken: time course and specificity of dendritic atrophy following deafferentation. *J Comp Neurol*, 229, 66-79.
- DONOGHUE, J. P. & WISE, S. P. 1982. The motor cortex of the rat: cytoarchitecture and microstimulation. *J Comp Neurol*, 212, 76-88.

- DOUGHERTY, K. J., SAWCHUK, M. A. & HOCHMAN, S. 2005. Properties of Mouse Spinal Lamina I GABAergic Interneurons. *Journal of Neurophysiology*, 94, 3221-3227.
- DREW, T. & ROSSIGNOL, S. 1990a. Functional organization within the medullary reticular formation of intact unanesthetized cat. I. Movements evoked by microstimulation. *Journal of Neurophysiology*, 64, 767-781.
- DREW, T. & ROSSIGNOL, S. 1990b. Functional organization within the medullary reticular formation of intact unanesthetized cat. II. Electromyographic activity evoked by microstimulation. *Journal of Neurophysiology*, 64, 782-795.
- DU BEAU, A., SHAKYA SHRESTHA, S., BANNATYNE, B. A., JALICY, S. M., LINNEN, S. & MAXWELL, D. J. 2012. Neurotransmitter phenotypes of descending systems in the rat lumbar spinal cord. *Neuroscience*, 227, 67-79.
- DUM, R. P. & STRICK, P. L. 1996. Spinal cord terminations of the medial wall motor areas in macaque monkeys. *J Neurosci*, 16, 6513-6525.
- ECCLES, J. C., FATT, P. & KOKETSU, K. 1954. Cholinergic and inhibitory synapses in a pathway from motor axons collaterals to motoneurons. *J Physiol Lond*, 126, 524-562.
- ECCLES, J. C., FATT, P. & LANDGREEN, S. 1956. Central pathway for direct inhibitory action of impulses in largest afferent nerve fibers to muscle. *J. Physiol.*, 19, 75-98.
- EDGLEY, S. A. & JANKOWSKA, E. 1987. An interneuronal relay for group I and II muscle afferents in the midlumbar segments of the cat spinal cord. *The Journal of Physiology*, 389, 647-674.
- EDGLEY, S. A., JANKOWSKA, E. & HAMMAR, I. 2004. Ipsilateral Actions of Feline Corticospinal Tract Neurons on Limb Motoneurons. *The Journal of Neuroscience*, 24, 7804-7813.
- ELGER, C. E., SPECKMANN, E. J., CASPERS, H. & JANZEN, R. W. C. 1977. Corticospinal connections in the rat. I. Monosynaptic and polysynaptic responses of cervical motoneurons to epicortical stimulation. *Experimental Brain Research*, 28, 385-404.
- EL-YASSIR, N., FLEETWOOD-WALKER, S. M. & MITCHELL, R. 1988. Heterogeneous effects on serotonin in the dorsal horn of rat: the involvement of 5-HT₁ receptor subtypes. *Brain Res*, 456, 147-158.
- ERICSON, H. & BLOMQUIST, A. 1988. Tracing of neuronal connections with cholera toxin subunit B: light and electron microscopic immunohistochemistry using monoclonal antibodies. *J Neurosci Methods*, 24, 225-235.
- ERLANDER, M. G., TILLAKARATNE, N. J. K., FELDBLUM, S., PATEL, N. & TOBIN, A. J. 1991. Two genes encode distinct glutamate decarboxylases. *Neuron*, 7, 91-100.

- FANG, X., DJOUHRI, L. & LAWSON, S. N. 2000. Sensory receptor properties of isolectin B4-positive (IB4+) and -negative (IB4-) dorsal root ganglion (DRG) neurones in vivo in the rat. *Soc Neurosci Abstr*, 26.
- FELDBLUM, S., DUMOULIN, A., ANOAL, M., SANDILLON, F. & PRIVAT, A. 1995. Comparative distribution of GAD65 and GAD67 mRNAs and proteins in the rat spinal cord supports a differential regulation of these two glutamate decarboxylases in vivo. *J Neurosci Res*, 15, 742-57.
- FENIK, V., DAVIES, R. O. & KUBIN, L. 2004. Combined antagonism of aminergic excitatory and amino acid inhibitory receptors in the XII nucleus abolishes REM sleep-like depression of hypoglossal motoneuronal activity. *Arch Ital Biol*, 142, 237-249.
- FIELDS, H. & BASBAUM, A. I. 1978. Brainstem control of spinal pain-transmission neurons. *Ann. Rev. Physiol.*, 40, 217-48.
- FINKELSTEIN, R. A., BOESMAN, M., NEOH, S. H., LARUE, M. K. & DELANEY, R. 1974. Dissociation and recombination of the subunits of the cholera enterotoxin (cholera toxin). *The Journal of Immunology*, 113, 145-150.
- FREMEAU JR, R. T., TROYER, M. D., PAHNER, I., NYGAARD, G. O., TRAN, C. H., REIMER, R. J., BELLOCCHIO, E. E., FORTIN, D., STORM-MATHISEN, J. & EDWARDS, R. H. 2001. The Expression of Vesicular Glutamate Transporters Defines Two Classes of Excitatory Synapse. *Neuron*, 31, 247-260.
- FREMEAU, R. T., VOLGLMAIER, S., SEAL, R. P. & EDWARDS, R. H. 2004. VGLUTs define subsets of excitatory neurons and suggest novel roles for glutamate. *Trends in Neuroscience*, 27, 98-103.
- GAME, C. J. & LODGE, D. 1975. The pharmacology of the inhibition of dorsal horn neurones by impulses in myelinated cutaneous afferents in the cat. *Exp Brain Res*, 23, 75-84.
- GANSER, A. L., KIRCHNER, D. A. & WILLINGER, M. 1983. Ganglioside localization on myelinated nerve fibres by cholera toxin binding. *J Neurocytol*, 12, 921-938.
- GARRAWAY, S. M. & HOCHMAN, S. 2001. Modulatory actions of serotonin, norepinephrine, dopamine, and acetylcholine in spinal cord deep dorsal horn neurons. *J Neurophysiol*, 86, 2183-2194.
- GIBSON, S. J., POLAK, J. M., BLOOM, S. R. & WALL, P. D. 1981. The distribution of nine peptides in rat spinal cord with special emphasis on the substantia gelatinosa and on the area around the central canal (lamina X). *J Comp Neurol*, 201, 65-79.
- GIBSON, S. J., POLAK, J. M., BLOOM, S. R. & WALL, P. D. 1981. The distribution of nine peptides in rat spinal cord with special emphasis on the substantia gelatinosa and on the area around the central canal (lamina X). *J Comp Neurol*, 201, 65-79.
- GIEROBA, Z. J., LI, Y. W. & BLESSING, W. W. 1992. Characteristics of caudal ventrolateral medullary neurons antidromically activated from rostral ventrolateral medulla in the rabbit. *Brain Research*, 582, 196-207.

- GIOCOMO, L. & HASSELMO, M. 2007. Neuromodulation by Glutamate and Acetylcholine can Change Circuit Dynamics by Regulating the Relative Influence of Afferent Input and Excitatory Feedback. *Molecular Neurobiology*, 36, 184-200.
- GIUFFRIDA, R. & RUSTIONI, A. 1989. Glutamate and aspartate immunoreactivity in corticospinal neurons of rats. *The Journal of Comparative Neurology*, 288, 154-164.
- GOBEL, S. 1975. Golgi studies of the substantia gelatinosa neurons in the spinal trigeminal nucleus. *Journal of Comparative Neurology*, 162, 397-416.
- GOBEL, S. 1978. Golgi studies of the neurons in layer I of the dorsal horn of the medulla (trigeminal nucleus caudalis). *Journal of Comparative Neurology*, 180, 375-393.
- GOLDSTEIN, I. J. & WINTER, H. G. 1999. The Griffonia simplicifolia I-B4 isolectin. A probe for alpha-D-galactosyl end groups. *Subcell Biochem*, 32, 127-141.
- GOULDING, M. 2009. Circuits controlling vertebrate locomotion: moving in a new direction. *Nat Rev Neurosci*, 10, 507-518.
- GRAS, C., HERZOG, E. & BELLENCHI, G. C. 2002. A third vesicular glutamate transporter expressed by cholinergic and serotonergic neurons. *J Neurosci*, 22, 5442-5451.
- GRILLNER, S. & DUBUC, R. 1988. Control of locomotion in vertebrates: spinal and supraspinal mechanisms. *Adv Neurol*, 47, 425-453.
- GRILLNER, S. & JESSELL, T. M. 2009. Measured motion: searching for simplicity in spinal locomotor networks. *Curr Opin Neurobiol*, 19, 572-86.
- GRILLNER, S. & WALLEN, P. 1980. Does the central pattern generation for locomotion in lamprey depend on glycine inhibition? *Acta Physiol Scand*, 110, 103-105.
- GRUDT, T. J. & PERL, E. R. 2002. Correlations between neuronal morphology and electrophysiological features in the rodent superficial dorsal horn. *The Journal of Physiology*, 540, 189-207.
- GWYN, D. G. & FLUMERFELT, B. A. 1971. Acetylcholinesterase in non-cholinergic neurones: A histochemical study of dorsal root ganglion cells in the rat. *Brain Research*, 34, 193-198.
- HAJNIK, T., LAI, Y. Y. & SIEGEL, J. M. 2000. Atonia-Related Regions in the Rodent Pons and Medulla. *Journal of Neurophysiology*, 84, 1942-1948.
- HALEY, J. E., DICKENSON, A. H. & SCHACHTER, M. 1992. Electrophysiological evidence for a role of nitric oxide in prolonged chemical nociception in the rat. *Neuropharmacology*, 31, 251-258.
- HALLET, M. 2001. Functional reorganization after lesions of the human brain: studies with transcranial magnetic stimulation. *Rev Neurol*, 157, 822-826.
- HAMMAR, I., BANNATYNE, B. A., MAXWELL, D. J., EDGLEY, S. A. & JANKOWSKA, E. 2004. The actions of monoamines and distribution of noradrenergic and

serotonergic contacts on different subpopulations of commissural interneurons in the cat spinal cord. *European Journal of Neuroscience*, 19, 1305-1316.

HAMMAR, I., KRUTKI, P., DRZYMALA-CELICHOWSKA, H., NILSSON, E. & JANKOWSKA, E. 2011. A trans-spinal loop between neurones in the reticular formation and in the cerebellum. *The Journal of Physiology*, 589, 653-665.

HAMMOND, C. 2001. *Cellular and Molecular Neurobiology*, second edition. Institut de la Mediterranee. Marseille, France. Academic Press.

HAYES, N. L. & RUSTIONI, A. 1981. Descending projections from brainstem and sensorimotor cortex to spinal enlargements in the cat. Single and double retrograde tracer studies. *Exp Brain Res*, 141, 89-107.

HECKMAN, C. J., HYGSTROM, A. S. & JOHNSON, M. 2008. Active properties of motoneurone dendrites: diffuse descending neuromodulation, focused local inhibition. *J Physiol*, 586, 1225-1231.

HELLSTRÖM, J., OLIVEIRA, A. L. R., MEISTER, B. & CULLHEIM, S. 2003. Large cholinergic nerve terminals on subsets of motoneurons and their relation to muscarinic receptor type 2. *The Journal of Comparative Neurology*, 460, 476-486.

HERZOG, E., LANDRY, M., BUHLER, E., BOUALI-BENAZZOUZ, R., LEGAY, C., HENDERSON, C. E., NAGY, F., DREYFUS, P., GIROS, B. & MESTIKAWY, S. 2004. Expression of vesicular glutamate transporters, VGLU1 and VGLUT2 in cholinergic spinal motoneurons. *Eur J Neurosci*, 20, 1752-1760.

HICKS, S. P. & D'AMATO, C. J. 1977. Locating corticospinal neurons by retrograde axonal transport of horseradish peroxidase. *Exp Neurol*, 56, 410-420.

HIOKI, H., FUJIYAMA, F., TAKI, K., TOMIOKA, R., FURUTA, T., TAMAMAKI, N. & KANEKO, T. 2003. Differential distribution of vesicular glutamate transporters in the rat cerebellar cortex. *Neuroscience*, 117, 1-6.

HOLMES, C. J. & JONES, B. E. 1994. Importance of cholinergic, GABAergic, serotonergic and other neurons in the medial medullary reticular formation for sleep-wake states studied by cytotoxic lesions in the cat. *Neuroscience*, 62, 1179-1200.

HOLMQVIST, B. & LUNDBERG, A. 1959. On the organization of the supraspinal inhibitory control of interneurons of various spinal reflex arcs. *Arch Ital Biol*, 97, 340-356.

HOLMQVIST, B. & LUNDBERG, A. 1961. Differential supraspinal control of synaptic actions evoked by volleys in the fictive reflex afferents in alpha motoneurons. *Acta Physiol Scand*, 54 [Suppl 186], 1-5.

HOLSTEGE, G. & KUYPERS, H. G. 1982. The anatomy of brain stem pathways to the spinal cord in cat: a labeled amino acid tracing study. *Prog Brain Res*, 57, 145-175.

- HOLSTEGE, G. 1998. The emotional motor system in relation to the supraspinal control of micturition and mating behavior. *Behavioural Brain Research*, 92, 103-109.
- HOLSTEGE, J. 1991. Ultrastructural evidence for GABAergic brain stem projections to spinal motoneurons in the rat. *The Journal of Neuroscience*, 11, 159-167.
- HOLSTEGE, J. C. & BONGERS, C. M. 1991. A glycinergic projection from the ventromedial lower brainstem to spinal motoneurons. An ultrastructural double labeling study in rat. *Brain Research*, 566, 308-15.
- HOLZER-PETSCHKE, U., RINNER, I. & LEMBECK, F. 1986. Distribution of choline acetyltransferase activity in rat spinal cord--influence of primary afferents? *J Neural Transm*, 66.
- HONDA, C. N. & PERL, E. R. 1981. Properties of neurons in lamina X and the midline dorsal horn of the sacrococcygeal spinal cord of the cat. *Soc Neurosci Abstr*, 7, 610.
- HONIG, M. C. & HUME, R. I. 1986. Fluorescent carbocyanine dyes allow living neurons of identified origin to be studied in long-term cultures. *Cell Biol*, 103, 171-187.
- HOSSAINI, M., GOOS, J. A. C., KOHLI, S. K. & HOLSTEGE, J. C. 2012. Distribution of Glycine/GABA Neurons in the Ventromedial Medulla with Descending Spinal Projections and Evidence for an Ascending Glycine/GABA Projection. *PLoS ONE*, 7, e35293.
- HOUK, J. C. 1989. in *Models of Brain Function* (Cotterill, R.M.J., ed.). Cambridge University Press, 309-325.
- HOUK, J. C., KEIFER, J. & BARTO, A. G. 1993. Distributed motor commands in the limb premotor network. *Trends in Neurosciences*, 16, 27-33.
- HOUSER, C. R., CRAWFORD, G. D., BARBER, R. P., SALVATERRA, P. M. & VAUGH, J. E. 1983. Organization and morphological characteristics of cholinergic neurons: an immunocytochemical study with a monoclonal antibody to choline acetyltransferase. *266*, 1, 97-119.
- HUANG, A., NOGA, B. R., CARR, P. A., FEDIRCHUK, B. & JORDAN, L. M. 2000. Spinal Cholinergic Neurons Activated During Locomotion: Localization and Electrophysiological Characterization. *Journal of Neurophysiology*, 83, 3537-3547.
- HUGHES, D. I., SIKANDER, S., KINNON, C. M., BOYLE, K. A., WATANABE, M., CALLISTER, R. J. & GRAHAM, B. A. 2012. Morphological, neurochemical and electrophysiological features of parvalbumin-expressing cells: a likely source of axo-axonic inputs in the mouse spinal dorsal horn. *The Journal of Physiology*, 590, 3927-3951.
- HULTBORN, H., BROWNSTONE, R. M., TOTH, T. I. & GOSSARD, J. P. 2004. Key mechanisms for setting the input-output gain across the motoneuron pool. *Prog Brain Res*, 143, 77-95.

- HULTBORN, H., JANKOWSKA, E., LINDSTRÖM, S. & ROBERTS, W. 1971. Neuronal pathway of the recurrent facilitation of motoneurons. *The Journal of Physiology*, 218, 495-514.
- HUME, R. I. & PURVES, D. 1981. Geometry of neonatal neurones and the regulation of synapse elimination. *Nature*, 293, 469-471.
- ITO, M., UDO, M. & MANO, N. 1970. Long inhibitory and excitatory pathways converging onto cat reticular and Deiters' neurons and their relevance to reticulofugal axons. *J Neurophysiol*, 33, 210-226.
- JÄNIG, W., SCHMIDT, R. F. & ZIMMERMANN, M. 1967. Presynaptic depolarization during activation of tonic mechanoreceptors. *Brain Research*, 5, 514-516.
- JANKOWSKA, E. & EDGLEY, S. A. 2006. How can corticospinal tract neurons contribute to ipsilateral movement? A question with implications for recovery of motor function. *The Neuroscientist*, 12, 67-79.
- JANKOWSKA, E. & EDGLEY, S. A. 2010. Functional subdivision of feline spinal interneurons in reflex pathways from group Ib and II muscle afferents; an update. *Eur J Neurosci*, 32, 881-893.
- JANKOWSKA, E. 1992. Interneuronal relay in spinal pathways from proprioceptors. *Prog Neurobiol*, 38, 335-378.
- JANKOWSKA, E. 2001. Spinal interneuronal systems: identification, multifunctional character and reconfigurations in mammals. *J Physiol*, 533, 31-40.
- JANKOWSKA, E. 2007. Spinal interneuronal networks in the cat: elementary components. *Brain Research Reviews*, 2-10.
- JANKOWSKA, E. 2013. Mammalian spinal interneurons. In: PFAFF, D. W. (ed.) *Neuroscience in the 21st Century From Basic to Clinical*. Springer.
- JANKOWSKA, E., HAMMAR, I., CHOJNICKA, B. & HEDÉN, C. H. 2000. Effects of monoamines on interneurons in four spinal reflex pathways from group I and/or group II muscle afferents. *Eur J Neurosci*, 12, 701-714.
- JANKOWSKA, E., HAMMAR, I., DJOUHRI, L., HEDEN, C., LACKBERG, Z. S. & YIN, X. K. 1997. Modulation of responses of four types of feline ascending tract neurons by serotonin and noradrenaline. *Eur J Neurosci*, 9, 1375-1387.
- JANKOWSKA, E., HAMMAR, I., SLAWINSKA, U., MALESZAK, K. & EDGLEY, S. A. 2003. Neuronal Basis of Crossed Actions from the Reticular Formation on Feline Hindlimb Motoneurons. *The Journal of Neuroscience*, 23, 1867-1878.
- JANKOWSKA, E., RIDDELL, J. S., SKOOG, B. & NOGA, B. R. 1993. Gating of transmission to motoneurons by stimuli applied in the locus coeruleus and raphe nuclei of the cat. *The Journal of Physiology*, 461, 705-722.
- JESKE, I., MORRISON, S. F., CRAVO, S. L. & REIS, D. J. 1993. Identification of baroreceptor reflex interneurons in the caudal ventrolateral medulla. *American*

Journal of Physiology - Regulatory, Integrative and Comparative Physiology, 264, R169-R178.

JESSELL, T. M. 2000. Neuronal specification in the spinal cord: inductive signals and transcriptional codes. *Nat Rev Genet*, 1, 20-29.

JIANG, Z., CARLIN, K. P. & BROWNSTONE, R. M. 1999. An in vitro functionally mature mouse spinal cord preparation for the study of spinal motor networks. *Brain Research*, 816, 493-499.

JIANG, Z., CARLIN, K. P. & BROWNSTONE, R. M. 1999. An in vitro functionally mature mouse spinal cord preparation for the study of spinal motor networks. *Brain Research*, 816, 493-499.

JOHNSON, R. G. 1988. Accumulation of biological amines into chromaffin granules: a model for hormone and neurotransmitter transport. *Physiol. Rev.*, 68, 232-307.

JONES, S. L. & LIGHT, A. R. 1990. Termination patterns of serotonergic medullary raphespinal fibers in the rat lumbar spinal cord: an anterograde immunohistochemical study. *J Comp Neurol*, 297, 267-282.

JORDAN, L. M. & SCHMIDT, B. J. 2002. Propriospinal neurons involved in the control of locomotion: potential targets for repair strategies? *Prog Brain Res*, 137, 125-139.

JORDAN, L. M. & SCHMIDT, B. J. 2002b. Propriospinal neurons involved in the control of locomotion: potential targets for repair strategies. In: MCKERRACHER, L., DOUCHET, G. & ROSSIGNOL, S. (eds.) *Spinal cord trauma: regeneration, neural repair, and functional recovery*. Amsterdam: Elsevier Science.

JORDAN, L. M. 1998. Initiation of locomotion in mammals. *Ann N Y Acad Sci*, 860, 83-93.

JORDAN, L. M., LIU, J., HEDLUND, P. B., AKAY, T. & PEARSON, K. G. 2007. Descending command systems for the initiation of locomotion in mammals. *Brain Research Reviews*, 57, 183-191.

JOSHUA, M., ADLER, A., MITELMAN, R., VAADIA, E. & BERGMAN, H. 2008. Midbrain dopaminergic neurons and striatal cholinergic interneurons encode the difference between reward and aversive events at different epochs of probabilistic classical conditioning trials. *J. Neurosci.*, 28, 11673-11684.

KANEKO, T., FUJIYAMA, F. & HIOKI, H. 2002. Immunohistochemical localization of candidates for vesicular glutamate transporters in the rat brain. *The Journal of Comparative Neurology*, 444, 39-62.

KARCZMAR, A. G., NISHI, S., MINOTA, S. & KINDEL, G. 1980. Electrophysiology, acetylcholine and acetylcholinesterase of immature spinal ganglia of the rabbit--an experimental study and a review. *Gen Pharmacol*, 11, 127-134.

KATZ, L. C. & CROWLEY, J. C. 2002. Development of cortical circuits: lessons from ocular dominance columns. *Nat Rev Neurosci*, 3, 34-42.

- KATZ, L. C. & SHATZ, C. J. 1996. Synaptic activity and the construction of cortical circuits. *Science*, 274, 1133-1138.
- KENNEDY, P. R. 1990. Corticospinal, rubrospinal and rubro-olivary projections: a unifying hypothesis. *Trends in Neuroscience*, 13, 474-479.
- KEPLER, J. 1596. *The Sacred Mysteries of the Cosmos. Mysterium cosmographicum*. Tübingen, Germany.
- KIEHN, O. & KJAERULFF, O. 1996. Spatiotemporal characteristics of 5-HT and dopamine-induced rhythmic hindlimb activity in the in vitro neonatal rat. *Journal of Neurophysiology*, 75, 1472-1482.
- KIM, G. & KANDLER, K. 2003. Elimination and strengthening of glycinergic/GABAergic connections during tomotopic map formation. *Nat Neurosci*, 6, 282-290.
- KIMURA, H., MCGEER, P. L., PENG, J. H. & MCGEER, E. G. 1981. The central cholinergic system studied by choline acetyltransferase immunohistochemistry in the cat. *The Journal of Comparative Neurology*, 200, 151-201.
- KITTO, K. F., HALEY, J. E. & WILCOX, G. L. 1992. Involvement of nitric oxide in spinally mediated hyperalgesia in the mouse. *Neurosci Lett*, 148, 1-5.
- KNEISLEY, L. W., BIBER, M. P. & LAVAIL, J. H. 1978. A study of the origin of brainstem projections to monkey spinal cord using the retrograde transport methods. *Exp Neurol*, 60, 116-139.
- KRIEGSTEIN, A. N. & DICHTER, M. A. 1983. Morphological classification of rat cortical neurons in cell culture. *J Neurosci*, 3, 1634-1647.
- KUCHLER, M., FOUAD, K., WEINMANN, O., SCHWAB, M. E. & RAINETEAU, O. 2002. Red nucleus projections to distinct motor neuron pools in the rat spinal cord. *J Comp Neurol*, 448, 349-359.
- KUDO, N., FURUKAWA, F. & OKADO, N. 1993. Development of descending fibres to the rat embryonic spinal cord. *Neurosci Res*, 16, 131-141.
- KULLANDER, K. 2005. Genetics moving to neuronal networks. *Trends in Neurosciences*, 28, 239-247.
- KUMER, S. & VRANA, K. 1996. Intricate regulation of tyrosine hydroxylase activity and gene expression. *J Neurochem*, 67, 443-462.
- KUYPERS, H. G. & BRINKMAN, J. 1970. Precentral projections to different parts of the spinal intermediate zone in the rhesus monkey. *Brain Res* 24, 29-48.
- KUYPERS, H. G. 1960. Central cortical projections to motor and somato-sensory cell groups. An experimental study in the rhesus monkey. *Brain*, 83, 161-184.
- KUYPERS, H. G. 1981. *Handbook of Physiology Section 1, Vol. II: Motor Control* (Brooks, V.B., ed.). American Physiological Society. 597-666.
- LAI, Y. & SIEGEL, J. 1988. Medullary regions mediating atonia. *The Journal of Neuroscience*, 8, 4790-4796.

- LAI, Y. Y. & SIEGEL, J. M. 1992. Corticotropin-releasing factor mediated muscle atonia in pons and medulla. *Brain Research*, 575, 63-68.
- LAWRENCE, D. G. & HOPKINS, D. A. 1976. The development of motor control in rhesus monkey: evidence concerning the role of corticomotoneuronal connections. *Brain*, 99, 235-254.
- LAWRENCE, D. G. & KUYPERS, H. G. 1968. The functional organization of the motor system in the monkey. I. The effects of bilateral pyramidal lesions. *Brain*, 91, 1-14.
- LAWRENCE, J. J. 2008. Cholinergic control of GABA release: emerging parallels between neocortex and hippocampus. *Trends in neurosciences*, 31, 317-327.
- LEMON, R. N. & GRIFFITHS, J. 2005. Comparing the function of the corticospinal system in different species: organizational differences for motor specialization? *Muscle Nerve*, 32, 261-279.
- LEMON, R. N. 2008. Descending pathways in motor control. *Annu. Rev. Neurosci.*, 31, 195-218.
- LEONG, S. K. 1983. Localizing the corticospinal neurons in neonatal, developing and mature albino rat. *Brain Res*, 265, 1-9.
- LI, X. G., FLORENCE, S. L. & KAAS, J. H. 1990. Area Distributions of Cortical Neurons Projecting to Different Levels of the Caudal Brain Stem and Spinal Cord in Rats. *Somatosensory and Motor Research* 7, 315-335.
- LI, Y. W. & BAYLISS, D. A. 1998. Electrophysical properties, synaptic transmission and neuromodulation in serotonergic caudal raphe neurons. *Clin Exp Pharmacol Physiol*, 25, 468-473.
- LI, Y. W., WESSELINGH, S. L. & BLESSING, W. W. 1992. Projections from rabbit caudal medulla to C1 and A5 sympathetic premotor neurons, demonstrated with phaseolus leucoagglutinin and herpes simplex virus. *J Comp Neurol*, 317, 379-395.
- LIANG, F. Y., MORET, V., WIESENDANGER, M. & ROUILLER, E. M. 1991. Corticomotoneuronal connections in the rat: evidence from double-labeling of motoneurons and corticospinal axon arborizations. *J Comp Neurol*, 311, 356-366.
- LINDSAY, K. A., MAXWELL, D. J., ROSENBERG, J. R. & TUCKER, G. 2007. A new approach to reconstruction models of dendritic branching patterns. *Mathematical Biosciences*, 205, 271-296.
- LOPEZ-GARCIA, J. A. & KING, A. E. 1996. Pre- and post-synaptic actions for 5-hydroxytryptamine in the rat lumbar dorsal horn in vitro: implications for somatosensory transmission. *Eur J Appl Physiol*, 8, 2188-2197.
- LOPEZ-GARCIA, J. A. 1998. Serotonergic modulation of the responses to excitatory amino acids of rat dorsal horn neurons in vitro: implications for somatosensory transmission. *Eur J Neurosci*, 10, 1341-1349.

- LU, J., GRECO, M. A., SHIROMANI, P. & SAPER, C. B. 2000. Effect of Lesions of the Ventrolateral Preoptic Nucleus on NREM and REM Sleep. *The Journal of Neuroscience*, 20, 3830-3842.
- LU, T., RUBIO, M. E. & TRUSSELL, L. O. 2008. Glycinergic Transmission Shaped by the Corelease of GABA in a Mammalian Auditory Synapse. *Neuron*, 57, 524-535.
- LU, Y. & PERL, E. 2007. Selective action of noradrenaline and serotonin on neurones of the spinal superficial dorsal horn in the rat. *J Physiol*, 582.1, 127-136.
- LUMSDEN, A. & KRUMSTAUF, R. 1996. Patterning the vertebrate neuraxis. *Science*, 274, 1109-1115.
- LUNDBERG, A. 1982. Inhibitory control from the brainstem of transmission from primary afferents to motoneurons, primary afferent terminals and ascending pathways. Amsterdam, Elsevier.
- LUQUE, J. M., NELSON, N. & RICHARDS, J. G. 1995. Cellular expression of glycine transporter 2 messenger RNA exclusively in rat hindbrain and spinal cord. *Neuroscience*, 64, 525-535.
- MA, W., BEHAR, T. & BARKER, J. L. 1992. Transient expression of GABA immunoreactivity in the developing rat spinal cord. *J Comp Neurol*, 325, 271-290.
- MACKAY-LYONS, M. 2002. Central Pattern Generation of Locomotion: A Review of the Evidence. *Physical Therapy*, 82, 69-83.
- MACKIE, M., HUGHES, D. I., MAXWELL, D. J., TILLAKARATNE, N. J. K. & TODD, A. J. 2003. Distribution and colocalisation of glutamate decarboxylase isoforms in the rat spinal cord. *Neuroscience*, 119, 461-472.
- MADRIAGA, M. A., MCPHEE, L. C., CHERSA, T., CHRISTIE, K. J. & WHELAN, P. J. 2004. Modulation of Locomotor Activity by Multiple 5-HT and Dopaminergic Receptor Subtypes in the Neonatal Mouse Spinal Cord. *Journal of Neurophysiology*, 92, 1566-1576.
- MARSDEN, C. D., ROTHWELL, J. C. & DAY, B. L. 1984. The use of peripheral feedback in the control of movement. *Trends in Neuroscience*, 7, 253-258.
- MARTELLA, G., TASSONE, A., SCIAMANNA, G., PLATANIA, P., CUOMO, D., VISCOMI, M. T., BONSI, P., CACCI, E., BIAGIONI, S., USIELLO, A., BERNARDI, G., SHARMA, N., STANDAERT, D. G. & PISANI, A. 2009. Impairment of bidirectional synaptic plasticity in the striatum of a mouse model of DYT1 dystonia: role of endogenous acetylcholine. *Brain*, 132, 2336-2349.
- MARTIN, E. M., DEVIDZE, N., SHELLEY, D. N., WESTBERG, L., FONTAINE, C. & PFAFF, D. W. 2011. Molecular and neuroanatomical characterization of single neurons in the mouse medullary gigantocellular reticular nucleus. *The Journal of Comparative Neurology*, 519, 2574-2593.

- MARTIN, G. F., CABANA, T., CULBERSON, J. L., CURRY, J. J. & TSCHISMADIA, I. 1980. The early development of corticobulbar and corticospinal systems. Studies using the North American opossum. *Anat Embryol*, 161, 197-213.
- MARTIN, G. F., HUMBERTSON, A. O., LAXSON, C. & PANNETON, W. M. 1979. Evidence for direct bulbospinal projections to laminae IX, X and the intermediolateral cell column. Studies using axonal transport techniques in the North American opossum. *Brain Research*, 170, 165-171.
- MARTIN, G. F., VERTES R.P., WALTZER R. 1985. Spinal projections of the gigantocellular reticular formation in the rat. Evidence for projections from different areas to lamina I and II and lamina IX. *Exp Brain Res*, 58, 154-162.
- MARTIN, J. 2005. The corticospinal system: from development to motor control. *The Neuroscientist*, 11, 161-173.
- MASKOS, U., MOLLES, B. E., PONS, S., BESSON, M., GUIARD, B. P., GUILLOUX, J. P., EVRARD, A., CAZALA, P., CORMIER, A. & MAMELI-ENGVALL, M. 2005. Nicotine reinforcement and cognition restored by targeted expression of nicotinic receptors. *Nature*, 436, 103-107.
- MASON, P. & LEUNG, C. G. 1996. Physiological functions of pontomedullary raphe and medial reticular neurons. *Prog Brain Res*, 107, 269-282.
- MASON, P. 1997. Physiological identification of pontomedullary serotonergic neurons in the rat. *J Neurophysiol*, 77, 1087-1098.
- MASON, P. 2001. Contributions of the medullary raphe and ventromedial reticular region to pain modulation and other homeostatic functions. *Annu Rev Neurosci*, 24, 737-777.
- MASON, P. 2001a. Contributions of the medullary raphe and ventromedial reticular region to pain modulation and other homeostatic functions. *Annu Rev Neurosci*, 24, 737-777.
- MASUKO, S., NAKAJIMA, Y., NAKAJIMA, S. & YAMAGUCHI, K. 1986. Noradrenergic neurons from the locus ceruleus in dissociated cell culture: culture methods, morphology, and electrophysiology. *The Journal of Neuroscience*, 6, 3229-3241.
- MATSUYAMA, K., MORI, F., KUZE, B. & MORI, S. 1999. Morphology of single pontine reticulospinal axons in the lumbar enlargement of the cat: a study using the anterograde tracer PHA-L. *J Comp Neurol*, 410, 413-430.
- MAXWELL, D. J. & RIDDELL, J. S. 1999. Axoaxonic synapses on terminals of group II muscle spindle afferent axons in the spinal cord of the cat. *Eur J Neurosci*, 11, 2151-2159.
- MAXWELL, D. J., KERR, R., JANKOWSKA, E. & RIDDELL, J. S. 1997. Synaptic connections of dorsal horn group II spinal interneurons: Synapses formed with the interneurons and by their axon collaterals. *The Journal of Comparative Neurology*, 380, 51-69.
- MAXWELL, D. J., RIDDELL, J. S. & JANKOWSKA, E. 2000. Serotonergic and noradrenergic axonal contacts associated with premotor interneurons in spinal

pathways from group II muscle afferents. *European Journal of Neuroscience*, 12, 1271-1280.

MAXWELL, L., MAXWELL, D. J., NEILSON, M. & KERR, R. 1996. A confocal microscopic survey of serotonergic axons in the lumbar spinal cord of the rat: co-localization with glutamate decarboxylase and neuropeptides. *Neuroscience*, 75, 471-480.

MCCREA, D. A. & RYBAK, I. A. 2008. Organization of mammalian locomotor rhythm and pattern generation. *Brain Research Reviews*, 57, 134-146.

MELLER, S. T., DYKSTRA, C. & GEBHART, G. F. 1992a. Production of endogenous nitric oxide and activation of soluble guanylate cyclase are required for N-methyl-D-aspartate-produced facilitation of the nociceptive tail-flick reflex. *European Journal of Pharmacology*, 214, 93-96.

MELLER, S. T., PECHMAN, P. S., GEBHART, G. F. & MAVES, T. J. 1992b. Nitric oxide mediates the thermal hyperalgesia produced in a model of neuropathic pain in the rat. *Neuroscience*, 50, 7-10.

MENA-SEGOVIA, J., WINN, P. & BOLAM, J. P. 2008. Cholinergic modulation of midbrain dopaminergic systems. *Brain Res. Rev.*, 58, 265-271.

MENTIS, G. Z., SIEMBAB, V. C., ZERDA, R., O'DONOVAN, M. J. & ALVAREZ, F. J. 2006. Primary afferent synapses on developing and adult Renshaw cells. *J Neurosci*, 26, 13297-13310.

MESNAGE, B., GAILLARD, S., GODIN, A. G., RODEAU, J.-L., HAMMER, M., VON ENGELHARDT, J., WISEMAN, P. W., DE KONINCK, Y., SCHLICHTER, R. & CORDERO-ERAUSQUIN, M. 2011. Morphological and functional characterization of cholinergic interneurons in the dorsal horn of the mouse spinal cord. *The Journal of Comparative Neurology*, 519, 3139-3158.

METZ, G. A., PIECHARKA, D. M., KLEIM, J. A. & WHISHAW, I. Q. 2004. Preserved ipsilateral-to-lesion motor map organization in the unilateral 6-OHDA-treated rat model of Parkinson's disease. *Brain Res*, 1026, 126-135.

MILLER, M. W. 1987. The origin of corticospinal projection neurons in rat. *Experimental Brain Research*, 67, 339-351.

MIZUKAWA, K., VINCENT, S. R., MCGEER, P. L. & MCGEER, E. G. 1989. Distribution of reduced-nicotinamide-adenine-dinucleotide-phosphate diaphorase-positive cells and fibers in the cat central nervous system. *J Comp Neurol*, 279, 281-311.

MOLANDER, C., XU, Q. & GRANT, G. 1984. The cytoarchitectonic organization of the spinal cord in the rat. *J Comp Neurol*, 230.

MOORE, P. K., OLUYOMI, R. C., BABBEDGE, P., WALLACE, P. & HART, S. L. 1991. L-NG -nitro arginine methyl ester exhibits antinociceptive activity in the mouse. *Br J Pharmacol*, 102, 198-202.

- MORALES, F. R., SAMPOGNA, S., RAMPON, C., LUPPI, P. H. & CHASE, M. H. 2006. Brainstem glycinergic neurons and their activation during active (rapid eye movement) sleep in the cat. *Neuroscience*, 142, 37-47.
- MUENNICH, E. A. L. & FYFFE, R. E. W. 2004. Focal aggregation of voltage-gated, Kv2.1 subunit-containing, potassium channels at synaptic sites in rat spinal motoneurons. *The Journal of Physiology*, 554, 673-685.
- MUIR, G. D. & WHISHAW, I. Q. 2000. Red nucleus lesions impair overground locomotion in rats: a kinetic analysis. *Eur J Neurosci*, 12, 1113-1122.
- NAIM, M. Y., SPIKE, R. C., WATT, C., SHEHAB, S. A. S. & TODD, A. J. 1997. Cells in laminae III and IV of the rat spinal cord that possess the neurokinin-1 receptor and have dorsally directed dendrites receive a major synaptic input from techykinin-containing primary afferents. *J Neurosci*, 17, 5536-5548.
- NAKAMURA, K., HIOKI, H., FUJIYAMA, F. & KANEKO, T. 2005. Postnatal changes of vesicular glutamate transporter (VGLUT1) and VGLUT2 immunoreactivities and their colocalization in the mouse forebrain. *J. Comp. Neurol.*, 492, 263-288.
- NEHER, E. 1998. Vesicle Pools and Ca²⁺ Microdomains: New Tools for Understanding Their Roles in Neurotransmitter Release. *Neuron*, 20, 389-399.
- NGUYEN, Q. T., SANES, J. R. & LICHTMAN, J. W. 2002. Pre-existing pathways promote precise projection patterns. *Nat Neurosci*, 5, 861-867.
- NI, B., ROSTECK, P., NADI, S. & PAUL, S. 1994. Cloning and expression of a cDNA encoding a brain-specific Na⁺-dependent inorganic phosphate cotransporter. *Proc Natl Acad Sci U S A*, 91, 5607-5611.
- NI, B., WU, X., YAN, G., WANG, J. & PAUL, S. 1995. Regional expression and cellular localization of the Na(+)-dependent inorganic phosphate cotransporter of rat brain. *The Journal of Neuroscience*, 15, 5789-5799.
- NISHIMARU, H. & KAKIZAKI, M. 2009. The role of inhibitory neurotransmission in locomotor circuits of the developing mammalian spinal cord. *Acta Physiologica*, 197, 83-97.
- NISHIMARU, H., RESTREPO, C. E., RYGE, J., YANAGAWA, Y. & KIEHN, O. 2005. Mammalian motor neurons corelease glutamate and acetylcholine at central synapses. *Proc Natl Acad Sci U S A*, 102, 5245-5249.
- NORTH, R.A. & YOSHIMURA, M. 1984. The action of noradrenaline on neurones of the rat substantia gelatinosa in vitro. *J Physiol*, 349, 43-55.
- NYBERG-HANSEN, R. & MASCITTI, T. A. 1964. Sites and mode of termination of fibers of the vestibulospinal tract in the cat. An experimental study with silver impregnation methods. *Exp Neurol*, 122, 369-83.
- NYBERG-HANSEN, R. 1965. Sites and mode of termination of reticulo-spinal fibers in the cat: an experimental study with silver impregnation methods. *J Comp Neurol*, 124, 71-99.

- NYBERG-HANSEN, R. 1966. Functional organization of descending supraspinal fibre systems to the spinal cord. Anatomical observations and physiological correlations. *Ergeb Anat Entwicklungsgesch*, 39, 3-48.
- OLAVE, M., PURI, N., KERR, R. & MAXWELL, D. 2002. Myelinated and unmyelinated primary afferent axons form contacts with cholinergic interneurons in the spinal dorsal horn. *Experimental Brain Research*, 145, 448-456.
- OLIVEIRA, A. L. R., HYDLING, F., OLSSON, E., SHI, T., EDWARDS, R. H., FUJIYAMA, F., KANEKO, T., HÖKFELT, T., CULLHEIM, S. & MEISTER, B. 2003. Cellular localization of three vesicular glutamate transporter mRNAs and proteins in rat spinal cord and dorsal root ganglia. *Synapse*, 50, 117-129.
- ORNUNG, G., SHUPLIAKOV, O., OTTERSON, O. P., STORM-MATHISEN, J. & CULHEIM, S. 1994. Immunohistochemical evidence for coexistence of glycine and GABA in nerve terminals on cat spinal motoneurons: an ultrastructural study. *Neuroreport*, 5, 889-892.
- OTTERSEN, O. P., STORM-MATHISEN, J. & SOMOGYI, P. 1988. Colocalization of glycine-like and GABA-like immunoreactivities in Golgi cell terminals in the rat cerebellum: a postembedding light and electron microscope study. *Brain Res*, 450.
- PAULI, W. M. & O'REILLY, R. C. 2008. Attentional control of associative learning—A possible role of the central cholinergic system. *Brain Research*, 1202, 43-53.
- PAXINOS, G. & WATSON, C. 2003. *The rat brain in stereotaxic coordinates*. 3rd ed. New York: Academic Press.
- PERSSON, S., BOULLAND, J.-L., ASPLING, M., LARSSON, M., FREMEAU, R. T., EDWARDS, R. H., STORM-MATHISEN, J., CHAUDHRY, F. A. & BROMAN, J. 2006. Distribution of vesicular glutamate transporters 1 and 2 in the rat spinal cord, with a note on the spinocervical tract. *The Journal of Comparative Neurology*, 497, 683-701.
- PETERSON, B. W., MAUNZ, R. A., PITTS, N. G. & MACKEL, R. G. 1975. Patterns of projection and branching of reticulospinal neurons. *Exp Brain Res*, 23, 333-351.
- PETERSON, B. W., PITTS, N. G., FUKUSHIMA, K. & MACKEL, R. G. 1978. Reticulospinal connections with limb and axial motoneurons. *Exp Brain Res*, 36, 1-20.
- PETRAS, J. M. 1967. Cortical, tectal and tegmental fiber connections in the spinal cord of the cat. *Brain Res*, 6, 275-324.
- PFLIEGER, J. F., CLARAC, F. & VINAY, L. 2002. Postural modifications and neuronal excitability changes induced by a short-term serotonin depletion during neonatal development in the rat. *J Neurosci*, 22, 5108-5117.
- PHELPS, P. E., BARBER, R. P. & VAUGHN, J. E. 1988. Generation patterns of four groups of cholinergic neurons in rat cervical spinal cord: A combined tritiated thymidine autoradiographic and choline acetyltransferase immunocytochemical study. *The Journal of Comparative Neurology*, 273, 459-472.

- PHELPS, P. E., BARBER, R. P., HOUSER, C. R., CRAWFORD, G. D., SALVATERRA, P. M. & VAUGH, J. E. 1984a. Postnatal development of neurons containing choline acetyltransferase in rat spinal cord: an immunocytochemical study. *J Comp Neurol*, 229, 347-361.
- PITUELLO, F. 1997. Neuronal specification: generating diversity in the spinal cord. *Curr Biol*, 7, 701-704.
- POTREBIC, S., FIELDS, H. L. & MASON, P. 1994. Serotonin immunoreactivity is contained in one physiological cell class in the rat rostral ventromedial medulla. *Journal of Neuroscience*, 14, 1655-1665.
- PRENTICE, S. D. & DREW, T. 2001. Contributions of the reticulospinal system to the postural adjustments occurring during voluntary gait modifications. *Journal of Neurophysiology*, 85, 679-698.
- PURVES, D. & HUME, R. 1981. The relation of postsynaptic geometry to the number of presynaptic axons that innervate autonomic ganglion cells. *The Journal of Neuroscience*, 1, 441-452.
- QU, S., ONDO, W. G., ZHANG, X., XIE, W. J., PAN, T. H. & LE, W. D. 2006. Projections of diencephalic dopamine neurons into the spinal cord in mice. *Experimental Brain Research*, 168, 152-156.
- RAMANATHAN, D., TUSZYNSKI, M. H. & CONNER, J. M. 2009. The Basal Forebrain Cholinergic System Is Required Specifically for Behaviorally Mediated Cortical Map Plasticity. *The Journal of Neuroscience*, 29, 5992-6000.
- REED, W. R., SHUM-SIU, A. & MAGNUSON, D. S. 2008. Reticulospinal pathways in the ventrolateral funiculus with terminations in the cervical and lumbar enlargements of the adult rat spinal cord. *Neuroscience*, 151, 505-517.
- RIBEIRO-DA-SILVA, A. & CUELLO, A. C. 1990a. Choline acetyltransferase-immunoreactive profiles are presynaptic to primary sensory fibers in the rat superficial dorsal horn. *J Comp Neurol*, 295, 370-384.
- RIBEIRO-DA-SILVA, A. & CUELLO, A. C. 1990b. Ultrastructural evidence for the occurrence of two distinct somatostatin-containing systems in the substantia gelatinosa of rat spinal cord. *J Chem Neuroanat*, 3, 141-153.
- ROBBINS, A., SCHWARTZ-GIBLIN, S. & PFAFF, D. W. 1992. Reticulospinal and reticuloreticular pathways for activating the lumbar back muscles in the rat. *Exp Brain Res*, 92, 46-58.
- ROBERTS, A., DALE, N., ENVOY, W. H. & S.R., S. 1985. Synaptic potentials in motoneurons during fictive swimming in spinal *Xenopus* embryos. *J Neurophysiol*, 54, 1-10.
- ROBLES-DE-LA-TORRE, G. 2008. Principles of haptic perception in virtual environments. In: M., G. (ed.) *Human Haptic Perception*. BirkHauser Verlag.

- ROSSIGNOL, S., BOUYER, L., BARTHÉLEMY, D., LANGLET, C. & LEBLOND, H. 2002. Recovery of locomotion in the cat following spinal cord lesions. *Brain Research Reviews*, 40, 257-266.
- RUDOMIN, P. & SCHMIDT, R. F. 1999. Pre-synaptic inhibition in the vertebrate spinal cord revisited. *Exp Brain Res*, 129, 1-37.
- SAKAI, S. T., DAVIDSON, A. G. & BUFORD, J. A. 2009. Reticulospinal neurons in the pontomedullary reticular formation of the monkey (*Macaca fascicularis*). *Neuroscience*, 163, 1158-1170.
- SAKATA-HAGA, H., KANEMOTO, M., MARUYAMA, D., HOSHI, K., MOGI, K., NARITA, M., OKADO, N., IKEDA, Y., NOGAMI, H., FUKUI, Y., KOJIMA, I., TAKEDA, J. & HISANO, S. 2001. Differential localization and colocalization of two neuron-types of sodium-dependent inorganic phosphate cotransporters in rat forebrain. *Brain Research*, 902, 143-155.
- SCHAFER, M. K., VAROQUI, H., DEFAMIE, N., WEIBE, E. & ERICKSON, J. D. 2002. Molecular cloning and functional identification of mouse vesicular glutamate transporter 3 and its expression in subsets of novel excitatory neurons. *J Biol Chem*, 277, 50734-50748.
- SCHEIBEL, M. E. & SCHEIBEL, A. B. 1969. Terminal patterns in cat spinal cord. III. Primary afferent collaterals. *Brain Res*, 13, 417-443.
- SCHENKEL, E. & SIEGEL, J. M. 1989. REM sleep without atonia after lesions of the medial medulla. *Neuroscience Letters*, 98, 159-165.
- SCHEPENS, B. & DREW, T. 2003. Strategies for the Integration of Posture and Movement During Reaching in the Cat. *Journal of Neurophysiology*, 90, 3066-3086.
- SCHEPENS, B. & DREW, T. 2004. Independent and convergent signals from the pontomedullary reticular formation contribute to the control of posture and movement during reaching in the cat. *Journal of Neurophysiology*, 92, 2217-2238.
- SCHERRER, G., LOW, S. A., WANG, X., ZHANG, J., YAMANAKA, H., URBAN, R., SOLORZANO, C., HARPER, B., HNASKO, T. S., EDWARDS, R. H. & BASBAUM, A. I. 2010. VGLUT2 expression in primary afferent neurons is essential for normal acute pain and injury-induced heat hypersensitivity. *Proceedings of the National Academy of Sciences*, 107, 22296-22301.
- SCHOMBURG, E. D. & STEFFENS, H. 1988. The effect of DOPA and clonidine on reflex pathways from group II muscle afferents to alpha-motoneurons in the cat. *Exp Brain Res*, 71, 442-446.
- SCOTT, S., PATEL, N. & LEVINE, J. 1990. Lectin binding identifies a subpopulation of neurons in chick dorsal root ganglia. *The Journal of Neuroscience*, 10, 336-345.
- SCULLION, K., BOYCHUK, J. A., YAMAKAWA, G. R., RODYCH, J. T. G., NAKANISHI, S. T., SETO, A., SMITH, V. M., MCCARTHY, R. W., WHELAN, P. J., ANTLE, M. C.,

- PITTMAN, Q. J. & TESKEY, G. C. 2013. Serotonin 1A Receptors Alter Expression of Movement Representations. *The Journal of Neuroscience*, 33, 4988-4999.
- SEMWOGERERE, D. & WEEKS, E. 2005. Confocal Microscopy. *Encyclopedia of Biomaterials and Biomedical Engineering*.
- SERRIAN, D. J., STRENS, L. H., CASSIDY, M. J., THOMPSON, A. J. & BROWN, P. 2004. Functional significance of the ipsilateral hemisphere during movement of the affected hand after stroke. *Exp Neurol*, 190.
- SCHMITZ, C. & HOF, P.R. 2005. Design-based stereology in neuroscience. *Neuroscience*, 130, 813-831.
- SHATZ, C. J. 1983. The prenatal development of the cat's retinogeniculate pathway. *J Neurosci*, 3, 482-499.
- SHERRIFF, F. E. & HENDERSON, Z. 1994. A cholinergic propriospinal innervation of the rat spinal cord. *Brain Research*, 634, 150-154.
- SHERRIFF, F. E., HENDERSON, Z. & MORRISON, J. F. B. 1991. Further evidence for the absence of a descending cholinergic projection from the brainstem to the spinal cord in the rat. *Neuroscience Letters*, 128, 52-56.
- SIEGEL, J. M. 1989. Brainstem mechanisms generating REM sleep. In: KRYGER, M. H., ROTH, T. & DEMENT, W. C. (eds.) *Principles and practice of sleep medicine*. Philadelphia: Saunders.
- SIEGEL, J. M., NIENHUIS, R., FEHRINGER, H. M., PAUL, R., SHIROMANI, P., DEMENT, W. C., MIGNOT, E. & CHIU, C. 1991. Neuronal activity in narcolepsy: identification of cataplexy-related cells in the medial medulla. *Science*, 252, 1315-8.
- SILVERMAN, J. D. & KRUGER, L. 1990. Selective neuronal glycoconjugate expression in sensory and autonomic ganglia: relation of lectin reactivity to peptide and enzyme markers. *J Neurocytol*, 19, 789-801.
- SKAGERBERG, G. & LINDVALL, O. 1985. Organization of diencephalic dopamine neurones projecting to the spinal cord in the rat. *Brain Research*, 342, 340-351.
- SMETANA, R., JUVIN, L., DUBUC, R. & ALFORD, S. 2010. A parallel cholinergic brainstem pathway for enhancing locomotor drive. *Nat Neurosci*, 13, 731-738.
- SNIDER, W. 1988. Nerve growth factor enhances dendritic arborization of sympathetic ganglion cells in developing mammals. *The Journal of Neuroscience*, 8, 2628-2634.
- SOGHOMONIAN, J.-J. & MARTIN, D. L. 1998. Two isoforms of glutamate decarboxylase: why? *Trends in Pharmacological Sciences*, 19, 500-505.
- SOJA, P. J., MORALES, F. R., BARANYI, A. & CHASE, M. H. 1987. Effect of inhibitory amino acid antagonists on IPSPs induced in lumbar motoneurons upon stimulation of the nucleus reticularis gigantocellularis during active sleep. *Brain Res*, 423, 353-358.

- SPIKE, R. C., TODD, A. J. & JOHNSTON, H. M. 1993. Coexistence of NADPH diaphorase with GABA, glycine, and acetylcholine in rat spinal cord. *J Comp Neurol*, 335, 320-333.
- SPITZER, N. C. 2004. Coincidence detection enhances appropriate wiring of the nervous system. *Proc Natl Acad Sci U S A*, 101, 5311-5312.
- SQALLI-HOUSSAINI, Y., CAZALETS, J. R. & CLARAC, F. 1993. Oscillatory properties of the central pattern generator for locomotion in neonatal rats. *Journal of Neurophysiology*, 70, 803-813.
- STEPANYANTS, A. & CHKLOVSKII, D. B. 2005. Neurogeometry and potential synaptic connectivity. *Trends in neurosciences*, 28, 387-394.
- STEPIEN, A. E., TRIPODI, M. & ARBER, S. 2010. Monosynaptic Rabies Virus Reveals Premotor Network Organization and Synaptic Specificity of Cholinergic Partition Cells. *Neuron*, 68, 456-472.
- STEWART, W. & MAXWELL, D. J. 1999. A population of lamina III/IV neurokinin-1-immunoreactive cells are targeted by serotonin-immunoreactive axons in the rat dorsal horn. *Journal of Physiology-London*, 518p, 166.
- STOKKE, M. F., NISSEN, U. V., GLOVER, J. C. & KIEHN, O. 2002. Projection patterns of commissural interneurons in the lumbar spinal cord of the neonatal rat. *The Journal of Comparative Neurology*, 446, 349-359.
- STORM-MATHISEN, J., DANBOLT, N. C. & OTTERSEN, O. P. 1995. Localization of glutamate and its membrane transport proteins. In: STONE, T. S. (ed.) *CNS neurotransmitters and neuromodulators: glutamate*. New York: CRC Press.
- SUGIUCHI, Y., KAKEI, S., IZAWA, Y. & SHINODA, Y. 2004. Functional synergies among neck muscles revealed by branching patterns of single long descending motor-tract axons. *Prog Brain Res*, 143, 411-421.
- SUMNER, B. E. & WATSON, W. E. 1971. Retraction and expansion of the dendritic tree of motor neurones of adult rats induced in vivo. *Nature*, 233, 273-275.
- TAAL, W. & HOLSTEGE, J. C. 1994. GABA and glycine frequently colocalize in terminals on cat spinal motoneurons. *Neuroreport*, 5, 2225-2228.
- TAKAHASHI, M., FREED, R., BLACKMER, T. & ALFORD, S. 2001. Calcium influx-independent depression of transmitter release by 5-HT at lamprey spinal cord synapses. *The Journal of Physiology*, 532, 323-336.
- TAKAMORI, S., HOLT, M. & STENIUS, K. 2006. Molecular anatomy of a trafficking organelle. *Cell*, 127, 831-846.
- TAKAMORI, S., RHEE, J. S., ROSENMUND, C. & JAHN, R. 2000. Identification of a vesicular glutamate transporter that defines a glutamatergic phenotype in neurons. *Nature*, 407, 189-194.
- TANAKA, H., AMAMIYA, S., MIURA, N., ARAKI, A., OHINATA, J. & FUJIEDA, K. 2006. Postnatal development of brainstem serotonin-containing neurons projecting to lumbar spinal cord in rats. *Brain and Development*, 28, 586-591.

- THOMAS, E. & PEARSE, A. G. E. 1964. The solitary active cells. Histochemical demonstration of damage-resistant nerve cells with a TPN-diaphorase reaction. *Acta Neuropathol.*, 3, 238-249.
- TODD, A. J. & SPIKE, R. C. 1993. The localization of classical transmitters and neuropeptides within neurons in laminae I-III of the mammalian spinal dorsal horn. *Progress in Neurobiology*, 41, 609-645.
- TODD, A. J., HUGHES, D. I., POLGAR, E., NAGY, G. G., MACKIE, M., OTTERSEN, O. P. & MAXWELL, D. J. 2003. The expression of vesicular glutamate transporters VGLUT1 and VGLUT2 in neurochemically defined axonal populations in the rat spinal cord with emphasis on the dorsal horn. *Eur J Neurosci*, 17, 13-27.
- TODD, A. J., SPIKE, R. C., CHONG, D. & NEILSON, M. 1995. The relationship between glycine and gephyrin in synapses of the rat spinal cord. *Eur J Neurosci*, 7, 1-11.
- TODD, A., WATT, C., SPIKE, R. & SIEGHART, W. 1996. Colocalization of GABA, glycine, and their receptors at synapses in the rat spinal cord. *The Journal of Neuroscience*, 16, 974-982.
- TOHYAMA, M., SAKAI, K., SALVERT, D., TOURET, M. & JOUVET, M. 1979. Spinal projections from the lower brain stem in the cat as demonstrated by the horseradish peroxidase technique: origins of the reticulospinal tracts and their funicular trajectories. *Brain Research*, 173, 383-403.
- TRICOIRE, L. & TANIA, V. 2012. Neuronal nitric oxide synthase expressing neurons: A journey from birth to neuronal circuits. *Frontiers in Neural Circuits*, 82, 1-16.
- TROJANOWSKI, J. Q., GONATAS, J. O. & GONATAS, N. K. 1982. Horseradish peroxidase (HRP) conjugates of cholera toxin and lectins are more sensitive retrogradely transported markers than free HRP. *Brain Research*, 231, 33-50.
- VALTSCHANOFF, J. G., PHEND, K. D., BERNARDI, P. S., WEINBERG, R. J. & RUSTIONI, A. 1994. Amino acid immunocytochemistry of primary afferent terminals in the rat dorsal horn. *Comp Neurol*, 346, 237-252.
- VALTSCHANOFF, J. G., WEINBERG, R. J. & RUSTIONI, A. 1992. NADPH diaphorase in the spinal cord of rats. *J Comp Neurol*, 321, 209-222.
- VALTSCHANOFF, J. G., WEINBERG, R. J. & RUSTIONI, A. 1993. Amino acid immunoreactivity in corticospinal terminals. *Exp Brain Res*, 93, 95-103.
- VAN DIJKEN, H., DIJK, J., VOOM, P. & HOLSTEGE, J. C. 1996. Localization of dopamine D2 receptor in rat spinal cord identified with immunocytochemistry and in situ hybridization. *Eur J Neurosci*, 8, 621-628.
- VANDERHORST, V. G. J. M. & ULFHAKE, B. 2006. The organization of the brainstem and spinal cord of the mouse: Relationships between monoaminergic, cholinergic, and spinal projection systems. *Journal of Chemical Neuroanatomy*, 31, 2-36.

- VANDERHORST, V. G., TERASAWA, E., RALSTON, H. J. R. & HOLSTEGE, G. 2000. Monosynaptic projections from the lateral periaqueductal gray to the nucleus retroambiguus in the rhesus monkey: implications for vocalization and reproductive behavior. *J Comp Neurol*, 424, 251-268.
- VAROQUI, H., SCHÄFER, M. K.-H., ZHU, H., WEIHE, E. & ERICKSON, J. D. 2002. Identification of the Differentiation-Associated Na⁺/PI Transporter as a Novel Vesicular Glutamate Transporter Expressed in a Distinct Set of Glutamatergic Synapses. *The Journal of Neuroscience*, 22, 142-155.
- VETRIVELAN, R., FULLER, P. M., TONG, Q. & LU, J. 2009. Medullary Circuitry Regulating Rapid Eye Movement Sleep and Motor Atonia. *The Journal of Neuroscience*, 29, 9361-9369.
- VINCENT, S. R. & KIMURA, H. 1992. Histochemical mapping of nitric oxide synthase in the rat brain. *Neuroscience*, 46, 755-784.
- WALL, P. D. & LIDIERTH, M. 1997. Five sources of a dorsal root potential: their interactions and origins in the superficial dorsal horn. *J Neurophysiol*, 78, 860-871.
- WALLEN, P., BUCHANAN, J. T., GRILLNER, S., HILL, R. H., CHRISTENSON, J. & HOKFELT, T. 1989. Effects of 5-hydroxytryptamine on the afterhyperpolarization, spike frequency regulation, and oscillatory membrane properties in lamprey spinal cord neurons. *Journal of Neurophysiology*, 61, 759-768.
- WANG, Z., KAI, L., DAY, M., RONESI, J., YIN, H. H., DING, J., TKATCH, T., LOVINGER, D. M. & SURMEIER, D. J. 2006. Dopaminergic control of corticostriatal long-term synaptic depression in median spiny neurons is mediated by cholinergic interneurons. *Neuron*, 50, 443-452.
- WANG, Z.-W. E. 2008. *Molecular Mechanisms of Neurotransmitter Release*, Farmington, CT, Humana Press.
- WEN, Q. & CHKLOVSKII, D. B. 2008. A Cost-Benefit Analysis of Neuronal Morphology. *Journal of Neurophysiology*, 99, 2320-2328.
- WESS, J. 2003. Novel insights into muscarinic acetylcholine receptor function using gene targeting technology. *Trends in Pharmacological Sciences*, 24, 414-420.
- WESTLUND, K. N., LU, Y., COGGESHALL, R. E. & WILLIS, W. D. 1992. Serotonin is found in myelinated axons of the dorsolateral funiculus in monkeys. *Neuroscience Letters*, 141, 35-38.
- WHELAN, P. J. 1996. Control of locomotion in the decerebrate cat. *Progress in Neurobiology*, 49, 481-515.
- WHELAN, P., BONNOT, A. & O'DONOVAN, M. J. 2000. Properties of Rhythmic Activity Generated by the Isolated Spinal Cord of the Neonatal Mouse. *Journal of Neurophysiology*, 84, 2821-2833.

- WHISHAW, I. Q. 2000. Loss of the innate cortical engram for action patterns used in skilled reaching and the development of behavioral compensation following motor cortex lesions in the rat. *Neuropharmacology*, 39, 788-805.
- WHITE, S. R., FUNG, S. J., JACKSON, D. A. & IMEL, K. M. 1996. Serotonin, norepinephrine and associated neuropeptides: effects on somatic motoneuron excitability. *Prog Brain Res*, 107, 183-199.
- WILLIS, W. D. 1971. The case for the Renshaw cell. *Brain Behav Evol*, 4, 5-52.
- WILSON, J. M., REMPEL, J. & BROWNSTONE, R. M. 2004. Postnatal development of cholinergic synapses on mouse spinal motoneurons. *The Journal of Comparative Neurology*, 474, 13-23.
- WILSON, V. J. & PETERSON, B. W. 1978. Peripheral and central substrates of vestibulospinal reflexes. *Physiological Reviews*, 58, 80-105.
- WILSON, V. J. & YOSHIDA, M. 1969. Comparison of effects of stimulation of Deiters' nucleus and medial longitudinal fasciculus on neck, forelimb, and hindlimb motoneurons. *Journal of Neurophysiology*, 32, 743-58.
- WINDHORST, U. 1996. On the role of recurrent inhibitory feedback in motor control. *Prog Neurobiol*, 49, 517-587.
- WINDHORST, U. 2007. Muscle proprioceptive feedback and spinal networks. *Brain Research Bulletin*, 73, 155-202.
- WISE, S. P. & JONES, E. G. 1977. Cells of origin and terminal distribution of descending projections of the rat somatic sensory cortex. *J Comp Neurol*, 175, 129-158.
- WOLPAW, J. R. 2010. What Can the Spinal Cord Teach Us about Learning and Memory? *The Neuroscientist*, 16, 532-549.
- YASAKA, T., TIONG, S. Y., HUGHES, D. I., RIDDELL, J. S. & TODD, A. J. 2010. Populations of inhibitory and excitatory interneurons in lamina II of the adult rat spinal dorsal horn revealed by a combined electrophysiological and anatomical approach. *Pain*, 151, 475-488.
- ZAGORAIYOU, L., AKAY, T., MARTIN, J. F., BROWNSTONE, R. M., JESSELL, T. M. & MILES, G. B. 2009. A cluster of cholinergic premotor interneurons modulates mouse locomotor activity. *Neuron*, 64, 645-662.
- ZEILHOFER, H. U., MÖHLER, H. & DI LIO, A. 2009. GABAergic analgesia: new insights from mutant mice and subtype-selective agonists. *Trends in pharmacological sciences*, 30, 397-402.

Publication